

Geomaterial behavior and testing

Comportement et essai de Geomaterial

Paul W. Mayne

Georgia Institute of Technology, Atlanta, GA USA; Email: paul.mayne@ce.gatech.edu

Matthew R. Coop

Imperial College, London, UK; Email: m.coop@imperial.ac.uk

Sarah M. Springman

Swiss Federal Institute of Technology, Zürich, Switzerland; Email: sarah.springman@igt.baug.ethz.ch

An-Bin Huang

National Chiao Tung University, Taiwan, Republic of China; Email: abhuang@mail.nctu.edu.tw

Jorge G. Zornberg

University of Texas, Austin, TX USA; Email: zornberg@mail.utexas.edu

ABSTRACT

A complete characterization detailing the intricate and complex response of geomaterials remains a challenging task that can only be realized on a partial basis via a careful drilling and sampling program coupled with detailed laboratory testing and comprehensive series of in-situ tests and field geophysics. As now evidenced from results reported from over 60 international geotechnical experimentation sites at worldwide locations, such extensive efforts directed at a particular soil formation take decades of time and considerable funding for completion. For a practical approach in routine site characterizations, the minimal standard of work should be seismic piezocone tests (SCPTu) or seismic flat dilatometer tests (SDMT), as up to 5 separate measurements of soil behavior are captured during a single sounding. These results should be supplemented with sampling and laboratory testing directed at defining parameters within a rational effective stress framework, and in particular, critical state soil mechanics (CSSM). Even then, a number of challenges remain, including the appreciation of rate effects, fabric, particle breakage, weathering, and diagenesis. Furthermore, nontextbook geomaterials (e.g., silty sands, carbonate clays, diatomaceous earth, peats, organic silts) will require a considerably higher level of testing and investigative effort because of greater uncertainty in understanding their anomalous behavior. Also, the characterization of geosynthetics, often used to complement or replace the function of earthen materials in many structures (e.g., reinforcement, drainage) requires the characterization of product-specific hydraulic, mechanical, and rheological properties.

RÉSUMÉ

Une caractérisation complète des géomatériaux devrait inclure toutes les complexités de leur comportement. Cela reste un défi, qui ne peut être réalisé que partiellement, et seulement si un programme de carottage et un programme d'essais en laboratoire, in-situ et géophysiques, sont tous suivis, sans exclusion et avec soin. On a maintenant la preuve, grâce aux données de plus de soixante sites géotechniques internationaux distribués dans le monde entier, que de tels efforts, plutôt consacrés à une formation géologique particulière, demandent des dizaines d'années et des fonds considérables pour aboutir. En pratique, un programme minimal d'essais pour une caractérisation in-situ devrait comprendre des essais au sismopiezocône ou des essais sismiques au dilatomètre plat, où jusqu'à cinq mesures séparées de la réponse du sol sont capturées pendant un seul sondage. Ces données devraient être supplémentées de carottage et essais en laboratoire afin de définir les paramètres pour un modèle rationnel de contrainte effective, et en particulier le modèle à l'état critique de Cambridge. Même ces essais de routine posent des problèmes ; par exemple il faut savoir apprécier les effets de taux de chargement, de fabrication du sol, de fracture des grains, de détérioration et de diagenèse sur la réponse du sol. De plus, pour les géomatériaux atypiques tels que les sables limoneux, argiles carbonatées, diatomées, tourbe, limons organiques, on a besoin d'un niveau d'essai et d'effort d'investigation bien plus élevé, à cause des incertitudes nombreuses liées à leur comportement hors norme. Enfin, l'utilisation dans beaucoup de structures de géosynthétiques, pour compléter ou remplacer les sols naturels, par exemple pour le renforcement du sol ou les barrières hydrauliques, demande une caractérisation appropriée et spécialisée des interfaces sol-géosynthétique.

Keywords: behaviour, clay, field tests, geomaterial, geosynthetics, in-situ test, modelling, modulus, sampling, sand, laboratory test, shear strength, shear modulus, shear wave velocity

1 INTRODUCTION

Soils and rocks are inherently complicated and often mysterious in their observed behavior because their constituency is made up of natural components formed over millenia. The diversity of the types of earthly geomaterials is vast and essentially limitless because of the infinite number of possible combinations and permutations regarding their geologic origin and global location, as well as long eonian histories involving changes in

climatology, temperature, elevation, environment, weathering, solutioning, and moisture, as well as any mechanical-chemical alterations. The advent of geosynthetics, i.e., polymeric materials used as integral part of earthen structures, augments the range of geomaterials and brings additional needs for proper material characterization. A selection of various geomaterials is shown in Figure 1.1 to illustrate the variegation. No formalized documented records on the beginnings, experiences, and histories of these soils and rocks are available for consultation

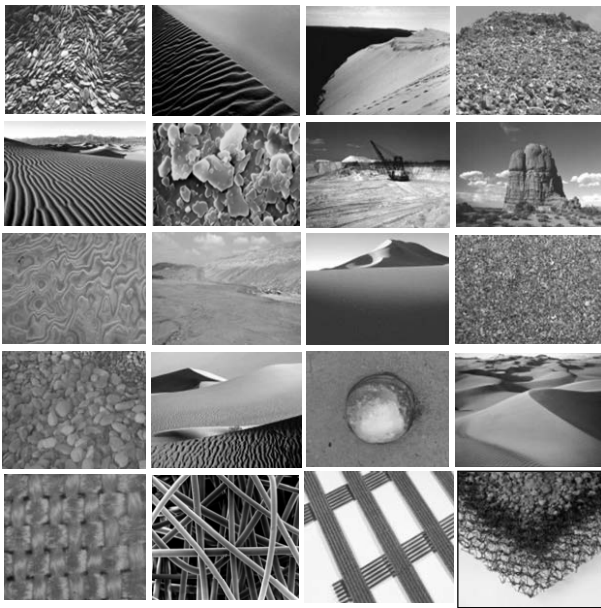


Figure 1.1. Selection of geomaterials showing their diversity.

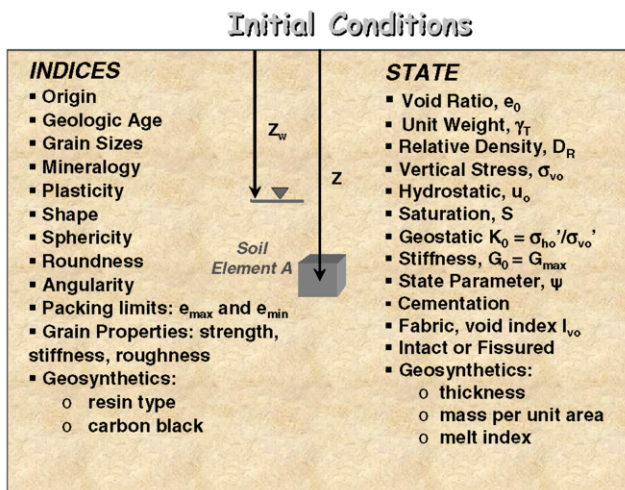


Figure 1.2. Geoparameters for representation of the initial conditions: (left) material indices and (right) state.

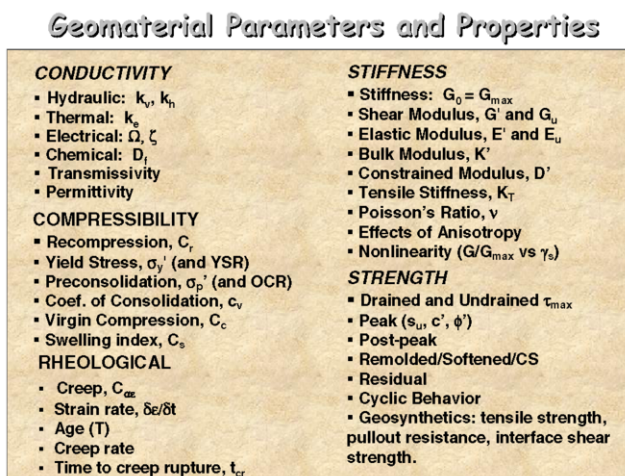


Figure 1.3. Geoen지니어ing parameters defined in terms of empirical, analytical, and/or theoretical solutions to problems.

when construction operations are undertaken. Therefore instead, representative and selected specimens of these natural materials must be procured in advance that are subjected to series of tests and examinations in an attempt to quantify their properties.

It is indeed quite a formidable task to undertake a comprehensive geotechnical characterization of a particular soil formation because of the many tasks and obstacles faced with in assigning quantifiable measures to describe all of the features, including: composition, gradation, particle shape, angularity, mineralogy, initial void ratio, density, packing arrangement, microstructure, fissuring, and/or degree of cementation. For the case of geosynthetics, additional properties should be quantified, including tensile strength, stiffness, transmissivity, permittivity, creep rate, interface shear strength, and pullout resistance.

For each stratum, numeric values must be assigned that adequately represent the characteristic parameters for stiffness, strength, prestress, permeability, rheological aspects, and anisotropy. The sheer number of parameters defined by our profession for soil engineering purposes is quite daunting (for example: $e_0, n_0, G_s, \gamma_t, D_R, e_{max}, e_{min}, R, \Psi, K_0, \kappa, \lambda, \Lambda, \Gamma, G_0, k, c_v, c_{az}, c', \phi', \sigma_p', CRR, OCR, YSR, OCD, s_u, E', G', D', K', \theta, T_{ult}, AOS,$ and J to name but a few). Supposedly, within a given layer, these should be independent variables and yet many may actually be interlinked or partially dependent upon one another, although the degree or reliance of their interrelationships may be in fact dependent on the type of geomaterial. The *initial conditions* can be established in terms of two sets of parameters: (a) indices; and (b) state parameters; as presented in Figure 1.2. The *index parameters* provide a measure on the types, shapes, ranges, and descriptive values on the particles that make up the composition. Indices can be performed on remoulded or disaggregated samples from the field. The *state parameters* represent quantification on how the particles are arranged or packed with respect to each other, thus lending to concepts such as "loose" vs. "dense" and "soft" vs. "hard", as well as special facets concerning bonding, cementation, fracturing, sensitivity and structural fabric. The initial state reflects the long-term geostatic conditions, often over many thousands to millions of years, and the value of these state parameters is given a subscript "nought" to indicate its beginning, such as initial void ratio (e_0), initial effective overburden stress (σ_{v0}'), initial hydrostatic porewater pressure (u_0), and initial lateral stress state (K_0). Primary findings in geotechnical research over the past two decades have established that the originally-defined dynamic shear modulus (G_{dyn}) is actually a fundamental stiffness at nondestructive strains (G_{max}) that applies to static, cyclic, and dynamic loading, as well as to both drained and undrained conditions, thus now termed G_0 (e.g., Tatsuoka & Shibuya 1991). As such, G_0 is a state parameter. It is determined from the shear wave velocity (V_s) and total mass density (ρ_t) using either or both laboratory or field tests:

$$G_0 = G_{max} = G_{dyn} = \rho_t \cdot V_s^2 \tag{1.1}$$

Beyond the initial conditions, geoen지니어ing concerns must deal with problems involving stability, structural loading, deformations, flow through porous media, compression, swelling and creep. While shear and compression have been the stress conditions of relevance for traditional soils, the advent of geosynthetic reinforcements brought up the need also to characterize tensile conditions, including tensile strength, tensile stiffness, as well as creep and stress relaxation under tensile conditions. Solutions to these situations rely on material parameters defined on the basis of analytical models, theoretical frameworks, or empiricism from observation of prior behavior. A selection of these mechanical-type parameters is shown in Figure 1.3 and includes such variables as shear strength (τ_{max}), compression index (C_c), coefficient of permeability (k), and constrained modulus (D'). With so many individual variables, a thorough and accurate assessment requires both a substantial

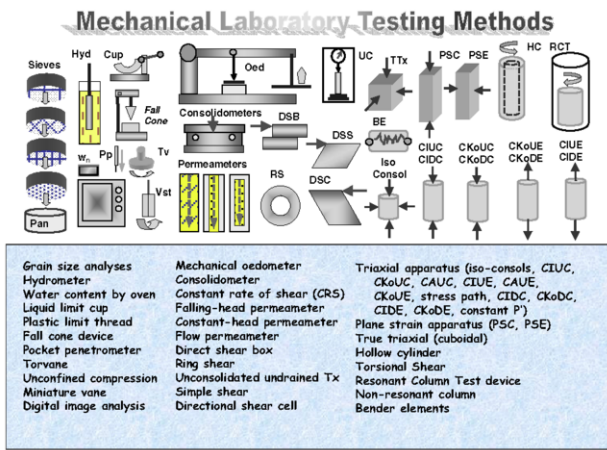


Figure 1.4. Laboratory testing devices for soil parameter determination.

budget and considerable time for experimentation, in order to acquire and test sufficient samples and obtain the data.

In most cases, each of the soil engineering parameters has been defined on the basis of laboratory reference tests. Towards these goals, the geotechnical profession has devised many apparatuses, with a selection presented in Figure 1.4. Only mechanical type measurements for soils are considered herein, and tests for chemical and electrical properties are not included. Tests for mechanical and hydraulic characterization of geosynthetics are also not included in the figure. The higher end laboratory devices presume that a representative, "undisturbed" specimen has been carefully obtained from the field sampling operations. Only then will the interpreted results bear resemblance to a soil element in the subsurface regime. It is likely, however, that some degree of sample disturbance has occurred during procurement of these geomaterials. The increased use of in-situ testing is an attempt to circumvent the issues of "representative" and "undisturbed" by the insertion of probes and widgets that measure a reaction of the soil that is interpreted into a geotechnical parameter directly.

Moreover, a good number of innovative and clever in-situ devices have been invented for the direct field testing of geomaterials, while still situated in the ground, as depicted in Figure 1.5. For each instrument, a different measurement on one or more aspects of soil behavior can be deduced, depending upon the method of insertion, direction of loading, strain rate, device geometry, duration of testing, and other factors.

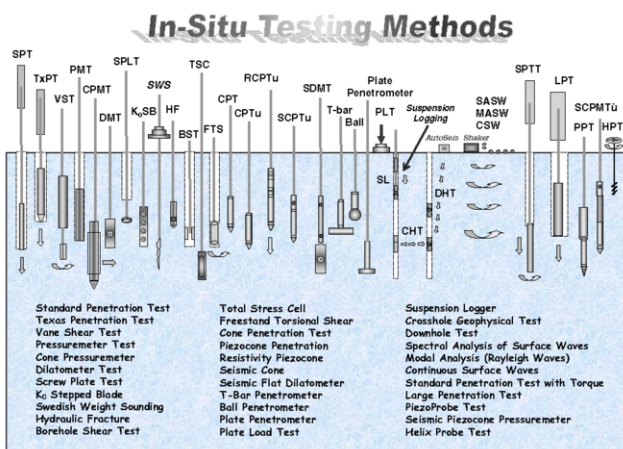


Figure 1.5. In-situ field probes for evaluating soil parameters.

Standardized test procedures should be followed so that consistent results are obtained among various users. Within a given country, standards may be imposed by the government, usually at a national level, or also by the state or province. On a more general basis, standards for testing soil and rock under field and laboratory conditions are given by the American Society for Testing and Materials (ASTM), and the Standards are generally employed in North American practice, or similar procedures produced for the European Union (CEN) or International Standards Organization (ISO). A summary of common ASTM procedures for laboratory and field testing of soils and rocks is given in Mayne et al. (2002). A summary of common ASTM procedures for laboratory testing of geosynthetics is given in Zornberg & Christopher (2007).

1.1 Experimentation Sites

Of particular value towards the understanding soil behavior and the interpretation of test data has been the advent of geotechnical test sites (e.g. Benoit & Lutenecker 2000). Recent symposia held in Singapore produced four volumes on the theme: *Characterization and Engineering Properties of Natural Soils*. In these proceedings, technical papers summarize the efforts of various prominent geotechnical research institutions and universities in the detailed field and laboratory testing of 60 different geomaterials, each within a particular geologic setting of a country. These locations are hereforth termed *international geotechnical experimentation sites* (IGES). In all cases, the IGES research programs have been underway for many years, often many decades, with most having not yet fully answered all of the behavioral subtleties within that particular soil formation.

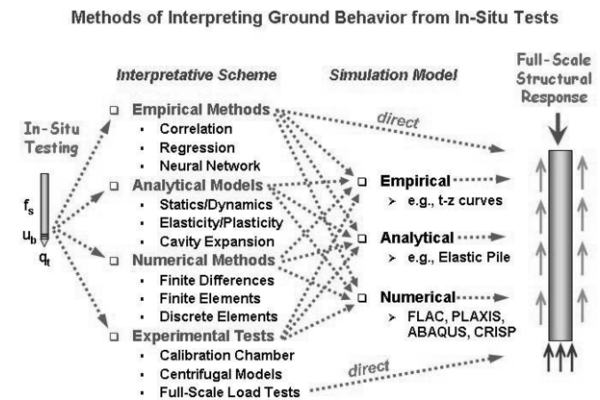


Figure 1.6. Various paths to interpretation of in-situ tests.

One example is the Holmen sand site, established and researched by the Norwegian Geotechnical Institute since 1956 (Lunne et al. 2003). Note that a number of other well-documented sites exist that were not included in this set of proceedings yet would certainly qualify for IGES status, for instance the Saugus, Massachusetts site underlain by the infamous Boston Blue Clay (Whittle et al. 2001). In the USA, six national test sites have been established (Benoit & Lutenecker, 2000), yet only 2 of these are considered within the aforementioned 60 IGES. Worth a final mention is another likely prospect for an IGES at the Canadian national test site in Gloucester, Ontario that is underlain by the well-known Champlain Sea sensitive clays and has been subjected to geotechnical research for almost 60 years (McRostie & Crawford 2001).

The geotechnical experimentation sites are of great value because many different types of measurements are taken in the same geomaterials in the same vicinity and location, hopefully minimizing issues of variability. It is possible here to obtain a

form of "ground truth" in terms of interpretation, and the laboratory test data can be compared with field test results. Geotechnical parameters acquired from analytical methods and numerical models can be calibrated properly with the recorded performance of full-scale geostructures. Also, statistical or empirical correlations can be developed amongst different test methods. An illustrative example is shown in Figure 1.6, where the measurements from cone penetration tests are shown to allow various paths to interpretation in the assessment of the axial load-displacement-capacity response of piling foundations. Having alternative methods of interpretation is actually helpful in geotechnical site characterization because there is no single consensus procedure for assessing parameters for all types of geomaterials, thus multiple methods can be adopted in parallel towards their evaluation or range of values.

Although these research sites have been thoroughly studied using an arsenal of multiple field and laboratory tests, several unexpected facets in soil behavior have come to light following subsequent construction and monitoring of full-scale shallow foundations, embankments, and pilings at these and other sites. For instance, short-term footing load tests on soft clay taken to failure indicated significant drainage and induced pore water pressures less than expected for "undrained conditions", as well as deviations from traditional linear elastic behavior (Jardine et al. 1995). Both facets were shown to affect our ability to calculate reliably the bearing capacity and vertical displacement of shallow foundations. Similarly, reported results from a prediction exercise with 22 calculation entries indicated the profession does not agree to a consensus approach to the interpretation of laboratory and field data for bearing capacity evaluation of footings on soft clays (Lehane 2003). Predictions ranged six-fold with estimates as low as one-half to as much as three times the measured bearing capacity of the full-scale load tests. Another example of deviant behavior comes from the case study of a recent highly-instrumented embankment constructed for the Venetian gates project (Simonini 2007) whereby the backfigured field stiffnesses are greater than laboratory oedometer values at stress levels less than the preconsolidation stress profile ($OCR > 1$) but field stiffnesses are significantly lower than laboratory values for stresses beyond σ_p' ($OCR = 1$).

Additional unexpected behavior from recent full-scale field testing programs has showed the considerable effects of creep on settlement magnitudes. For instance, long-term footing load tests on soft clay showed that the magnitude of creep settlements over an 11-year period were comparable to those caused by primary consolidation (Lehane & Jardine 2003). An instrumented circular embankment constructed on soft stratified sediments experienced 360 mm of primary consolidation settlements in 180 days, followed by an additional 80 mm of creep displacements over the next 180 days (Marchetti et al. 2004).

The benefit in observations of such anomalous behavior is to rethink the standard analytical methods and/or re-tune working numerical codes to address and include these facets in their predictions.

1.2 Interpretative Framework

In the evaluation of test data, it is advantageous to have an adopted framework within which to assess the results and assign parameter or property values based on the measured responses. For laboratory strength tests, this may include a total stress framework (e.g., Ladd 1991) or an effective stress framework (e.g., Lambe & Whitman 1979), otherwise a work-energy method such as critical state soil mechanics, CSSM (e.g., Schofield & Wroth 1968). The latter actually encompasses both the total and effective stress approaches and therefore should be adopted by the geotechnical engineering community towards a consensus framework. Moreover, a number of well-known and advanced constitutive models have been developed on the basis

Table 1.1. Undrained strength ratios (S) for normally-consolidated Boston Blue Clay (data from Ladd et al. 1980; Ladd & Lambe 1963).

Test Method/Mode	$S = (s_u/\sigma_{vo}')_{NC}$
Plane strain compression (PSC)	0.34
Triaxial compression (CK_0UC)	0.33
Iso-consolidated triaxial compression (CIUC)	0.32
Iso-consolidated triaxial extension (CIUE)	0.24
Direct simple shear (DSS)	0.20
Plane strain extension (PSE)	0.19
Unconsolidated Undrained (UU)	0.185
Triaxial extension (CK_0UE)	0.16
Unconfined compression (UC)	0.14

of CSSM and many of these have also been implemented into numerical computer codes for commercial use.

1.3 Test Modes

In terms of in-situ tests, for the most part, each device has developed somewhat independently since its inception and consequently the interpretations are based on mixed types of theories, analytics, numerics, and empiricism. As a result, inconsistent answers may be obtained when comparing different tests. For instance, the vane shear test (VST) is usually interpreted in terms of limit equilibrium analyses, results from plate load tests (PLT) are examined via plasticity solutions, while the pressuremeter test (PMT) is evaluated using cavity expansion theory. Moreover, it has been common to calibrate in-situ tests with the results of laboratory tests on supposedly "undisturbed" samples taken from the field. This causes additional difficulties because there are multiple laboratory tests for discerning a particular geo-parameter and different reference benchmark values are obtained from the different tests.

Consider the various types of laboratory test devices for measurement of undrained shear strength of clays. The undrained shear strength is not a unique value for a given soil deposit, but depends upon the type of test mode used to measure its value. This creates problems when trying to assess a representative value for s_u in clays, as the user will have already selected a bias in his or her choice of the test mode used to obtain a reference value for s_u .

Results of s_u compiled from different laboratory tests conducted on normally-consolidated Boston Blue Clay ($OCR = 1$) are presented in Table 1.1. The values are given in dimensionless form in terms of their normalized undrained shear strength ratios $S = (s_u/\sigma_{vo}')_{NC}$ that vary from a low of 0.14 for the unconfined compression mode (UC) to a high value of $S = 0.34$ for plane strain compression (PSC). All the tests were conducted and reported by MIT, a credible and reputable testing facility. Yet, a fairly healthy range in s_u is clearly evident for Boston Blue Clay, giving rise to the notion that a family of values or hierarchical suite of s_u modes exists. Of further note, an overall reasonable and representative s_u would correspond to the simple shear mode that provides an intermediate value for stability problems (Ladd 1991).

If both laboratory and field values for s_u are compared, the observed ranges become even more widespread. For example, various sets of undrained shear strength measurements for the

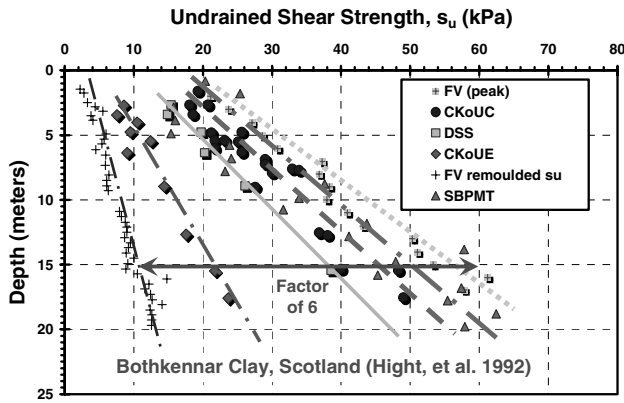


Figure 1.7. Six-fold variance of s_u from different laboratory and field tests at well-documented test site in soft Bothkennar clay. (Data replotted from Hight et al. 1992).

well-documented Bothkennar soft clay site in the UK are presented in Figure 1.7. These include results from in-situ pressuremeter tests (PMT) and vane tests (VST), as well as laboratory series from triaxial compression, direct simple shear and triaxial extension tests on undisturbed samples (Hight et al. 1992; 2003). At any given depth, these various values might range up to a factor of six, depending upon the particular test mode and strength under consideration. How does the geotechnical engineer in practice choose the correct value for stability problems involving footings, embankments, and/or excavations without being unsafe, yet not overly conservative?

The noted differences in the various undrained shear strength modes can be attributed to several factors: initial stress state (iso- vs. K_0 -consolidation), direction of loading (e.g., compression vs. extension paths), boundary conditions (triaxial vs. plane strain), rate of loading, inherent fabric anisotropy, sensitivity, strain compatibility, and other variables. The non-uniqueness of s_u must be addressed rationally if a clear and consistent framework is to be adopted by the geotechnical community in its practice.

1.4 Undisturbed Clay Specimens and Disturbance Issues

Results from laboratory testing depend significantly on the quality of the specimens cut from "undisturbed" samples. For soft clays and silts, the issue of sample disturbance is of paramount concern and depends on the drilling procedures, type of sampler, extraction, level of stress relief, sealing methods, transport, storage time, moisture conditions, tube extrusion of specimens, mounting, and laboratory care (Ladd & DeGroot 2003). Research studies by Tanaka (2000) comparing six different samplers in various soft clays found that the quality depended upon inside and outside diameter of the tube, sampler design, wall thickness, cutting angle, piston geometry, and other details. Generally, the highest quality specimens showed more pronounced peaks with higher s_u values, greater post-peak softening, and stiffer stress-strain responses during undrained compression loading than samples of inferior quality.

The effects of sample quality are illustrated by the anisotropically-consolidated triaxial compression (CAUC) test results presented in Figures 1.8 and 1.9 for Bothkennar clay and Lierstranda clay, respectively. In Figure 1.8a, for samples taken at depths of approximately 11.5 m, the high-quality JPN sampler is shown to give a significantly higher peak strength ($s_u = 42$ kPa) vs. the lower quality ELE sampler ($s_u = 30$ kPa), yet after strains have reached 15%, the two specimens indicate a softened strength value of about 16 kPa. Notably, the effective

stress paths for the Bothkennar tests converge to the same effective stress envelope, as evident in Figure 1.8b.

Similarly, Figure 1.9a shows results from three specimens on Lierstranda clay from 6 m depths, whereby the highest quality block sample gives a peak $s_u = 30$ kPa, the larger 75-mm tube gave $s_u = 24$ kPa, and the poorer quality test reflected by the small 50-mm tube with $s_u = 22$ kPa. Notably again, all three effective stress paths can be observed in Figure 1.9b and join the same effective stress strength envelope represented by $c' = 0$ and $\phi' = 34.4^\circ$.

The important findings here can be stated: (1) undrained shear strength in triaxial compression (s_{uTC}) is significantly affected by sample disturbance; (2) the effective friction angle (ϕ') is essentially not affected by disturbance effects. Additional support for these conclusions can be found in the triaxial data on other clays reported by Lacasse et al. (1985) and Lunne et al. (2006).

Another consideration regarding sample disturbance is with regard to the type of laboratory test. Laboratory data from triaxial compression (TC), direct simple shear (DSS), and extension tests (TE) on three Norwegian clays sampled by both blocks and tubes showed that the TC results for s_u and undrained stress-strain-strength behavior were much more affected than their companion DSS or TE series (Lacasse et al. 1985). This would lend support towards the use of DSS tests as perhaps a more reliable mode, since less variability and loss in strength and stiffness may occur.

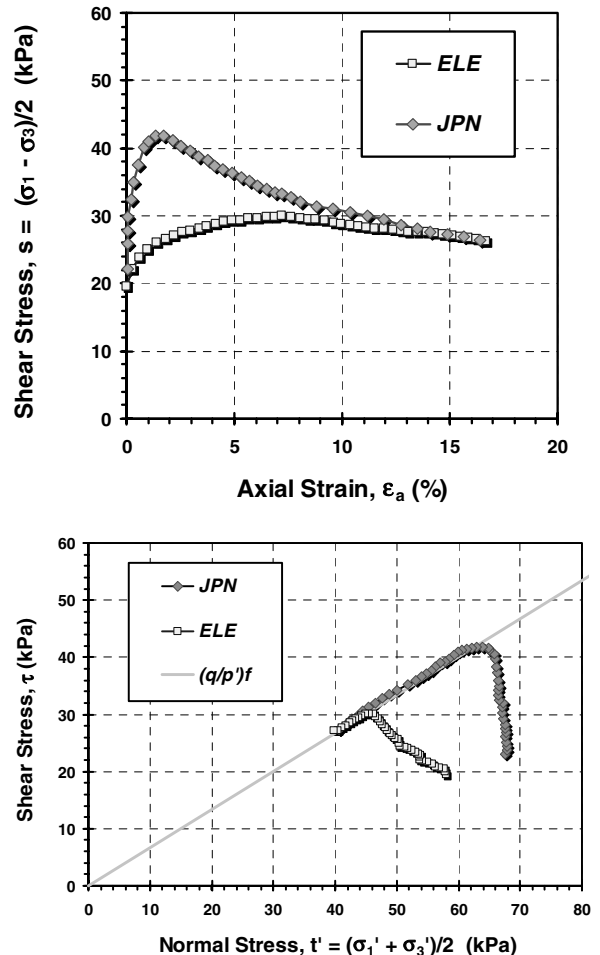


Figure 1.8. Sample disturbance effects for CAUC triaxial compression tests on Bothkennar clay showing (a) undrained stress-strain response; (b) effective stress paths (data from Tanaka 2000).

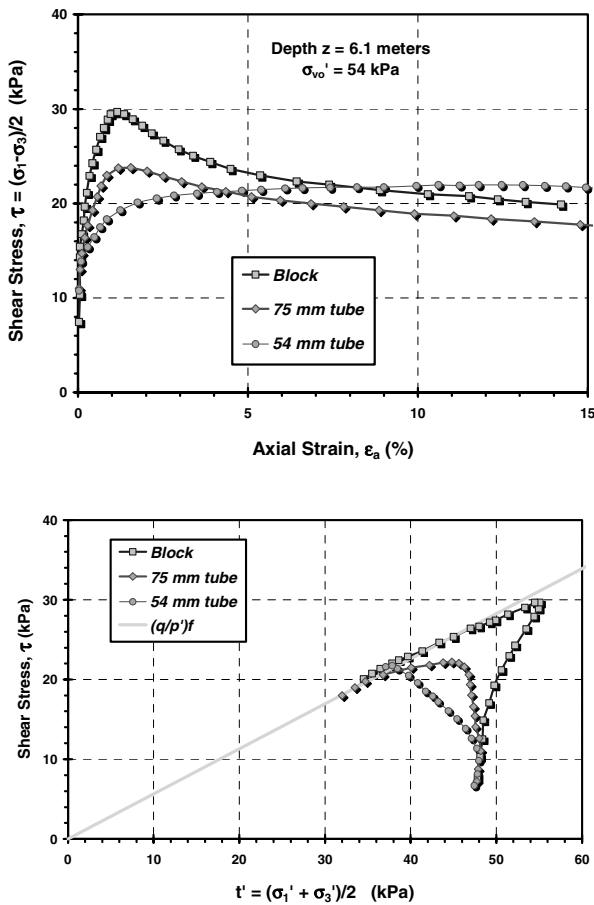


Figure 1.9. Sample disturbance effects for CAUC triaxial compression tests on Lierstranda clay showing (a) undrained stress-strain response; (b) effective stress paths (data from Lunne et al. 2006).

The results from one-dimensional consolidation tests are also well-recognized as being susceptible to disturbance effects, and consequently, a fair good number of graphical construction techniques have been proposed to correct the data, primarily towards defining the magnitude of yield stress or effective preconsolidation stress better ($\sigma'_p = \sigma'_{vmax} = P_c'$) that is obtained from the test (e.g., Grozić et al. 2003). However, the authors do not know of a comparable approach to correcting undrained stress-strain-strength curves based on issues of sample disturbance.

1.5 Undisturbed vs. Reconstituted Sand Specimens

For many early georesearch projects involving sands, specimens were created in the laboratory by reconstitution. Clean quartz to siliceous sands are cohesionless and therefore difficult to impossible to sample using conventional thin-walled tube techniques. Therefore, researchers resorted to taking easy-to-acquire bulk quantities of the natural sands back to their laboratories where artificial samples were prepared using one or more of a variety of placement techniques, including: air pluviation, compaction, slurry, sedimentation, vibration, and moist tamping. These laboratory-prepared sands were reconstituted to the estimated in-place void ratio (e_0) and supposed relative density (D_R) of the natural sand deposits, primarily evaluated on the basis of penetration tests in the field. Specimens were then tested to determine a particular parameter or behavior, such as friction angle or undrained cyclic liquefaction response that could be used in design. More

recently, special 1-d freezing techniques have been developed such that true undisturbed sands can be evaluated in the laboratory.

There are two major shortcomings with the preparation of artificial sand samples: (1) various reconstitution methods result in different fabric and structure, thus affecting the measured behavior; and (2) the in-situ e_0 or D_R of sands is rather poorly evaluated on the basis of penetration tests, including SPT, CPT, and DMT (e.g., Mayne 2006). For point 1, examine the undrained stress-strain-strength curves from undisturbed frozen sand samples reported by Hoeg et al. (2000) with triaxial specimens of the same sand artificially prepared using two different reconstitution techniques, as presented in Figure 1.10. The measured porewater pressure responses for these three triaxial tests are also considerably different (Fig. 1.11). This particular case is a reliable and solid example of sand behavior, as the freezing method truly determined an accurate in-situ e_0 (and D_R) to which the density of artificial specimens could be prepared. In many prior research studies, however, the field SPT-N and/or CPT- q_c resistances were utilized to merely estimate the D_R of the natural deposits, likely resulting in laboratory samples with different densities than those in-situ.

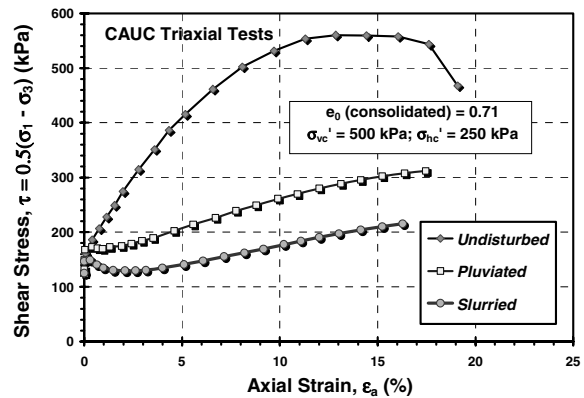


Figure 1.10. Comparison of undrained triaxial stress-strain-strength response for silty sand in undisturbed and reconstituted states. (Note: data from Hoeg et al. 2000).

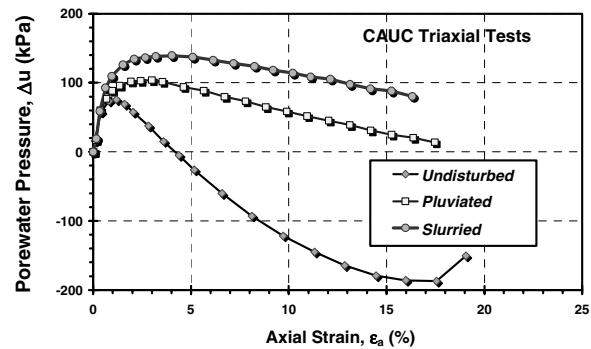


Figure 1.11. Various excess porewater pressure responses for silty sand in undisturbed and reconstituted states. (data from Hoeg et al. 2000).

The good news is that when sands are actually prepared artificially to the same densities as field values, the measured undrained triaxial response in terms of effective stress conditions reaches the same effective stress envelope. Consider the aforementioned sand in terms of MIT type q-p' plots in Figure 1.12, where all three specimens converge to the same frictional envelope represented by $c' = 0$ and $\phi' = 35.7^\circ$. Thus, the in-situ state (e_0 or D_R) should probably be measured by more accurate means, such as: freezing, nuclear methods, time

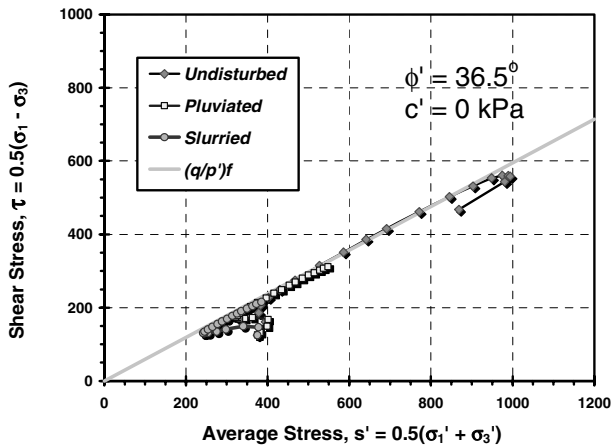


Figure 1.12. Common effective strength envelope for silty sand in undisturbed and reconstituted states. (data from Hoeg et al. 2000).

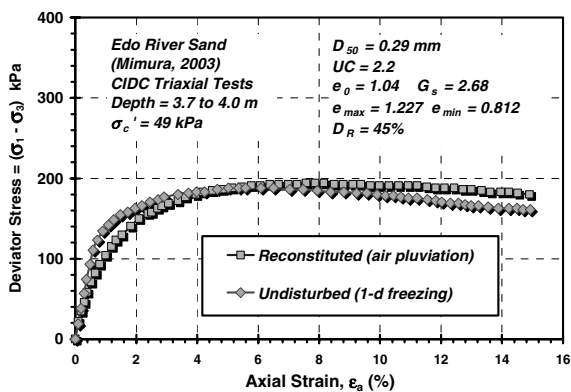


Figure 1.13. Comparison of stress-strain-strength curves for undisturbed and reconstituted Edo River sand (after Mimura 2003).

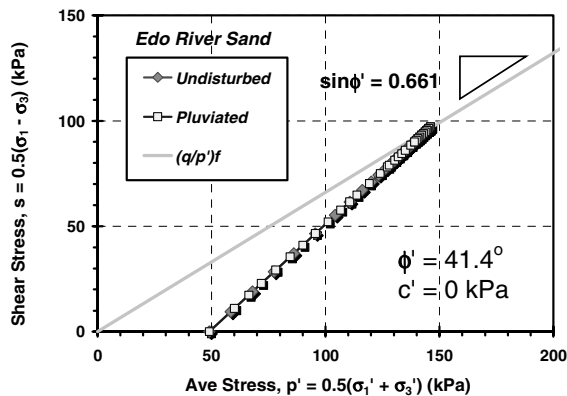


Figure 1.14. Common friction angle and effective stress paths for undisturbed and reconstituted Edo River sand (after Mimura 2003).

domain reflectometry, or geophysical logging tools, in order to determine the sand density properly.

More good news is that the drained triaxial response is adequately represented in terms of the stress-strain-strength curves if the artificial samples are prepared at the same density as in-situ specimens. Data from Edo River sand tested under isotropically-consolidated drained triaxial compression tests (CIDC) are shown in Figure 1.13 for both undisturbed (frozen) specimens and reconstituted by pluviation. Consequently, the derived strength, corresponding to maximum deviator stress, as

well as corresponding friction angle ($\phi' = 41.4^\circ$) are correctly obtained (Fig. 1.14) from both types of specimens. Note also, for the example shown, the stiffness (e.g., modulus at 50% strength, E_{50}') appears somewhat stiffer for the undisturbed specimen in comparison with the pluviated specimen. This phenomenon will be discussed in further detail in Section 4.

In summary, this section has shown several important and new findings on soil behavior of clays and sands, based upon recent research with undisturbed sampling methods. For both clays and sands, there is a non-uniqueness and thus low reliability in the expected undrained shear response, particularly in the triaxial compression mode. Clays are affected by sample disturbance in their peak undrained triaxial response, tending to lower their s_u and stiffness E_u values with increasing levels of remolding. In contrast, the effective frictional response ($c' = 0, \phi'$) is unaffected by sample disturbance, thus giving it a higher degree of reliability. For sands, artificially-created samples behave considerably different than undisturbed specimens in undrained triaxial shear, thus questioning their certainty and use in design. Notably, however, in terms of effective stress paths, the effective friction angle is common ground to both undisturbed and reconstituted sand specimens, thus a reliable and attainable value for use by the geotechnical community.

1.6 Generic vs. Project-Specific Geosynthetic Specimens

Unlike clays (Section 1.4) and sands (Section 1.5), geosynthetics are geomaterials manufactured in controlled environments that generally include strict quality control procedures. This has often led to the erroneous practice of minimizing the determination of project-specific properties of geosynthetics. Yet, relevant hydraulic and mechanical properties of geosynthetics may vary significantly. Section 6 of this paper provides an overview of recent advances in the characterization of the interface shear strength between soil and several geosynthetics. However, the need for appropriate characterization of geosynthetics spans through multiple applications in geotechnical engineering.

To illustrate the relevance of project-specific geosynthetic testing, the variability of a specific test (internal shear strength) using a specific type of geosynthetic (Geosynthetic Clay Liner, or GCL) is described herein. GCLs are prefabricated geocomposite materials used in hydraulic barriers as an alternative to compacted clay liners. They consist of sodium bentonite clay bonded to one or two layers of geosynthetic backing materials (carrier geosynthetics). Advantages of GCLs include their limited thickness, good compliance with differential settlements of underlying soil or waste, easy installation, and low cost. Yet, stability is a major concern for liners that include GCLs because of the very low shear strength of hydrated sodium bentonite (Mesri & Olson 1970). Consequently, proper shear strength characterization is needed for the different materials and interfaces in these hydraulic barriers. In particular, the failure surface of a liner system may develop internally (within the GCL), either through its bentonite core or along the bentonite/carrier geosynthetic interface.

A detail of the specimen configuration for GCL internal shear strength testing is shown in Figure 1.15 (Zornberg et al. 2005). A water bath may be used for testing GCLs under submerged conditions, although the most common procedure involves testing of GCL specimens after hydration, without a water bath. Internal strength testing of the GCL specimen typically involves constraining the GCL specimen in a modified direct shear apparatus so that shearing is only allowed to occur within the bentonite component of the GCL. As shown in the figure, the specimens can be constrained by bonding the two carrier geotextiles to porous rigid substrates using textured steel gripping surfaces. In this case, extensions of each carrier geotextile are secured using a second porous rigid substrate.

Conditioning of specimens plays an important role in GCL

internal shear strength testing, as moisture interactions should simulate correctly those anticipated in the field. GCL conditioning involves hydration and (in some cases) subsequent consolidation of the sodium bentonite. Hydration of the sodium bentonite leads to swelling. Although hydration times as high as 250 hs may be required, hydration times beyond 72 hs have been reported not to increase the GCL water content significantly, especially under high normal stresses (Stark & Eid 1996). Shearing is conducted after GCL conditioning by applying a shear load under a constant shear displacement rate.

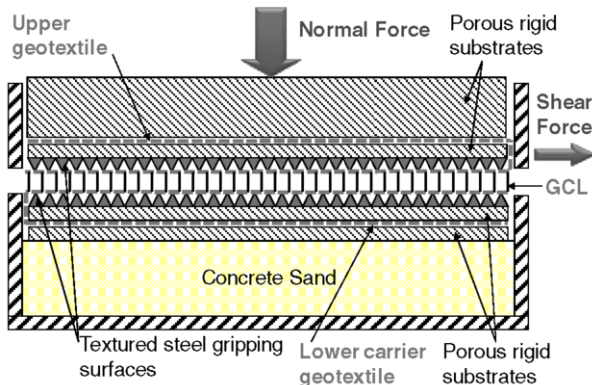


Figure 1.15. Large-scale direct shear device used for internal shear strength testing of GCLs (Zornberg et al. 2005).

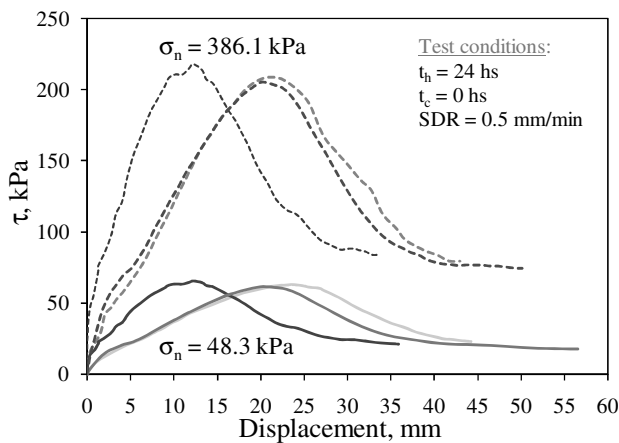


Figure 1.16. Repeatability of test results on needle-punched GCL specimens using rolls taken from the same lot (Zornberg et al. 2005).

The fact that this geomaterial (i.e. GCL) is manufactured under controlled conditions is reflected by the good repeatability of test results shown in Figure 1.16. The results correspond to internal shear of GCLs with needle-punched woven and nonwoven carrier geotextiles (Zornberg et al. 2005). However, it should be noted that these results were obtained using specimens collected from a single manufacturing lot and tested with the same conditioning procedures. These results illustrate that good repeatability can be achieved in the stress-strain-strength response when tests are conducted using same-lot specimens. Zornberg et al. (2005) report a maximum relative difference between shear strength results conducted in same-lot specimens is less than 6%.

Figure 1.17 shows GCL internal peak shear strength values reported in the literature for a wide range of GCLs (Zornberg & McCartney 2007). The wide range in shear strength reported by the different studies is in clear contrast with the good

repeatability of internal shear strength results obtained when using single-lot specimens. While some of the variability can be explained by differences in testing procedures and equipment used in the various studies, significant intrinsic material variability is still apparent. Generally, reinforced GCLs show higher shear strength and greater variability than unreinforced GCLs.

The overall material variability was also assessed by evaluating internal shear strength results obtained using the same GCL product (from a single manufacturer) and the same conditioning procedures, but using specimens from different manufacturing lots. In this case, The maximum relative differences of internal shear strength results is 55%, which is significantly higher than the differences obtained for tests conducted using same-lot GCL specimens. The results shown in the Figure 1.18 include data from 141 internal shear strength tests on the same GCL used to assess repeatability (Figure 1.16), and conducted using the same test conditions (hydration time of 168 hs, consolidation time of 48 hs, and shear displacement rate of 0.1 mm/min). The tests were conducted at three different normal stresses. The spread in shear strength values increases with normal stress, with a spread of 150 kPa at a normal stress of 310 kPa.

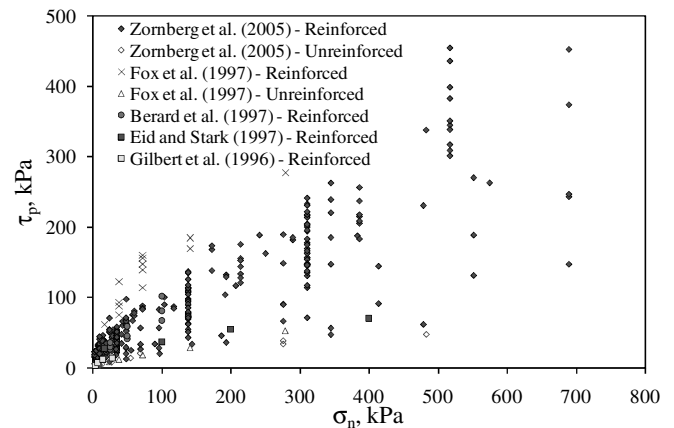


Figure 1.17. Overview of GCL internal peak shear strength values (Zornberg & McCartney 2009).

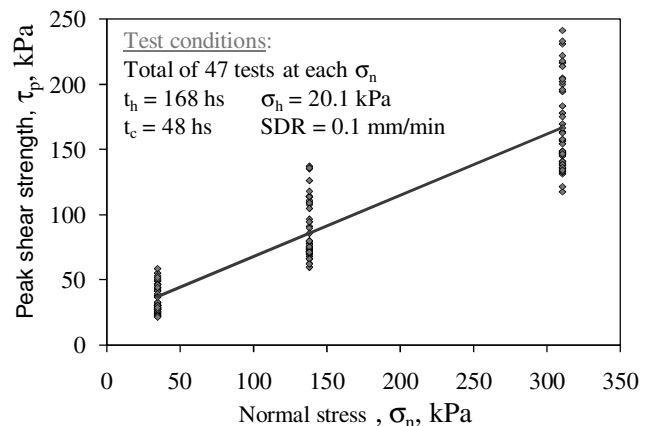


Figure 1.18. Variability of shear strength results obtained using needle-punched GCL A specimens from different lots, tested using same conditioning procedures and normal stress (Zornberg et al. 2005).

While the information discussed herein involves a single type of geosynthetics (i.e. GCLs), it illustrates the good repeatability of results that can be expected for tests conducted by the same laboratory using specimens from the same manufacturing lot. However, as in the case of soils, significant variability can

result from tests conducted using geosynthetic specimens obtained from different lots over a period time. Accordingly, the material properties of geomaterials manufactured in controlled environments should not be based only on tests conducted using generic products, but it may often require tests conducted using project-specific specimens.

1.7 Local Strain Measurements

In laboratory triaxial testing, strains at small stiffnesses must be measured internally and directly on the soil specimen in order to accurately assess deformations. These are termed local strain measurements and require special sensors for the proper resolution of small movements. Standard triaxial equipment available from a number of commercial suppliers use the easier route by measuring deformations external to the triaxial cell, thus averting the difficulties of placing electrical devices inside a water-pressurized chamber and mounting problems. However, a number of key research laboratories have successfully overcome these obstacles using superglues (cyanoacrylates) and special sealants, therefore obtaining data on clays, sands, rocks, and cemented geomaterials (e.g., Burland & Symes 1982; Jardine et al. 1984; Clayton & Khatrush 1986; Ackerley et al. 1987; Tatsuoka & Shibuya 1991; Cuccovillo & Coop 1997). In fact, the significance of this work spurred sufficient interest to establish a series of international symposia on the topic of *Deformation Characteristics of Geomaterials* that have been held in Japan (Shibuya et al. 1994), London (Jardine et al. 1997), Italy (Jamiolkowski et al. 1999), France (DiBenedetto et al. 2003), and the USA (Burns et al. 2008).

Local strain measurements have confirmed three major findings: (1) $E_0 = 2G_0(1+v)$ at small strains is the beginning of all stress-strain curves, as noted earlier; (2) soils are much stiffer than originally assessed by older conventional triaxial apparatuses; (3) Poisson's ratio is generally smaller than previously measured by older equipment. Examples to illustrate each of these points will be presented.

Point 1: The small-strain stiffness of soils has been conventionally determined in the laboratory using resonant column tests (RCT), where data are confined to non-destructive shear strains on the order of 10^{-4} to 10^{-2} % (Woods 1978). In contrast, traditional triaxial equipment provides data at strains up to 15% with the smallest resolution at around 0.1%. With the advent of local strain measurements, accurate stiffnesses at smaller strains can now be identified in triaxial tests (Tatsuoka et al. 1997). Figure 1.19 shows results from both RCT and CIUC triaxial tests on Vallerica clay with the overlapping match of stiffnesses in the strain range from 0.01 to 0.05% (Georgiannou et al. 1991). Measured shear moduli from both tests tend towards a maximum shear stiffness represented by $G_0 = 80$ MPa.

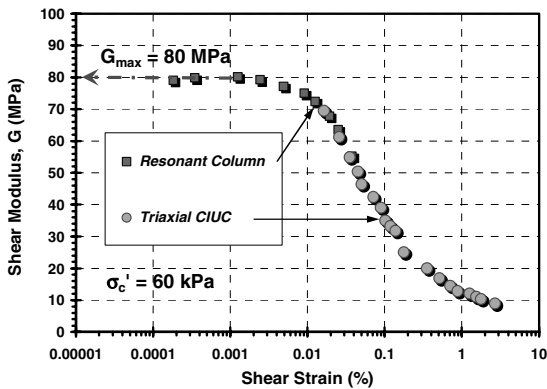


Figure 1.19. Compatibility of RCT and TX results for Vallerica clay (data from Georgiannou et al. 1991).

Point 2: The stiffnesses of soils are best measured internal to the triaxial cell with deformation gages mounted directly on the specimen (e.g., Jamiolkowski et al. 1994). This is because the standard triaxial readings of deformations include primary issues related to bedding errors and apparatus compliance, as well as additional minor effects due to ram-cap seating, rod friction, compressibility of filter stone and filter paper at specimen ends, specimen boundary effects, and membrane corrections. Local strains measured directly on the specimen abdomen omit these errors. Consider the example of triaxial tests on North Sea clay where the conventional (external) deformations can be compared with the special (internal) local measurements on the same specimen in Figure 1.20. At the initial to intermediate loading stages, the conventional method gives a rather low elastic modulus $E_u = 48$ MPa in contrast to the much stiffer $E_u = 600$ MPa obtained from the local strain gages. At the much latter stages of shearing near the peak strength, the two sets of measurements converge.

Point 3: For similar arguments made above, characteristic values of Poisson's ratio ($v' = -\Delta\epsilon_r/\Delta\epsilon_a$) are actually lower when measured by internal deformation gages mounted directly on the specimen, than when taken using conventional equipment. Figure 1.21 shows the development of Poisson's ratio with strain as determined from both traditional (external) and local (internal) measurements. It is clear that the latter indicate lower values of v' throughout the range, in fact about half the conventional values from external measurements at strains < 0.5%. For loading of the soil continuum by footings, piles, and walls, Burland (1989) has shown that mobilized strains are on the order of 0.05% to 0.2%, averaging around 0.1%.

Figure 1.22 shows a selection of v' from local strain measurements in terms of mobilized stress level (q/q_{max}). Initial values of v' are between 0.1 and 0.2. Note that the ratio q/q_{max} can be considered as the reciprocal for the factor of safety ($FS = q_{max}/q$). For many geotechnical situations, the corresponding range: $10 > FS > 2.5$ applies to working loads, consequently a characteristic value of $v' = 0.2$ can be adopted for many soils.

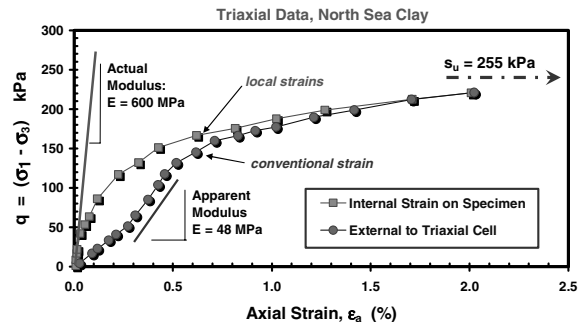


Figure 1.20. Local- and conventional-strain measurements for stress-strain-strength on same specimen (data from Jamiolkowski 1998).

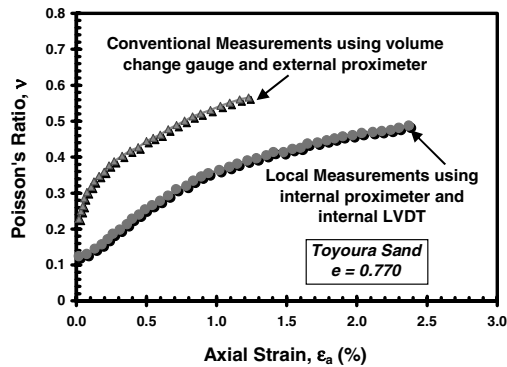


Figure 1.21. Conventional external vs. local internal measurements of Poisson's ratio (data from Jamiokowski et al. 1994).

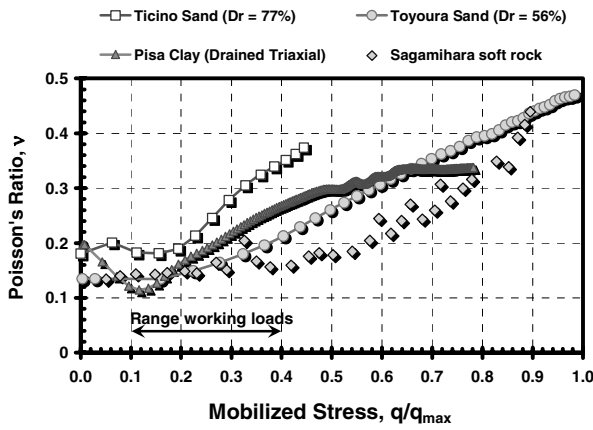


Figure 1.22. Response of Poisson's ratio with mobilized stress level from local strain measurements on different geomaterials.

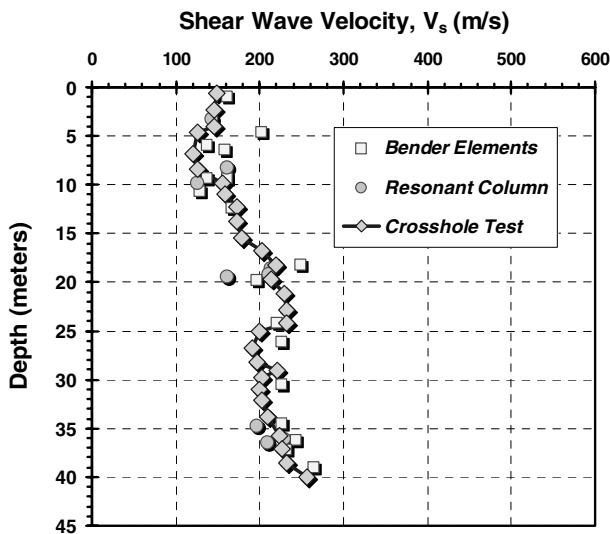


Figure 1.23. Comparison of shear wave velocities from BE, RCT, and CHT at Garigliano site (after Jamiolkowski et al. 1994).

For a cross-anisotropic soil, using a combination of bender elements and local strain readings from static probes, we can get the full set of elastic parameters (E_{th} , E_v , G_{vh} , G_{hv} , G_{hh} , v_{hh} , v_{hv} , v_{vh}) (although the set reduces to five independent parameters). For example, a set of cross-anisotropic parameters for London clay are presented by Gasparre et al. (2007) and similar tests of other materials are shown elsewhere (e.g., Lings 2001; Lings et al. 2000; Tatsuoka et al. 2001).

1.8 Bender elements

Bender elements (BE) permit a quick and economical determination of G_0 on all sizes of laboratory soil samples. In the traditional RCT, a full specimen of 75 mm diameter and 150 mm height is required. The RCT costs approximately US \$2000 for one specimen and takes several days for completion. In contrast, the new bender elements uses a pair of small plates that can be mounted on existing oedometer, triaxial, direct shear, or even RCT specimens, thus being more versatile. The BE determination of G_0 can be made expeditiously by sending a wavelet from one element to the other. Also, BE tests are conducted at a fraction of the cost of RCT. Results for obtaining V_s are comparable for BE and RCT, as well as field methods provided that sample quality is high, as illustrated by test data reported for Garigliano clayey silt shown in Figure 1.23.

A more recent development is to use lateral T-elements to get G_{hh} and G_{hv} (Pennington et al. 1997), as well as, or instead of, the platen mounted elements to get G_{vh} . The T-elements are necessary if the full set of cross-anisotropic parameters are desired.

1.9 Critical state soil mechanics

Critical state soil mechanics (CSSM) offers a rational, yet simple, framework that can be used to organize and present field and laboratory results. In essence, CSSM is a linkage between compression, swelling, volume change, shear behavior, and porewater pressure response in terms of effective stresses. In consideration of work-energy models, the mathematical forms are given by the Original Cam-Clay (Schofield and Wroth 1968), Modified Cam Clay (Roscoe & Burland 1968; Muir Wood 1990), NorSand (Jefferies 1993; Jefferies & Shuttle 2005), and higher-order constitutive relationships (e.g., Whittle & Kavvas 1994; Pestana & Whittle, 1999). Surprisingly, CSSM is not always taught as a fundamental section or chapter in undergraduate and graduate courses, nor is it mentioned or discussed in most textbooks on soil mechanics. It is often missing from the educational backgrounds of our practising engineers with the repercussions that their evaluation of soil parameters may have incompatibilities and contradictions. Towards improving the theory-to-practice and bridging this gap, the authors offer the following simplified version of CSSM to show its versatility and elegance.

In its basic form, CSSM is merely a linkage between two well-known facets of soil behavior: (a) compression, in terms of void ratio vs. logarithm effective stress (e - $\log \sigma'_v$) graphs; and (b) shearing, in terms of shear stress vs. normal stress (τ - σ'_v) or equivalent Mohr-Coulomb type friction response. An example of one-dimensional consolidation response for clay is shown in Figure 1.24. The conventional interpretation puts emphasis on the determination of the preconsolidation stress (σ'_p), virgin compression index (C_c), and swelling index (C_s), although additional parameters can be defined as well (e.g., $D' = 1/m_v$, c_v , k_v , and $C_{\alpha e}$). In this instance, the value of $\sigma'_p = 45$ kPa is determined by the Pacheco Silva procedure (Clementino 2005). The normalized form of the preconsolidation is termed the overconsolidation ratio ($OCR = \sigma'_p / \sigma'_{vo}$), and for this clay specimen: $OCR = 1.15$. Portions of the curve beyond σ'_p are in the normally-consolidated (NC) region and are at stress levels never before experienced by this natural clay deposit. This virgin compression line (represented by C_c), when projected backward to higher void ratios, would reflect a state and condition similar to that occurring during the original sedimentation process, provided that mechanical loading and/or unloading alone occurred since that time (Burland 1990).

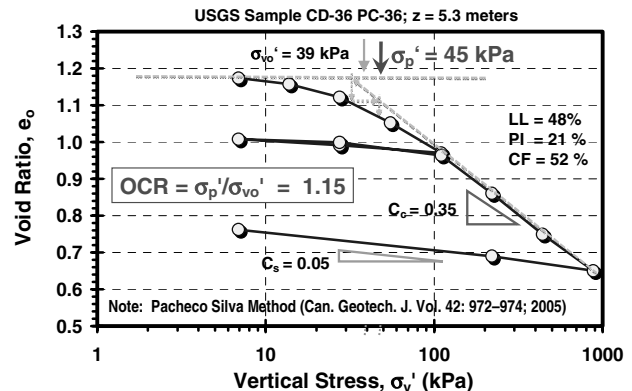


Figure 1.24. One-dimensional consolidation test results for offshore clay from the Atlantic continental slope.

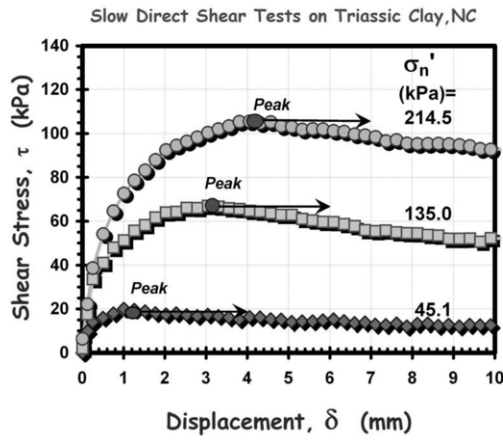


Figure 1.25. Slow drained direct shear test results for clay specimens from Raleigh, NC (Mayne et al. 2002).

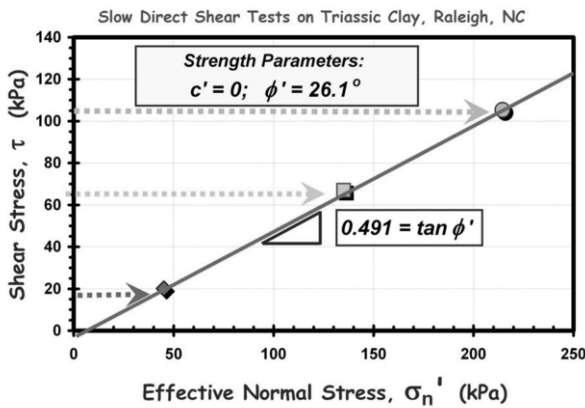


Figure 1.26. DS results plotted in terms of shear stress vs normal stress for determining effective friction angle (Mayne et al. 2002).

An example of shear behavior is afforded from direct shear tests (DST) on clay from Raleigh, North Carolina in Figure 1.25. Here, identical specimens from one tube sample have been subjected to a slow drained DST after consolidation at three different applied normal stresses of 45, 135, and 214 kPa. In the DST, the measured horizontal shear stress (τ) is plotted vs. shear displacement (δ) and the maximum or peak shear stress (τ_{max}) is termed the shear strength. Plotting the maximum shear stress (τ_{max} = shear strength) vs. the applied effective normal stress for all 3 points defines the effective stress friction angle (ϕ') of the soil ($c' = 0$), as shown in Figure 1.26.

A close cousin testing device is the direct simple shear (DSS), whereby the sides move as a parallelogram rather than as two split box halves as in the DST (see Fig. 1.27). Nevertheless, results from DST and DSS on the same soil are quite similar (e.g., Potts et al. 1987; Tang et al. 1995). The advantage of the DSS is that the angle of movement is the shear strain (γ_s), a more fundamental measurement than horizontal displacement δ . If needed, a pseudo-strain can be defined as $\gamma_s \approx \delta/h$, where h = height of the specimen.

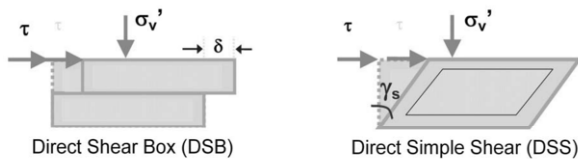


Figure 1.27. Direct shear (DS) box and direct simple shear (DSS).

In CSSM, consolidation and shearing are interlinked by their stress state spaces, as depicted in Figure 1.28. The consolidation response is shown in e - $\log \sigma'_v$ space and the shearing behavior is represented by τ - σ'_v space. A third and intermediate space is also shown (e - σ'_v) only to allow projection between the other two spaces, but this requires no new information as it is just an arithmetic scaling of the consolidation space. The CSSM premise is that, regardless of the initial state of the soil, any shearing will tend towards and eventually reach the critical state line (CSL). In the τ - σ'_v space, the CSL is synonymous with the effective frictional envelope defined by ϕ' . In the e - $\log \sigma'_v$ space, the CSL lies parallel to the VCL given by C_c , yet offset to the left, as shown by the (red) dashed line in Figure 1.28.

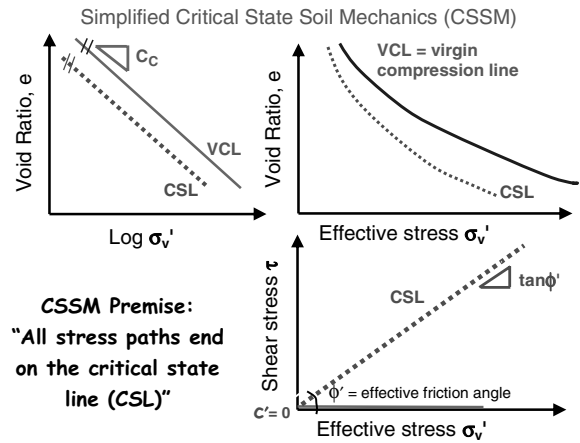


Figure 1.28. State spaces for NC soil using simplified CSSM.

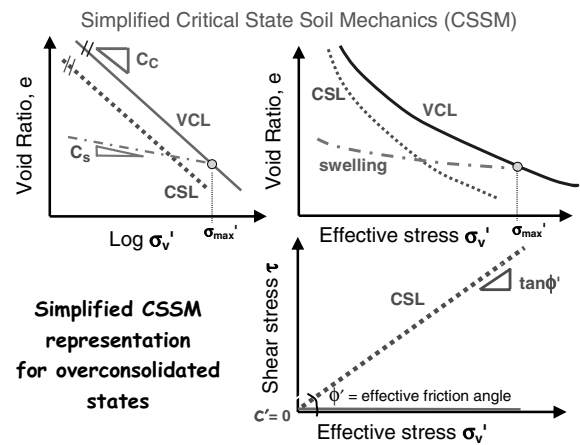


Figure 1.29. State spaces for OC soil using simplified CSSM.

The first step is to define an initial state for the geomaterial, specifically: initial void ratio (e_0), initial effective vertical stress (σ'_{v0}), and degree of preconsolidation (NC or OCR). If the soil is NC at OCR = 1, the soil state lies at some point on the VCL. If the soil is overconsolidated, the initial state would lie along a swelling line, as indicated by Fig. 1.29.

In the second step, a type of stress path or shearing condition is imposed, the two most common cases being: (a) *undrained loading*, whereby no volume change is allowed; i.e., $\Delta V/V_0 = 0$, which also requires $\Delta e = 0$; or (b) *drained loading*, in which case no excess porewater pressures occur: $\Delta u = 0$. Using those rules, undrained stress paths can move only horizontally (either left or right) in the e - $\log \sigma'_v$ (and e - σ'_v) spaces. For drained cases, movement can only occur vertically in all three spaces.

The corresponding stress paths for 4 common cases are presented in Figure 1.30: (1) NC undrained; (2) OC undrained; (3) NC drained; and (4) OC drained. For the undrained tests, the induced excess porewater pressure is simply equal to the horizontal distance on the x-axis that corresponds to the difference between the initial and final vertical stresses, or $\Delta u = \sigma_{vo}' - \sigma_{vf}'$. For the NC undrained case (soft clay), this produces positive porewater pressures that reduce the effective stress state, while in contrast, for OC undrained (stiff clay), negative porewater pressures are obtained. For NC drained loading (loose sand), the void ratio decreases corresponding to a volumetric reduction (contractive behavior), whilst for the OC drained case (dense sand), a corresponding increase in void ratio and volumetric strain must occur (dilative response). Note that the volumetric strain could be defined as $\epsilon_{vol} = \Delta u / (1 + e_0)$. Additional observations show that the drained strength > undrained strength in NC soils, while for OC soils, the opposite occurs. Note also that within this framework, it is easy to devise intermediate stress paths that could correspond to those of partial drainage, strain rate effects, cyclic loading, and so forth.

Despite the evidence and arguments (e.g., Schofield 2005), a simple Mohr-Coulomb strength envelope can be adopted to represent the basic frictional characteristics of soil. In the general case: $\tau_{max} = c' + \sigma' \tan \phi'$ where the c' is best left equal to zero, for arguments discussed later. Thus, the strength of soil can be represented simply by a friction angle (ϕ'), although alternative stress paths to a drained condition may occur due to porewater pressure effects, imposed loadings in addition to shearing, partial drainage, and other effects.

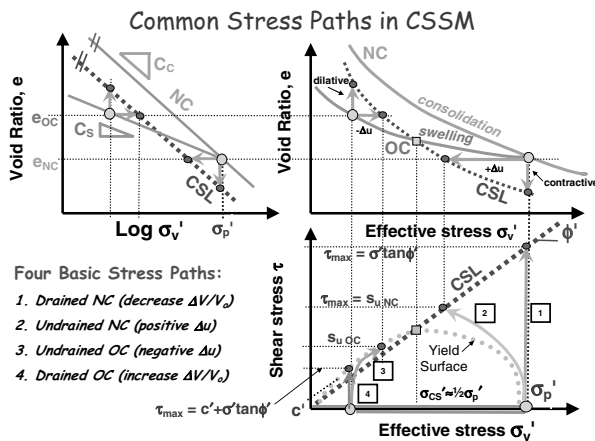


Figure 1.30. Four common stress paths (drained and undrained) for NC and OC soil within the simplified CSSM spaces.

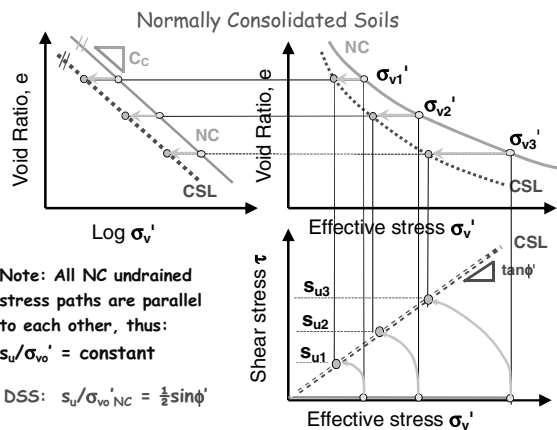


Figure 1.31. NC undrained paths for three specimens in CSSM spaces.

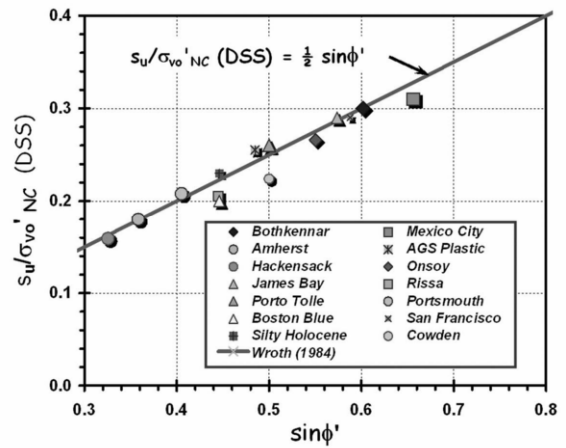


Figure 1.32. Undrained strength ratios from DSS tests on NC clays.

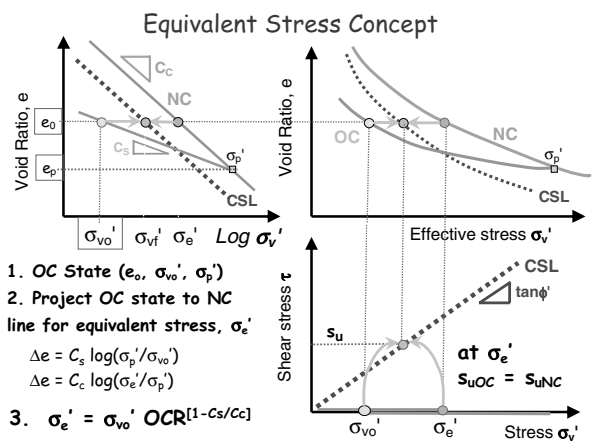


Figure 1.33. Equivalent stress concept in CSSM spaces.

In summary, the basics of CSSM lie in the definition of only three soil constants: effective friction angle (ϕ'), compression index (C_c), and swelling index (C_s). The initial state (e_0, σ_{vo}' , and OCR) must also be known.

1.9 Simple Shear Testing of Clays

For NC soils, Figure 1.31 shows that all curves emanating from the VCL along undrained stress paths are in fact parallel, thus confirming the well-recognized observance that the normalized undrained strength ratio $S = (s_u / \sigma_{vo}')_{NC}$ is a constant for a given clay (e.g. Ladd 1991). For the simple shear mode, Wroth (1984) suggested that:

$$DSS \text{ mode: } S = (s_u / \sigma_{vo}')_{NC} = \frac{1}{2} \sin \phi' \tag{1.2}$$

Therefore, for any initial point on the VCL, the undrained shear strength can be obtained by merely multiplying the S value times the effective overburden stress: $s_u = S \cdot \sigma_{vo}'$. The validity of (2) can be cross-checked with laboratory data now available from a variety of clays. For NC clays, the measured value of $S = (s_u / \sigma_{vo}')_{NC}$ is plotted vs. $\sin \phi'$ in Figure 1.32 with good agreement evident.

The strength evaluation can be extended to OC soils by use of the equivalent stress concept. Figure 1.33 shows that for every OC state, there is an associated equivalent NC state to essentially obtain the same value of s_u . If we project the OC state back along the swelling/recompression line to the preconsolidation stress, and then backwards along the VCL line

to this point, we have reached an equivalent effective stress on the NC side.

As shown in Figure 1.33, the equivalent effective overburden stress (σ'_e) on the NC line is given as a function of the actual OC overburden stress (σ_{vo}'), OCR, C_s , and C_c . Combining with (2) provides an evaluation of undrained shear strength for overconsolidated soils:

$$DSS \text{ mode: } S = (s_u/\sigma_{vo}')_{OC} = \frac{1}{2} \sin\phi' OCR^\Lambda \quad (1.3)$$

where $\Lambda = 1 - C_s/C_c$. The parameter Λ has been observed to lie within a relatively narrow range of 0.8 ± 0.1 for low-medium sensitive clays up to around 0.9 ± 0.1 for sensitive and structured soils (Kulhawy & Mayne 1990).

For OC clays tested under DSS conditions, Figure 1.34 shows that (3) provides a very reasonable evaluation of the normalized undrained shear strength. While the importance of ϕ' is clear, the much larger effect of OCR must be realized as impacting this relationship. This is supported also by the empirical approach developed over four decades of testing by the MIT group that concluded a good estimate on the DSS strength is afforded for homogeneous lean to plastic sedimentary clays of low to moderate sensitivity (Ladd & DeGroot 2003):

$$DSS \text{ mode: } S = (s_u/\sigma_{vo}')_{OC} = 0.22 OCR^{0.80} \quad (1.4)$$

Note that (4) is in fact a subset of the CSSM expression (3) in the case of $\phi' = 28^\circ$. For sensitive marine clays, varved clays, silts, and organic soils, the above coefficients can be slightly adjusted (e.g., Ladd 1991). Notably, for fissured geomaterials, the undrained strengths can be reduced by one-half or more, depending upon the extent, closeness, and frequency of the discontinuities, as indicated in by the dashed line in Figure 1.34 for London clay at Brent Cross.

Additional corroboration to (3) is found in the backanalyses of failure case studies involving vane shear tests in soft intact clays and associated correction factors where Mesri (1975) showed:

$$\text{Mobilized strength: } s_{uMOB} = 0.22 \sigma_p' \quad (1.5)$$

For the NC case where $OCR = 1$, the preconsolidation stress equals the effective vertical overburden stress, so that (5) is a subset of both (4) and (3).

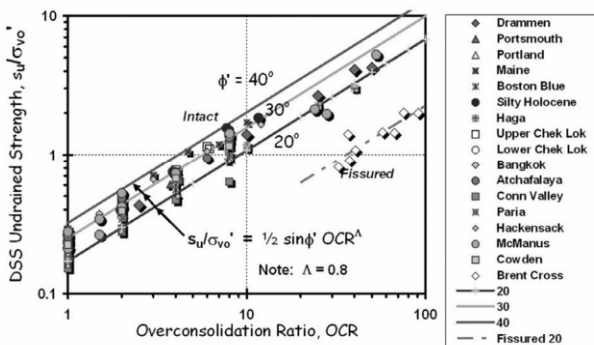


Figure 1.34. Undrained strength ratios from DSS tests on OC clays.

1.10 Yield Surfaces

For a full family of specimens with a common preconsolidation stress, where each are consolidated to initially different OCRs, the suite of undrained stress paths forms a yield surface, as shown in Figure 1.35. This clearly shows that soils tend towards an optimal packing arrangement (i.e., critical state). The yield

surface is curved and envelopes the overconsolidated states. The top of the yield surface crosses the frictional strength at a key stress point, about half the magnitude of the preconsolidation stress. For stresses above this top value, the yield surface lies beneath the frictional strength, while at stresses below this value, the yield envelope extends above the frictional envelope. In essence, the effective yield surface is a multi-dimensional parameter.

Whereas the conventional σ_p' is derived as the yield stress in one-dimensional consolidation testing, the yield surface is a 4-dimensional preconsolidation that reflects changes in the effective principal stress directions (σ_1' , σ_2' , σ_3') that can vary with time (t) and strain rate (dε/dt). As such, generalized stress paths that can consider compression, shearing, and extension, as well as increases in normal octahedral stresses and directions of loading should be more rigorously plotted in terms of Cambridge q-p' space, where the deviator stress $q = (\sigma_1' - \sigma_3')$ and $p' = (\sigma_1' + \sigma_2' + \sigma_3')/3$, as presented in Figure 1.36. In this space (e.g., Wood 1990), a conventional drained triaxial compression test rises at a slope of 3(V):1(H) towards the frictional strength envelope that is now represented by the parameter $M_c = (6 \cdot \sin\phi')/(3 - \sin\phi')$. Undrained stress paths behave similarly as before, with NC curving left from initial conditions and OC curving right. Figure 1.36 also shows an expression for the undrained strength ratio (S) corresponding to isotropically-consolidated triaxial compression tests (CIUC). As mode of shear and direction of loading are important, the CIUC value of S is higher than that for DSS given by (3).

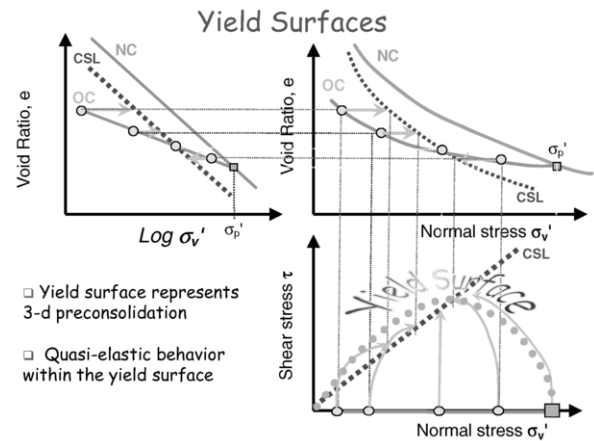


Figure 1.35. Family of undrained stress paths forming a yield surface.

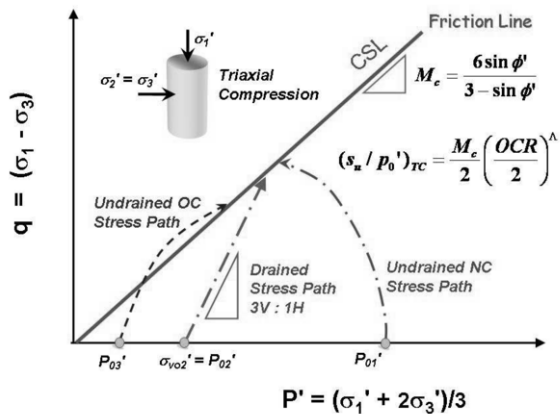


Figure 1.36. Stress path principles extended to 3-d invariant q-p' space.

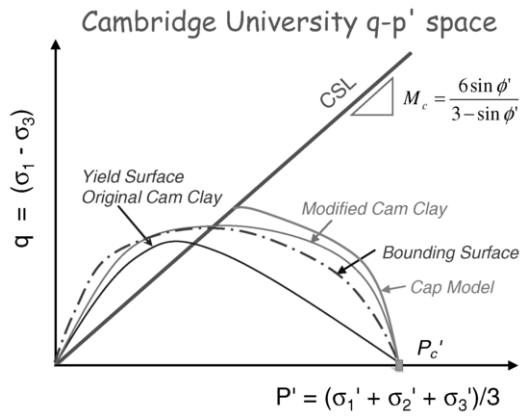


Figure 1.37. Yield surfaces for various constitutive soil models.

The CSSM principles can be formulated in terms of work-energy relationships to express stress paths and stress-strain curves in mathematical terms called constitutive soil models. One key distinction of these models is the derived (e.g., Original Cam Clay) or adopted yield surface (e.g., Modified Cam Clay). A few examples are shown in Figure 1.37.

As the mathematical versions of CSSM evolve and the models grow more complex in their ability to handle various nuances and aspects of soil behaviour, some formulations have added additional inner yield surfaces or nested zones that separate true elastic response (i.e., G_{max}) from pseudo-elastic and elastic-plastic regions. The yield surfaces depicted in Figure 1.38 have been rotated up and centered along the K_0 consolidation line to capture anisotropy associated with the strength and stiffness features that are inherent in geomaterials.

Experimental data have also been collected on a variety of geomaterials to delineate the true shape of these yield surfaces. Using special series of stress paths with constant Δq and $\Delta p'$ maintained during compression and extension loading have been used to identify yielding loci that may be combined to show the yield surface shapes. In a summary study by Diaz-Rodriguez et al. (1992), the yield surfaces of 50 natural clays appear to be similar to a rotated oval as per Figure 1.38. The general shape is depicted in MIT t - s space, as presented in Figure 1.39, where $t' = \frac{1}{2}(\sigma_1' - \sigma_3')$ and $s' = \frac{1}{2}(\sigma_1' + \sigma_3')$.

As the yield surface is curved, herein lies the difficulty in the force fitting of a linear equation (e.g., $y = mx+b$) which is commonly adopted for the Mohr-Coulomb strength criteria: $\tau_{max} = \sigma' \cdot \tan \phi' + c'$. The values of the forced slope ($m = \tan \phi'$) and forced intercept ($b = c'$) will depend upon which particular stresses and/or range of stresses are chosen for the fitting. In most commercial labs, the convention is to run a series of three specimens at different confining stresses. No real basis or rationale exists of course for why only three points are used. In fact, three points is not sufficient. In careful studies using many data points (e.g., Singh et al. 1973), research has found that the envelope is truly curved and shear strength tends to zero as the normal stresses tend toward the origin. As a consequence, the choice of Mohr-Coulomb parameters is rather subjective and an infinite number of paired c' - ϕ' strength parameters can be assigned in the unfortunate consequences of neglecting CSSM in the consideration of laboratory data.

The application of CSSM concepts to sands were initially quite challenging because of the following: (1) difficulties related to undisturbed sampling, (2) recognition of the initial state and possible multi-VCL at different relative densities; and (3) flatness of the VCL slope and rebound (i.e., small values of C_c and C_s). These issues can be resolved in part by defining a state parameter (ψ_s) which is the void ratio difference between the initial void ratio and critical state line (CSL) at constant

value of mean effective stress (p'), as discussed by Jefferies & Been (2006):

$$\psi = e_i - e_{csl} \tag{1.6}$$

Figure 1.40 illustrates the state parameter in e - $\ln(p')$ space. Due to dilatancy effects, most sands show primarily negative ψ values and only very loose or unstable sands exhibit positive values of ψ (Jefferies 1993). In a similar approach, an adopted log-log relationship between e and p' has been successfully utilized (Pestana & Whittle 1999).

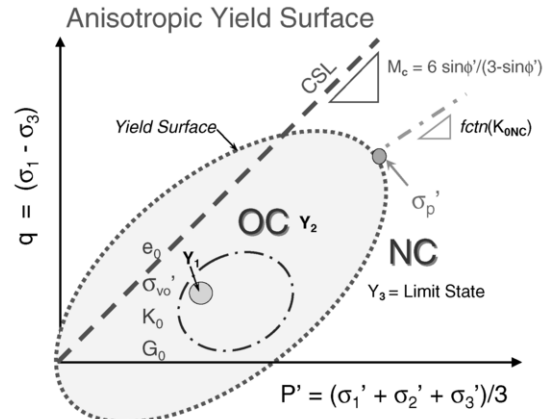


Figure 1.38. Anisotropic yield surface with zone Y1 for small-strain stiffness (after Jardine et al. 2005).

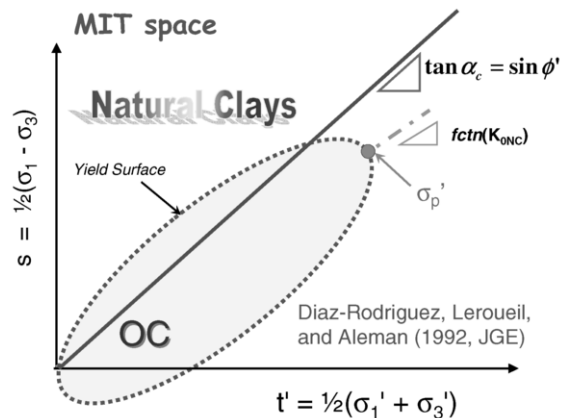


Figure 1.39. Observed anisotropic yield surface shape for various natural clays with rotated symmetry in the MIT s - t' space (after Diaz-Rodriguez et al. 1992).

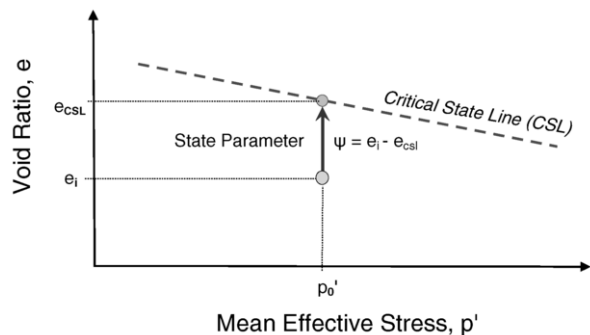


Figure 1.40. State parameter defined for sands in CSSM framework (after Jefferies & Been 2006).

2 SOIL BEHAVIOR

While much recent research on in-situ testing and physical and numerical modeling has revolved around the application and/or interpretation within Critical State Soil Mechanics, laboratory research on soil behavior has tended to concentrate on the limitations of the theory, since the basic concepts have long since been established. It might be argued that this is a slightly hazardous direction to follow, because Critical state Soil Mechanics is our only truly unifying framework, and its dismantling could lead to the anarchy of everybody's particular soil being unique, which would only be to the advantage of ambitious academics anxious to expand their list of publications on obscure soil behavior at the expense of a wider understanding amongst the geotechnical community. Inevitably, for materials with such diversity of origins and complexities of geological histories, we must expect simple frameworks to have faults and there to be exceptions, but we must also be on our guard against defective data, the limitations of our simple laboratory tests and interpretations of data that are sometimes almost willfully poor, leading to yet another chip in the cornerstone of our science; after all, it is far easier to publish a paper on some spurious unusual feature than it is to admit that after years of work and several PhDs that a particular soil has no especially interesting aspect of behavior.

The critical state framework was largely based on laboratory element tests on simple soils such as reconstituted clays and sands. The major developments of Critical State Soil Mechanics in the 1980s and 1990s were its more complete application to the mechanics of sands, including the effects of damage to the sand particle under loading (Been & Jefferies 1985; Coop & Lee 1993; Pestana & Whittle 1995; Lade & Yamamoto 1996; Verdugo & Ishihara 1996; McDowell & Bolton 1998), its use as the basic framework within which the behavior of natural clays and the influence of their structure could be understood (Burland 1990; Leroueil & Vaughan 1990; Cotecchia & Chandler 2000) and its application to the mechanics of partially saturated soils (e.g. Alonso et al. 1990; Wheeler & Sivakumar 1995).

For sands, the effects of the element of structure arising from inter-particle cementing has been extensively investigated, both for artificial cementing (e.g. Clough et al. 1981; Lade & Overton 1989; Reddy & Saxena 1993; Coop & Atkinson 1993; Huang & Airey 1998; Fernandez & Santamarina 2001; Rotta et al. 2003) and natural cementing (e.g. Airey 1993; Lagioia & Nova 1995; Zhang et al. 1998; Cuccovillo & Coop 1999; Coop & Willson 2003), and some progress has been made by interpreting such behavior within a critical state framework. Much less progress has been made on investigating the effects of the natural fabric of sands (e.g. Mimura 2003; Cresswell & Powrie 2004; Ventouras & Coop 2009) largely because of the difficulty of sampling an uncemented sand, but a rather greater research effort has been directed towards the effects of various fabrics created in reconstituted sands in the laboratory (e.g. Oda 1972a & b; Ladd 1974, 1977; Miura & Toki 1982; Tatsuoka et al. 1986; Zlatovic & Ishihara 1997; Jang & Frost 1998; Chu et al. 2003; Vaid & Sivathalayan 2007; Wood et al. 2008; Yang et al. 2008).

The limitations of critical state arising from strain localization were apparent from an early stage, and Roscoe himself invested considerable effort in devising apparatus, particularly the simple shear, which would ensure a more uniform strain distribution, allowing the true critical state to be evaluated more clearly. Much progress has been made in recent years in evaluating how and why strain localization occurs, particularly using powerful new imaging techniques such as False Relief Stereophotogrammetry, Digital Image Correlation or X-ray Computed Tomography or CT (Desrues et al. 1996; Viggiani & Desrues 2004; Rechenmacher 2005). Through the use of CT Desrues et al. (1996) found that within the dilatational

shear band formed in a sand sample, the soil did reach a unique critical state volume that, at any given stress state, was independent of the initial density of the sample (Fig. 2.1). This does, however, emphasize the impossibility of assessing critical state volumes of soil samples accurately where there is localization, when using our usual techniques of measuring the displacements at the boundaries of soil element tests.

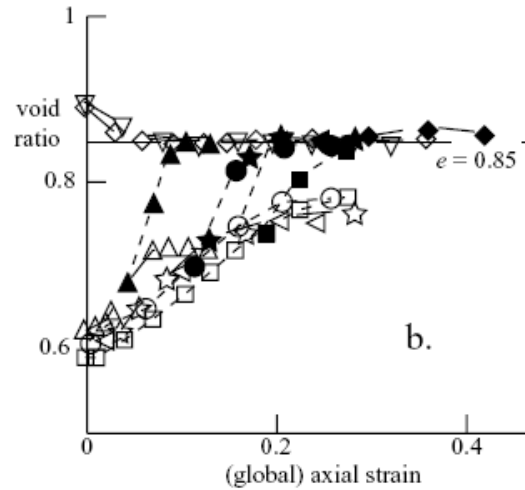


Figure 2.1. Variation of void ratio during triaxial tests on Hostun sand (global e: open symbols, local e: solid symbols).

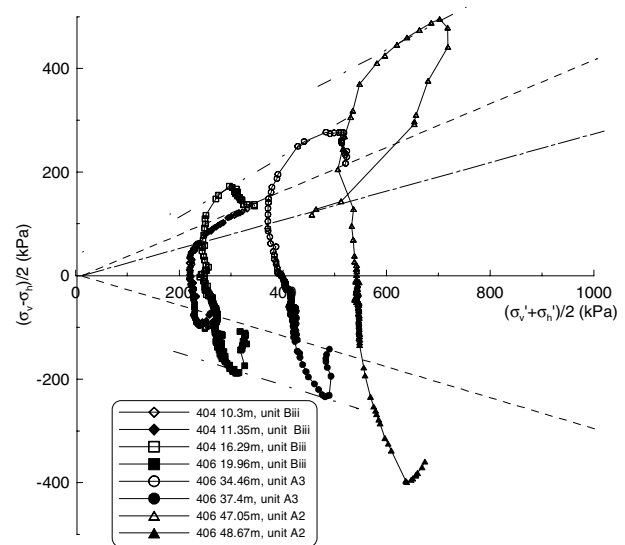


Figure 2.2. Undrained triaxial stress paths for rotary London clay: an example of the curtailment of undrained shear strength through strain localization (Hight et al. 2002).

The most severe restriction resulting from strain localization is perhaps on the undrained strength of stiff, overconsolidated clays. As illustrated in Figure 2.2, once the stress paths crosses the critical state line, strain localization within the sample causes the path to drop back rather than climb the Hvorslev surface towards the ideal critical state. This results in the undrained strength of the soil not being uniquely related to the void ratio, as suggested in Figure 1.27, but being also a function of the stress level. Continued displacement along the shear surface leads eventually to the residual strength being

developed (Lupini et al. 1981), but Burland (1990) and Georgiannou & Burland (2001) identified that immediately after rupture of triaxial samples a constant strength could often be identified that they referred to as "Post Rupture" strength, since it could not correctly be called a critical state as it was not a continuum failure. Because of the localization, they argued that the use of invariants (such as p' and q') was incorrect and that the strength being mobilized could only be assessed by using a Mohr's circle analysis of the stress state within the sample, to obtain the shear and normal stress on the shear plane from its measured inclination. Having done this for a number of tests at different stress levels, it was found that the Post-Rupture failure envelope was close to the critical state line (referred to as the intrinsic strength envelope), which was defined by a series of tests on normally consolidated reconstituted samples, for which there was no strain localization (Figure 2.3). Within the accuracy of an analysis in two-dimensions for a three dimensional stress state, and given the difficulty in defining accurately the current area of shear planes developed in triaxial samples, it might be argued that the Post-Rupture state on Figure 2.3 corresponds to a local critical state on the shear surface.

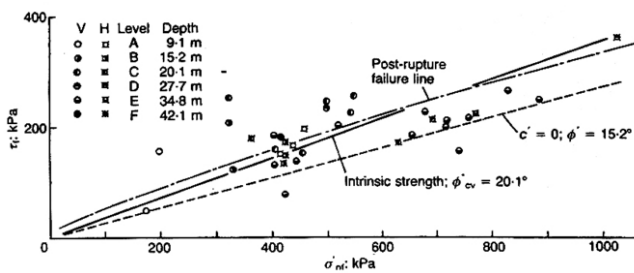


Figure 2.3. Post-Rupture and critical state (Intrinsic) failure envelopes for a stiff intact clay (Burland 1990).

Atkinson & Richardson (1987) showed that, for a reconstituted clay, the development of localized shearing during undrained loading was a function of local drainage into the developing plane, so that locally the constant volume condition was not maintained and the soil dilated, allowing it to reach a critical state at lower stress at point E rather than point F on Figure 2.4. The development of the shear plane could therefore be prevented by loading the sample rapidly enough to prevent internal drainage, and this, they observed, is one reason for strain rate effects on the undrained shear strength. The extent to which this argument may be applied to natural clays is unclear, since a component of their strain softening might result from the breakage of inter-particle cementing.

Although there is much current research on the causes and nature of strain localization, it is less clear how this new knowledge might be applied to predictive design. Strain localization cannot easily be described within a continuum mechanics framework such as Critical State Soil Mechanics nor by Finite Element constitutive models based on its precepts (e.g. Roscoe & Burland 1968; Stallebrass & Taylor 1997; Kavvas & Amorosi 2000; Rouainia & Muir Wood 2000; Li & Dafalias 2002).

Discontinuous models such as DEM (Distinct or Discrete Element Modeling) are much better adapted to capture the effects of strain localization (e.g. Thomas & Bray 1999; Wang et al. 2007), but as yet the modeling of the individual soil particles is so far from reality that the method can only be used with any degree of success to model relatively simple boundary value problems, such as laboratory element tests (e.g. Cui & O'Sullivan 2006; Liu 2006; Cui et al. 2007; Sitharam et al.

2008) or to investigate the fundamental mechanics and how they are related in particular to particle shape, soil fabric and particle damage (e.g. Thornton 2000; McDowell & Hareche 2002; Mirghasemi et al. 2002; Cheng et al. 2003, 2004; Noguier-Lehon et al. 2003; Ng 2004; Powrie et al. 2005; Lobo-Guerrero & Vallejo 2005). Any accurate reproduction of the behavior of a particular soil requires considerable calibration of the model against laboratory test data and direct modeling of engineering applications is, as yet, much less common (e.g. Maynar & Rodriguez 2005; Deluzarche & Cambou 2006).

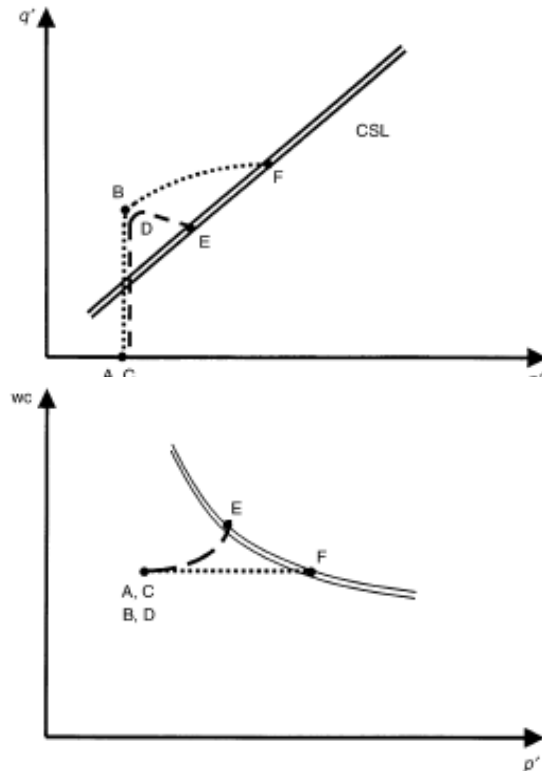


Figure 2.4. Schematic diagram illustrating the influence of internal drainage on the undrained shear strength of an overconsolidated clay (Atkinson & Richardson 1987; Atkinson 2000).

Perhaps one case where a continuum approach may still be used with some success is when the spacing of the planes of localization is so small, as for example for the naturally formed fissures in many clay shales (e.g. Picarelli et al. 2002; Fearon & Coop 2002) that the soil may be again considered as a continuum with the numerous planes of localization forming part of the fabric and the size of our laboratory tests are sufficiently large that the soil is a Representative Element Volume (REV).

Although strain localization is a severe limitation for CSSM, particularly for many natural soils for which inter-particle bonding emphasizes strain softening, such problems do not invalidate its basic usefulness as a unifying framework; the critical state may be regarded as an unreachable target and other aspects of pre-peak behavior may still be analyzed within the framework. However, as highlighted in the following sections, there are a number of areas of research that are challenging even more basic aspects of CSSM, notably work on the effects of the particulate nature of sands on their behavior, on the mechanics of intermediate and mixed grain size soils, for which fabric seems to play a particularly strong role, and the effects of rate of loading.

2.1 Particulate Behavior

As a continuum framework, CSSM cannot easily account for all aspects of soil behavior that arise from its particulate nature. There is an increasing amount of research examining the nature and properties of individual particles, both of a qualitative and quantitative nature, the latter mostly for sands for which the particles are large enough to make precise measurements of particle scale properties such as size, shape, strength, stiffness, roughness and inter-particle friction. However, rather than posing a specific threat to the critical state framework the aim of this work is largely either to examine the relationship between the properties of individual particles and the values of continuum based parameters within Critical State Soil Mechanics or is aimed at a better modeling of particles within a DEM approach. For example, as part of a wider debate about the causes of dilatancy of sands and its relationship to the applied stresses, Skinner (1969) showed how the critical state angle of shearing resistance, ϕ'_{cs} is independent of the inter-particle friction angle. This has been challenged more recently through DEM modeling (Thornton 2000) as shown in Figure 2.5. Using DEM, it is clearly much easier to vary the inter-particle friction while keeping all other particle characteristics constant than it is in physical tests.

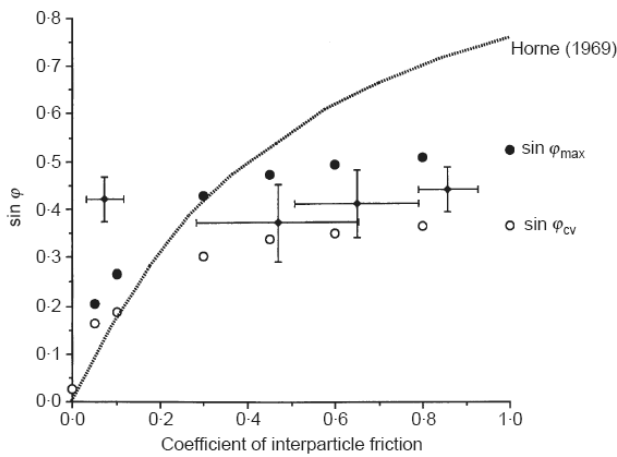


Figure 2.5. The influence of the coefficient of inter-particle friction on the critical state angle of shearing resistance (Thornton 2000).

It might be imagined that a greater threat to CSSM might come from those properties of particles that change under loading. Perhaps because it is the most easily quantified, changes to particle size have received rather more attention than changes to roughness or shape. Initially it was believed that the effects of particle breakage could be accounted for with very little modification to the critical state framework. Through high pressure triaxial testing Coop & Lee (1993) and Pestana & Whittle (1995) showed how a unique Normal Compression Line (NCL) could be identified at higher pressures to which samples of all initial densities would converge (Figure 2.6). As assumed by CSSM it was straight in the $e:\ln p'$ plane (although they used specific volume, v rather than e , where $v=1+e$). One-dimensional compression was found to give a NCL parallel to that defined by isotropic compression, with a lower location in the $e:\ln p'$ plane, as also expected from a critical state framework.

Shearing to as large strains as the triaxial apparatus permitted defined a critical state line (CSL) that was again parallel to the NCL at these higher pressures, as again assumed in the model, although the work of others (e.g. Verdugo & Ishihara 1996; Been & Jefferies 1985; Konrad 1998) emphasized that at lower pressures the CSL is shallower in the

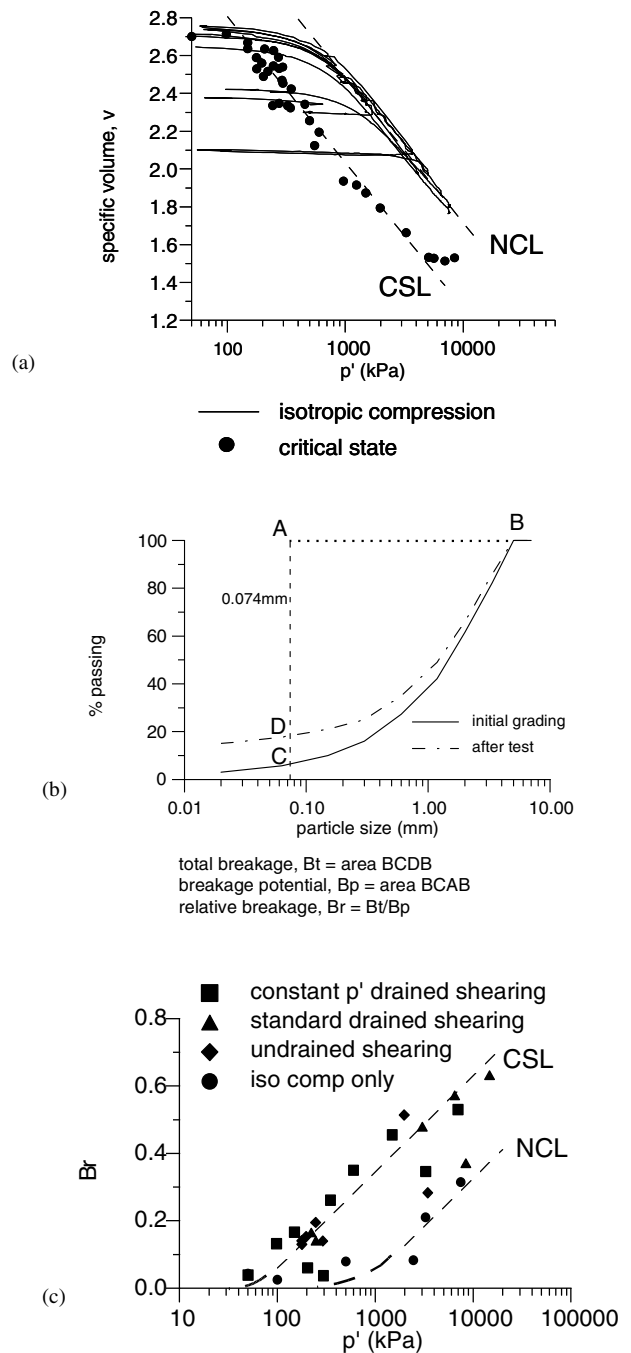


Figure 2.6. Compression and shearing behavior of Dog's Bay carbonate sand (Coop 1990) (a) isotropic compression and critical states (b) definition of Relative Breakage (Hardin 1985) (c) B_r measurements for Dog's Bay sand (Coop & Lee 1993).

$e:\ln p'$ plane (Figure 2.7), leading the CSL to be modeled as bi-linear (e.g. Konrad 1998) or curved with a horizontal asymptote (e.g. Verdugo & Ishihara 1996). It has been assumed in the hypoplasticity constitutive model of Gudehus (1996) that the horizontal asymptote corresponds to the e_{max} of the soil. It might indeed be argued that on a semi-logarithmic graph there is necessarily a horizontal asymptote, otherwise the void ratio would be infinite on the CSL at zero stress. One of the key differences between sands and clays is therefore that the curvature of the CSL occurs within the range of engineering stresses, whereas for clays it occurs at such large values of void ratio and such low stresses that it is usually of no relevance. Sands will also not generally reach their NCL, when they are

compressed from a typical depositional density until they are again beyond the usual range of stresses. This led Coop & Lee (1993), Been & Jefferies (1985) and others to emphasize the importance of depositional density in sands. Whereas in clays the density at deposition is generally of little importance to the current stress and volume state, for sands it is of key importance, since the initial density would only be “forgotten” if the sand ever reached its NCL,

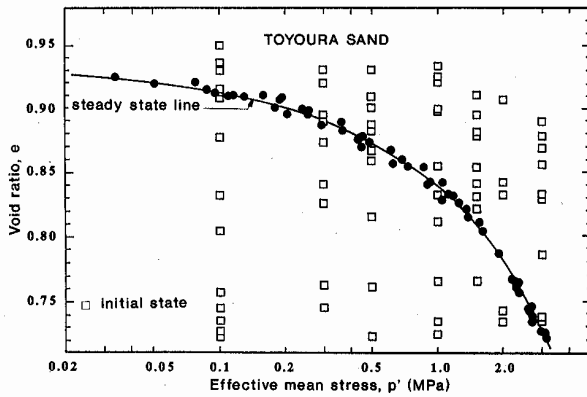


Figure 2.7. An example of the curvature of the critical state line at lower stress levels (Verdugo & Ishihara 1996).

Coop & Lee (1993) found that the gradual yield as the initial compression paths reached the NCL corresponded to the onset of the major part of particle breakage, which they quantified with Hardin's Relative Breakage, B_r , defined in Figure 2.6(b), although their breakage data were of relatively poor quality and fairly scattered, being calculated using manual grading measurements from sieving. Kwag et al. (1999) correlated the yield in compression with the strength of individual particles. Similarly, the onset of breakage on the CSL seemed to correspond to the point of its curvature in the $e:\ln p'$ plane, leading to the general assumption that the flatter part of the CSL at lower stress levels is that part for which particle breakage is not dominant. At higher stress levels, where there was significant breakage, each stress level on the NCL and CSL seemed also to correspond to a unique amount of breakage, regardless of the stress path followed. Examining the role of breakage during compression in greater detail, McDowell & Bolton (1998) highlighted that, as a sand is compressed down its NCL, a fractal grading evolves as the grading curves of an initially poorly graded soil tends to rotate around its top end (Figure 2.8), indicating that coarser particles tend to survive. When plotted with a logarithmic percentage passing axis, the fractal grading is a straight line. This they attributed to the fact that although larger particles tend to be more prone to breakage because of a greater likelihood that they might contain defects within them, larger particles tend also to have higher coordination numbers (i.e. the number of particle contacts per particle). The larger particles therefore tend to be surrounded by a number of smaller particles supporting them, while smaller particles can often be trapped in between two larger particles, making them more prone to breakage. The use of sieving to assess particle damage is relatively crude, as it does not distinguish changes of shape arising from different forms of damage. Bolton et al. (2008) have used their DEM model of breakable particles to examine how the different types of breakage (asperity breakage, internal shear and tensile cracking) related to different loading conditions.

Initially, the work on the effects of particle breakage tended to concentrate on soils with weaker particles such as carbonate (calcareous) sands. During the 1980s and 90s, interest in these soils was provoked by the difficulties encountered with a

number of piled foundations for offshore structures, such as the Rankin platform (King & Lodge 1988). However, it was soon realized that their susceptibility to breakage arose not only from delicate particles but also from their very high void ratios and so low coordination numbers and high contact stresses, which were a result of the particle shape rather than strength (Coop 2003). Nevertheless, the basic mechanics of carbonate sands and those of other mineralogies, such as quartz, was essentially similar, the only real differences being that the denser quartz sands, with stronger particles tended to reach their NCL and the steeper part of their CSL at much higher stresses that were less likely to be a problem for practical applications.

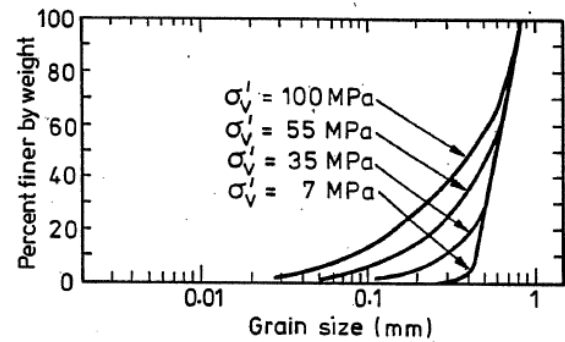


Figure 2.8. Evolution of grading during one-dimensional compression of Ottawa sand (Fukumoto 1992).

The influence of breakage was therefore incorporated within Critical State Soil Mechanics, with only minor modification to the framework. Apart from the influence of depositional density, the other important differences for sands that arose from the particle breakage were: (1) Rendulic's principle was not obeyed, and in general undrained tests were not found to identify the State Boundary Surface on either wet or dry sides of critical (e.g. Coop 2003); (2) the spacings between CSL and the NCL are rather greater than for clays; and (3) the CSL is not at the apex of the State Boundary Surface, and so normality cannot apply. Chandler (1985) proposed a model for materials with deformable grains that assumed non-associated flow, which was adopted by Baharom & Stallebrass (1998) for use with sands for which the particles break rather than deform. Perhaps surprisingly, particle breakage, and the consequent change in grading, was not found to affect significantly the value of ϕ'_{cs} , which was typically found to remain constant with increasing breakage at higher stress levels (e.g. Coop & Lee 1993).

This type of critical state model of behavior was then extended to analyze the behavior of various in-situ tests, such as the CPT (Been et al. 1986, 1987; Konrad 1998), pressuremeters (e.g. Yu et al. 1996), driven pile behavior (Klotz & Coop 2001; Coop et al. 2005), relating the behavior observed to the State Parameter, i.e. the distance of the current state from the CSL in the $e:\ln p'$ plane, either defined in terms of volumes (Bassett & Wroth 1965; Been & Jefferies 1985), or in terms of stresses (Coop & Klotz 2001).

A defect in this simple critical state type of model for sands was highlighted by Cheng et al. (2005), who modeled the particle breakage of sands in DEM by using “blackberries” or agglomerates of spherical particles that could break under load, with which they were able to reproduce the pattern of change of gradings curve seen in Figure 2.8. They found that samples that were taken to a NCL, and subsequently unloaded, had a substantially different critical state in the $e:\ln p'$ plane to those that had never reached the NCL, and so had not undergone significant breakage prior to shearing (Figure 2.9). Muir Wood

(2008) has modeled this in a modified version of the ‘‘Severn-Trent’’ constitutive model (Gajo & Muir Wood 1999) by assuming that as the stress level increases and particle breakage progresses, the soil is actually traversing an infinite number of CSLs, each appropriate for the current grading (Figure 2.10). The single CSL apparently seen experimentally in Figure 2.6 was only the locus of end points of current CSLs for the changing grading as breakage moved the soil from one CSL to the next. Muir Wood (2008) introduced a Grading State Index, I_g , to quantify the current grading relative to an assumed limiting grading.

Einav (2007a, b) has defined a very similar method of quantifying breakage to Muir Wood (2008), in which the current grading is again related to the ultimate grading but the initial reference is the initial gradings curve rather than d_{max} . By analogy with fracture mechanics, he then used this as the basis for a Continuum Breakage Model that accounted for energy dissipation from particle breakage as well as frictional rearrangement, which he showed should be coupled. This model was able to reproduce the isotropic hardening with a unique Normal Compression Line typical of sands through breakage alone and without plastic straining with frictional dissipation.

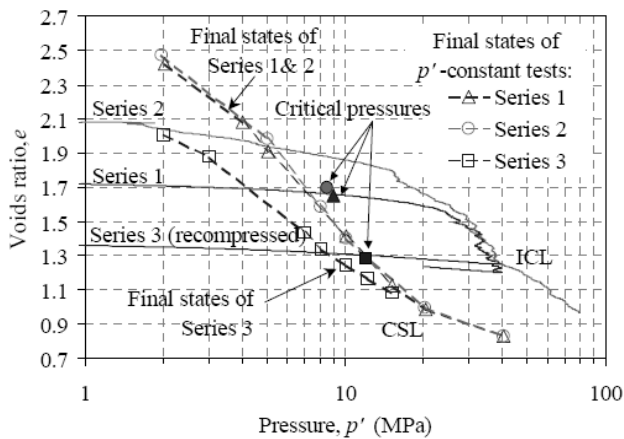


Figure 2.9. DEM analysis of the effect of particle breakage through overconsolidation on apparent critical states (Cheng et al. 2005).

The assumption of an ultimate grading was based on some experimental evidence, firstly that McDowell & Bolton (1998) had observed a limiting grading in compression with a fractal dimension of about 2.5. Coop et al. (2004) had also reached a limiting breakage and grading in ring shear tests on Dog’s Bay sand at very large strains (Figure 2.11). At the higher stress levels used, the final grading was fractal, although the fractal dimension was slightly higher at 2.57. Testing a very well graded glacial till, Altuhafi et al. (2006) had found a grading of a non-plastic glacial till that was not susceptible to further breakage, no matter what loading was applied, which was taken as further evidence of a limiting grading. Again the grading of this soil was fractal. A central assumption of these models is that the soil ‘‘knows’’ what is its current grading, i.e. that the behavior of the soil that has undergone some breakage would be the same as that of the same soil that had been reconstituted at the new grading. This might be expected to be the case if the critical state is independent of the initial fabric, but is an assumption that needs to be checked experimentally. The model of Muir Wood (2008) also assumes that the value of ϕ'_{cs} is not affected by the particle breakage during shearing. It had already been established that compression to high confining pressures did not affect the value of ϕ'_{cs} during subsequent shearing, and the ring shear tests of Coop et al. (2004) now showed that

continued breakage during shearing also had no measurable effect on ϕ'_{cs} .

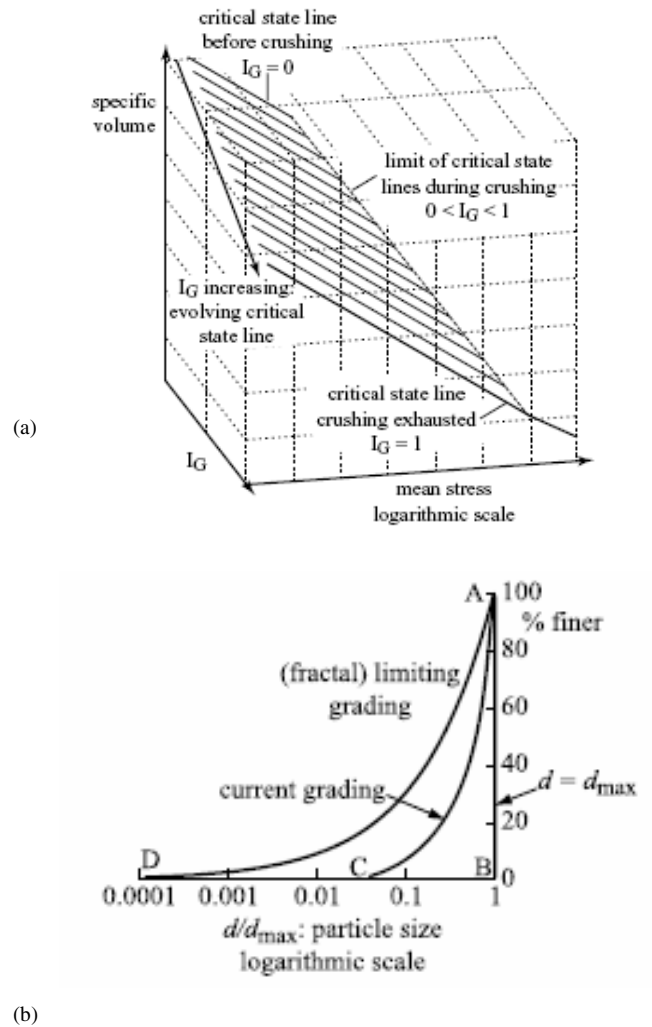


Figure 2.10. (a) Suggested evolution of critical state Line with particle breakage (b) definition of grading state index $I_g = \text{area ABC}/\text{area ABD}$ (Muir Wood 2008).

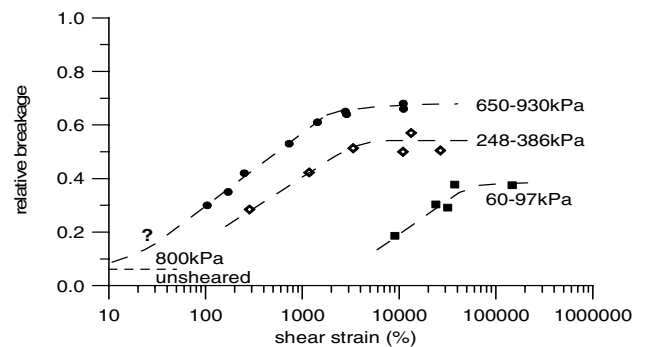


Figure 2.11. Development of relative breakage for Dog’s Bay sand in ring shear tests (modified from Coop et al. 2004).

Examining the ring shear data in greater detail (Fig. 2.11), it can be seen that although there was a unique grading at the higher stress levels used by Coop et al. (2004), which was fractal, the final gradings at other stress levels were

significantly different and they were not fractal. The basis for the existence of a single limiting grading may therefore not be secure. The final grading was also found to change with the initial grading, which was the reason why Einav (2007a) used the initial grading as his reference rather than d_{max} . Finally, there was no evidence that a state could be reached at which the I_g value would stabilize at a value less than unity during shearing as continued shearing resulting in continued breakage until the final grading was reached, and the compressive volumetric strain only ceased when the breakage stopped.

As Muir Wood (2008) identified, it would be convenient for modeling that the breakage should be linked either to the stress state or the work done. At smaller strains, Miura & Yamanouchi (1977) and Miura & O-Hara (1979) successfully correlated the amount of particle breakage with energy input. Neither is actually the case since the stresses remain constant while this breakage continues and the soil eventually reaches a state at which breakage stops, even if work continues to be done in shearing. It therefore appears that the central assumption of Chandler's (1985) model was correct; a critical state that is reached at modest strains in a triaxial apparatus represents only a transient balance between volumetric compression resulting from particle breakage (or particle deformation in his model) and dilation resulting from particle rearrangement.

2.2 The Influence of Fabric on the Behavior of Soils

For clays, there is evidence that the intrinsic fabric is often relatively robust. Through an examination of Scanning Electron Micrographs, Cotecchia & Chandler (1998) found that although the fabric of their stiff natural clay changed as it yielded, the fabric remained very different to that of the same soil in a reconstituted state up to very high stresses. The oedometric compression path of the natural soil therefore never fully converged with that of the reconstituted soil. Similar evidence for a robust component of structure that could not be removed by compression was given by DeGroot & Lutenecker (2003), Masin et al. (2003) and Coop et al. (1995). Other authors (e.g. Rampello & Silvestri 1993; Coop & Cotecchia 1995) have postulated that not only are the compression paths of their clays offset from the NCL of the reconstituted soil, but the CSLs were too, which may be again attributed to the effects of a natural fabric surviving even shearing to a critical state. This led Baudet & Stallebrass (2004), in their critical state based constitutive model for natural clays, to assume that while the component of structure arising from inter-particle bonding could be broken down at modest strains, structure arising from fabric was much more robust and so there were components (of structure) that could survive both compression and shearing (Figure 2.12).

In other constitutive models for natural clays (e.g. Kavvas & Amorosi 2000; Rouainia & Muir Wood 2000), a similar effect can be achieved by having a slow rate of destructuration, different rates of destructuration being assumed for compression and shearing. More extreme forms of fabric, such as aggregation of particles, were even found to survive reconstitution by traditional means (e.g. Fearon & Coop 2002) so that different intrinsic properties could be created by reconstituting with different energies. For such soils, the effects of structure could not easily be determined by a comparison between the behavior of the natural soil with that of the same soil in a reconstituted state, as there was no means of knowing which reconstituted state was appropriate.

The debate about the robustness of fabric has been reopened for sands in recent years as highlighted by Muir Wood (2008). In sands, fabric might be quantified by the orientation of the particles (provided they are non-spherical), the void spaces or the contacts between particles (Oda & Iwashita 1999; Chen et al. 1988).

There is considerable evidence that different fabrics created by different sample preparation methods affect the small to intermediate strain region, so for example Jefferies & Been

(2006) and Chu et al. (2003) have found that moist tamped samples are stiffer at small strains than those prepared by water pluviation methods. However, there is also evidence (Vaid & Sivathayan 2007; Chu et al. 2003; Chen & Chuang 2001; Riemer & Seed 1997) that even the critical state in the $e:ln p'$ plane is affected, which is of key importance since sand behavior is related to the location of the CSL through state parameters. Again the evidence is not in consensus and agreement, and Jefferies & Been (2006) found no significant difference in the critical states of their samples. Following similar techniques to Kuo & Frost (1996) and Jang et al. (1999), Yang et al. (2008) cut coupons from resin impregnated samples of Toyoura sand from which Scanning Electron Microscope images were taken that were reduced to a binary image for analysis. The rosette of particle orientations in Figure 2.13 indicates a significantly different anisotropy in dry deposited and moist tamped samples.

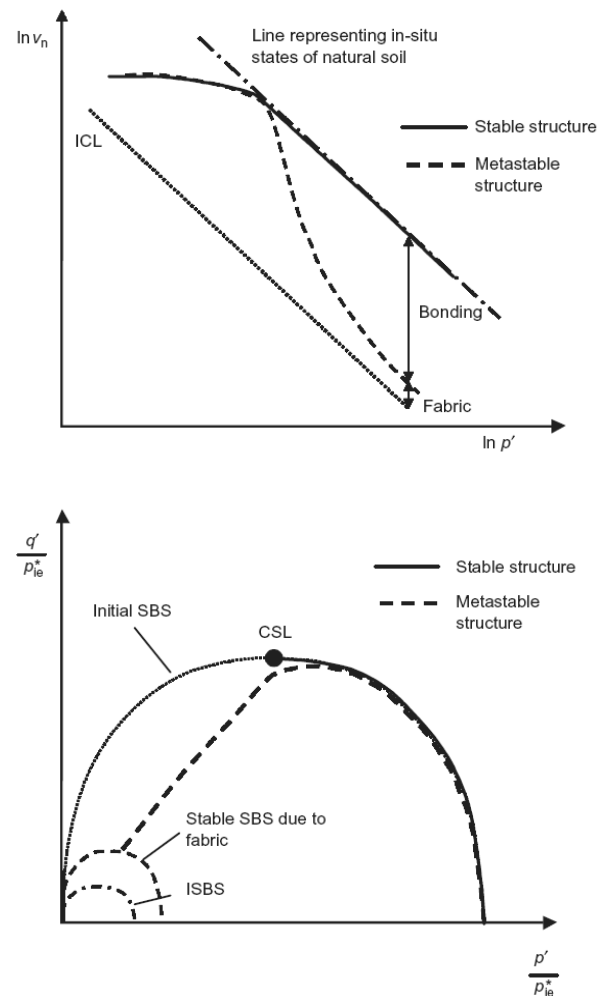


Figure 2.12. A constitutive model for clays assuming stable and unstable elements of structure (Baudet & Stallebrass 2004) (v_n is a specific volume normalized for the nature of the soil, p_{ic}^* is an equivalent pressure on the intrinsic isotropic normal compression line, SBS State Boundary Surface).

The stress paths for the undrained extension tests in Figure 2.14 appear to confirm that tests are tending towards different CSL locations in the $e:ln p'$ plane, since the final values of p' on the stress paths are significantly different. In contrast, undrained triaxial compression tests showed that the stress path was affected by the method of preparation but not the critical states.

The predictions shown on the figures were made using a constitutive model developed by the authors from that of Li & Dafalias (2002), which includes the effects of fabric anisotropy. Here the model was extended to allow for different CSLs in the $e:lnp'$ plane for different loading paths and different fabrics. Following Li & Dafalias (2000), the dilatancy was related to the state parameter. Papadimitiou & Bouckovalas (2002) have also developed a bounding surface plasticity model, based on the model of Manzari & Dafalias (1997) that incorporates the effects of fabric evolution during cyclic loading.

Rather less experimental data are available for the effects of fabric in natural or intact uncemented sands, largely because of the difficulty of sampling. Through comparisons of intact and reconstituted samples, significant effects of fabric have been observed by Mimura (2003), Yoshimi et al. (1989) and Ventouras & Coop (2009), generally at small to intermediate strains in quartzitic sands. For the rather extreme case of a locked fabric (Dusseault & Morgenstern 1979) in which pressure solution has created flattened particle contacts, Cresswell & Powrie (2004) found much more dramatic effects of fabric, with not only very different small strain stiffnesses for the natural and reconstituted soil, but also very much higher rates of dilation resulting in much higher peak strengths (Figure 2.15). The higher rates of dilation and peak strengths could not be attributed solely to differences of initial density, and it was clear that even at the same density, the behavior would be very significantly different as a result of the fabric.

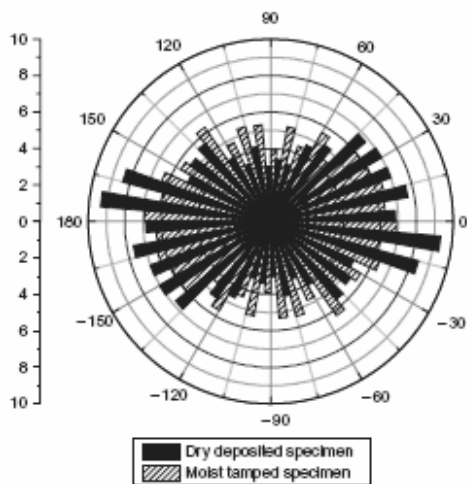


Figure 2.13. Particle orientations for vertical section through Toyoura sand samples (Yang et al. 2008).

With reference to the critical state framework for sands of Figure 2.6, it is perhaps unlikely that the soil would have forgotten its initial fabric as a result of compression before the NCL was reached, since the current volume is so directly linked to that at deposition, but it might be hoped that shearing to a critical state would erase the initial fabric, so that it represented not only a state of constant volume and stress state, but also of constant fabric. Through DEM analyses, Muir Wood (2008) showed that at least the coordination number would reach a constant value at the critical state, and while the value of the final coordination number increased with stress level, it was independent of the initial density. Again using DEM, but with particles of elongated shape so that an initial fabric could be created, Nougier-Lehon et al. (2005) found that a unique critical state would eventually be reached at which the volume and stress state would be constant as well as the fabric (Figure 2.16). The example given is for the largest aspect ratio of 3 that was considered by the authors. Three loading cases were also

analyzed, with different angles α of the major principal stress to the fabric. The deviatoric fabric in this case represents the directions of contact normals rather than particle orientations, which are defined for the simpler case of circular disks in Figure 2.17.

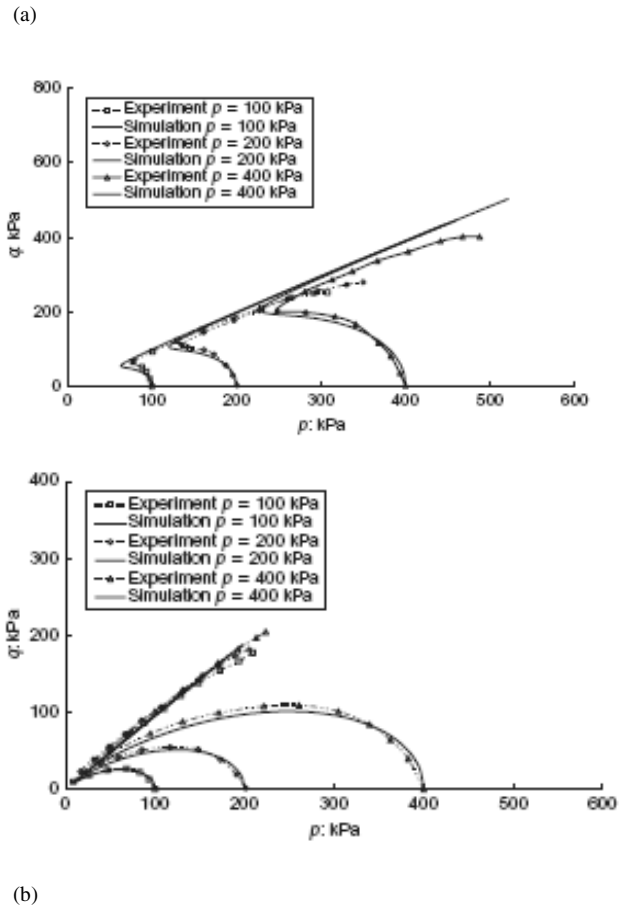


Figure 2.14 Comparison of undrained triaxial extension tests on (a) moist tamped and (b) dry deposited samples of sand (Yang et al. 2008).

Even for the simple case of triaxial compression of a sample with an initially horizontally orientated fabric ($\alpha=0$), strains of over 20% were required to reach a final stress ratio, void ratio and fabric. For the more extreme case of a passive compression test in which the contact normals need to realign from an initial vertical direction to the new horizontal direction of the major principal stress, strains of up to 100% still did not quite produce a final fabric, although a state of almost constant stress was reached far more quickly. Zlatovic & Ishihara (1997) postulated that the effective angle of friction is independent of the fabric because the initial fabric is erased at the critical state. The analyses of Nougier-Lehon et al. (2005) confirm this, but reveal that much larger strains than are common in most laboratory tests are required to reach that state.

The lag between the orientation of the fabric and the applied major principal stress that is seen in the DEM simulations of Nougier-Lehon et al. (2005) means that when complex stress paths are followed in which there is a change in principal stress direction acting on an anisotropic soil, non-coaxiality may occur, in which the directions of the principal stresses do not coincide with those of the plastic strain increments, as has been highlighted by Yu (2008). Non-coaxiality cannot exist in an isotropic soil and is most significant at smaller strains, being erased as the soil is loaded in a particular direction towards critical state. It has been demonstrated experimentally by

measuring the applied stresses and resulting boundary strains in various element tests (e.g. Roscoe 1970; Arthur et al. 1986) but is not accounted for in most constitutive models.

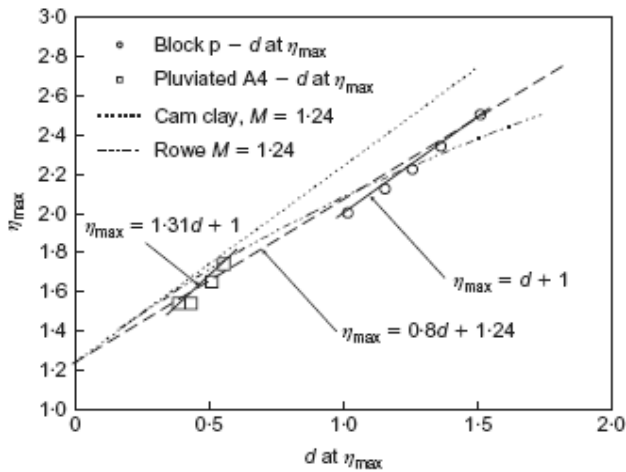


Figure 2.15 Comparison between behavior of intact (block) and reconstituted (pluviated) samples of a locked sand (Cresswell & Powrie 2004) ($\eta=q/p'$, d rate of dilation).

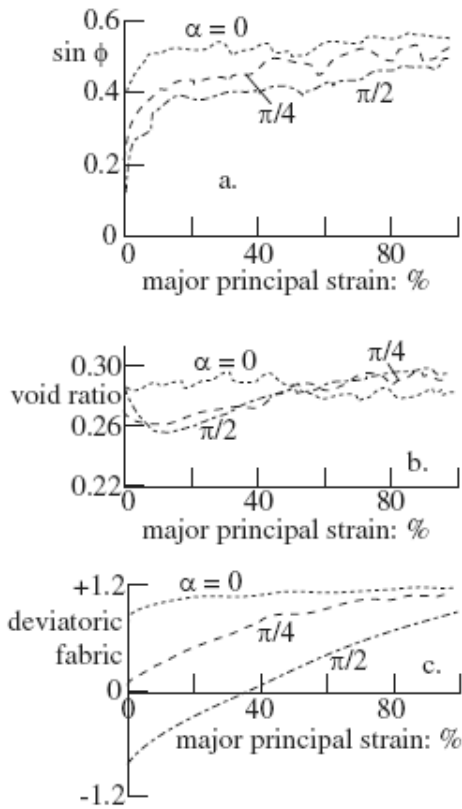


Figure 2.16. DEM analysis of stress-strain behavior for shearing of angular particles (Nougier-Lehon et al. 2005, modified by Muir Wood 2008).

There have been a number of attempts to model non-coaxiality in DEM analyses, and Figure 2.18 shows data from a two dimensional analysis of Yu (2008), in which the direction of the major principal stress was rotated while the stress ratio and mean normal stress were held constant. There is a significant

lag between θ_σ , the direction of the major principal stress and θ_ϵ , the direction of the major principal strain increment. Figure 2.19 shows the directions of contact normals at two angles of rotation. The stress induced anisotropy of the fabric that is necessary for non-coaxiality is evident, but there is also a slight lag in the contact normal direction compared to the principal stress. Although the causes of non-coaxiality may be again illustrated and better understood through DEM, Yu (2008) has used this to define a continuum constitutive model that allows non-coaxiality which accounts for fabric and its evolution during loading.

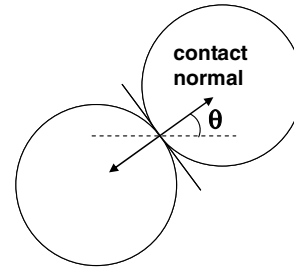


Figure 2.17. Definition of contact normal.

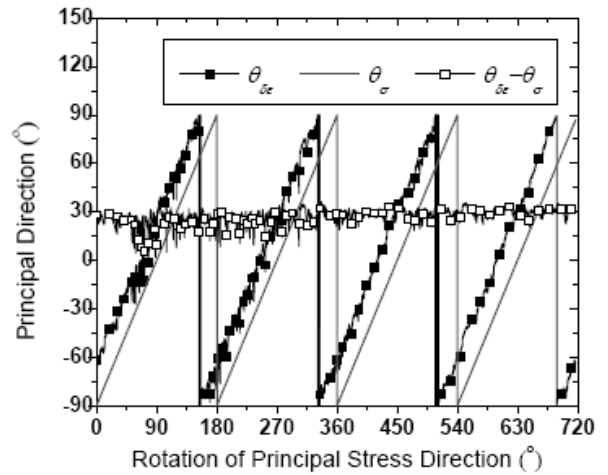


Figure 2.18. DEM simulation of rotation of major principal stress (Yu 2008). (θ_σ direction major principal stress, θ_ϵ direction major principal strain increment.)

Experimentally it is often difficult to know whether the natural or reconstituted samples of a sand that apparently defined a CSL that was unique regardless of initial fabric did so because the fabric was not a strong one, or whether those that apparently did give different CSLs in the $e:lnp'$ plane did so because they were not sheared far enough, which could be impossible in many standard element tests if strains of 100% are really required. The extension tests of Yang et al. (2008) were terminated at axial strains of 8-16% because of necking, which is indeed much smaller than the strains reached in the analyses of Nougier-Lehon et al. (2005), and the stresses were still changing slowly when the tests were terminated. This illustrates the difficulty of verifying experimentally whether the CSL is unique. Their observation of a single CSL in compression seems also to agree with the prediction that a critical state can be reached at much smaller strains for the $\alpha=0$ case. However, it is difficult to believe that the test data of Vaid & Sivathalayan (2007), shown in Figure 2.20 could converge had the tests been continued to larger strains. These considerations may in any case be rather academic, if the critical state that we see in laboratory tests is an apparent transitory state while breakage

continues to allow the volume to decrease to extremely large strains.

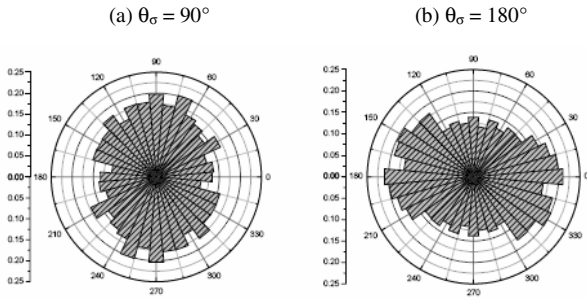


Figure 2.19. Rotation of contact normals during rotation of principal stresses (Yu 2008).

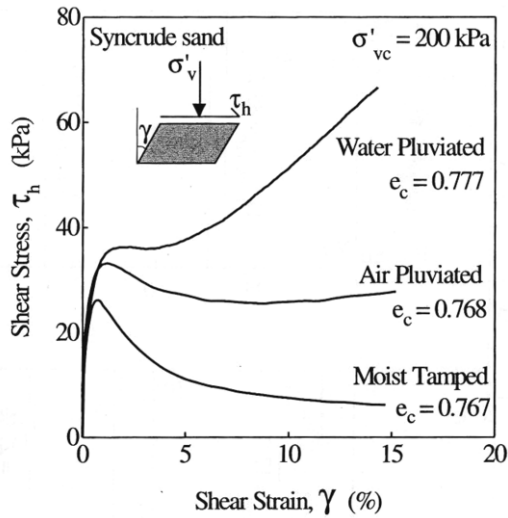


Figure 2.20. The effects of preparation technique on the undrained simple shear behavior of a sand (Vaid & Sivathalayan 2007).

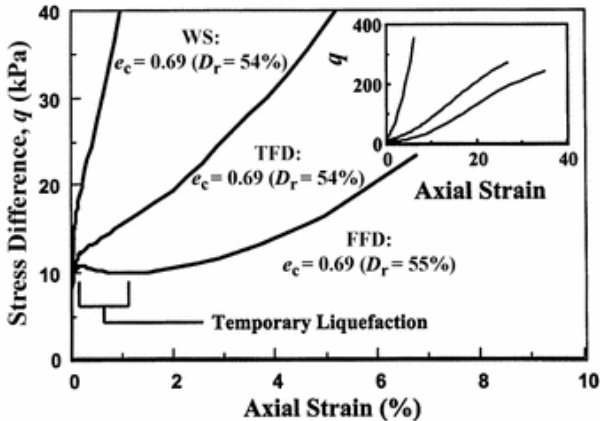


Figure 2.21. An example of the effect of fabric on the undrained behavior of a silty sand (18% silt content; WS water sedimented; TFD tapped dry funnel; FFD fast funnel deposition) (Wood et al. 2008).

2.3 Soils of Intermediate Grading and Transitional Soils

There has perhaps been an implicit assumption for some years that if clays broadly follow a critical state framework and sands do with a few modifications, then everything between is also likely to in some way or other, but recent research has highlighted that this is often not the case. As the evidence

mounts, it becomes clear that there are many deviations from previously established behavior, with soils that have additional complexities and nuances of behavior that require special attention.

There has been a considerable amount of work investigating the effects of adding fines of different types to sands and there is considerable evidence that the effects of fabric are particularly pronounced in these mixtures (e.g. Wood et al. 2008; Fig. 2.21). It has been postulated that the different modes of behavior can be explained by the different type of particle contact illustrated in Figure 2.22 that may be created and the different proportions of each of them for different preparation methods. Yamamuro et al. (2008) argued that while large to large particle contacts (L-L) were stable, large to small to large (L-S-L) were unstable. Where small particles simply rested on large ones with a large to small to void contact (L-S-V), the contact was passive in nature.

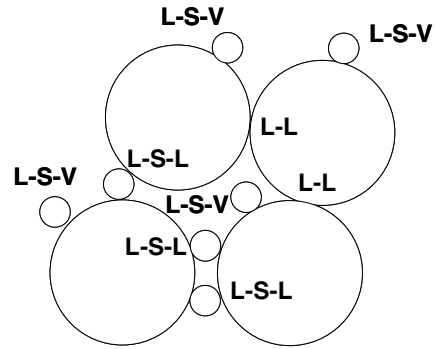
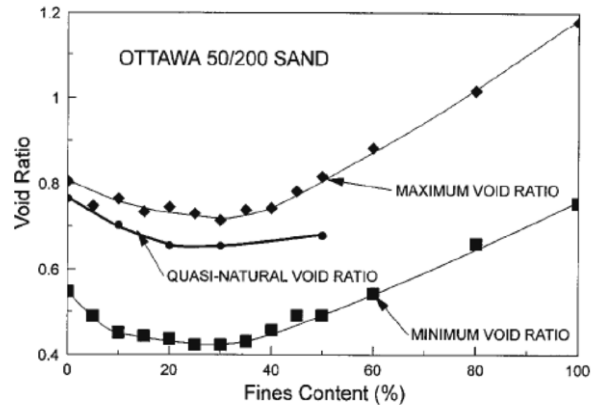


Figure 2.22. Particle contacts in a gap-graded soil (based on Yamamuro et al. 2008).

Figure 2.23. The influence of adding non-plastic fines on the density of



a sand (Lade & Yamamuro 1997).

Typically, as fines are added to a sand, the maximum and minimum densities initially decrease before increasing again (Kurbis et al. 1988, Lade & Yamamuro 1997; Pitman et al. 1994) as shown in the example in Figure 2.23. In the $e:ln p'$ space (Fig. 2.24), the CSLs generally move initially downwards but remain substantially parallel, before moving back up again (Thevanayagam et al. 2002; Murthy et al. 2007). Some authors have only seen a downwards movement (Fourie & Papageorgiou 2001), while others have seen significant changes in gradient (Coop & Atkinson 1993; Adrianopoulos et al. 2003). However, as Muir Wood (2008) has observed, the primary

effect of the change of grading is on the vertical location of the CSL, which is the basis for the assumed parallel CSLs in his model (Fig. 2.10) and which Muir Wood & Maeda (2007) had predicted through DEM analyses and Daouadji et al. (2001) had incorporated into their constitutive model that accounts for grain damage. This movement of the CSL has been explained by the fines initially filling the void space, but not contributing to the mechanical behavior, but as more are added, the coarse particles eventually “float” within a fines matrix and the behavior is then dominated by the fines. The fines content at which the trends in behavior reverse is generally around 15 to 40% and is defined to be the limiting or transitional fines content, as the behavior moves from sand dominated to fines dominated (Polito & Martin 2001; Pitman et al. 1994).

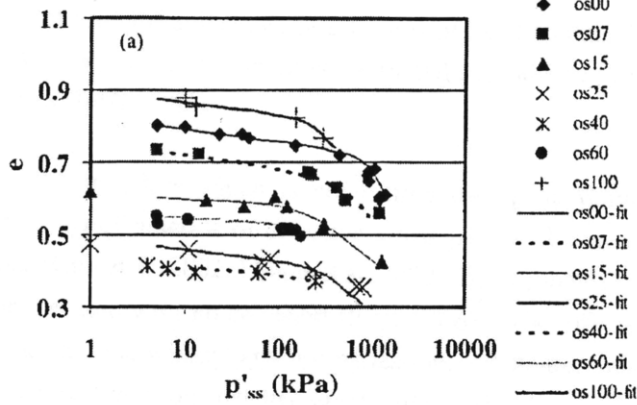


Figure 2.24. The influence of fines on the location of the CSL of a sand (Thevanayagam et al. 2002).

A number of attempts (Thevanayagam & Mohan 2000; Vaid 1994; Chu & Leong 2002) have been made to remove the effect of the fines content (FC) on the calculation of void ratio by defining an “intergranular” or “skeletal” void ratio (Mitchell 1976). If the specific gravity of the fines and sand are the same, this reduces to:

$$e_{sk} = \frac{e + (FC/100)}{1 - (FC/100)} \quad (2.1)$$

This type of approach is largely limited to low to medium fines contents, and cannot apply beyond the transitional fines content. Thevanayagam & Mohan (2000) found that a unique critical state line could be defined at higher pressures for their sand mixed with various quantities and types of fines using a skeletal void ratio, although at lower stress levels the CSLs were not unique (Fig. 2.25). Thevanayagam et al. (2002) recognized that fines of different natures would have different effects on the overall behavior, and they defined an equivalent skeletal void ratio:

$$e_{sk,eq} = \frac{e + (1 - b)(FC/100)}{1 - (1 - b)(FC/100)} \quad (2.2)$$

So that if $b=1$, the fines have no effect on behavior and $e_{sk,eq}$ reduces to e_{sk} . They suggested that generally b should be between 0 and 1 for all fines, but Ni et al. (2004) found it necessary to allow b values to be negative for plastic fines.

Even using a granular void ratio (e_g), Geogiannou et al. (1990) found that the small to medium strain behavior was not unique for different clay contents (Fig. 2.26). Bouferra & Shahrouh (2004) made similar observations for the undrained

stress paths of sand: clay mixtures, but chose to make their comparisons at similar void ratios. This raises the question of what is the appropriate means of comparison of samples with different fines contents, e , e_{sk} (or e_g), or relative density, or simply creating samples by similar methods, whatever their densities then turn out to be. Fourie & Papageorgiou (2001) attributed the often contradictory evidence for the effect of fines on sand behavior to the lack of a consistent means of comparison. Perhaps some form of state parameter would be the more logical choice which would account for the different location of CSL that each grading would exhibit.

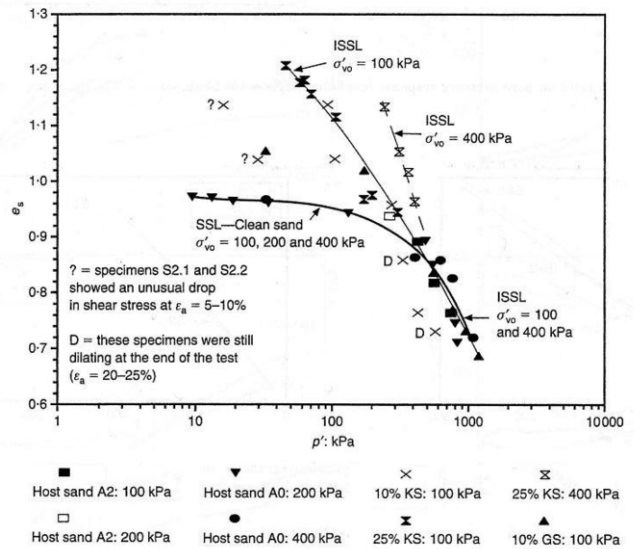


Figure 2.25. Use of skeletal void ratio to define a unique CSL for mixed soils (Thevanayagam & Mohan 2000).

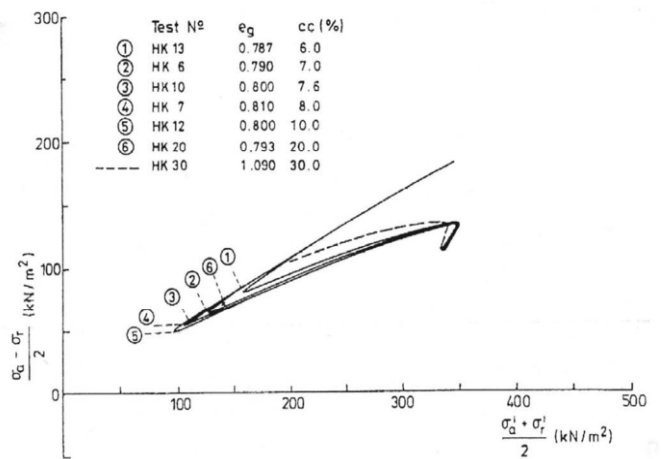


Figure 2.26. Undrained stress paths of sandy samples with varying clay contents (Geogiannou et al. 1990)

However, it is not really clear why this type of normalization for grading using $e_{sk,eq}$ or e_{sk} is really necessary. After all, we do not try to normalize in some way the nature of clay soils to produce a unique CSL regardless of their grading and mineralogy. Instead, the approach has been to treat each individually, defining intrinsic properties that are dependent on the nature of the soil (i.e., grading, particle shape and

mineralogy) which we then use as a basis for understanding the influence of the structure on the behavior of the soil in its natural state (Burland 1990). While Burland and others have suggested empirical correlations between plasticity and the location of the intrinsic Normal Compression Line, this was only intended for use in cases where no intrinsic properties were available, rather than any attempt to remove variation due to soil nature through normalization.

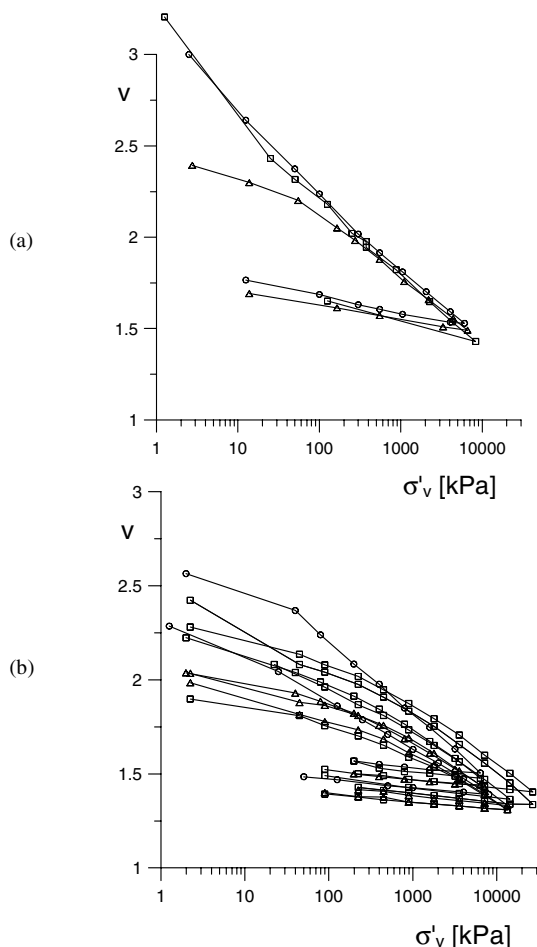


Figure 2.27. Oedometer compression curves for a silt with (a) 45% clay content (b) 8% clay content (Nocilla et al. 2006).

It may be the case that a concentration on trying to normalize away the intrinsic behavior of a soil has tended to conceal a rather more serious problem, which is that central assumptions of CSSM break down for these soils. An example is shown in Figure 2.27, which shows the oedometric compression data for a silt, which has been prepared with different proportions of clay fines. Samples with clay contents of 45, 25, 8 and 3.5% were prepared, with a variety of initial void ratios. At high fines contents, the various samples converged to unique Normal Compression Lines, but as the fines content reduces the different compression paths no longer converge, but tend to remain parallel, so no NCL can be defined. Of course there is no normalization process such as e_{sk} or e_{skeq} by which the void ratio could be modified that would cause the various compression curves to converge, since they all have the same grading. Such behavior had previously been seen for gap-graded soils by Martins et al. (2002), but these data now showed that this type of behavior might be much more widespread than had been thought. It has been termed “transitional” behavior. The same term has been used both to refer to the fines content at which trends of behavior tended to reverse, as discussed above,

and also by Lupini et al. (1981) for soils that were between sands that did not have a residual strength and the more plastic clays that had a very well defined drop in strength from critical state to residual. It is not yet known what is the relationship between the various usages of the term “transitional”, but it is unlikely that the three definitions are coincident. Sipton et al. (2006) went on to demonstrate that this type of behavior could be found in soils with both plastic and non-plastic fines and whether particle breakage was observed or not. Finding a relationship between grading or mineralogy and whether transitional behavior is seen or not has therefore proven elusive; there are plenty of soils with apparently similar gradings that conform quite happily to our expectations from Critical State Soil Mechanics.

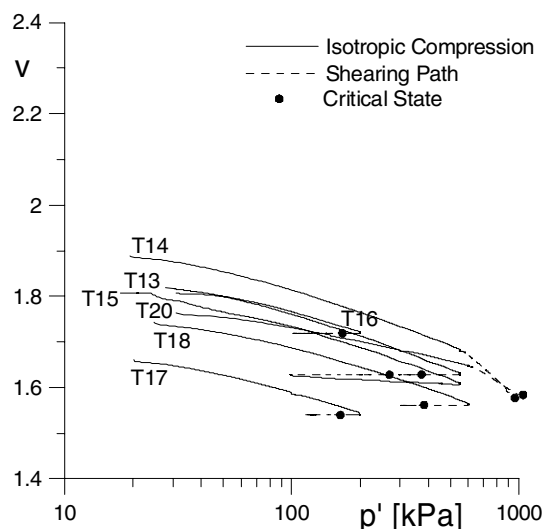


Figure 2.28. Isotropic compression and “critical states” for silt with 8% clay content (Nocilla et al. 2006).

The lack of convergence of compression paths from different initial void ratios must reflect a stability of the initial fabric that cannot be broken down by compression alone. Nocilla et al. (2006) had used various different sample preparation techniques to make their samples (slurry, dry compaction and wet compaction), but it was clear that the lack of convergence was very much more a function of the initial void ratio than the preparation technique per se and differences in fabric were impossible to distinguish under the Scanning Electron Microscope. Such behavior is probably more widespread than realized in the literature; while many authors emphasize the effects of fabric on the behavior they observe, few then recognize the consequences for a critical state interpretation, and that their soil is actually transitional.

For clays, Burland (1990) emphasized that reconstituted samples should be made with an initial water content significantly above the Liquid Limit, if robust and repeatable intrinsic properties were to be measured that were independent of the initial state, but Figure 2.27(a) shows that for a wide range of initial void ratios, for plastic soils the compression curves may eventually converge. Unfortunately, for the transitional soils, there is no evidence so far that any such guidance can be given for a limit on the initial state, above which the properties would be independent of initial void ratio, and so it is impossible for such soils to find a unique “intrinsic” behavior, which might act as the reference to determine the effects of structure in the natural soil (Ferreira & Bica 2006). The “correct” initial void ratio for reconstitution might be viewed as the one at which the soil had been deposited, but how would that be determined?

Perhaps it might have been expected from the work of Nougier-Lehon et al. (2005) that one-dimensional compression would not be able to erase initial fabric, since the strains are limited to tens of percent and there is no change in the direction of the principal stresses compared to that during sample deposition or preparation that might aid in the disruption of an anisotropic fabric. However, the lack of a unique Normal Compression Line does limit the applicability of critical state Soil Mechanics. For clays, as discussed above, the stability of fabric as a form of structure and the persistence of fabric effects during compression is well established and even included in a number of constitutive models that account for structure (e.g. Baudet & Stallebrass 2004).

Even more serious for the applicability of the critical state framework is whether a unique critical state may be reached during shearing, or whether, as assumed by these models for clays, fabric effects may still persist. Nocilla et al. (2006) also carried out a series of triaxial tests, and their data for 8% fines are shown in Figure 2.28. It is clear that in the $v:lnp'$ plane the isotropic compression paths are non-convergent and that the shearing paths for different initial states also do not converge towards any unique critical state Line. The scatter in the data appears rather too large to be explained by incomplete testing. Ferreira & Bica (2006) found that for reconstituted samples of a residual soil, different critical state lines could be identified for different initial void ratios at reconstitution.

For a sand/fines mixture, Yamamuro & Lade (1998) made the similar observation that the location of the CSL in the $e:lnp'$ plane depended on the initial density of the samples. In other cases, forms of transitional behavior have been seen in which there is a unique critical state line, but no unique normal compression line (Altuhaifi 2007) indicating that the effects of initial fabric can be removed in some cases.

Transitional soils are therefore an extreme example of soils for which initial fabric dominates behavior. It is not yet clear how a critical state framework, formulated in $q':p':e$ space, might be modified to account for fabric and what parameter might be used to do that.

2.4 Rate Effects

Within the critical state framework, the soil behavior is independent of time, so that the rate of loading has no effect in compression or shearing and constant load or constant strain stages would not lead to creep or stress relaxation. There is now a wealth of evidence that this is not correct and that there are significant time related effects. Typical data for the one-dimensional compression of a soft clay are shown in Figure 2.29, in which shearing at different rates gives rise to different compression curves for different rates, there being a general downward movement of the curve as the compression becomes slower, so that the curves may be characterized by the pre-consolidation pressure as in Figure 2.30. Leroueil & Marques (1996) went on to identify that temperature would also have an effect on the viscous behavior of soils, so that the pre-consolidation pressure is a function of strain rate and temperature. The only exception to the general trend on Figure 2.30 is the slowest test for which Leroueil et al. (1985) believe that the rate was so slow that the soil was re-establishing some structure. With this exception, the pattern of behavior is termed "Isotach" or "Isotache" and analogous behavior can be seen for some soils during shearing (Figure 2.31).

As the rate of shearing is changed so the stress: strain curve and stress path steps from the curve appropriate to the previous rate of loading to that for the new rate. However, the response of soils to changes of strain rate in shearing is generally more complex than in compression, and several other characteristic patterns of behavior have been seen.

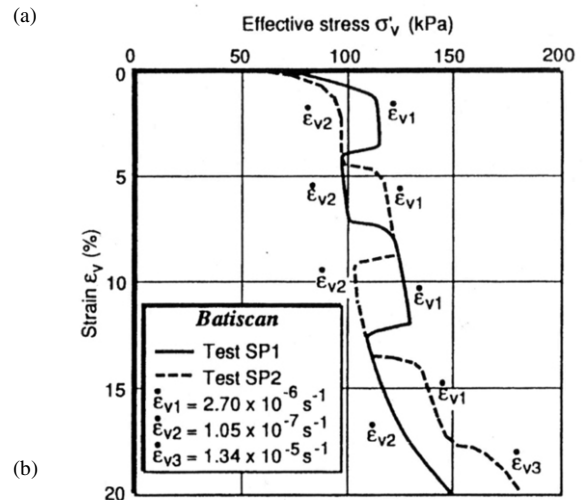
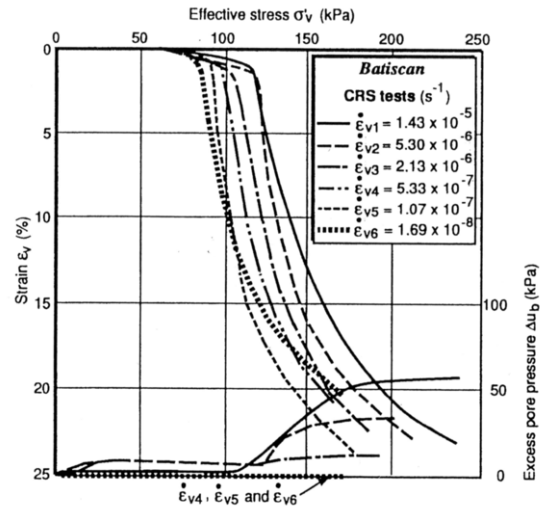


Figure 2.29. Typical oedometer test data for a soft clay (a) Constant Rate of Strain tests (b) Step-changed Rate of Strain test (Batiscan clay, Leroueil et al. 1985).

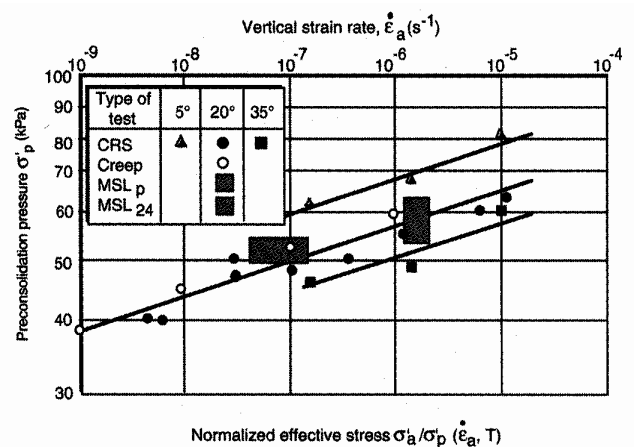
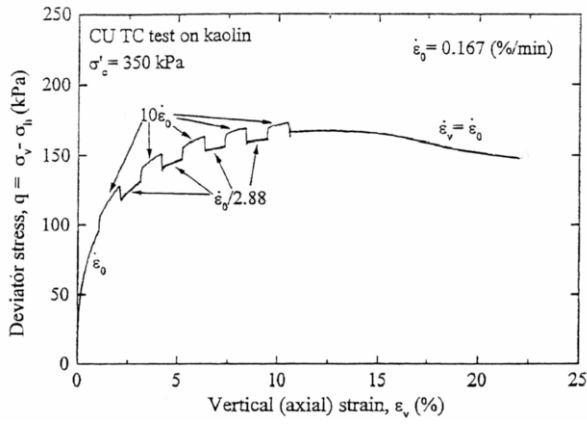
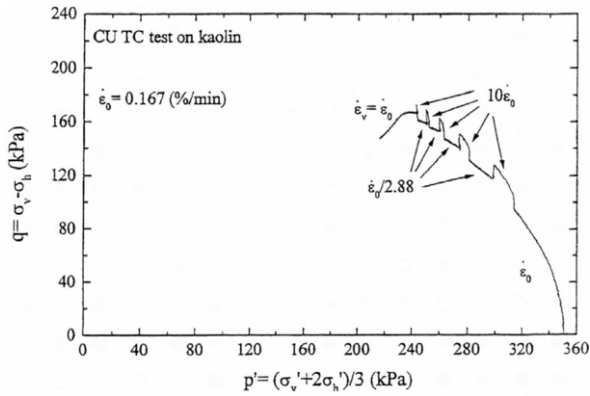


Figure 2.30. Dependency of preconsolidation pressure on rate of loading for Berthierville clay (Boudali et al. 1994).



(a)



(b)

Figure 2.31. Isotach behavior for normally consolidated reconstituted kaolin (a) stress:strain data (b) stress path (Tatsuoka et al. 2002).

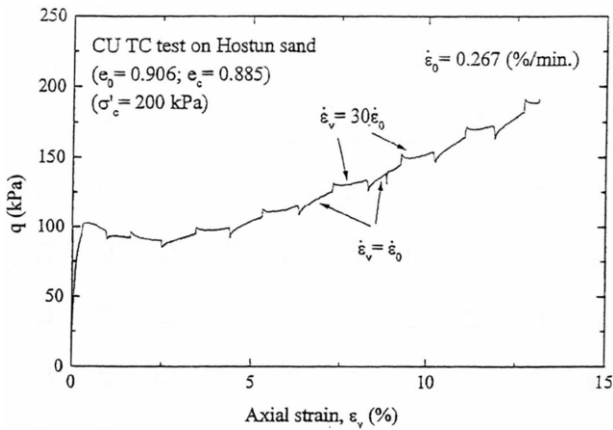


Figure 2.32. An example of pure TESRA behavior in undrained tests on Hostun sand (Tatsuoka et al. 2002).

The second common mode of behavior is “TESRA” Temporary (or transient) Effect of Strain Rate and strain Acceleration, in which step changes to the rate of shearing only cause a transient peak in the stress: strain curve before it returns to the same curve as at the previous rate of loading (Fig. 2.32). For some soils, combinations of Isotach and TESRA behavior occur, and while the behavior at small strains is essentially Isotach, at larger strains there is an increasing temporary effect with

overshooting on a strain rate increase or undershooting for a decrease, but still some persistent effects of strain rate after the immediate peak. This is illustrated schematically in Figure 2.33 and has been referred to as General TESRA or Intermediate behavior (Oka et al. 2003; Tatsuoka et al. 2002; Tatsuoka 2006).

Sorensen et al. (2007) have made a summary of the types of strain rate effect seen in different soil types, and while Isotach is often more prominent at smaller strains and pure or general TESRA at larger strains, Isotach is more likely to be seen in soft clays, both intact and reconstituted, weak rocks and intact stiff clays and general TESRA in cemented soils, some dense gravels, dense silty sands and reconstituted stiff clays. Pure TESRA throughout the strain range was only seen in clean sands. In comparing their own tests on samples of intact London clay with normally and overconsolidated reconstituted samples, Sorensen et al. (2007) concluded that the reconstituted soil was Isotach at small strains, tending towards pure TESRA a large strains, but the intact soil was Isotach throughout the strain range. This showed that the structure of the soil rather than its overconsolidation had a significant influence on the nature of the strain rate effect. Similarly Komoto et al. (2003) found a change from Isotach to general TESRA between intact and reconstituted samples of a stiff clay, although they did not model the overconsolidation of the soil and so could not separate stress history and structure effects. Soga & Mitchell (1996) identified that strain rate effects generally increase with the degree of structure or sensitivity of a soil.

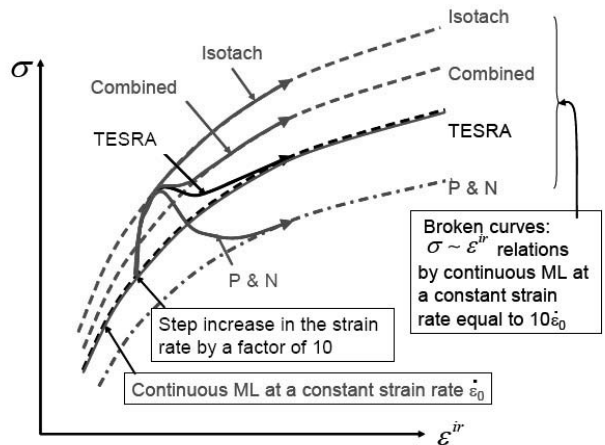


Figure 2.33. Schematic illustration of the various types of strain rate effect during shearing (Tatsuoka 2006).

Table 2.1. Factors affecting the type of strain rate effect (Tatsuoka 2006).

Viscosity type (θ)	Isotach \rightarrow Combined \rightarrow TESRA \rightarrow P & N
	($\theta = 1$) ($0 < \theta < 1.0$) ($\theta = 0$) ($\theta < 0$: could be less than -1.0)
Influencing factors	
Particle shape (in case of stiff particles)	More angular \rightarrow More round
Grading characteristics	Better graded \rightarrow More uniformly graded
Particle size (if saturated)	Smaller (clay) \rightarrow Larger (sand/gravel)
Particle crushability	More crushable ?? \rightarrow Less crushable ??
Inter-particle bonding	Stronger \rightarrow Weaker \rightarrow Null (e.g., rock/cement-mixed soil (unbound granular materials) /bituminous-mixture)
Strain level	Pre-peak \rightarrow Post-peak (in particular, at residual state)
Inter-particle contact point	More stable (better bound, better interlocking & larger co-ordination numbers) \rightarrow Less stable (less bound, less interlocking & smaller co-ordination numbers)

More recently Tatsuoka has identified that the persistent or Isotach strain rate effect need not necessarily be positive, i.e. with a higher stress: strain curve at faster rates of shearing. This led to the discovery of the “Positive and Negative” category of behavior in which, although the effect of the initial strain rate acceleration on applying a step change is to give an overshooting as for general TESRA, the persistent effect is in the opposite direction (Fig. 2.33). From a survey of a very wide range of data, Tatsuoka proposed the factors shown in Table 2.1 as a general guide to the influences on strain rate effects. In most tests investigating the effects of rate of strain and acceleration, the changes to the rate of strain have been applied in a step-wise manner, with a rate of acceleration that is uncontrolled and unmeasured, so that the relationship between the behavior observed, and the acceleration, is unclear.

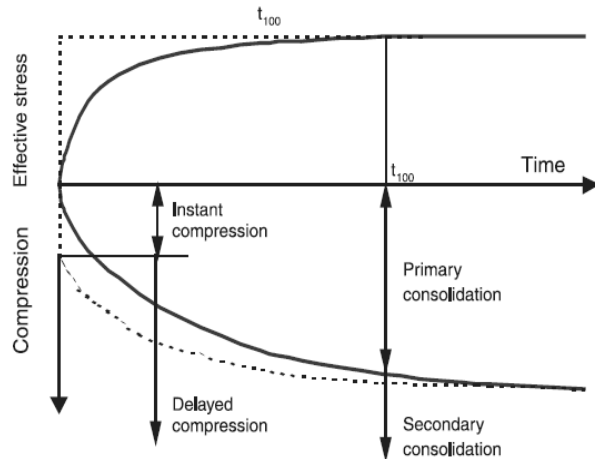
or axi-symmetric triaxial tests (e.g. Yin et al. 2002; Leoni et al. 2008). Figure 2.34 illustrates that the equivalent time concept that forms the basis of the model of Yin et al. (2002), allows creep and strain rate effects to be modeled for both normally and overconsolidated states. Based on Bjerrum’s (1967) suggestion for one-dimensional compression, strain is divided into instant and delayed components, and in this case the instant component is assumed to be elastic and time-independent and the delayed viscoplastic. The model as shown in Figure 2.34 is formulated in terms of volumetric strain rather than void ratio or specific volume, but the reference time or λ -line is essentially the normal compression line for a reference zero equivalent time; this, the authors state, could be close to the end of primary.

Equivalent time lines above the reference time line have negative equivalent times and those below positive. The instant time or κ -lines are the swelling lines, and so there are an infinite number of them. The concept of equivalent time is that if a sample is loaded from i to $(i+1)^{II}$ it will initially travel down an instant time line and then creep with time to say $(i+1)$, but the equivalent time and hence the creep rate at that point will be the same as if the soil had reached the same point by overconsolidation following the path i to $(i+1)^{II}$ to $(i+2)^I$, with creep to $(i+2)$ and unloading to $(i+1)$. Within the model, the soil can therefore reach an overconsolidated state below the reference time line either by unloading or creep. The creep is modeled with a non-linear logarithmic function to overcome earlier problems with a linear function that the creep strains are infinite at infinite time. A limit time line then forms the limit of creep, and the behavior of any heavily overconsolidated soil beneath it is time independent.

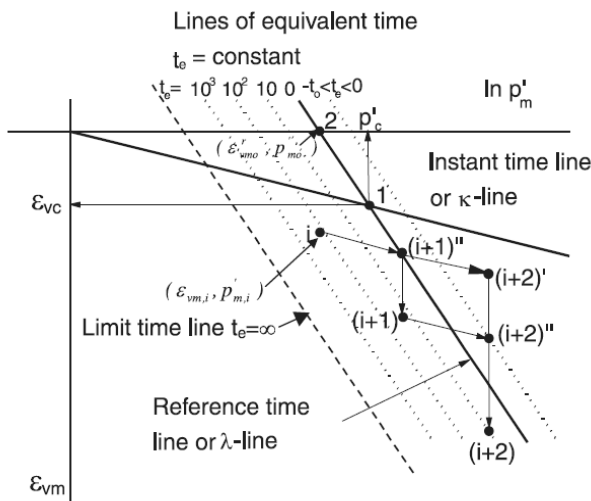
The main limitation of equivalent time models is that they are only able to model Isotach behavior and cannot capture either the effects of acceleration that are evident in TESRA, the influence of structuration due to ageing or the effects of tertiary creep in which the creep starts to accelerate with time rather than decelerate. Tatsuoka et al. (2003) have proposed a model that separates the loading rate effects from ageing effects by means of defining three components of strain; hypo-elastic, plastic and viscous. This is able to reproduce temporary acceleration effects as well as Isotach behavior but is limited to relating a stress ratio to single component of strain and strain rate.

A key assumption of the models that are developed in generalized stress space for the influence of strain rate effects is that the locations of the normal compression and critical state lines in the $e:\ln p'$ plane suffer from similar time dependent effects. Clearly this cannot be the case for pure TESRA unless there is no strain rate effect in compression. For many soils with general TESRA, the persistent effects at large strains become quite small or even disappear at the critical state, so that Sorensen et al. (2007) have found a unique CSL for reconstituted London clay. In some cases, even for Isotach behavior, such as in Figure 2.31, it is far from clear that there will be a significant difference in the critical states for different strain rates, often because the step changes are ceased before the critical state is reached. At least it is difficult to convince oneself that the effect will be as large as typical differences in the Isotachs for compression (e.g. Fig. 2.29). In other cases (e.g. Yin et al. 2002; Jung et al. 2008), there do seem to be more significant effects of strain rate on the CSL location. Clearly there needs to be more research on the relationship between strain rate effects on the relative locations of the NCL and CSL.

Soil behavior continues to be an advancing and exciting dynamic area within geotechnical research because of the complexities, nuances, uniqueness, and fine technical details associated with natural geomaterials. This requires extensive experimental efforts based on high-quality samples and careful examination of the results within a rational framework, such as that established by CSSM.



(a)



(b)

Figure 2.34. The equivalent time model of Yin et al. (2002).

There have been a number of models proposed in recent years that can account for time dependent behavior, that are based on critical state concepts and in particular on simple models such as Modified Cam Clay and that have been extended into generalized stress space rather than simulating simply one aspect of behavior, such as oedometric compression

3. PHYSICAL MODELING

3.1 Introduction

Physical modeling may be adopted to make predictions about specific modes of soil behavior. Leonardo da Vinci is renowned for using physical models in the Renaissance period, during his highly creative prime as one of the world's first 'scientists' (White 1990; Ferguson 1992). Around 1500, he also sketched a large helical propeller, which would drill itself into the ground by mechanics and rotation, as discussed by Broms & Flodin (1988). The art and science of physical modeling with soil is to be able to predict prototype soil behavior consistently with the simplest possible model, while being aware of the limitations and extent of validity of the physical model and the ensuing prediction.

This section discusses how physical modeling can contribute to investigating soil behavior, building on knowledge gained from element tests discussed in section 2, and extending the understanding of soil behavior and modes of testing in a more integrated fashion to either aspects, or specific prototypes, of boundary value problems.

3.2 Modeling or testing?

It is important to differentiate between the dual acts of modeling and testing, which are carried out for two different, yet complementary, purposes. Lee (2002) contended that the difference between modeling and testing was that modeling leads to a prediction, whereas the latter may not represent a specific or idealized prototype, even though it is nonetheless definitive and should lead to validation. A test accepts certain conditions, for example, in the form of natural ground or samples extracted without disturbance from the ground or lack of complete similitude. Perturbations may be imposed to investigate a hypothesis, which may be useful for engineering design or be upheld until disproven.

Prediction obtained from a model leads onto observation of a 'real' physical event, which could be described as a form of 'ground truth'. The interpretation may then require other models and will ultimately lead to reflection of whether the model was appropriate or not. The circle will then be joined by further interventions and predictions as required until a satisfactory coherence has been achieved.

3.2.1 A brief philosophical digression

The English poet, William Cowper (1731-1800) opined that 'absence of evidence is not the same as evidence of absence', which may also be applied to physical modeling. Karl Popper (1902-1994) commented that 'good tests kill flawed theories' so it could be that a definition of falsehood or error is required more than the elusive truth. Russell (1912, 1998) referred to the possibility of the existence of more than one version of the truth, in pointing out that *error* can creep into knowledge of truth. Beliefs may encompass what is false as well as what is true since incompatible and very strong opinions may be held on many subjects; so some of the beliefs must be erroneous. He opined that truth and falsehood are properties dependent upon the relationship of the belief to a known past series of events.

In science, two or more hypotheses may be coherent and account for all the known facts on a subject. Russell examined whether *coherency* would be sufficient as a requirement for truth, in that falsehood would be the failure of a body of beliefs to be coherent, leading to the conclusion that there can be only

one coherent body of belief! Certain truths might also be self evident, ensuring infallibility and constituting *knowledge* of the fact.

Even if coherence cannot define truth, it may be used as a criterion. Knowledge is mostly *probable opinion*, which as a body of individually probable opinions may be mutually coherent, and become more probable than one opinion alone. This is how scientific hypotheses acquire probability. Order and coherence lead to probable opinion delivering near certainty of truth. This impinges on testing hypotheses in that those responsible should take care not to assume non-existence of certain behavior exhibited in a test, if the model had failed to predict this response.

3.2.2 A return to physical representation

Bolton (2009) surmised that engineers need to base their judgments and actions on theories that have stood a test of examination so far by making references to literature, and declaring the hypothesis on which it is proposed to build. This embodies the publication of scaling laws for physical modeling that have arisen by performing physical tests, analyzing them, deriving dimensionless groups, and showing that "modeling of models" produces consistent predictions of a prototype.

If a geotechnical physical model is defined as a simplified physical representation of a more complex boundary value problem, it may represent a class of generic problems or a prototype chosen to reveal behavior under certain conditions, which Schofield (1980) introduces as an imaginary full-scale construction obtained by applying scaling laws to the results of a model test. While this will differ from a real construction, it may offer an insight into the response expected.

Following the 'problem definition', relevant boundary conditions and perturbations to be applied contribute to the decision making about what type of physical model is both required and affordable in resource terms (money, available equipment and time).

A key aspect of physical modeling is the idealization process for representing soil behavior, such as geometrical, loading, environmental and construction effects. These must be incorporated within any similitude requirements and will lead to model design. Contributing behavior sets should be identified individually and then in concert. Springman (2001) described such a sequence in developing models from the simplest possible boundary value problem to a more realistic representation of the prototype for centrifuge modeling of a piled bridge abutment. Pile deformations and bending moments were predicted during embankment construction and in service (Ellis & Springman 2001a&b).

On the one hand, a geotechnical model will be constructed principally with soil or rock (or equivalent analogues), which have been artificially constituted, or transported from their natural location to the laboratory. Subsequently data will be obtained representing a 'real' physical event and a successful demonstration of appropriate idealization, modeling and prediction will be a faithful characterization of the key aspects of the prototype behavior. Provided this is achieved, there is confidence in the modeling method.

On the other hand, model tests either to contribute to engineering design or to falsify a previously held hypothesis or to calibrate soil properties or additional modeling methods (e.g. new numerical algorithms).

Advanced physical models may be used to establish predictions of soil-structure interaction, environmental geotechnical response and for problems that can benefit from a

multi-scaled, multi-modeling method approach. Predictions of the behavior of a prototype system based on physical models can offer a midway house between those derived from constitutive models that are embedded in numerical analysis programs, and validated by element tests, and reality.

Since geotechnical design decisions in some countries may be founded on predictions made from physical modeling (e.g. SIA 2003), this offers tremendous opportunities as well as putting the onus on the designer to be able to determine what is a sound, or appropriate, physical model. Most Japanese major design and construction corporations, or public bodies acting as clients, rely on input from careful physical model and test studies. This may be at the design stage for mega-projects that present challenges outside prior experience, in developing further understanding of technology or methods, or to achieve an entrepreneurial advantage while engaged in innovation cycles (e.g. Kitazume et al. 2000; Miyake et al. 2001; Imamura et al. 2006a&b).

3.2.3 Summary

Consequently, both physical modeling and physical (model) tests will be discussed in this section. Muir Wood (2002) presented a reflective practice loop that advances scientific understanding (Fig. 3.1).

Primary forms of physical modeling will be introduced with their main advantages and disadvantages. These emerge from books and the conference literature focused initially on a single mode of physical modeling (e.g. Craig 1984; Corté 1988; Craig et al. 1988; Ko & McLean 1991; Huang 1991; Leung et al. 1994; Taylor 1995; Kimura et al. 1998) before attempting to cover the entire range of physical modeling (Phillips et al. 2002; Ng et al. 2006) or the extremes between centrifuge and constitutive modeling (Springman 2002).

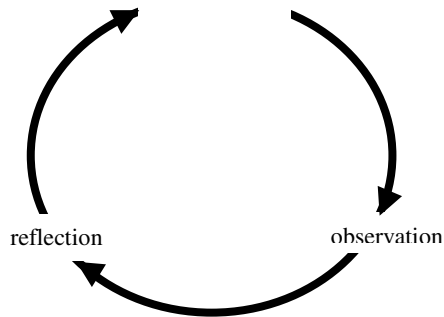


Figure 3.1. Reflective practice loop (Muir Wood 2002).

The state of the art will consider some crosscutting themes from increasing sophistication of the prototype systems, to the evolution of miniature mechatronics, robotics, digital imaging, data capture, storage and mining. Applications will be discussed of the foremost techniques that demonstrate key aspects of, and make significant contributions to, understanding soil behavior.

3.3 Modes of physical modeling

Lee (2002) noted that there is never an 'only possible way' to model, although methods can be ranked in terms of the most suitable for the task in hand. Modeling must be appropriate and effective, according to the level of risk and cost expected for the purpose or project in hand, as well as the desired accuracy of prediction. Table 3.1 summarizes some opportunities available

in physical modeling, and the main advantages and their disadvantages.

Early physical modeling focused on small scale model tests to investigate processes, explore physical response to loading and to develop fundamental theories in soil mechanics, for example, lateral earth pressure distribution (Terzaghi 1934) or bearing capacity of shallow foundations (Vesic 1963).

Full scale pile load tests using Statnamic rigs (Bermingham & Janes 1991) or Osterberg Cell (Osterberg 1991) to differentiate pile resistance at the base and along the shaft, are now standard industry practice for predicting axial pile capacity. Using the ground insitu constitutes rather a physical test, such as unmetalled road construction on geosynthetic reinforced unpaved roads (Hufenus et al. 2006), which incorporates variability in natural soil properties, than a model, per se, in which control of events and ground conditions are greatly facilitated.

There are many other examples also of reduced scale field tests on shallow foundations (e.g. 1:2.5 scale 1g, 3 m x 3 m footings, Steenfelt et al. 2003) or in using simple plate load tests (e.g. Costa et al. 2003) to interpret complex soil conditions, for example due to natural variability and partial saturation.

With the exception of full scale loading tests, relatively few full scale physical modeling series (Hertweck 2000; Edelmann 1998; Edelmann et al. 1999; Bathurst et al. 2002; Bathurst & Hatami 2006; Tefera et al. 2006a&b) are conducted nowadays.

The resources required, measured in terms of qualified people, time, money, space, mean that there is a far greater tendency to benefit from technological advances in using a calibration chamber, a centrifuge or a shaking table or in carrying out 1g small scale physical model tests (e.g. White 2002; Walz 2005).

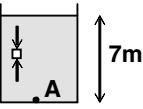
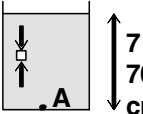
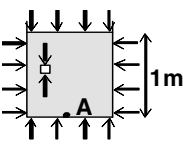
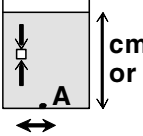
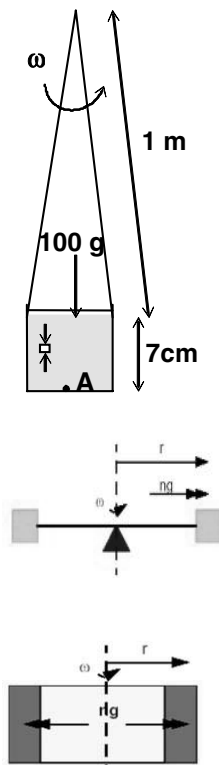
Basic soil behavior may be investigated cheaply through physical modeling at small scale under single gravity, and may be appropriate for preliminary tests for any boundary value problem. Such models are suitable for making predictions for cases in which insitu stress is not greatly significant. They should be used with great care for prediction of deformations and failure mechanisms.

Unconservative predictions of the Ultimate Limit State are likely to be obtained from 1g small scale models under some modes of kinematic constraint due to a high dilatancy angle ψ (Rowe 1962), exhibited at the low stress levels and increased wall friction. Quite often the interpretation of peak strengths has relied upon an apparent effective cohesion intercept c' and associated (apparent) friction angle, which is then lower than the critical state angle of friction, when in fact it would be more appropriate to adopt a peak friction angle that includes ϕ'_{cv} and a component for ψ (e.g. Bolton 1986).

Calibration chamber and 1g shaking tables are suitable for specific problems. Calibration chambers became particularly popular in the eighties, leading to an international symposium (Huang 1991); however other techniques seem to have attracted more usage in the last decade. Shaking tables are common in Japan and such facilities have become quite widespread in the United States, following a multimillion dollar 15 year research Network for Earthquake Engineering Simulation (NEES, <http://www.nees.org>). They have mainly been used for investigating structural response to earthquakes, yet do cover aspects related to geotechnical seismic ground hazards.

Funding packages are provided to upgrade seismic (See: http://www.nees.org/Research_Sites/ShakeTableLabs/) research sites in the United States in order to advance understanding of how earthquakes and tsunamis affect man-made infrastructure, such as roads, buildings, port facilities, and public utility systems. 1g shaking tables and geotechnical centrifuges are included in the facilities to be upgraded too.

Table 3.1. Physical modeling options, EQ: Earthquake, DAQ: Data Acquisition, d.o.f.: degree of freedom (after Springman 2001).

Type	Sketch of Model/Prototype	σ_v @ A (kPa)	Advantages	Disadvantages
1g, full or large scale		100 - 140	<ul style="list-style-type: none"> stress correct soil conditions controlled 1:1 to 1:4 models feasible & useful 	<ul style="list-style-type: none"> time to construct model time for diffusion processes time for flow processes boundary effects manpower & cost
1g, small scale		~ 1 - 10	<ul style="list-style-type: none"> time (quick) cost (cheap) ease of control suitable as preliminary test to check equipment & testing principles 	<ul style="list-style-type: none"> stresses incorrect potential for suctions & dilatancy to affect results time for flow processes boundary effects
Calibration chamber		10 - 20 + external pressure increment	<ul style="list-style-type: none"> can apply known boundary conditions normal to sample edges (stress or displacement) stress within element can represent full scale conditions soil conditions and geometry well controlled (mainly axisymmetric) 	<ul style="list-style-type: none"> stress gradients may be unrealistic can only represent small part of a boundary value problem limited to applying principal stresses in horizontal and radial directions construction & installation effects do not represent field conditions
1g, shaking table (see above for 1g models)		5 - 10+	<ul style="list-style-type: none"> application of simulated ground motions scaling to suitable EQ frequency unnecessary up to 6 d.o.f. possible offer opportunities for soil-structure interaction 	<ul style="list-style-type: none"> greater focus on area (and structures) than soil depth stresses in ground incorrect wave reflection at boundaries near field EQ may not be well modeled
100g, 1/100 th scale in a centrifuge		100 - 140	<ul style="list-style-type: none"> stress with depth modeled correctly idealization possible to reveal key mechanisms of behavior soil selected, design stress history, control loading systems testing time (relatively quick) expedites flow processes significantly cost (not expensive) observer witnesses deformation and failure mechanisms <p>BEAM</p> <ul style="list-style-type: none"> ideal for prototype problem with greater depth to surface area ng shaking tables can be mounted <p>DRUM</p> <ul style="list-style-type: none"> ideal for prototype problem with greater surface area to depth can be used as a 'beam' with strongboxes fixed to infill plates considerable real estate on central tool plate to mount actuators, imaging, DAQ devices 	<ul style="list-style-type: none"> factor n, on earth's gravity g, varies with depth Coriolis effect reconstituted soil relative size of particles, structural units, displacement controlled behavior scaling of interface roughness and length dimension of shear surface with particle size (strain localization) boundary effects size & accuracy of mini-instrumentation, site investigation devices, stress path may be different construction method different dynamic scaling challenges necessitating change of fluid viscosity or other solution <hr/> <ul style="list-style-type: none"> curvature of 'g' field curvature of water table <hr/> <ul style="list-style-type: none"> surface curved limited radius so only shallow soil depths feasible before depth variation errors dominate strongboxes cannot swing up so difficult to recreate some construction stress paths and retain stability at 1g

Early 'modern' justification for using a geotechnical centrifuge was presented in the Rankine lecture by Roscoe (1970), following earlier inspiration from Phillips (1869a&b), Bucky (1931) and Pokrovsky (1933) in France, USA and Russia (Craig 2002). Roscoe (1970) stated categorically that the centrifuge was the only satisfactory way of truly modeling a prototype problem to scale in which self-weight of the soil is significant.

Schofield (1980), in his Rankine lecture, complemented further developments in Critical State Soil Mechanics, and the use of Cam Clay models to describe the yield function, work hardening and flow rules based on conjugate work, with discussions of scaling effects, errors and the suitability of geotechnical centrifuges in examining response of boundary value problems in reconstituted clay. These developments have had far reaching effects on examining aspects of soil behavior over past decades using conjugate modeling methods.

More recently, Rankine lecturers Randolph (2003) and Mair (2008) relied upon centrifuge model tests to validate design approaches and provide new insights into mechanisms for various boundary value problems for suction caissons and piles, and pipe-soil interactions above tunnel excavations. Most modern beam centrifuge facilities have been set up with equipment to replicate seismic shaking (e.g. Kutter et al. 1994; Madabhushi et al. 1998; Shen et al. 1998; van Laak et al. 1998; Derx et al. 2006) with capacity available in Japanese centres.

Quite often several physical model test and modeling methods will be adopted, either for validation purposes, to investigate different aspects of the boundary value problem in question or to provide a range of competing prediction opportunities. For example, Newson (1998) validated a non-associated CSSM model by predicting centrifuge model behavior successfully. Adachi et al. (2004) proposed a new method for earthquake resistant pile reinforcement. This was validated by a combination of model shaking table tests under a 1g gravitational field and numerical simulation analyses, and then a full-scale model test of the proposed method was also conducted to examine the construction performance and the quality of reinforcement body in the pile foundation. The full-scale test included horizontal load tests, vibration tests, and excavation to observe the outcome and to confirm the applicability of the proposed reinforcement method for a prototype pile foundation.

3.3.1 1g small scale models and tests

Particular challenges exist to the use of 1g model tests in sand for the determination of deformations, which will later be used to predict behavior at full scale. These include the strongly nonlinear dependency of stiffness upon stress level, the highly exaggerated influence of dilatancy at the low stresses present in a small-scale model, and side friction on the model container walls.

Any influence of dilatancy exhibited between very low and intermediate stress levels may be allowed for subsequently during interpretation of the data. Although Bolton (1986) shows limited data from shear testing on poorly graded sands for mean effective stress $p' < 50$ kPa, the greater difference between peak and critical state angle of friction ($\phi_{max}' - \phi_{crit}'$) with low mean effective stress p' and high relative density I_D is clear (Fig. 3.2a). Care must be taken though in the use of relative density. While it is an understandable concept, it is much harder to measure well in reality, and several researchers have shown that the fabric within sands and silty sands at nominally identical relative density and stress level can influence soil behavior significantly (Vaid & Negusse 1988; Frost et al. 1999; Yamamuro & Wood 2004).

Furthermore, Klotz & Coop (2001) comment that some form of state parameter Ψ (Been & Jefferies 1985) should be adopted to account for the effect of stress level as well as relative

density, when analyzing the driving of piles in sands. In attempting to use the volume difference based derivation to define state, they found that the lack of straightness and a fixed location of the CSL (Klotz & Coop 2001) for this particular boundary value problem required the state parameter to be newly defined in terms of a ratio of stresses. The results demand that there is similitude between prototype and model in density and stress level, as well as particle crushing strength for cases in which significant crushing is expected.

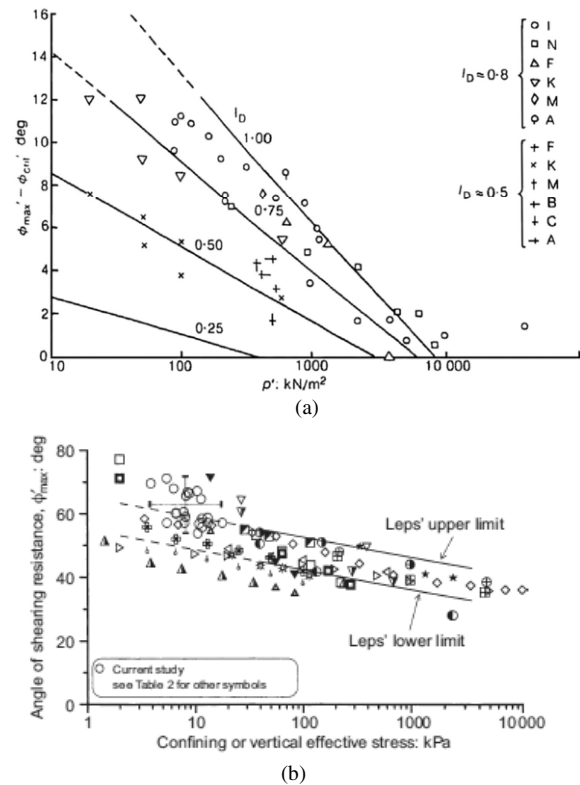


Figure 3.2. Comparison of: (a) difference between peak angle of shearing resistance and critical state angle against mean effective stress (Bolton 1986); (b) peak angle of shearing resistance against confining or vertical effective stress (Fannin et al. 2005).

Fannin et al. (2005) show similar trends for data obtained from both field insitu and laboratory tests (Fig. 3.2b) for peak angle of shearing resistance for well graded angular gravels, and crushed rockfill of similar grading, sheared under very low stresses. These datasets could be augmented by similar field and laboratory direct shear box tests on Swiss alpine soils (Springman et al. 2003a; Arnold et al. 2005) that likewise mobilized ϕ_{max}' between 50° and 66° for $\sigma_v' < 34$ kPa.

Springman (2000) has also discussed this for an example case history, on which peak angles of shearing resistance might lie 12° higher at depths of 100 mm than at 6 m depth for a medium dense sand (see also Fig. 3.2a). Models tested at lower stresses will tend to reproduce unconservative conditions in that 'design tables' derived from the data require extreme caution in their application, with the possible exception of preliminary design for very low risk projects.

Small scale models can be effective within a multi-scale modeling programme for boundary value problems investigated in the undrained state on normally consolidated soils, since undrained shear strength is linearly related to the effective vertical stress (e.g. Ladd 1991): indeed CSSM already predicts such behavior. Houlsby et al. (2005) based their design methods for suction caissons on small-scale model testing (e.g. Byrne &

Houlsby 2002, 2004) and the validation process relied upon a series of intermediate-scale field trials.

A recent contribution dealing with the transition from undrained loading to the consolidation process is described by Fang & Yin (2006). They installed band drains in reconstituted marine clay in a consolidometer, instrumented with pore pressure transducers, to which uniform normal load is applied and removed. Pore pressure response was consistent with practical experience. Fang & Yin commented that 'back-analysis of data from well-instrumented small-scale physical model tests and full-scale model tests based on analytical solutions and numerical models may provide a suitable approach to investigating the permeability changes and the influences on the consolidation process'. Comparison with predictions from larger scale models could be beneficial to encourage and aid reflection about validity of these highly instrumented small scale models.

3.3.2 1g large scale models and tests

Parametric studies can be extremely useful in exposing mechanisms of behavior relevant at both Serviceability Limit States and Ultimate Limit States. Such repetitive investigations are almost impossible if a full-scale model test option is adopted for most full-scale geo-structures, although there are other major advantages in carrying out full scale tests (see Table 3.1).

One notable exception is the extensive range of full scale physical models of well instrumented geosynthetic-reinforced walls and embankments, constructed in an indoor plane strain test facility that are unique with respect to scale of testing and the range, quality and quantity of measurements recorded (Bathurst et al. 2002; Bathurst & Hatami 2006). The influence on wall performance at the end of construction, and following subsequent surcharge loading, of reinforcement type, stiffness, strength, spacing, different facings, and backfilled with one of two types of sand, was investigated. These have provided opportunities to verify numerical codes (Hatami & Bathurst 2005) and to reduce conservatism in the wall design methods (Allen & Bathurst 2002).

Consequently, some researchers have constructed 1/n scale models (where $2 \leq n \leq 6$) that are operated at vertical stress levels to a maximum $\sigma_v' < 100$ kPa, an order of magnitude larger than typical small scale 1g tests ($\sigma_v' < 10$ kPa; Table 1), but yet do not acquire the scale to be considered as a 1:1 full scale model.

Tefera et al. (2006a&b) describe their work on a plane strain model of 2.5 m deep strutted flexible sheet pile wall, excavated in stages to over 2 m in loose sand. They compare their data of wall deformations, bending moments, strut loads and surface settlements with predictions made for all excavation stages, based on finite element analyses conducted in parallel.

Conventional triaxial and oedometer element tests were carried out at appropriate stress levels to propose parameters for sand for a constitutive model with a cap and deviatoric hardening (Brinkgreve 2002). It was proposed that future design processes could be enhanced by numerical modeling by elaborating the precise conditions for the laboratory element tests that would be required as a minimum standard.

The soil mobilized greater strength in plane strain (which was not allowed for from the values of friction angle defined under triaxial compression) and stress paths were dominated by extension rather than compression and these points were mentioned as causes of some discrepancies. The prediction was claimed to have been 'relatively good' nonetheless, and encouraging for future engineering practice for excavation depths applicable in service (up to 1.82 m in this case).

Bathurst et al. (2002) also conducted independent laboratory testing of component materials to calibrate their computational models. Like Tefera et al. (2006b), they confirmed that these

tests should be carried out in plane strain to obtain appropriate peak strengths.

3.3.3 Calibration chambers

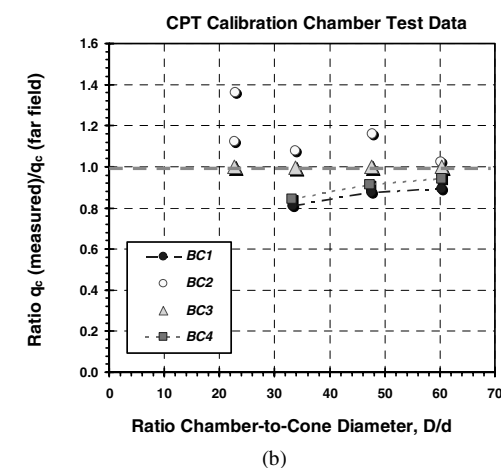
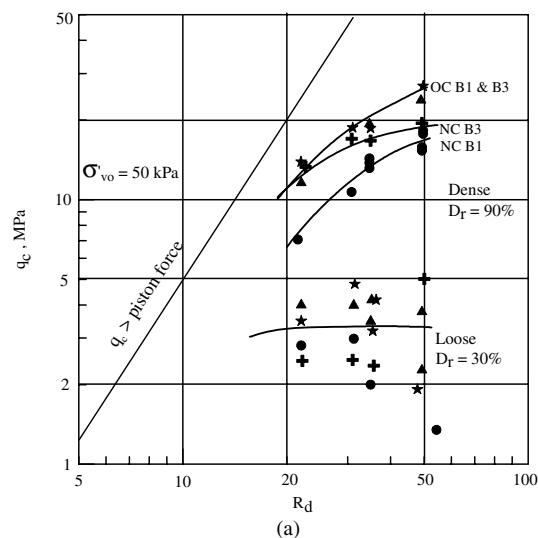


Figure 3.3. Calibration chamber size effect for cone penetration resistance a) for Høksund sand with $R_d =$ ratio of chamber to cone diameter (after Parkin & Lunne 1982) and b) for Ticino and Toyoura sand (Iwasaki et al. 1988).

Calibration chamber testing (CCT) has been found to be preferable for studying reduced scale loading conditions for axisymmetric systems such as piles, and full scale testing of standard penetration tests (SPTs), cone penetration tests (CPTs), pressuremeter testing (PMT), dilatometer testing (DMT), shear waves under known stress conditions and soil states, to deliver more generic analyses of the load–deformation response. Reconstituted or remolded soil models may be prepared in calibration chambers at any desired level of (relative) density under normal stresses acting vertically and radially, while under either stress or strain controlled boundary conditions.

Initially the walls of cylindrical chambers were rigid (K_0 condition) to prevent lateral strain (e.g. Last 1979a, b&c) however flexible walled chambers were introduced subsequently with any combination of controlled vertical and horizontal stresses and strains (BC1 (constant stress), BC2 (no strain), BC3 (constant vertical stress, no horizontal strain), BC4 (constant horizontal stress, no vertical strain)). Plane strain calibration chambers (BC5) tend to retain the rigid wall boundary condition similar to BC3, and are also generally adopted in a beam centrifuge (e.g. White & Bolton 2002).

Parkin & Lunne (1982, Fig. 3.3a) show that the boundary effects are also related to sand density (or dilatancy), so that there are essentially limited boundary effects regardless of boundary conditions applied, as long as the sand is loose and not dilatant. When sand is dilatant, q_c increases with sample dimensions even under BC3. Only when the dilatancy and stress state in the physical model test match that expected in the field, will the “correct” far field value be obtained. In BC3, the cone penetration induces too much lateral stress due to the rigid lateral boundary that inhibits dilatancy.

Lateral stress increase near the cone tip in BC1 is lacking because of the constant applied lateral boundary stress. When the sand is loose, the failure zone around the cone is very limited and much smaller than the lateral dimension of the chamber sample. Chamber boundary effects are minimal. The normalized chamber diameter must be close to 100 in dense sand (extrapolating from Fig. 3.3a) to eliminate boundary effects, implying that a calibration chamber suitable for CPT testing should be 4 m in diameter, which is unrealistic. BC5 simulates field stress conditions provoked by cone penetration near the cone tip, without needing a large chamber.

After a flurry of activity in the eighties and nineties, there would appear to have been rather less focus on this method recently. Perhaps, this is because tests performed in a conventional cavity-wall calibration chamber are affected by the ongoing quandary over boundary conditions (e.g. Huang & Hsu 2004; 2005).

Although attempts to make corrections to allow for q_c (determined in the laboratory) to q_c (far-field) have been proposed over the years to overcome various shortcomings with this method (see Table 1 and Parkin & Lunne 1982; Mayne & Kulhawy 1991), Lee & Salgado (2000) comment that ‘questions regarding the existence of calibration chamber size effects have not, to this date, been adequately addressed’.

According to Salgado et al. (1997; 1998), the BC3 boundary condition is ‘not practically attainable’ in a CCT, which they comment calls the data obtained in such tests into question. Local movements of individual particles around a penetrating tip are still able to achieve a greater degree of freedom than could be attained with a perfectly rigid wall.

In comparison, CPT data reported from centrifuge tests that represent the BC3 case (rigid lateral boundary) show that q_c reduces with increasing size of container, as the restrictions to particle movement caused by rigid boundaries becomes less significant. Gravitational forces on soil under ‘hyper gravity’ in a centrifuge may reduce strains in the vertical direction, which could then be considered to simulate BC2 (with zero vertical and horizontal strains, see Fig. 3.3b, Iwasaki et al. 1988). The correction factor would then become the reciprocal of that used for the most common CCT data, i.e. BC1 (vertical & horizontal stresses held constant).

The absolute rigidity of a radial boundary in a CCT is questionable. Although the net lateral displacement was required to be zero under the BC3 condition, there could still be local displacements at the depth of the stress bulb, as the CPT tip was pressed into soil.

Recent work by Huang & Hsu (2005) in developing a stack of expandable rings (as an axisymmetric field simulator, BC5) permitted CPT calibration tests to be conducted on a cylindrical sand specimen and under substantially reduced boundary effects. They found that increased horizontal stress had a much more significant and consistent effect on q_c than the initial horizontal stress existing in the soil prior to the CPT. For a given relative density, q_c was found to be most closely related to mean normal stress.

Huang & Huang (2006) back-analyzed liquefaction potential for sand sampled from a region adjacent to the districts in Central Western Taiwan close to the Chi Chi earthquake of September 21, 1999. Standard Penetration Test (SPT), CPT and

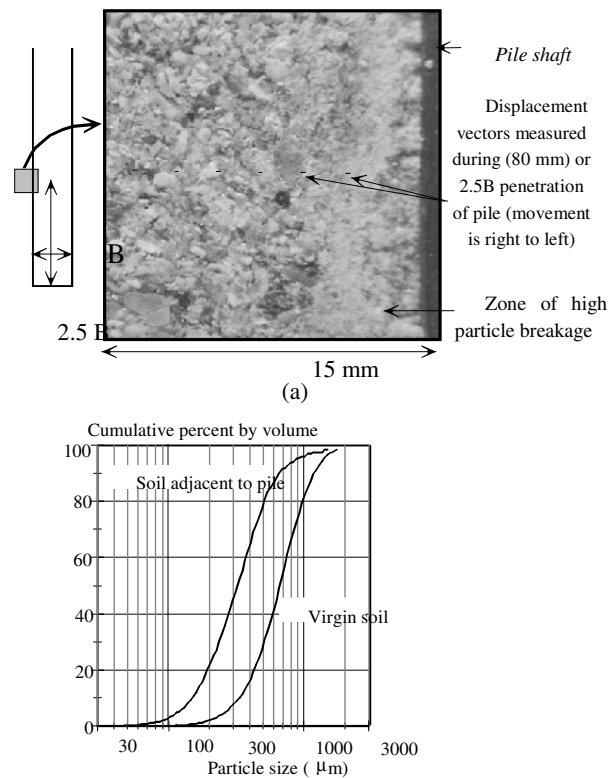


Figure 3.4. Friction fatigue in piles a) sand adjacent to a jacked pile shaft b) post-mortem grading analysis (White & Bolton 2002).

shear wave velocity (V_s) data had provided contradictory indications. They performed a series of CCTs on CPTs and cyclic triaxial tests on remolded sand with various fines contents and densities, to calibrate the correlations obtained between q_c and the cyclic resistance ratio.

Lee and Salgado (2000) justified the use of calibration chambers for pile base capacity studies. They calibrated finite element analyses to investigate both pile base and plate resistance for sands with various relative densities and stress states, against CCT data provided by Ghionna et al. (1994) and Salgado et al. (1998). Chamber size effects were postulated, in this case, to be small for settlement levels of interest in practice.

A further example demonstrates the opportunity to expose mechanisms when the influence of insitu stresses is subsumed in importance below other dominating effects. White and Bolton (2002) described investigations into friction fatigue of piles in a plane strain calibration chamber equipped with glass observation windows. They used digital image analysis (e.g. White et al. 2003) to expose the movement of sand particles crushed (McDowell & Bolton 1998) during pile jacking (Fig. 3.4b). Since the applied surcharge load was only 50 kPa, Dog’s Bay sand (Coop 1990) was used to emphasize the crushing mechanisms under investigation.

Displacement vectors revealed the migration of the crushed sand grains away from the zone under the pile tip, eventually into the voids adjacent to the shaft (Fig. 3.4a). This effect was emphasized; the further the zone of interest was located behind the model pile tip.

3.3.4 1g shaking tables

Usage of shaking tables has mainly been focused on investigating structural response to earthquake simulation. Typically, there is a greater surface area to depth aspect ratio

than for the other geotechnical physical modeling methods. Few of the 89 shaking tables recorded by NEA/CSRI/R (2004) and Roth & Cheney (2001) appear to be employed actively for geotechnical research. Payloads reach 100 tonnes in European facilities, up to 50 tonnes in North America (e.g. Ling et al. 2003), whereas Asian facilities (primarily in Japan) offer the opportunity to shake over 1000 tonnes.

The influence of dilatancy associated with stress profiles should not be forgotten when planning dynamic physical model tests. For example, stress-strain curves from undrained stress paths followed in dilatant soil were shown by Kutter (2006) to be counter-intuitive.

Ling et al. (2003) describe the behavior of a full-scale reinforced soil retaining wall, subjected to earthquake shaking, for validation of numerical analyses. The wall was instrumented with various transducers and was 2.8 m high (Fig. 3.5), which is the deepest soil model reported to have undergone excitation on a 1g shaking table to date. Kobe earthquake motions were simulated to excite the wall at a maximum base acceleration of 0.4g initially, followed by 0.8g.

The wall withstood the initial shaking (0.4g) with minimal deformation and an acceleration amplification of 1.35. The wall deformations, settlements and acceleration amplification were almost negligible (Fig. 3.6).

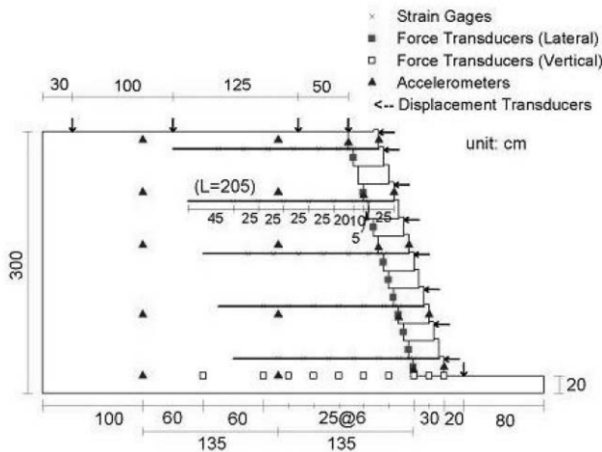


Figure 3.5. Cross section through an instrumented geogrid reinforced modular block retaining wall (Ling et al. 2003).

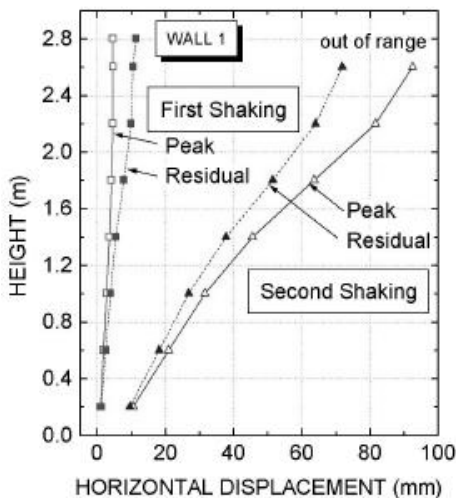


Figure 3.6. Horizontal displacement of the front of the retaining wall with height for both phases of shaking (Ling et al. 2003).

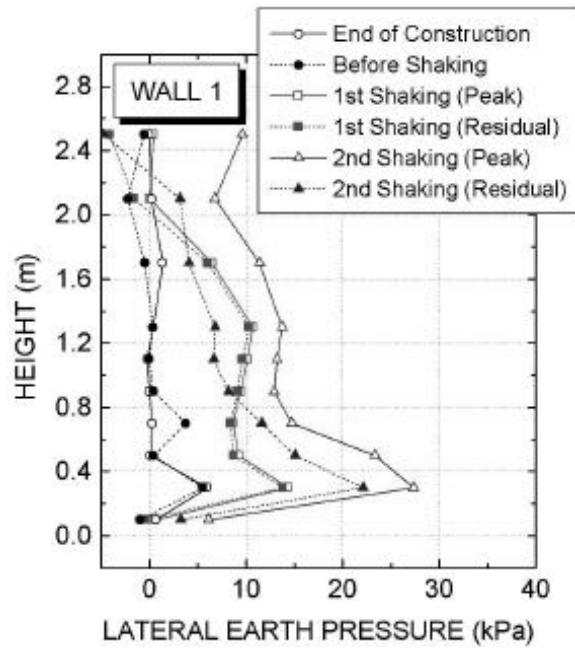


Figure 3.7. Peak and residual lateral earth pressure acting over height of retaining wall for the shaking phases (Ling et al. 2003).

Slightly larger horizontal deformations and settlements were observed during shaking with a peak acceleration of 0.8g, and the tension mobilized in the bottom two reinforcement layers increased noticeably. Lateral earth pressure (Fig. 3.7) acting behind the wall was only marginally larger at these lower depths, and the wall remained stable and serviceable. The 1g shaking table tests confirmed that the modular block system interacted effectively with the geogrid reinforcement to render this wall system stable when subjected to significant earthquake loading.

Bathurst et al. (2002) also cite a programme of 1/6th scale reinforced walls that were subjected to seismic base excitation. Subsequently, El-Emam et al. (2002) reported that the magnitude of accumulated lateral displacement in the facing decreased with reinforcement length and number of layers but that deformations were unaffected by the stiffness of the reinforcement materials used.

3.3.5 Dimensional analysis

Whereas centrifuge modeling is a powerful physical modeling technique, and diffusion and advection processes are modeled with advantageous, if contradictory, scaling laws on time in the model, care is still needed over creating a suitable stress history for the model to represent the current stress state and future stress paths. Validation of small scale modeling is critical to the growth of the use of this method.

Dimensional analysis has been used extensively to clarify whether similitude with a prototype can be achieved for a physical model. Ovesen (1975) was one of the early leaders in developing geotechnical centrifuge methods and technology. He investigated the influence of gravity level and scale on bearing capacity problems of footings on sand and wrote that although 'the idea of centrifugal testing of a soil model is simple in principle; the centrifugal testing technique involves serious difficulties in practical testing'. This remains true today and may even be more challenging through the increasing variety and complexity that is possible nowadays.

Ovesen confirmed through verification of models that ‘a model of a footing on sand built to the length scale $1/n_1$ subjected to an acceleration field n_1g yields the same bearing capacity as a model of the same footing built to a length scale $1/n_2$ subjected to an acceleration field n_2g – at least for $1 \leq n_1/n_2 \leq 3$.’ Subsequently, Ovesen (in Kerisel et al. 1979) compared similar tests to the previous ones carried out on a larger machine and elucidated the basic ideas of similitude and the importance of dimensional analysis in that:

- ‘the complete set of similarity requirements must be established by means of dimensional analysis’, and
- ‘departure from complete similarity must be justified by means of experimental evidence’.

Bucher (1996) lends further credence to the validity of centrifuge modeling through consideration of dimensional analysis for a slope of height H , soil density ρ and undrained shear strength s_u . $H\rho g/s_u$ (Table 3.2) becomes a key non-dimensional group related to the characteristic insitu stresses and strength.

Table 3.2. Unstable slopes: comparing key non-dimensional group for different modeling options (Bucher 1996)

Model	Prototype	1	2	3	4
Geometric scale	1:1	1:10	1:10	1:10	1:10
Acceleration	1g	1g	1g	1g	10g
H (m)	5	0.5	0.5	0.5	0.5
s_u (kPa)	15	15	1.5	15	15
ρ (t/m^3)	1.65	1.65	1.65	16.5	1.65
g (m/s^2)	10	10	10	10	100
$H\rho g/s_u$	5.5	0.55	5.5	5.5	5.5

Similitude of models, when defined by $H\rho g/s_u$, is guaranteed for the tenth scale models 2-4 but not for model 1, which is therefore not appropriate. Model 1 represents the traditional small-scale 1g laboratory test mentioned in Table 1. Adjusting either density (model 3), or undrained shear strength (model 2), without affecting the response (e.g. the deformation mechanisms), is challenging and so the recommended method remains to increase the gravity field (model 4). Despite achieving stress dependency with depth, errors may arise for a variety of reasons.

Ovesen (1979) carried out verification of models (known as modeling of models by Schofield 1980) by varying the gravity levels and scaling factors to represent exactly the same prototype. The proximity of lateral and base boundaries, the effect of particle size in comparison with a scaled down structural model (see also Craig 1994), interfaces and in shear zones, was described as scale and size effects. Schofield (1980) discusses the effect of the parabolic distribution of vertical stress with depth and different scaling relationships for dynamic load application and pore pressure dissipation and proposes effective modeling limitations and solutions that are still state of the art, whereas Palmer (2008) examines the use and misuse of models through dimensional analysis, pointing out where the latter can be misleading.

Some 32 years later, the ISSMGE TC2 Catalogue (Garnier et al. 2007) provides an up to date inventory of the scaling laws and similitude questions relating to centrifuge modeling. It bears testament to the significant progress made in understanding similitude issues, although some ‘unsolved problems’, still remain.

New scaling laws have been developed as geotechnical centrifuge modeling has been applied to solve multidisciplinary

problems within geotechnical engineering, and across other disciplines. For example, coupled transport including unsaturated phases, heat transfer, current propagation, electro-osmosis, aqueous and non-aqueous phase transport in soils and dynamics have been treated in the 2007 version, as well as fluid flow and erosion and sedimentation. The latter case was explored by Bezuijen & den Adel (2006) as they sought to model the influences of stress, groundwater flow and overtopping of dykes. Careful consideration of testing protocols is required in such cases. Additionally, the reliance of residual surfaces on a relative deformation scale cannot be scaled down in centrifuge model tests due to inaccurate scaling of strain localisation (e.g. Palmer et al. 2003).

The vast majority of nearly 100 geotechnical centrifuges in operation around the world today are beam centrifuges (see <http://www.tc2.civil.uwa.edu.au/>). Techniques have been refined over the past 30 years, and most new facilities (e.g. Ellis et al. 2006, Ha et al. 2006; Kim et al. 2006; Ma et al. 2006; Askarinejad et al. 2008) are able to mobilize their equipment and technology based on a significant prior learning curve. All of these new facilities have been installed and commissioned in the last half decade, and most are developing capacity to carry out seismic investigations with either one or two dimensional shakers, as well as in the more traditional areas of soil structure interaction and environmental geotechnics (e.g. Garnier et al. 2000). The first beam centrifuge has now been installed in Africa, close to the location of this conference, at the Mansoura Geotechnical Centrifuge Laboratory (El Nimr 2009).

Geotechnical drum centrifuges are relatively new, leaving room for significant further improvement in some testing methods and technologies. Drums have been installed by a few institutions in preference to a beam centrifuge, although the leading laboratories generally have both, to complement their capacity for physical modeling. Mostly, the more modern drums are oriented to rotate on a vertical axis, which creates challenging conditions in which to make models (Dean et al. 1990; Stewart et al. 1998; Springman et al. 2001; Miyake et al. 2002). Cambridge University (Barker 1998) and COPPE (Gurung et al. 1998; Fig. 3.8) have drums of diameters around 1 m that can rotate from the vertical plane to the horizontal during acceleration from stationary conditions to the nominal gravity level selected for the test. This facilitates preparation of models in ‘beam’ mode (see container in drum in Fig. 3.8).

Drums and beams have different yet compatible advantages and disadvantages. These are listed partially in Table 3.1. The examples following in sections 3.5 and 3.6 will focus mainly, but not exclusively, on activities in centrifuge modeling.



Figure 3.8. Drum centrifuge rotated on horizontal axis in soil preparation mode at COPPE, Rio de Janeiro (Photo: Springman).

3.4 Soil models

While physical modeling can be carried out on block samples extracted from the ground without significant further treatment or preparation for use in centrifuge models (e.g. Springman 1993), the parent soils are generally reconstituted or remoulded (Fearon & Coop 2000). Reconstituted or remoulded soils should create a more homogeneous deposit that would exhibit less spatial variation of soil types and be designed to achieve a specific distribution of strength and stiffness based on an applied stress history. Often such samples will be well modelled by CSSM (Schofield 1980).

More recently, Schofield (1998) commented that 'the geotechnical centrifuge model test solves the problem of applying Critical State Soil Mechanics to a wide range of boundary value problems' and that 'the geotechnical centrifuge is an ideal test apparatus for reconstituted soil, both on the wet and the dry side of critical states.' In the context of the backbone of this review, this confirms that discussions about soil behavior and testing should include a review of physical modeling, and especially that carried out on such soils in a geotechnical centrifuge.

Sands and clays have long been the traditional 'laboratory' soils used for small scale physical modeling, and are mainly provided by industrial suppliers to a given specification. Otherwise, characterisation of a local soil may be carried out in a reconstituted state (Küing 2003) and used in the same way (e.g. Nater 2002). Typically, clays are mixed under vacuum as slurry, and placed in strongboxes on the laboratory floor or in containers. Consolidation is carried out to a pre-defined stress history to achieve a specific strength profile with depth and may also take place under a hydraulic gradient to offer greater flexibility in the maximum effective vertical stress profile applied (Springman, 2003). Alternatively, slurry may be placed underwater and sedimented out in drum centrifuges in-flight, to create normally consolidated fine-grained deposits (e.g., Nater 2002; 2006; Weber 2007).

Sands are usually pluviated in air by means of point, line or plane hopper systems to produce dense sand samples (e.g. Ueno et al. 1998; Takemura 1998a&b) or through water to create deposits looser than relative density $I_D = 0\%$, as predicted by ASTM (2007), (Laue et al. 2005). Vaid & Negussey (1984) had postulated that the drop height effects are of no significance for pluviated through water, whereas the relative density achieved in air pluviated depends very much on the drop height, although the range of drop heights over which densification is effective depends on the average particle size. Size and shape of containers, wall friction, repeatability of density, inhomogeneity within the sample, effects of pluviated and saturation methods and mechanical properties achieved are the primary concerns.

Particular issues include both the way in which the grains fall, and the nature of the force alignment between the grains (Springman & Weber 2002). Hopper systems that promote sand heap formation should be avoided due to the tendency for these to adopt self-organized criticality, leading to creation of heterogeneous samples. Bolton et al. (1999) report the results of CPTs on centrifuge models prepared to the same specification by 5 European centrifuge laboratories, for which mainly hoppers and tubes were used to pluviate the sand deposit. They confirm that model-making that follows a common specification produces repeatable results when considered in terms of uniformity of q_c mobilized with depth.

Katagiri & Takemura (1998) describe a larger study, from ten laboratories, to investigate the influence of sample preparation of dry Toyoura sand on density determined from embedded sampling rings (Katagiri et al. 1998) and from CPTs (Takemura & Kouda 1998). Trends in data were very similar but a greater range of equipment was used, and this added to the variability in the measurements. A line pourer was preferred.

Automatisation of preparation methods for pouring large sand beds has seen improved consistency in desired relative density. Madabhushi et al. (2006) and Zhao et al. (2006) arranged to sweep a line pourer backwards and forwards over a container and achieved a variation of $\pm 4\%$ in I_D throughout the model, between a range from 50 to 90%. Generally, flow rate was demonstrated to be more significant at controlling the density than particle drop height, although boundary conditions influence results considerably (e.g. Garnier et al. 1992). This finding was supported by Grämiger (2001), from his pioneering sand placement tests using a rotating disc in a drum centrifuge, in which he obtained a linear correlation between flow rate and relative density within the range $20 < I_D < 70\%$. However, this method was also proven to produce a trend of density increasing across the sample width, i.e. from top to bottom in the drum (vertically) with the component of earth's gravity providing the stimulus for the tendency observed.

Nater (2006) and Weber (2007) discuss key considerations about constructing layered (sand-clay-sand) and soft clay models respectively in a large drum centrifuge. In both cases, the tests to be conducted on the soil lasted several weeks, so care was required to ensure the stability of the model as well as a consistency in the quality of clay model during several cycles of saturation and desaturation of sand layers, and between repeated application of 1 and ng. The stability calculations indicated that model would stand, although secondary effects, of which researchers should always beware, led to a dramatic slump failure during the first attempt at placing a 15 cm deep normally consolidated soft clay deposit. A geotextile had been placed below an underlying sand layer and caused the detachment. When successive 'charges' of 200 litres of slurry were placed under water and permitted to consolidate, vertical deformations during unloading dragged the geotextile down and away from the underlying sand layer, reducing the stabilising shear resistance mobilized between geotextile and sand, until failure occurred.

Maintaining humidity so that suction exists in sand layers, while continuing to ensure full saturation in the clay, so that it can respond immediately to fast loading in an undrained manner exhibiting constant volume, is a challenge. Further work is required from drum centrifuge users to bring the standard and consistency of model-making to the level of that achieved in beam centrifuges.

More recently, work has been reported on creating analogue rock materials and features to investigate (gypsum) rock toppling (Chen et al. 2006), stability of a jointed (sand-cement) rock wall with melting ice in sawtooth joints (Günzel & Davies 2006) and to enhance the occurrence of fragmenting in rock avalanches (Imre & Springman 2006; Imre et al. 2008).

Harris et al. (2008) froze silts with up to 25% clay in slopes with angles between 4-24°, from the surface downwards in a laboratory up to -10°C, before thawing under enhanced gravity in a centrifuge. Up to 4 model annual 'freeze at 1g, thaw at ng' cycles were conducted. Benefitting from the scaling of thaw consolidation, at n^2 faster than prototype, it was possible to examine soil behavior exhibited during periglacial solifluction and slope stability as a result of annual freezing cycles.

Centrifuge modellers are endeavouring to answer the criticism that their models are too homogeneous and do not represent the range of soil deposits found in practice. Recent work reported includes scaling studies to create centrifuge models of double porosity mine waste, with up to 1 m diameter clump sizes (Najser et al. 2009a). This has been stimulated by a desire to remediate significant tracts of land for further use for transportation corridors, for example to construct road embankments (Najser et al. 2008; 2009b) and investigate ground improvement options for bridge foundations (Pooley et al. 2007, 2008a&b, 2009) on these challenging deposits.

3.5 Crosscutting themes

Considerable progress has been made on many fronts in the last decade, all contributing to the current state of the art in physical modeling. Some crosscutting themes will be identified, a few examples will be cited and trends or special advances noted. In particular, the ability to work across the multiscale continuum from nano-, micro-, meso-, and macro- will be demonstrated subliminally.

3.5.1 Sensors

There has always been a focus on increasing miniaturization of devices. The technology has developed in two directions, either towards more cheap and cheerful sensors, which are less accurate but operate as a simple switch (e.g. Optoschmitt light detectors made by Honeywell 2003, in Chikatamarla et al. 2006) or the more expensive, sophisticated variety that deliver accurate measurement of a specific quantity. The trick is to combine them to obtain the best outcome for the physical model under investigation, without causing too much disturbance in the process.

Miniature transducers have been developed to determine stress (Garnier et al. 1999), pore pressure or suction within soil masses (Garnier et al. 2000; Take & Bolton 2003), and earth pressures on foundations and piles (e.g. Klotz & Coop 2001; White & Lehane 2004; Chen & Randolph 2007; Choy et al. 2007). Novel photometric probes have been designed to track groundwater pollutant tracers (Lynch et al. 2000; 2001). Some further examples are discussed in more detail.

3.5.1.1 Deformations

Whereas measurements of movements of surfaces or points may be achieved using laser systems, linear potentiometers or Linear Variable Differential Transformers (LVDTs), the ability to deduce measurements inside a soil body has been limited to insertions that may be excavated or photographed with X-rays after the test is complete (e.g. Springman 1993).

This misses an opportunity to determine when deformations along a future shear band have developed, which impoverishes the information received and misses an opportunity to expose such important data.

Whereas X-rays may be used effectively for observing shear banding in 1g physical models in the laboratory (e.g. Wolf et al. 2003), safety requirements in using X-rays in-flight in centrifuges are significant. As yet, in-flight Computed Tomography has not been reported in the literature, although it may only be a matter of time. Other forms of imaging will be discussed in Section 3.5.3.



Figure 3.9. TDR cables: 0.59 mm diameter 75 Ω (left), 1.02 mm diameter 50 Ω (right) (McAlister & Pierce 2001).

McAlister & Pierce (2001) present the concept of using miniature Time Domain Reflectometry cables in physical models to measure small, localized internal displacements. Coaxial cables were sheared in a modified direct shear device to acquire shear load and voltage reflection data as a function of shear box displacement. The results displayed the unique shear load and voltage reflection responses of each cable, with significant voltage reflections >50 mp produced at displacements up to 5 mm: a 75 Ω , 0.59 mm diameter miniature cable, was found to be slightly more compliant and weaker in shear than the 50 Ω , 1.02 mm diameter one (Fig. 3.9). Future trends will be towards even more diminutive and more compliant cables for instrumentation of small scale physical models, to locate shear zones as they develop.

Kitazume (2006) embedded carbon rods in pre-prepared columns for ground improvement in soft clays using the Deep Mixing Method (DMM), to improve temporal identification of column failure as part of the development of general kinematic mechanisms during embankment construction. Carbon exhibits low electrical resistance, which jumps to infinity when the columns fail (Kitazume & Maruyama 2007).

Hauswirth (2008) investigated the use of fiber optic cables (Brillouin Optical Time Domain Analysis BOTDA) in sandbox tests to make continuous measurement of distributed strain in a glass fiber cable, secured in the ground with a micro-anchor system. This technology will become more relevant in the future.

3.5.1.2 Normal total stress acting in soil

Lee et al. (2001) demonstrate adaptation of a Total Stress Transducer (TST) sensor for measuring total stress normal to it. The EPL-D12 TSTs (Fig. 3.10) were coated with a thin layer of silicone rubber before insertion into saturated clay beds. Calibration of the TSTs was conducted in soft clay inside a calibration chamber, under deadweight loading at 1 g. The registration ratio (Weiler & Kulhawy 1982) of this TST was about 0.7, indicating significant under-reading of the applied stress.

Attaching the transducer to an aluminum plate improved this ratio while also decreasing the amount of hysteresis between the loading and unloading phases. Lee et al. (2001; 2002) postulated that by altering the cell's aspect ratio, the stress arching effect over the TST was thereby reduced. One possible drawback was that the plate might interfere with any soil flow during the experiment, but this effect was minimized by keeping the width of the plate to a minimum.

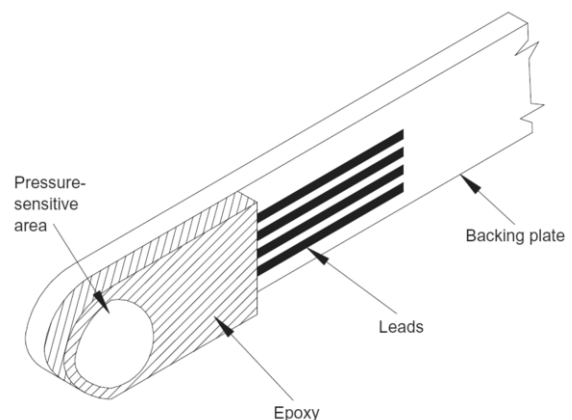


Figure 3.10. Entran EPL-D12 total stress transducer with backing plate measuring 7 mm wide 80 mm long 1.2 mm thick (Lee et al. 2001).

3.5.1.3 Normal total stress acting on an interface

Technology adopted from other fields (e.g. Springman et al. 2002; Laue et al. 2002b; Nater et al. 2003) has allowed real-time measurement of the bearing pressures up to a maximum of either 3.5 or 35 MPa (dependent on pressure range chosen), as they develop under a footing. A thin (0.1 mm) pressure sensor, as shown in Fig 3.11a, can be placed between footing and soil surface. Various shapes and sizes of sensor are available. Following careful calibration, normal stress may be determined at the crossing points of orthogonally oriented piezocables, which have a measuring cell area of 0.79 mm² and a spacing of 1.25 mm.

Total stress distributions were obtained for vertically loaded axisymmetric footings on homogeneous ground. There was initial concentration of load under the outer annulus at low percentages of failure loads, which became more uniformly distributed close to failure. Resistance was concentrated about the outer annulus throughout the entire loading range for vertically loaded footings on layered ground (Fig. 3.11b).

The same technology was also used by Chikatamarla et al. (2004) to measure the impact of rock falls on model protection galleries and to establish the optimal form of cushion material. These sensors are ideal for measuring normal pressures in a qualitative sense but may suffer from some time dependency in terms of drift or when there is a significant component of shear stress. Impact pressures are shown in Fig. 3.12a&b, for a gallery with, and without, a sand cushion.

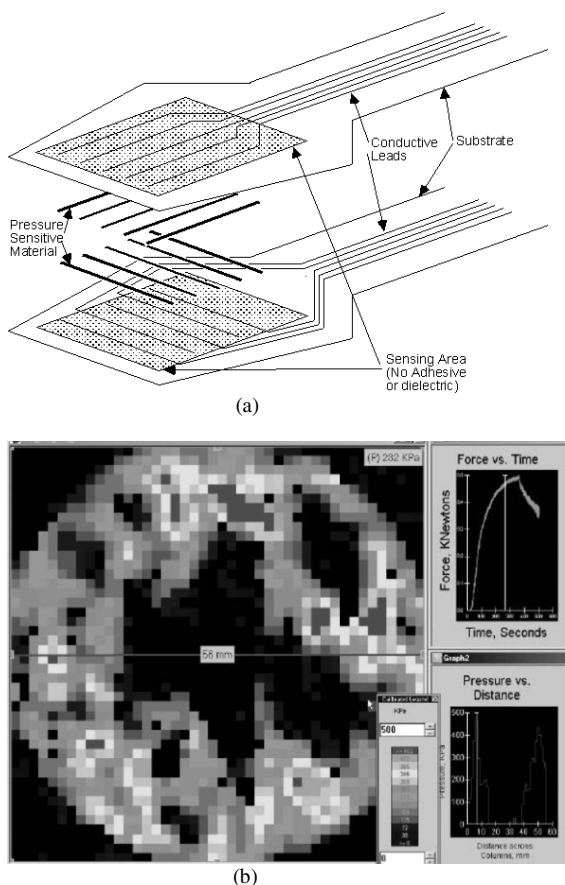


Figure 3.11. Contact stress measurement: (a) pressure sensor (Tekscan 2002); (b) stress distribution (above left), contact stress profile underneath an axisymmetric footing (below right) with a model diameter of 56 mm, mean sand grain diameter of 0.28 mm at a g-level of 12.5g on layered ground close to peak load (above right) (Springman et al. 2002; Nater 2006).

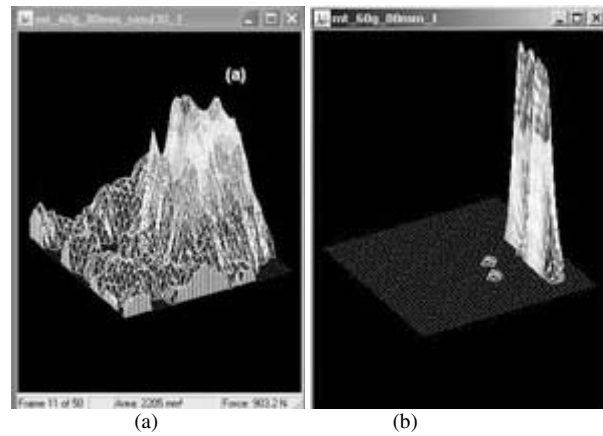


Figure 3.12. Contact stress measurement of the impact of a boulder on a model protection gallery: (a) with a sand cushion; (b) with no protection (Chikatamarla et al. 2004).

3.5.2 Mechatronics & Robotics

Laue (2002a) and Sharma (2002) both note the increasing sophistication of models that require realistic simulation of geotechnical construction processes. Improved control through miniaturized electronics and microcomputers enables finer steering of actuation that can be conducted under more degrees of freedom than previously was possible. Additionally, more data have been obtained and stored through increasingly powerful data acquisition systems (more data, more frequently).

3.5.2.1 Actuation

With rapid advances in mechatronics and robotics, each centrifuge laboratory has created their own multipurpose actuation system to examine soil behavior. Derkx et al. (1998) from the Laboratoire de Ponts et Chaussées LCPC, Nantes, reported the design of an on board remote controlled centrifuge robot. It is mounted on top of the strong box container on a beam centrifuge (Fig. 3.13) to handle materials with a device with pincers, and to apply loads in any direction: x, y, z, θ .

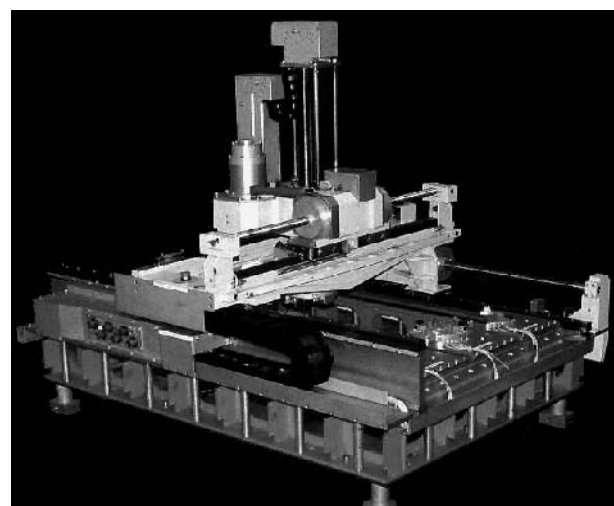


Figure 3.13. LCPC Nantes Robot (Derkx et al. 1998).

Ng et al. (2002) followed on in creating a 4 axis robotic simulator that is capable of carrying out a multitude of

activities: excavation, fill, compaction, soil extraction, all in-flight without stopping the centrifuge. More recent examples include pile tests in the x - y - z - θ planes under lateral and torsional loading (Kong & Zhang 2006). Ubilla et al. (2006) loaded stiff monopile foundations laterally and Hao et al. (2006) tightened ground anchors to pre-stressing levels in the centrifuge.

Actuation benefits greatly in a drum centrifuge from the space available in the centre, as well as that for run out experiments. Following development of an earlier run out chute (Bowman et al. 2006; 2007), Imre (2008) designed diametrically opposed bottom opening hoppers (Fig. 3.14; A & B). These were packed with cubic soft analogue rock boulders that could be released at the base by pneumatic control, from a pressure vessel charged with air at 8 MPa to create a rock avalanche.

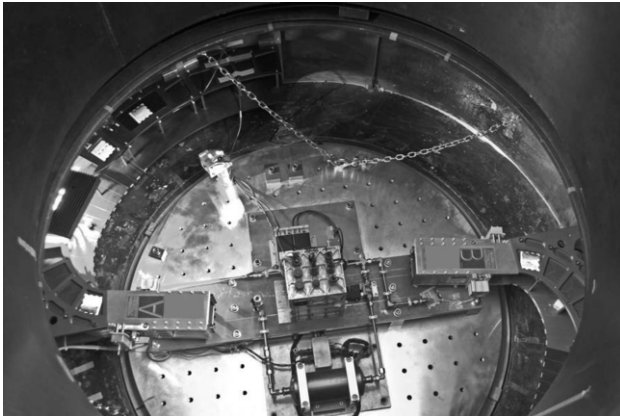


Figure 3.14. Hopper and chute system for rock avalanches mounted in the ETHZ drum centrifuge, with pressure vessel at bottom centre of the figure (Imre 2008).

3.5.2.2 Installation devices

In order to replicate soil behavior in physical models, guidance has been taken over the years from the response of soil in element tests, as summarized in Section 2. Consequently, sophisticated installation devices have been developed to replicate the prototype stress paths. Some recent examples that lean heavily on the advances in mechatronics and robotics are discussed.

An in-flight miniature pile hammer was first reported by Allard (1984). Since then, the state of the art robot systems offer opportunities to drive or jack-in piles as well as devices designed exclusively for this purpose (e.g. De Nicola & Randolph, 1997; Pan et al. 1999). In the last half decade, this has become standard actuation equipment. Dyson & Randolph (2001) show the effect on lateral pile resistance of installation methods and confirm the importance of replicating the prototype stress paths during construction in the model.

Gaudin & Lehane (2006) describe the complete in-flight installation of a pile group (Fig. 3.15). Each pile is jacked into the ground independently through a template and then the cap is lowered over the pile heads and fitted in place. This avoids the need to cycle the centrifuge gravity from n -1- n gravities, while fixing the pile cap, which is advantageous from the point of view of the soil response.

Al-Khafaji & Craig (2000) placed sand columns beneath a tank foundation as ground reinforcement at 1g in a grid of pre-bored holes. Subsequently, Lee et al. (2001) advanced the physical modeling of ground improvement further by constructing sand compaction piles 'in-flight' in the centrifuge in order to represent the influence of stress paths on the system

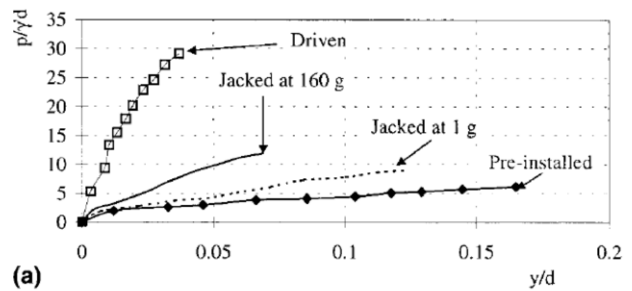


Figure 3.15. Installation of piles; a) influence of methods, in-flight or on ground, on pile normalized lateral pressure $p\gamma/d$ with γ unit weight and d pile diameter (Dyson & Randolph 2001); b) pile group (Gaudin & Lehane 2006).

response. These authors examined the performance of Sand Compaction Piles (SCPs) installed using three different methods: the frozen pile method, a 1 g displacement method that injected sand into a soft clay bed (Lee et al. 1996), and a high-g displacement method that was achieved by injecting sand forcibly using an Archimedes screw into a soft clay bed at high-g (Ng et al. 1998).

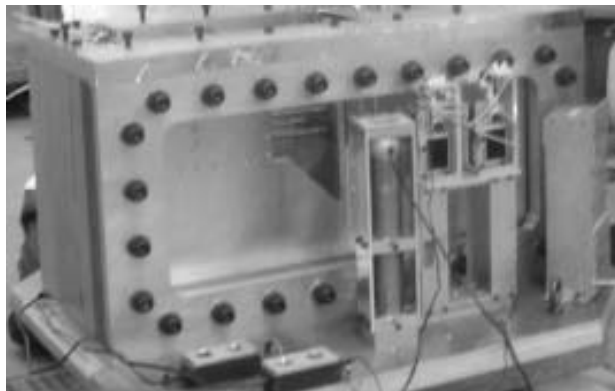
Weber (2007) used a different method for improving ground beneath base reinforced embankments. He developed a tool to transfer sand to a lightly over-consolidated clay deposit, which could then advance and withdraw from a cylindrical hole created in-flight for this purpose. Sand was poured through the tool from outside the drum centrifuge, and compacted through this process, increasing the lateral earth pressure coefficient in the surrounding clay and improving the settlement response and the bearing capacity of the sand compaction piles.

Several studies have been conducted to represent the performance of geosynthetic walls in the centrifuge. Notwithstanding the difficulties in modeling the construction techniques and representing the mobilisation of strain along the reinforcing layers, some useful insights have been obtained (Springman et al. 1997).

Ilamparuthi & Dickin (2001) model belled piles embedded in various forms of geogrid layers and rings, the latter system providing the most stiffness and strength. Pullout resistance increased with diameter of the geogrid ring, sand density, bell diameter and embedment.

Suction pumping has also been adopted to install anchors (Gaudin et al. 2006a&b) and suction caissons (Senders et al. 2006; Chen & Randolph 2007) in normally to lightly over-consolidated clays. Chen & Randolph (2007) investigated the external radial stress changes around the caisson and varied the state of the soil by adding sodium hexametaphosphate ($\text{Na}_6\text{O}_{18}\text{P}_6$) solvent to the kaolin slurry to increase the sensitivity

by a factor of 2. As consolidation proceeded, there was some relaxation of the radial total stress around the caisson, and since such soil response would be greatly affected by the stress paths followed during installation, this confirmed the necessity of modeling installation as faithfully as possible to deliver relevant predictions.



(a)



(b)

(c)



(d)

Figure 3.16. Devices and set up for excavation in front of a retaining wall in-flight a) cross section, b) close up on wall and struts, c) birds' eye view on top of wall, d) cutting device with cutouts for the parallel struts (Photographs Sarah Springman).

3.5.2.3 Construction techniques

The challenge of modeling the stress paths during installation and excavation in front of embedded wall has been considerable. Initially, in-flight excavation in front of such walls was achieved by draining heavy fluids from a bag, which was recently enhanced by Richards & Powrie (1998), who added props during the modeling of the construction process after Powrie and Kantartzi (1996) had earlier managed to concrete diaphragm walls in-flight.

A cutting blade can be advanced and lowered into soil in front of a wall, which is then scraped horizontally to excavate a layer into a collecting bucket (e.g. Kimura et al. 1994; Loh et al. 1998; Takemura et al. 1999; Laue 2002a). Gaudin et al. (2002) describe the use of the LCPC robot to execute the same construction process. Figure 3.16 shows the equipment developed recently in Cambridge (Bolton et al. 2006).

3.5.2.4 Environmental chambers

An environmental chamber has been designed by Take & Bolton (2002) to impose appropriate environmental boundary conditions on centrifuge models of clay embankments (Fig. 3.17). The chamber is sealed to prevent moisture transfer from the model to the external surroundings, and regulates the relative humidity of the air in the chamber, and subjects the embankment to model rainfall from atomising mist nozzles.

Tristancho et al. (2006) describe the design of the next generation of such chambers that proposes to control insolation, wind velocity, atmospheric pressure, air temperature, rain intensity and relative humidity.

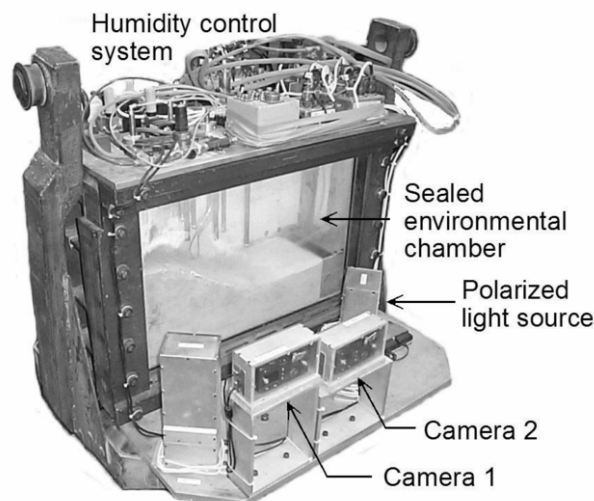


Figure 3.17. Environmental chamber and multi-camera image acquisition system (Take & Bolton 2002).

3.5.3 Imaging

The digital imaging revolution in geotechnical physical modeling has been stimulated by the work of Take and White in Cambridge (e.g. Take & Bolton 2002; White & Bolton 2002; White et al. 2003), who processed digital images taken in-flight (Fig. 3.17) using Particle Image Velocimetry (PIV) and close range photogrammetry, in which the texture of the soil is used to track movements rather than using automatic target tracking systems (Taylor et al. 1998; Paikowsky & Xi 2000). Based on earlier developments in experimental fluid mechanics (e.g. Adrian 1991), they created a functional, cost effective system with precision finer than 0.1 pixels, such accuracy being essential when amplifying displacements measured under the centrifugal factor n .

Take & Bolton (2002, Fig. 3.18) used PIV initially to show development of tension cracks prior to progressive failure in overconsolidated embankments. Subsequently, segments of overconsolidated clayey rubble formed a mass movement event. Such a mode of failure cannot be modelled using finite element analysis, even with the benefit of the Schofield model, a variation of Original Cam Clay on the wet side of critical state

with a tension crack failure criterion and a Hvorslev rupture criterion on the dry side (Britto & Gunn 1987).

Gourvenec & O’Loughlin (2006) conducted half-footing tests against a Plexiglas window in a modified strongbox in a drum centrifuge for semi-circular shallow foundations with short skirts on reconstituted normally consolidated kaolin, subjected to combined load paths. Digital photography and Particle Image Velocimetry (PIV) exposed the kinematic mechanism accompanying failure of the foundation (Fig. 3.19; White et al. 2005).

X-ray techniques portray differences in density of the granular material in 1g models, as a precursor to shear band formation, and thus offer the opportunity to record changes in

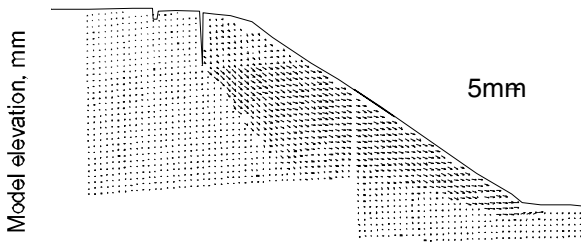
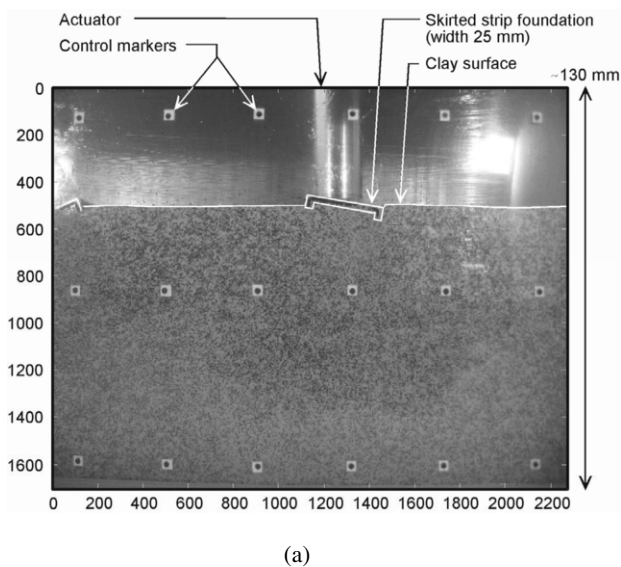
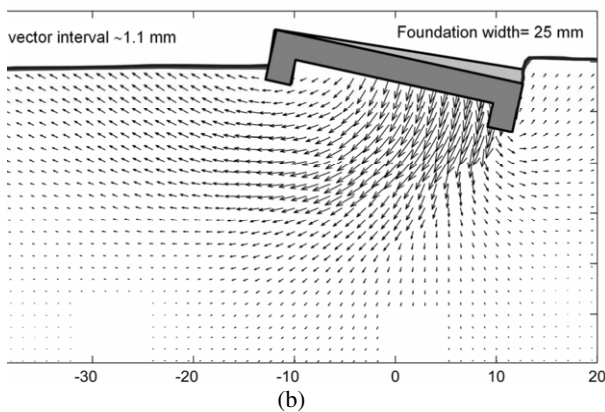


Figure 3.18. Deformations induced by rainfall, exhibiting tension cracks at the crest determined from PIV analysis (Take & Bolton 2002).



(a)



(b)

Figure 3.19. Half skirted strip foundation, (a) on clay with artificial texture, (b) Displacement vectors derived from PIV image following loading (White et al. 2005).

the granular structure inside a specimen (Oda et al. 2004; Borsic et al. 2005). Wolf et al. (2003) made continuous observation of shear band formation and spacing using X-ray techniques (Fig. 3.20) and matched the data with measurements made within a precision of 0.125 mm, also using image analysis with PIV, to determine strains and rotations in the granular structure.

Moving to the nano-microscale, recent growth in Environmental Scanning Electron Microscopy (ESEM) has revealed valuable information about changes in fabric and structure at particle scale that explain modes of soil behavior occurring under field scale stresses in centrifuges. Soil stabilization (Rittirong et al. 2006; 2007) and changes in soil structure invoked by installation effects (Weber et al. 2009) are examples that will be described briefly.

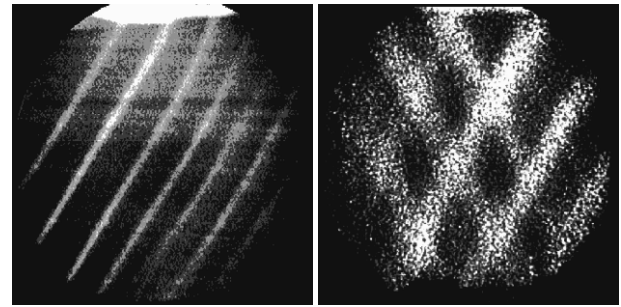


Figure 3.20. X-ray photographs showing effect of average grain size d_{50} on shear band formation: (a) $d_{50} = 0.35$ mm and (b) $d_{50} = 1.58$ mm in quartz sand (Wolf et al. 2003).

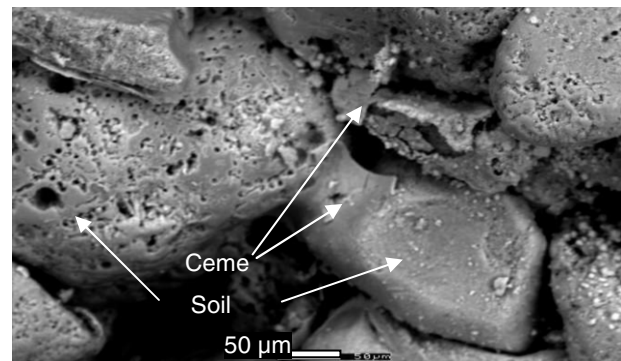
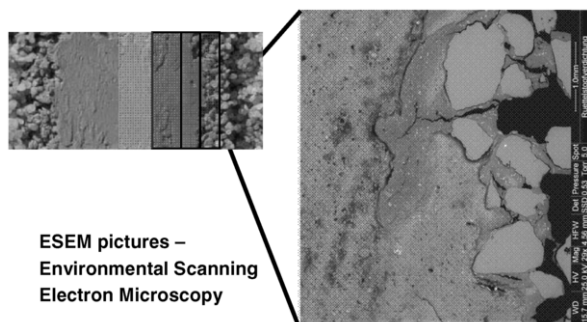


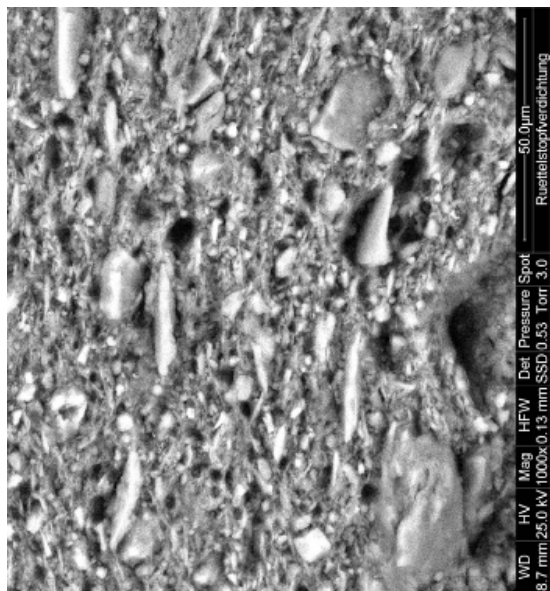
Figure 3.21. Electron microscopic image of calcareous sand after electrokinetic treatment (Rittirong et al. 2007).

Electrokinetic and electrochemical stabilization of model caissons embedded in offshore calcareous sand was investigated by Rittirong et al. (2006; 2007), who used X-ray diffraction analysis (XRD) to determine changes in mineralogy, X-ray fluorescence analysis (XRF) to investigate precipitated iron, as well as ESEM to inspect the new microscale structure (Fig. 3.21).

The pullout resistance of an identical model caisson in stabilized soil increased by up to 120% compared to data from untreated soil. Polarity reversal and application of a stabilization agent enhanced the effectiveness of the electrical treatment and increased resistance to pull out significantly, confirming the potential for this mode of ground improvement.



(a)



(b)

Figure 3.22. Environmental Scanning Electron Microscopy of the zone around the sand compaction pile: (a) showing the indentation of sand particles into the clay, and successively less disturbed zones in the clay; (b) 120x120 μm ESEM picture at from the centre of the box in a) (Weber et al. 2009).

Weber et al. (2009) investigated the nano-micro-mechanical response around a sand column installed by penetration of a bottom feed poker, which was withdrawn in cycles of extraction and penetration to compact sand into the surrounding soft clay. Detail of the soil structure was revealed by ESEM pictures (Figs. 3.22a&b) showing a residual shear (smear) zone in the clay around the sand column (Fig. 3.22b). This would be likely to have a lower radial permeability, even before any clogging might develop when the sand compaction pile was acting as a drain in service. Local densification of the annulus beyond this zone due to radial cavity expansion was also exposed by Mercury Intrusion Porosimetry.

Driving mechanisms behind frozen fringe and ice lens formation in fine-grained ‘frost susceptible’ soils (Fig. 3.23) were examined in small scale models at 1g by Arenson et al. (2007; 2008). Improvements in measuring techniques using a fluorescent tracer exposed to Ultraviolet light, linked to PIV analysis of displacements, led to detailed observations of ice lens formation under 1D confinement. A single cycle of freezing (from the top down) was applied to the silt. Water migrated through the frozen fringe from the unfrozen soil towards the warmest ice lens, with clearly paradigmatic response, while colder ice lenses continued to grow without access to the unfrozen zone, as water was sucked from soil beds between ice lenses.

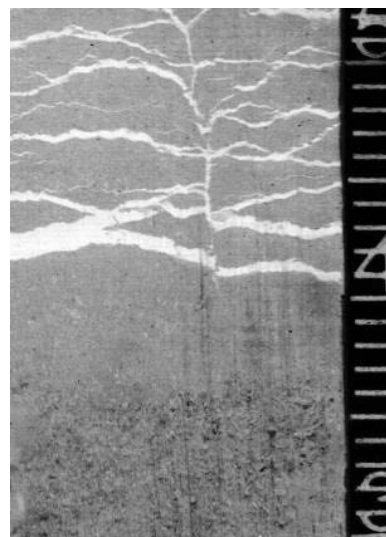


Figure 3.23. Devon silt frozen from the top, with fluorescent tracer showing saturated zone at the base, frozen fringe and ice lens formation (Arenson et al. 2008).

A study involving centrifuge testing and digital image analysis was conducted by Zornberg & Arriaga (2003) in order to obtain the strain distribution within geosynthetic-reinforced slopes under prefailure conditions. Specifically, digital image analysis techniques were used to determine the displacement distribution along reinforcement layers in reduced-scale models subjected to increasing g levels. Analysis of reinforcement strain results showed that the location of the reinforcement maximum peak strain did not occur near the toe of the structure, but was located approximately at midheight of the reinforced slopes, at the point along the critical failure surface directly below the crest of the slope. The pattern of reinforcement peak strain with height obtained for prefailure conditions was similar to that obtained for failure conditions. The estimated factor of safety was found to be a good indicator of the magnitude of the reinforcement maximum peak strain for geosynthetic-reinforced slopes built with different configurations.

3.5.4 Data capture & storage

In the spirit of creating open access to data, Schaminée et al. (2006) describe a data exchange standard that was being used for CPT data in the Netherlands. Data were archived in a repository for autonomous analysis with data handling achieved through a geotechnical exchange format (GEF) language, which offered both efficiency and flexibility.

Swift et al. (2004) describe a similar idea used for the NEES groups so that soil behavior could be experienced from physical modeling hosted by one research node and shared with others over an Internet access, which could also steer the direction of the tests. Access to the data repository would then be permitted to those interested in further analysis.

Given the vast amount of digital data that is stored, partially unused and without analysis to date, the idea of a GEF (Schaminée et al. 2006) for physical modeling has some merit. Members of a TC2 subgroup are currently working towards establishing standards for saving, exchanging and archiving model test data. This would promote easy viewing, manipulation and comparison of test data within the physical modeling community and allow sharing of post-processing software within and between institutes, based on data archived in a standard form.

3.6 Applications

This section focuses on current key research 2gvdirections that may contribute to understanding soil behavior within boundary value problems. These opportunities enhance existing possibilities with laboratory and insitu testing and do not yet include issues that are necessarily easy to resolve under hyper gravity. On the other hand, models are often used when it is impossible or unpractical to create experimental environments to measure outcomes directly – so idealized conditions are controlled with some assumptions and a simplified view of complex reality. Some recent applications of physical modeling have been selected where this approach is particularly beneficial and where finite element analysis will be challenged to give accurate predictions. This cannot be a complete summary of the work conducted around the world, indeed soil dynamics, earthquake and geoenvironmental engineering will be treated in other State of the Art contributions, although a brief comment on the latter is included here.

3.6.1 Themes benefitting from physical modeling

Progress has been made in fundamental understanding of several processes in environmental geotechnics and the application in a centrifuge, where complete similarity of all relevant nondimensional groups is not possible (e.g. Culligan & Barry 1998; Gay & Azouni 2000; Levy et al. 2000; Marulanda et al. 2000; Barry et al. 2001; Garnier et al. 2002; Almeida et al. 2000; Oung et al. 2005). Non-aqueous phase liquids (NAPLs) add to the complexity of predicting transport phenomena through liquid density contrasts and interfacial tension between contaminant interstitial fluids. Physical model tests have been used many times to test hypotheses and understand fundamentals of multiphase flow and other significant modes of behavior.

Culligan & Soga (2006) discuss, in a recent state of the art report, flow of contaminants in various media including heterogeneous models and fractures. Examples relating to source zone characterization, source plume remediation, NAPL remediation and air sparging were cited with key concerns and lessons learnt.

Physical modeling earns a valued place in the spectrum of investigatory techniques for problems dominated by response outside the well bounded modes of analysis, such as for drained or undrained soil behavior, or when moving away from standard fields of investigation (e.g. Gaudin et al. 2006a,b&c), where scaling laws are well understood. Strain rate effects during soil characterization, installation of devices, load carrying members, equipment, or application of complex load histories may often be modeled more effectively with an appropriate physical model than numerically. The creation and dissipation of pore pressures, including partially drained (consolidation) processes form the focus of research in many institutions: for footings (Gaudin et al. 2006c), suction caissons (Senders et al. 2006), drag or plate anchors (O'Loughlin et al. 2006; Gaudin et al. 2006a) or pipelines (Gaudin et al. 2006d; 2007).

The formation and treatment of tension cracks and cavity formation in finite element analyses continues to present some challenges, whereas these modes of soil behavior may be revealed under appropriate replicated stress conditions in centrifuge tests. Take & Bolton (Fig. 3.18; 2002; 2003) demonstrated this for embankments of heavily overconsolidated clays, as Bolton and Powrie (1987, 1988) had done earlier for retaining walls in soils with a similar stress history.

More recent examples include two forms of physical modeling adopted by Van (2003) to investigate the sudden failure through uplift at the toe of an ancient peat embankment that had dried out during the hot summer in 2003. A wooden pile wall had been installed on the water side to reduce seepage,

however this provided a 'wound' in the ground and a preferential seepage path into the underlying gravel aquifer under full hydrostatic pressure.

Similarly, the catastrophic failure of the New Orleans embankments were exposed by Steedman (2006) as part of the IPET (2007) investigations, in which sheet pile walls had been driven into the crest of existing embankments to raise the effective protection height against river floods for the houses in the shadow of these dykes. Local pre-failure deformations led to additional modes of failure from those considered at the time of approval of this remediation method. Lateral deformation of the sheet pile wall opened up a crack on the river side of the wall, permitting the full hydraulic pressure to be transmitted to the base of the sheet pile wall, causing reduced effective stresses and hence lateral resistance in the passive zone on the land side.

Large deformation problems can be investigated beneficially in physical models, especially since influence on bearing capacity and resistance may be examined and parametric studies can deliver valuable insights. Richardson et al. (2006) investigated several aspects of behavior of deep penetrating anchors including the effect of tip shape on anchor embedment in the beam centrifuge. Mechanisms concerning punch through of spud footings, and cavities forming behind spudcans (Hossain et al. 2006) or anchors following installation and loading at depths greater than the controlling scalar dimension of the structure can all be informed by appropriately scaled centrifuge model tests.

Recent physical modeling experiments have investigated modes of limiting ground movements and compared outcomes with both field and numerical data. Addenbrooke et al. (1997) and, more recently, Franzius et al. (2005) noted that despite advances in constitutive models, anisotropy in the ground is still not represented well for calculating plane strain and three dimensional settlement troughs following excavation of tunnels. Jacobsz et al. (2001), followed by Chung et al. (2006a), investigated the loss of stiffness and bearing capacity of instrumented piles due to nearby tunnel construction in a beam centrifuge, showing interaction mechanisms between essentially elastic and plastic regimes as tunnel volume loss increased (Fig. 3.24). Ghahremannejad et al. (2006) collapsed tunnel sections in 1g model tests to observe settlements and increase in bending moment in the piles, although the low stress levels will have influenced dilatancy in the Sydney sand used.

Honda et al. (2001) used 0.58 mm diameter steel wire as nails, installed in a variety of modes in dense Toyoura sand. Three options were considered with nails vertical from the surface to roughly half the cover, radially from the upper half of the tunnel orthogonally to the lining and with inclined crossed nails extending to tunnel shoulders.

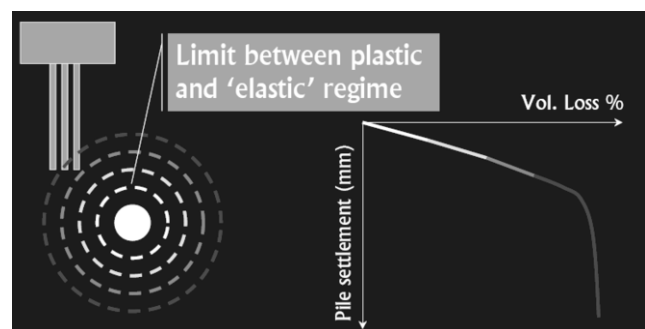


Figure 3.24. Tunnel-pile interaction mechanisms showing link between pile settlement and volume loss in the tunnel and relationship to elastic and plastic regimes (Mair 2003).

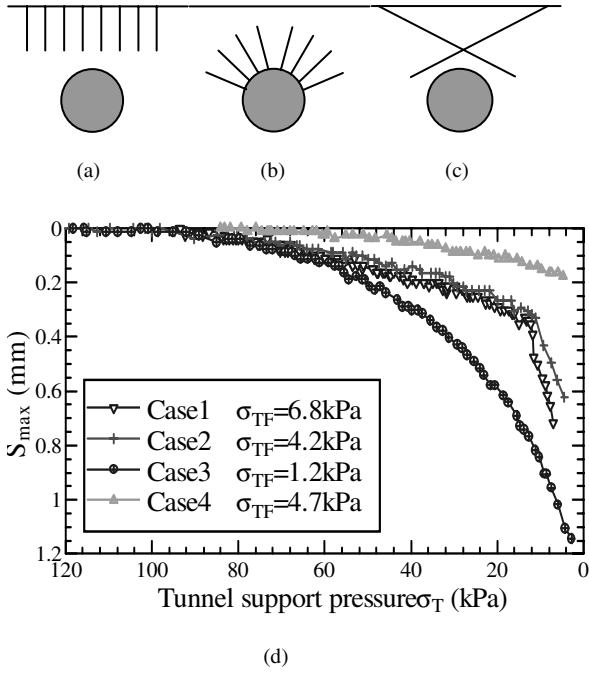


Figure 3.25. Tunnel in Toyoura sand with $I_D = 80\%$, Cover/Depth = 1, Tunnel Diameter = 50mm in 100g, no nails for Case 1, (a) vertical nails from the surface, Case 2, (b) radial nails in upper tunnel, Case 3, (c) diagonal nails, Case 4, (d) maximum settlement at ground surface above the tunnel S_{max} as a function of reducing tunnel support pressure σ_T with σ_{TF} denoting the value at failure (Taylor 2004 after Honda et al. 2001).

Figure 3.25 shows that stability was improved most by the radial nails whereas ground movement was limited most effectively by the crossed nails that stiffened up the circumferential response and prevented zones of high shear strain from developing.

Bilotta (2008) installed smooth and rough model diaphragm walls between a tunnel and a building (not shown on the right hand side of the model) to shield the latter from unwanted ground movements during excavation (Fig. 3.26a). Whereas the settlement troughs either side of a rough wall did not differ greatly from a reference solution without any walls at all, smooth diaphragm walls were very effective at limiting the movements to the right of the wall, shown with an arrow in Fig. 3.26b. However, the air pressure required to support the tunnel was greater. McNamara & Taylor (2002) installed settlement reducing piles in excavations in a beam centrifuge, lowering heave in front of the wall, lateral movements in the ground and limiting the settlement trough behind the wall (Fig. 3.27).

Katzenbach et al. (2006) calibrated a numerical model for pile, soil-wall interaction, from small scale 1g tests to make a very simplified allowance for dilatancy within the linear elastic perfectly plastic Mohr Coulomb constitutive model, and a constant angle of dilatancy of 10° .

Complex multi-degree of freedom loading combinations can be applied as well (Bienen et al. 2006). These can include torsional (Bienen et al. 2007), cyclic reversal of lateral loading on piles (Levy et al. 2007), cyclic loading of suction caissons (Watson & Randolph 2006; Senders et al. 2006) and many other variations.

3.6.2 Characterization

Following on from early efforts by Luong (1994) and Siemer (2000) to measure travel times for Rayleigh, compression (p) and shear (s) waves, recent development of wave propagation techniques in the centrifuge includes use of spectral analysis of surface waves (SASW) (Murillo et al. 2006) and seismic

tomography using arrays of bender elements (Rammah et al. 2006). Techniques used in the field and the laboratory have been transported effectively to the hyper gravity environment. Further growth is expected in this area.

In a reverse of the usual innovation cycle, Chung (2005) and Chung et al. (2006b) conducted miniature CPT, ball, T-bar penetrometer and extraction tests to compare predictions of undrained shear strength profiles for tests insitu, in reconstituted models in a beam centrifuge and also from undisturbed samples in triaxial tests. Bearing capacity factors were also determined for each device and cyclic soil response was investigated including partial drainage and possible time dependent, viscous effects. These methods, developed from early work by Stewart & Randolph (1991), are now in use in practice for characterization of fine-grained soils for both on and offshore engineering applications. The latest development is that of a miniature cone pressuremeter (Thorel et al. 2007) that is still in its infancy but offers promise for lightly overconsolidated fine-grained soils in which the strength and stiffness may not vary significantly over the length of the small scale probe.

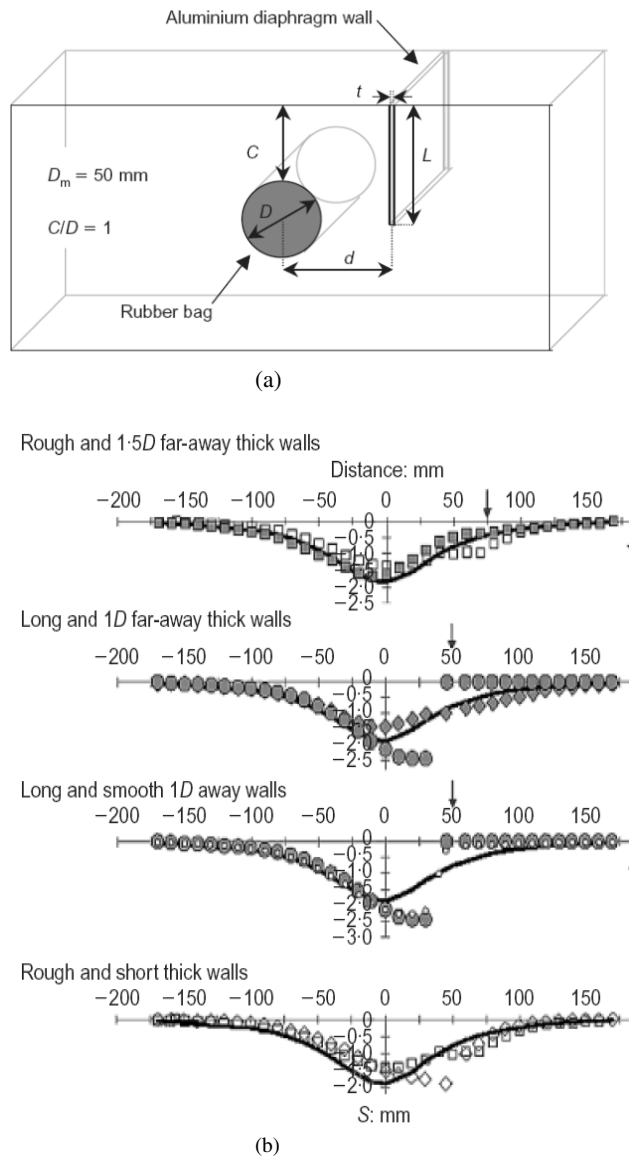


Figure 3.26. Diaphragm wall adjacent to a tunnel to mitigate ground movements during construction, (a) model geometry, (b) experimental data, compared to a reference test with no wall (line) and smooth walls denoted with a circle, the remainder being rough (Bilotta 2008).

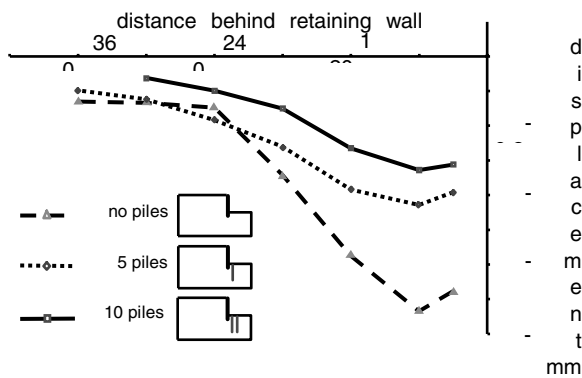


Figure 3.27. Settlement at model scale behind a retaining wall, with one, two or no rows of settlement reducing piles in the excavation (Taylor 2004 after McNamara & Taylor 2002).

3.6.3 Flow processes

Centrifugation has been used to increase the body forces on a porous media to alleviate the shortcomings of conventional characterization of unsaturated hydraulic properties. The centripetal acceleration field causes fluid to drain from the specimen at a rate quadratically proportional to the g -level (Dell'Avanzi et al. 2004).

Centrifuges were first used in the early 1930's to define the moisture retention curves by soil scientists (Gardner 1937) and petroleum engineers (Hassler & Bruner 1945). A saturated specimen was typically placed upon a saturated ceramic plate, which conducts only liquid. During centrifugation, the increased body force causes water to exit from the specimen through the ceramic. Air enters the specimen surface, and suction is developed.

Centrifuge testing has been used to define the relationship between hydraulic conductivity and suction in the design of evapotranspirative covers (Zornberg et al. 2003). Nimmo et al. (1987) developed the Internal Flow Control Steady-State Centrifuge method, which uses a system of reservoirs to control the fluid flow rate and suction at the upper and lower surfaces of a specimen. Conca & Wright (1994) developed the Unsaturated Flow Apparatus (UFA), which uses a rotary joint to provide a low fluid flow rate into the specimen.

Until recently, centrifuge technology did not allow the direct acquisition of relevant variables (suction, moisture, discharge velocity) for tests under very high g -levels. However, the shortcomings in characterization of the unsaturated hydraulic characteristic of porous materials have driven development of a Centrifuge Permeameter for Unsaturated Soils (CPUS). This device incorporates a low-flow hydraulic permeameter and a high- g (approx. 600 g 's) centrifuge capable of measuring suction, continuously, non-destructively and non-intrusively moisture content, and fluid flow rate in a single specimen during centrifugation (McCartney & Zornberg 2005). Accordingly, CPUS expedites determination of the moisture retention curve and hydraulic conductivity functions from a single specimen in a single test.

The CPUS is shown schematically (Fig. 3.28) with instrumentation layout, including heat dissipation units (HDU) for monitoring suction and time domain reflectometry probes (TDR) to monitor moisture content continuously. A low-flow fluid union has been developed to supply fluid from the stationary environment to the rotating specimen within the centrifuge. An infusion pump is used to supply flow rates ranging from 0.1 to 100 ml/min to the fluid union. The inflow is dispersed to the specimen using an overflow distribution cap.

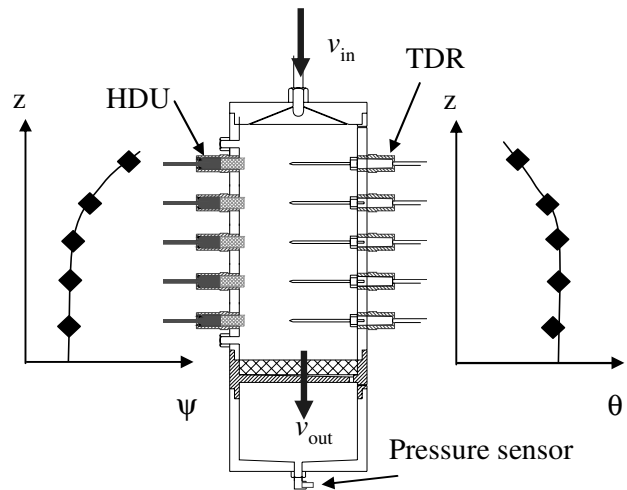


Figure 3.28. Moisture and suction measurements in centrifuge permeameter (McCartney & Zornberg 2005).

3.6.4 Natural hazards

Harris et al. (2008) modeled identical prototype shallow slopes (Fig. 3.29), frozen as discussed in Section 3.4, undergoing solifluction at different geometric scales and gravity levels, to show that deformations measured scaled consistently with time, according to $1/n^2$.

They attributed their results to plastic straining resulting from thaw consolidation, which could be represented by a coupled thermo-hydromechanical Cam Clay based CSSM, rather than at a direct 1/1 linear scale with time that would represent viscous flow.

Take et al. (2004) and Olivares & Picarelli (2006) cite the phenomenon of spontaneous static liquefaction arising due to small perturbations for loose saturated soils in connection with flowslides and hazard assessment (Fig. 3.30), in which it becomes clear that risk reduction may be best achieved by preventing failure in the first place. Static liquefaction (Chu et al. 2003) may be explained, within CSSM, by undrained effective stress paths reaching an Instability Line (IL), while mobilizing ϕ'_{IL} , and accompanied by contraction of the soil matrix. This causes sudden increase in pore pressures that reduce mean effective stress and lead to loss in mobilized deviatoric stress as the stress path approaches a state of full liquefaction.

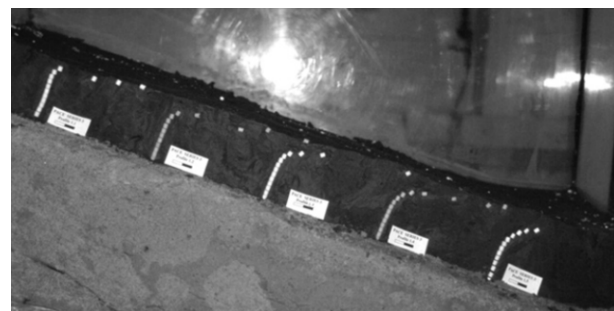


Figure 3.29. Soil movement shown by markers after 1 thawing cycle of thawing (Harris et al. 2008).

Take et al. (2004) obtained PIV data for loose fill slopes in which it was thought that either static liquefaction or a transition of landslide to flow slide could be expected to occur. Despite observing significant collapse settlements due to rainfall in a previously unsaturated loose fill (Fig. 3.31), high

excess pore pressures were dissipated through air mobility in the void space in the loose fill. More danger was witnessed for constricted flow in layered slope systems, which could transmit a slow moving slip into a rapid flow through localized transient pore pressure rise.

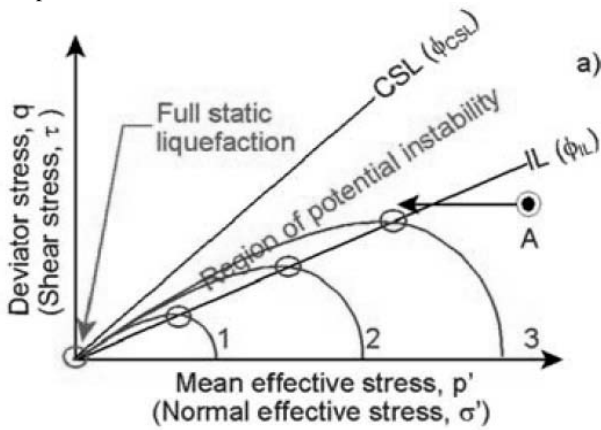


Figure 3.30. Static liquefaction landslide triggering mechanism (Take et al. 2004 after Chu et al. 2003).

Olivares and Picarelli (2006) rely on the Instability Line too (e.g. Fig. 3.30) to describe the flow and mobility demonstrated in loose pyroclastic or slope debris deposits. A variety of large and small scale (1g) flume experiments have been prepared with loose granular deposits and subjected to artificial rainfall (e.g. Iverson 1997; Moriwaki et al. 2004) with measurement of pore pressures. Flow slide mobility was dependent either upon:

- the locale of the excess pore pressures generated through shear strains triggering failure in a shear zone, or
- initial porosity and on time taken both to generate and dissipate pore pressures, with rapid fluidization developing due to high pore pressures.

Wang & Sassa (2001; 2006) describe soil behavior observed in flume tests including various failure modes at different flow rates in many such experiments.

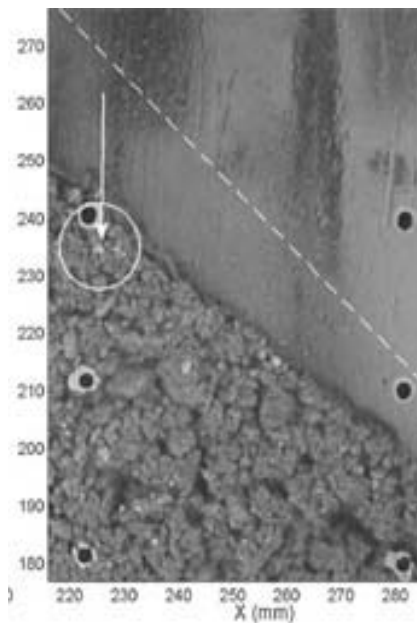


Figure 3.31. Moist tamped loose fill after rainfall in a beam centrifuge (Take et al. 2004).

Stabilizing slopes with bioengineering methods, using analogue roots or grown insitu vegetation, is discussed by Bransby et al. (2006). Flexible, rubber or more rigid, wooden roots were tested in taproot, herringbone or dichotomous forms. Further applications are expected in the future in this area.

Another esoteric series of centrifuge model tests follows on from earlier investigations into the thawing of ice in rock joints by Davies et al. (2003) that had showed that ice at -0.5°C led to less shear resistance in warm ice-filled joints than in dry ones.

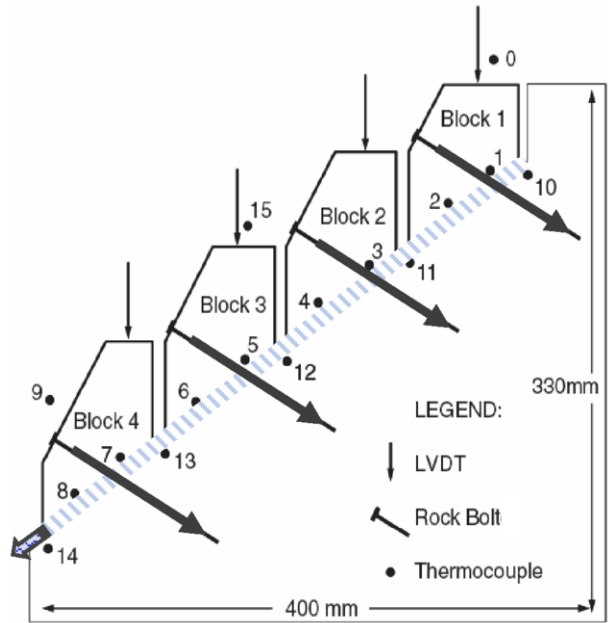


Figure 3.32. Loose, faulted rock anchored by rock bolts through ice filled joint (Günzel & Davies 2006).



Figure 3.33. Run-out chute showing fragmented boulders after a rock avalanche event (Imre 2008).

Unstable blocks were anchored by pre-stressed, instrumented rock bolts into sound (analogue) rock (Fig. 3.32). Loss of prestress was measured due to melting of ice and joint closure, indicating urgent need for ongoing monitoring and maintenance (Günzel & Davies 2006).

Drum centrifuges offer complementary opportunities for investigating geohazards with an advantageous plan area to permit simulation of run out for debris flow (Bowman et al. 2006; Rombi et al. 2006), rock avalanches or sturzstrom (Imre 2008; Fig. 3.33), of submarine slides and interaction with offshore pipelines and wave loading on river protection dykes

(Miyake et al. 2002). Processes linked to transitions from soil as a solid, transforming to a heavy viscous liquid during a debris flow, prior to run out and consolidation are not perfectly modeled in a centrifuge, however testing hypotheses on various aspects of the response can lead to useful insights.

3.7 Design

Successful design of a planned geo-structure to withstand a critical combination of perturbations often requires the effective application of a series of modeling processes that offer significant advantages to the geotechnical engineer. They may deliver their own pitfalls too. These may include the idealization of a prototype case and the creation of a suitable model, be it physical or numerical, followed by the modeling itself. Depending on the status of the model used, either a validation, verification or a calibration process may be necessary to determine how close the prediction will be to reality or indeed a prototype of the model.

Van (2003) describes an innovation cycle related to future safe and economic geotechnical design and construction of flood levees. He completed validation of the innovation cycle by comparing two forms of physical and numerical modeling, including predictions made using centrifuge data, against results obtained from a full scale prototype.

There are many such examples too, from the host of centrifuges in Japan. Most major construction companies, public research institutes and universities are equipped with large centrifuges to aid design, in which earthquake engineering is informed by hypotheses proposed prior to conducting parametric studies through dynamic centrifuge tests.

From USA, Ilankatharan et al. (2006) investigated structural aspects of bridge system seismic behavior in a 1g shaking table and then compared the geotechnical response obtained from dynamic centrifuge tests. Reconciling the different scaling laws adopted in each case required significant collaboration. Eventually, the bridge deck response was found to be modeled well by a specific geometrical set up of columns cantilevered at the equivalent depth of fixity on the 1g shaking table.

While there are many examples that could be cited for in this section, lessons learnt from experiments carried out in the ETHZ drum will be presented together with selected other mechanistic studies to aid design.

3.7.1 Base reinforced embankments on sand compaction piles

Benefitting from earlier work by Sharma & Bolton (2001), who constructed embankments on soft clay, with wick drains to speed consolidation and base reinforcement to provide short term resistance during this process in a beam centrifuge, embankments were placed 'in-flight' in a drum centrifuge on normally consolidated soft clay ($s_u = 0.24\sigma_v'(\text{OCR})^{0.9}$) in a drum channel and lightly overconsolidated clay (with $15 \leq s_u \leq 23$ kPa) in a container strongbox. Half of the tests were carried out with no ground improvement while the remainder were reinforced with sand compaction piles, constructed in-flight (Section 3.5.2.2, Weber 2007). Settlements and pore pressures were recorded throughout the test.

Centrifuge modeling cannot replicate the rate of settlement in a prototype exactly, in that the newly dominant radial drainage paths are considerably shorter than in a specific prototype. Nonetheless, the reduction in settlements caused by embankment construction can be compared between improved and unimproved ground for various pile spacings, and reported as a settlement reduction factor as a function of an area ratio of

columns in a unit cell (Fig. 3.34). Recommendations can also be made for design. Here, again, the experimental evidence has provided insights into behavior that has not been exposed in a parametric study using physical models until now, and may be used to inform predictions in future.

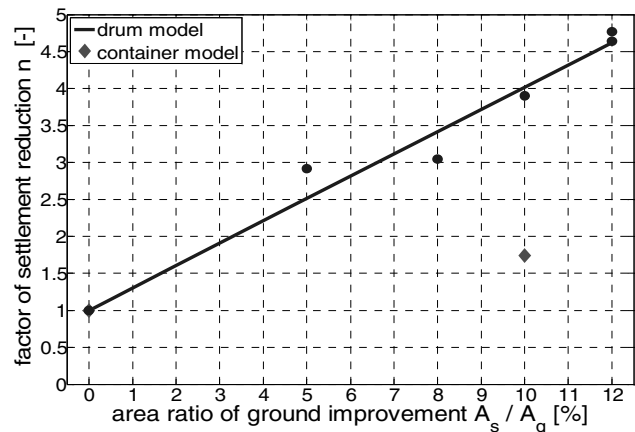


Figure 3.34. Settlement reduction factor determined for embankment crest with drum model representing 3D boundary conditions and the container model, plane strain (Weber 2007).

3.7.2 Footings

Nater (2006) investigated the bearing capacity of smooth axisymmetric footings on layered ground in which a soft clay layer of depth D_c was sandwiched between two sand layers of depth D_s . Geometry was quoted relative to the footing diameter D_f , in which solutions were presented as a function of D_s/D_f and D_c/D_f and their validity determined according to the appropriate range. Existing approaches to design were inaccurate due to a curious mixture of assumptions, and in most cases were based on kinematically inapplicable mechanisms. The bearing capacity mechanism was found to be dominated by extrusion (Nater et al. 2001) for small values of D_s/D_f and D_c/D_f and this was approximated by an equation based on silo theory (Terzaghi 1943) and found to be effective for $D_s/D_f < 0.5$ and $D_c/D_f < 0.5$. Outside this range, centrifuge models could be used in future to investigate the intermediate mechanisms between extrusion and the classical bearing capacity approaches.

Advanced contributions to design have considered soil behavior to be represented in a coupled mode by simple stress-strain data from an element test. Osman et al. (2004, 2006) validated deformation and failure mechanisms for a strip footing, respectively, as a function of a suitable kinematic mechanism, mobilized strain, a stress-strain relationship, and mobilized strength. The authors provide a coupled mode of analysis for the integrated response of a geotechnical system, and suggest that this approach may represent 'reality' better than decoupled methods and hence enable more accurate predictions to be made.

It is also important to consider structural elements for the design of foundations. Laue & Arnold (2008) showed the limitations of existing design methods, with centrifuge model tests using foundations of similar geometry and varying the loading arrangements.

The same load was applied via a central column, side walls or a mixture of both (Fig. 3.35). Arnold & Laue (2009) discuss the stiffening effect of unloaded side walls to the foundation response for foundations loaded by a middle column, which can clearly be verified both from the standard load settlement curve as well as by the evaluation of data from tactile pressure measurements.

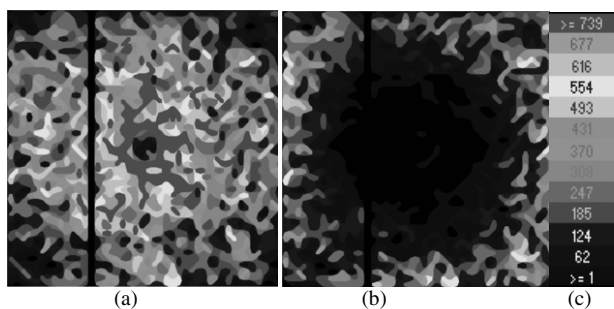


Figure 3.35. Vertical pressure underneath vertically loaded square model footing 11.2 x 11.2 cm, with central column, tested at 50g (a) maximum model load 4.25 kN, (b) after unloading to 1.8 kN at model scale, (c) scale of normal pressure measured by 11.2 x 11.2 cm Tekscan sensor in kPa (Arnold & Laue 2009).

3.7.3 Reinforced soil structures

The design of reinforced soil structures is based on limit equilibrium methods that incorporate the tensile forces induced by reinforcement elements. A centrifuge study was conducted by Zornberg et al. (1998a&b) to evaluate the suitability of current design methods. The results of this investigation indicated that the orientation of reinforcement forces should be consider to be horizontal, that significant contribution to stability is provided by the overlapping reinforcement layers, and that rigorous limit equilibrium analyses can predict the collapse of reinforced soil structures accurately when using the soil peak shear strength in the analysis (Zornberg 2003). The location of the failure surface observed experimentally was accurately predicted by limit equilibrium approaches currently used in design (Fig. 3.36). These findings support earlier findings by Springman et al. (1997), who instrumented geosynthetics with strain gauges and investigated deformation mechanisms arising during increase of gravity and vertical loading on top of the wall. Subsequent centrifuge studies conducted by Viswanadham & Mahajan (2007) confirm using digital image analysis the suitability of current design methods for geosynthetic-reinforced soil structures.

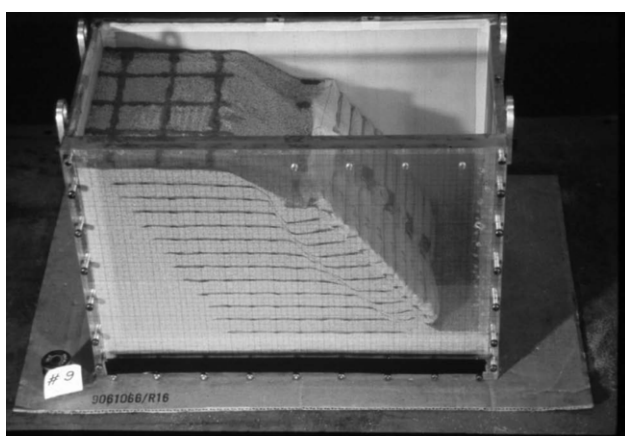


Figure 3.36. View of failure surface in the reduced-scale model of a geosynthetic-reinforced soil structure after testing in a geotechnical centrifuge. (Zornberg et al. 1998).

3.8 Teaching

Small scale physical models may be used successfully in lectures, laboratory classes, and virtually, to demonstrate soil behavior for a specific class of geotechnical structure (foundation, dam, retaining wall) in the form of mechanisms that can be understood at several levels. The younger cohorts are mainly interested in pure observation (Fig. 3.1), subconsciously learning by doing, creating collapse scenarios and being fully engaged in a fascinating activity (e.g. Fig. 3.37). Whereas combining the use of physical models to demonstrate stability and flow problems with background theory for undergraduate teaching (e.g. Bucher 2000; Springman et al. 2003b; Dewoolkar et al. 2003; Shiau et al. 2006) provides a mutually supportive observational approach to understanding and explaining soil behavior within a ‘blended’ style of teaching and learning (e.g. Sharma et al. 2001; Davison et al. 2002, Springman et al. 2003b; Laue et al. 2009; geotip.igt.ethz.ch) that should encourage reflection and enable students to engage successfully in prediction (Fig. 3.1).

Subsequent to the aforementioned, masters’ students can be exposed to conceptual constitutive modeling based on the theory of plasticity and add physical modeling in the centrifuge (e.g. Craig 1989; Springman 1997; Laue et al. 2002b; Madabhushi & Take 2002; Newson et al. 2002) and numerical analysis to investigate a specific boundary value problem thoroughly (e.g. Caprez et al. 2008). Introduction to (under)graduate courses on physical modeling, and access to teaching and other materials, may be achieved through the remit of TC2 (www.tc2.civil.uwa.edu.au).

It can be summarized that physical modelling is useful in obtaining valuable information and improved understanding of soil behaviour within the context of a boundary value problem. The benefits and deficits of the various modeling methods have been discussed in this section and related to predictions of soil behaviour and validation of numerical models. Physical modelling has become quite sophisticated with improvements in capacity and capability, including: automation, data acquisition, miniaturization, mechatronics, imaging techniques, handling and storage. Nevertheless, should the geotechnical aspects for creating a suitable model are forgotten or ill-considered due to greater complexity, the results will be less valid for full-scale applicability.



Figure 3.37. 11 year old girls attending a ‘KIDSINFO’ day in 2006 to expose them to geotechnical engineering by allowing them to discover how to build an embankment dam, test it under working loading conditions and then to cause overtopping and failure (Photograph: Sarah Springman).

4. IN-SITU TESTING

The utilization of in-situ tests has proven significant in the characterization of geomaterials in several aspects: (a) they can be done relatively quickly as compared with laboratory tests, (b) results are available immediately, (c) large numbers of data are obtained, and (d) vertical and lateral variability can be assessed over the site. Because of these vantages, in-situ testing has blossomed over the past few decades. In addition to the development of special instrumented probes that include electrical, mechanical, pneumatic, and/or hydraulic components and computerized and automated data recording, field testing has embraced the various geophysical methods of investigation.

Within a historical perspective, Lacasse (1985) summarized the types of technical tasks providing input and weight towards geoenvironment design starting with the advent of our discipline circa 1925 (see Figure 4.1). In our early years, considerable emphasis was placed on *judgment*, albeit this personal virtue has a rather vague and subjective quality that is reliant on both experience and common sense (as well as age of the individual). As the geotechnical profession became more formalized, decisions were made with a greater dependency on material testing both in the laboratory and in the field, later coupled with more robust theoretical frameworks based in analytical and numerical simulations, and of most recent vintage, probabilistic and reliability models. The consequences of having designs based on more substantial, varied, and diverse types of input information has resulted in an overall lesser need for judgment.

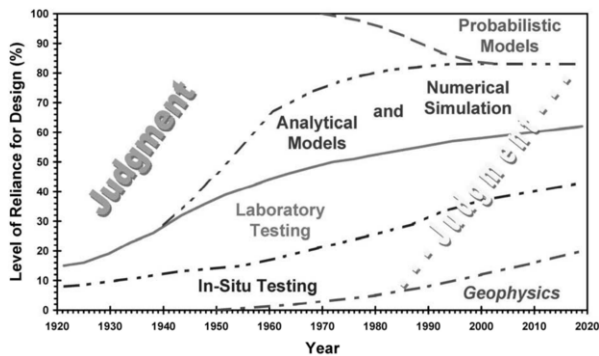


Figure 4.1. Evolution curve for geomaterial parameters evaluation in design (modified after Lacasse, 1985).

The development of field exploration methods dates back over two millennia with a concise overview of the various devices given by Broms & Flodin (1988). Within the domain of in-situ testing, one of the oldest methods of the profession is the standard penetration test (SPT) which made its advent beginning in 1902 and has now become a staple in subsurface site investigation practices (Fletcher, 1965).

Over the past century, the SPT has developed two key problems: (a) a variable energy inefficiency; and (b) overuse. The hammer energy rating (ER) issue has been recognized for quite some time and is still the focus of much research (e.g., Tsai, et al. 2004). An evolution of hammer types from pin weight ($ER_{ave} = 30\%$) to donut (40%) to safety (70%) to auto hammers (up to 100%) underlies the problem because of the refusal of the profession to give up older correlations based on the prior hammer reliance. In the USA and UK, the current practice is to energy correct the measured N-value to that for an equivalent $ER = 60\%$ (designated N_{60}), representing the average value over historical use, despite considerable variances at each hammer type. The newer automatic hammers have further exacerbated the situation because the various manufacturers have developed systems that provide the applied ER anywhere

from 100% (fully efficient) to the specified 60% (a direct N_{60} value). Most unfortunately, routine boring logs often fail to note which system has been employed.

The other issue with the SPT is a false sense of reality in the geotechnical engineer's ability to assess each and every soil parameter from the single N-value that is recorded (Figure 4.2). This nonsensical and irrational approach continues in textbook citations in the form of smoothed curves without benefit of the actual statistical scatter and data points shown for truthfulness.

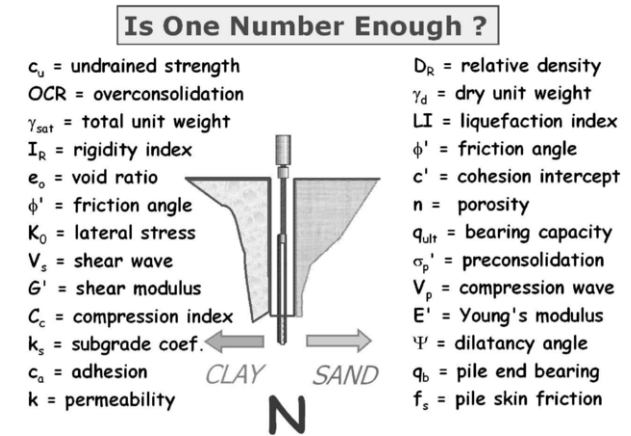


Figure 4.2. Unrealistic overreliance on the single N-value for design

4.1. Traditional and Direct-Push Site Characterization

The complexities of natural geomaterials requires that multiple types of measurements must be acquired in order to put some reasonableness towards their assessment. In this regard, the conventional approach would entail a series of soil borings with thin-walled tube samples procured for laboratory testing and intermittent SPT N-values taken at regular depth intervals, perhaps juxtaposed with occasional vane shear tests (VST) in clay layers and/or interspersed pressuremeter tests (PMT) made in sandy or clayey zones, and after casing and grouting the completed boreholes, supplemented with crosshole tests (CHT) to obtain the shear wave velocity profiles. Taken together, all of these are suitable towards achieving a comprehensive means for the characterization program, yet at considerable cost in time and expense (Figure 4.3).

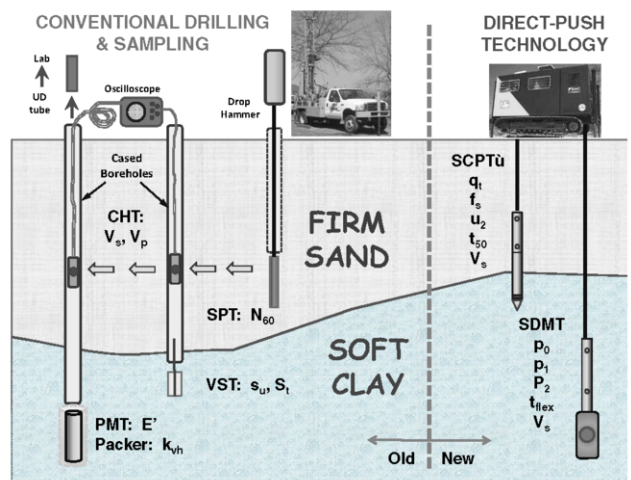


Figure 4.3. Conventional drilling & sampling methods vs. direct-push technology approach to site characterization

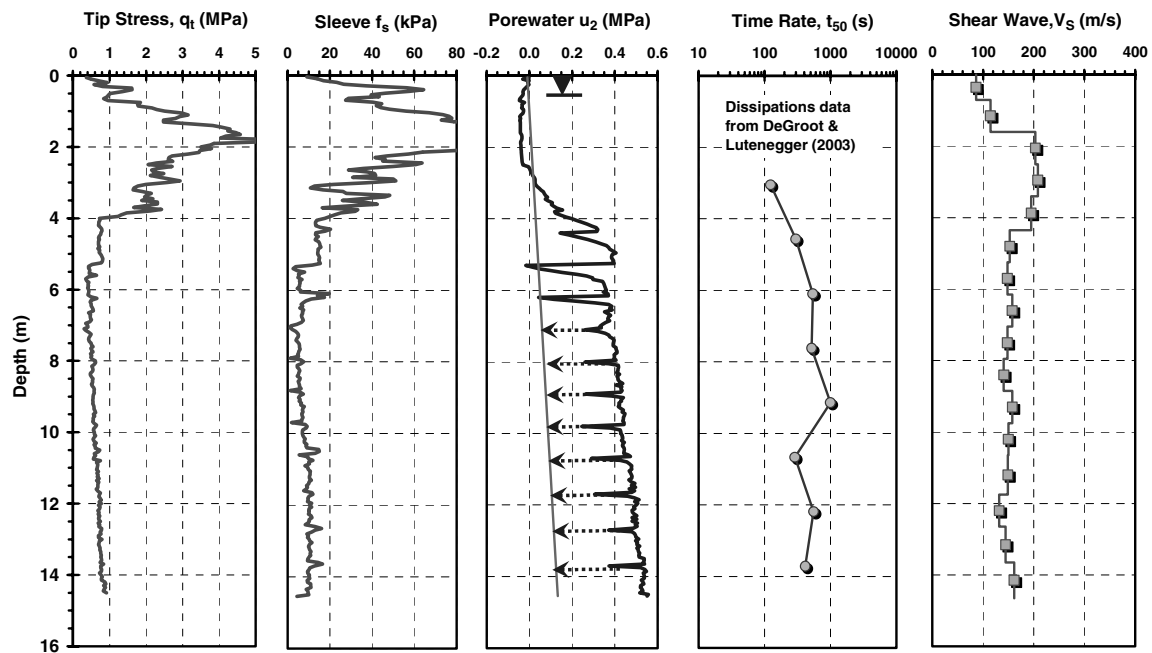


Figure 4.4. Seismic piezocone test with dissipations (SCPTu) in soft varved clays at Amherst national geotechnical test site, Massachusetts

In this fast-paced world of 2009, a more efficient approach to the task of geotechnical site characterization is the utilization of direct-push technology whereby multi-measurements are taken during the advance of in-situ devices. Here, hybrid tests that combine the advantages of full-displacement penetrometer probes with downhole geophysics can be appreciated. In particular, the seismic piezocone test with porewater pressures dissipations (SCPTu) and the seismic flat dilatometer with monitored decays of A-readings with time (SDMTu) offer clear opportunities in the economical and optimal collection of data.

An illustrative example of SCPTu results in soft lacustrine varved clay-silt from Amherst-Massachusetts is presented in Figure 4.4 indicating that as many as five independent readings can be obtained from a single sounding: cone tip resistance (q_t), sleeve friction (f_s), porewater pressure (u_2), timed dissipations (t_{50}), and shear wave velocity (V_s). The Amherst site serves as a national geotechnical experimentation site for calibrating field and laboratory tests, as well as the performance of full-scale civil engineering structures (DeGroot & Lutenege, 2003). Likewise, Fig. 4.5 shows a representative SDMTu taken to 45 m depth at the Treporti embankment test site near Venice to promote five separate readings with depth from a single probing: contact pressure (p_0), expansion pressure (p_1), closure pressure (p_2), time rate decay of A-reading (t_{lex}), and downhole shear wave velocity (V_s). The Treporti site served as a testing area for monitoring embankment performance for constructed levees on soft ground (McGillivray & Mayne, 2004). For this sounding, the downhole geophysics measurements included both true-interval readings to 16 m taken at every 0.2-m vertical depths and pseudo-interval values obtained to 30 m at the normal and regular 1-m depths. A V_s -profile from an adjacent SCPTu to 40 m is also shown.

It is suggested that the SCPTu and SDMT direct-push tests should serve as the basis for the minimum required level of effort in routine and daily site investigation practices by the profession in order that adequate amounts and sufficiently different types of data are collected for a given project. Thus, the emphasis herein this section will be placed on the interpretation of the SCPTu and SDMT.

4.2 Interpretation of Soil Parameters

Results of in-situ tests may be used to interpret soil parameters within the context of critical-state soil mechanics. As such, it cannot be expected that it will be possible to determine each and every possible soil parameter from these tests, but more rational to focus on their use in defining key parameters. Parametric values should be verified with companion laboratory tests on high-quality undisturbed samples as best as possible. In many instances, only the lab testing program will be able to determine certain characteristics and properties (e.g., PI, LL, C_c , C_{ov} , ...).

In this section, methodologies for evaluating four three key soil parameters from SCPTu and SDMT soundings will be presented: (a) unit weight (γ_t) for calculation of overburden stress profiles; (b) effective yield stress, or more commonly considered as an apparent preconsolidation ($\sigma'_p = P'_c = \sigma'_{vmax}$); (c) effective friction angle (ϕ), and (d) soil stiffness, expressed as either an equivalent shear modulus (G) or elastic Young's modulus, $E = 2G(1+\nu)$, where ν = Poisson's ratio.

4.2.1 Unit Weight Relationships

The total unit weight of soils (γ_t) has been shown to be related to the shear wave velocity (V_s) and depth (z) in a global trend relationship (Mayne, 2001). An updated grouping of various particulate geomaterials is presented in Figure 4.6 showing that the measured γ_t (kN/m^3) increases with V_s (m/s), and slightly decreases with depth, z (meters), according to:

$$\gamma_t = 8.63 \cdot \log(V_s) - 1.18 \cdot \log(z) - 0.53 \quad (4.1)$$

where n = number of data points ($n = 1018$), the coefficient of determination $r^2 = 0.822$, and the standard error of the dependent variable is $S.E.Y. = 1.17 \text{ kN/m}^3$. The effect of soil type (clay, silt, sand, gravel) may also have some nuance in the specific trending, yet not clearly apparent in the presented plot. Also shown in Figure 4.6 (but not included in the multiple regression analyses) are data from bonded and cemented types

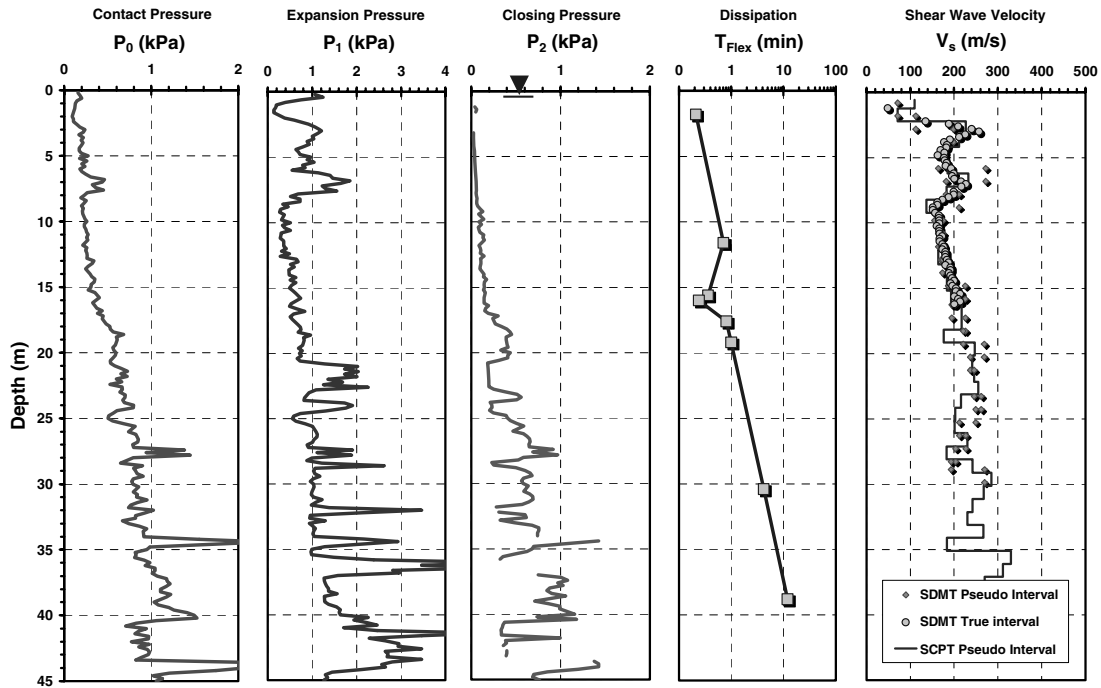


Figure 4.5. Seismic flat dilatometer test with dissipations (SDMT) in stratified sediments of Venetian lagoon at Treporti test embankment.

of geomaterials including intact rocks, weathered rocks, calcareous clays, and diatomaceous soils. A limiting condition for geomaterials of "normal" common mineralogy comprised of basic quartz-feldspar-kaolinite-illite constituency can be established at the focal (x,y) point given by a shear wave velocity of V_s (limit) = 3600 m/s and γ_t (limit) = 27 kN/m³ for solid intact rocks. Of course, in mining applications, higher unit weights might be applicable if heavy metals (iron, gold, hematite) are present.

A more fundamental relationship occurs between γ_t , V_s , and effective overburden stress (σ_{vo}'), since the effects of groundwater buoyancy are considered directly. However, this requires an initial estimate for the first soil layer and subsequent iteration of estimates with consecutive depths. With the same database, Figure 4.7 shows the corresponding trend for unit weights using an enlarged region for the soil materials with $V_s \leq 1000$ m/s. The relationship for γ_t (kN/m³) with V_s (m/s) and σ_{vo}' (kPa) from multiple regression analyses is ($n = 1018$; $r^2 = 0.806$; S.E.Y = 1.22):

$$\gamma_t = 8.64 \cdot \log(V_s) - 0.74 \cdot \log(\sigma_{vo}') - 0.40 \quad (4.2)$$

As the SCPTu and SDMT both provide a direct downhole measure of V_s with depth, a fairly reliable estimate on unit

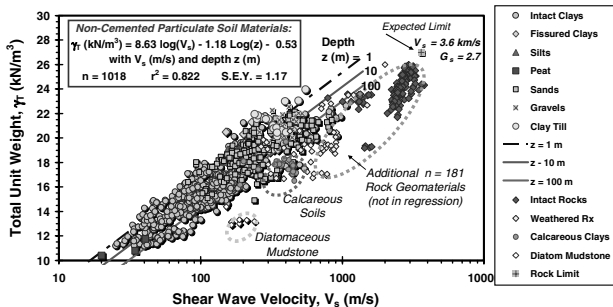


Figure 4.6. Observed trend for unit weight with shear wave velocity and depth in various geomaterials.

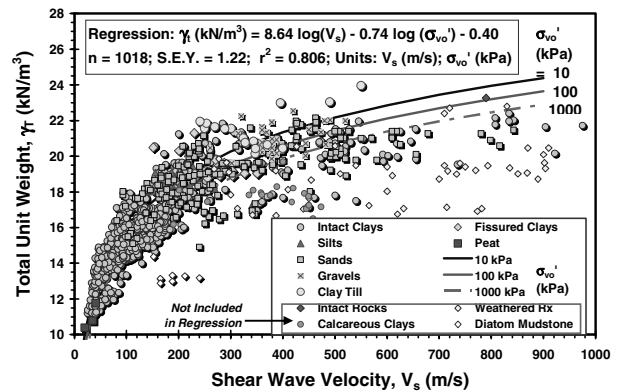


Figure 4.7. Relationship for unit weight with shear wave velocity and effective overburden stress in different soil materials.

weight can be made for overburden stress calculations. In addition, the correlation is useful for evaluating the total mass density ($\rho_t = \gamma_t/g_a$), where $g_a = 9.8 \text{ m/s}^2$, that is required for the determination of initial tangent shear modulus: $G_{max} = \rho_t \cdot V_s^2$. In the case where V_s measurements are not available, a database was compiled to investigate direct correlations between the unit weight and CPT readings. This resulted in some dependency upon the plasticity index for clay soil types, however not relevant for practical use as the PI is not known in such cases. As indicated in Figure 4.8, an estimate of total (saturated) unit weight (γ_t) can be made from the effective overburden stress (σ_{vo}'), and sleeve friction f_s according to ($n = 207$):

$$\gamma_t = \gamma_w \cdot [1.96 + 0.25 \log(\sigma_{vo}' / \sigma_{atm}) + 2.65 \log(f_s / \sigma_{atm})] \quad (4.3)$$

Similarly, a relationship for DMT readings has been developed for evaluating total unit weight in soils (Mayne, et al., 2002):

$$\gamma_t = 1.12 \cdot \gamma_w \cdot (E_D / \sigma_{atm})^{0.1} (I_D)^{-0.05} \quad (4.4)$$

where E_D = dilatometer modulus, σ_{atm} = atmospheric pressure (= 1 bar = 100 kPa), and I_D = material index, as detailed by Marchetti (1980). Figure 4.9 shows the measured vs. predicted graphs using a database from clays compiled by Lunne, et al. (1990) with additional data from two sands and a sandy silt, indicating an overall fair to good approach.

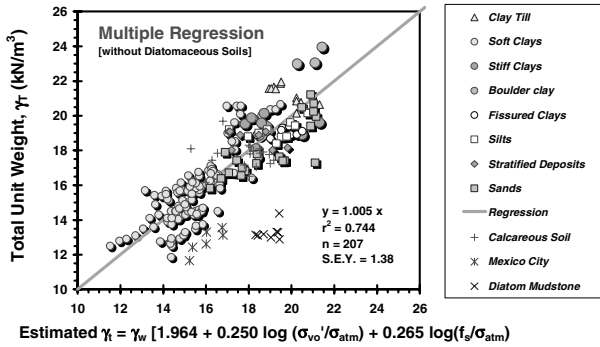


Figure 4.8. Unit weight relationship from CPT measurements

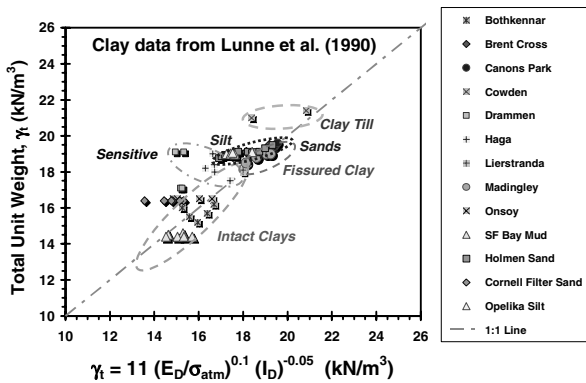


Figure 4.9. Unit weight relationship from DMT measurements

4.2.2 Soil Behavioral Type

As soil samples are not normally taken during direct push soundings, the classification of geomaterials is accomplished by inference using the measured probe readings in empirical soil behavioral type (SBT) charts or with normalized measurements to account for overburden stress effects (e.g., Lunne, et al. 1997; Robertson, 2004; Schneider et al. 2008).

With the piezocone tests, the three readings can be processed to obtain a CPTu material index, I_c (Jefferies & Been, 2006):

$$I_c = \sqrt{\{3 - \log(Q \cdot [1 - B_q] + 1)\}^2 + \{1.5 + 1.3 \cdot \log(F)\}^2} \quad (4.5)$$

where the corresponding dimensionless and normalized CPTu parameters are defined: $Q = (q_t - \sigma_{vo}')/\sigma_{vo}'$, $B_q = (u_2 - u_0)/(q_t - \sigma_{vo}')$, and $F = 100 \cdot f_s / (q_t - \sigma_{vo}')$. The index I_c can be used to evaluate approximate soil type per the guide given in Table 4.1 corresponding to different SBT zones. If only CPT readings are available (without the benefits of porewater pressures), a simplified version has been suggested (Robertson & Wride, 1998):

$$I_{cRW} = \sqrt{\{3.47 - \log(Q)\}^2 + \{1.22 + \log(F)\}^2} \quad (4.6)$$

with corresponding zones and SBT classifications also given in Table 4.1. In this case, the normalized cone tip resistance has

Table 4.1 Soil behavioral type by CPTu material index, I_c

Soil Classification	SBT Zone	Range CPTu Index, I_c	Range CPT Index I_{cRW}
Sands with gravels	7	$I_c < 1.25$	$I_{cRW} < 1.31$
Sands: clean to silty	6	$1.25 < I_c < 1.80$	$1.31 < I_{cRW} < 2.05$
Sandy mixtures	5	$1.80 < I_c < 2.40$	$2.05 < I_{cRW} < 2.60$
Silty mixtures	4	$2.40 < I_c < 2.76$	$2.60 < I_{cRW} < 2.95$
Clays	3	$2.76 < I_c < 3.22$	$2.95 < I_{cRW} < 3.60$
Organic soils	2	$I_c > 3.22$	$I_{cRW} > 3.60$
Sensitive soils	1	NA	NA

Notes: 1. Index I_c after Jefferies & Been (2006).

2. Index I_{cRW} after Robertson & Wride (1998).

been re-defined as (Robertson, 2004):

$$Q = \frac{(q_t - \sigma_{vo}')}{\sigma_{atm}} \cdot \left(\frac{\sigma_{atm}}{\sigma_{vo}'} \right)^n = \frac{(q_t - \sigma_{vo}')}{(\sigma_{atm} \cdot \sigma_{vo}')^n} \quad (4.7)$$

where $\sigma_{atm} = 1$ atmosphere ≈ 1 bar = 100 kPa and the exponent $n = 1.0$ in the general case of clays ($I_c > 3.30$), $n = 0.5$ for clean sands ($I_c < 1.64$), and intermediate values of n apply for inbetween and mixed soil types.

For the DMT, the material classification index (I_D) is defined by:

$$I_D = \frac{(p_1 - p_0)}{(p_0 - u_0)} \quad (4.8)$$

The DMT index I_D provides an approximate guide to soil type according to the following ranges: clays ($0.1 < I_D < 0.6$); silts ($0.6 < I_D < 1.8$), and sands ($1.8 < I_D < 10$), yet finer detailing of mixed soil classification is also possible (Marchetti, et al. 2006).

An approximate interrelationship between the CPT index (I_c) and DMT material index (I_D) has been studied by Robertson (1990) that can be expressed by:

$$I_c = 2.5 - 1.5 \log(I_D) \quad (4.9)$$

which is presented in Figure 4.10.

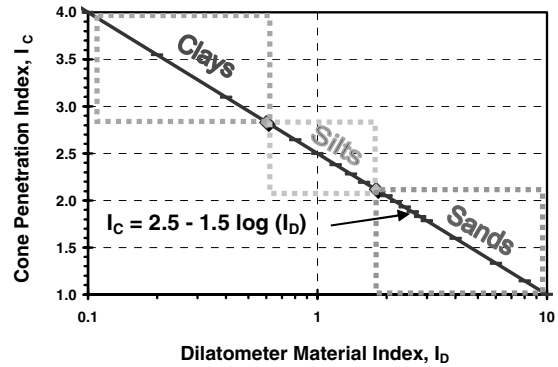
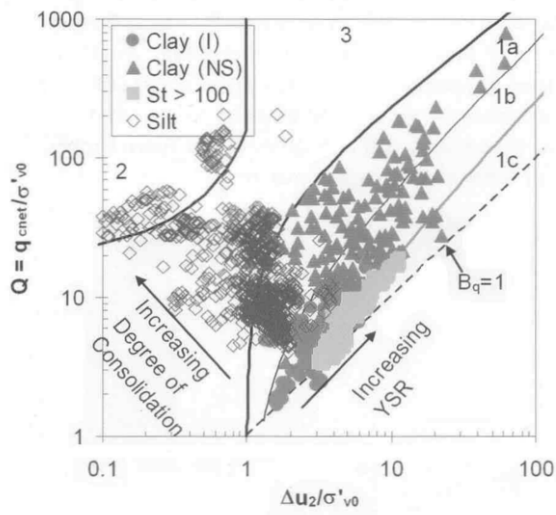


Figure 4.10. Correlation between in-situ geomaterial indices CPT I_c and DMT I_D for soil type identification (modified after Robertson, 2009).

An alternate CPT soil behavioral type (SBT) system has been proposed by Schneider et al. (2008) based on considerations of drainage by separation of undrained, drained, and partially-drained response. In this system, the groupings of SBT are found by plotting the normalized net cone tip resistance, $Q = (q_t - \sigma_{vo}')/\sigma_{vo}'$, versus a normalized porewater pressure parameter defined by $U^* = \Delta u_2/\sigma_{vo}'$, as presented in Figure 4.11. Three primary soil types include: Group 1 - clays and silts (undrained); Group 2 - sands (drained); and Group 3 - transitional soils (partially drained).



Zone	Soil Type
1a	SILTS and 'Low I _c ' CLAYS
1b	CLAYS
1c	Sensitive CLAYS
2	Essentially drained SANDS
3	Transitional soils

Figure 4.11. New CPT soil behavioral type chart using Q and normalized porewater pressure $U^* = \Delta u_2/\sigma'_{vo}$ (Schneider et al. 2008).

With the CPT I_c index, an estimate on the percent fines (PF) content (or fines content, FC) corresponding to grain sizes < 0.075 mm (i.e., No. 200 sieve) can be made. The PF content is then obtained from the following:

$$\text{For } I_c < 1.26: \quad \text{PF (\%)} = 0 \quad (4.10a)$$

$$\text{For } 1.26 < I_c < 3.50: \quad \text{PF (\%)} = 1.75 I_c^{3.25} - 3.7 \quad (4.10b)$$

$$\text{For } I_c > 3.50: \quad \text{PF (\%)} = 100 \quad (4.10c)$$

The reasonableness can be partially checked for one example case study using data from an intermediate type geomaterial, namely residual soils at the national geotechnical experimentation site (NGES) at Opelika, Alabama which is located in the Atlantic Piedmont geology (Mayne & Brown, 2003). Here, the natural soils are comprised of a near 50-50 mix of silt and sand (ave. PF = 48%) formed by the long-term disintegration of underlying gneiss, schist, and granite bedrock. For this example, the mean values of q_t , f_s , and u_2 from 22 piezocone soundings are presented in Figure 4.12. The derived dimensionless Q and F profiles are shown in Figure 4.13 with two stress normalization exponents of $n = 1.0$ and $n = 0.5$. Here, the normalized porewater pressure parameter B_q averages -0.025 in the very silty fine sands. The estimated percent fines content (PF) is presented in Figure 4.14a and shown in reasonable agreement with most of the laboratory reference values from sieve analyses, the exceptions being underestimations at shallow data at depths < 2 m.

The CPT I_c index is also useful in converting CPT data to equivalent SPT N-values (and vice-versa) using the expression:

$$q_t = \alpha_{qN} \cdot N_{60} \quad (4.11)$$

where the CPT-SPT parameter α_{qN} (bars/blows) is obtained

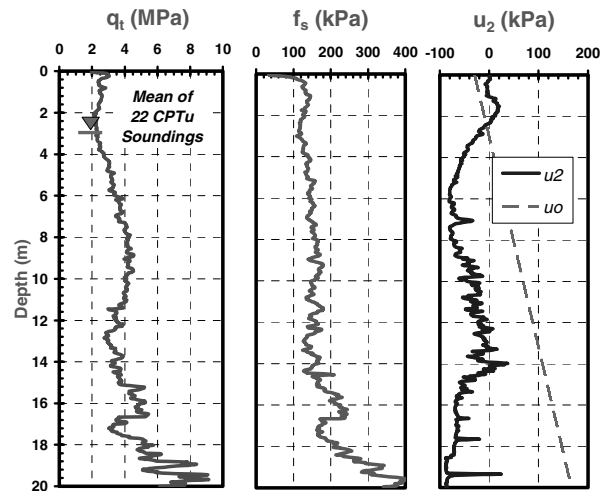


Figure 4.12. Mean piezocone readings in Opelika residual soils of the Atlantic Piedmont geology (silty fine sand).

from the empirical relationship (Jefferies & Been, 2006):

$$\alpha_{qN} = 8.5 \cdot (1 - 0.211 \cdot I_c) \quad (4.12)$$

In the Piedmont residuum at Opelika NGES, the mean $I_c = 2.77$ compared with $I_{cRW} = 2.70$, therefore little distinction needs to be made between the two in this case. Using the mean N-values at 1.5-m vertical intervals from 6 soil test borings at the site, together with the mean piezocone results, Figure 4.13b shows that the derived mean $\alpha_{qN} \approx 3.67$ provides a reasonable conversion factor between SPT and CPT in these residua, excepting the very shallow readings below 3 m depth that are somewhat overestimated.

Measured contact and expansion pressures with corresponding shear wave velocities from two SDMTs at the Opelika site are shown in Figure 4.15 (Mayne 2004). The dilatometer pressures can be processed using (4.8) to obtain the soil material index (I_D), as shown in Figure 4.16, that evaluates the soil is predominantly silty soils. The calculation of dilatometer modulus, $E_D = 34.7(p_1 - p_0)$, allows use of (4.4) for estimating soil unit weight.

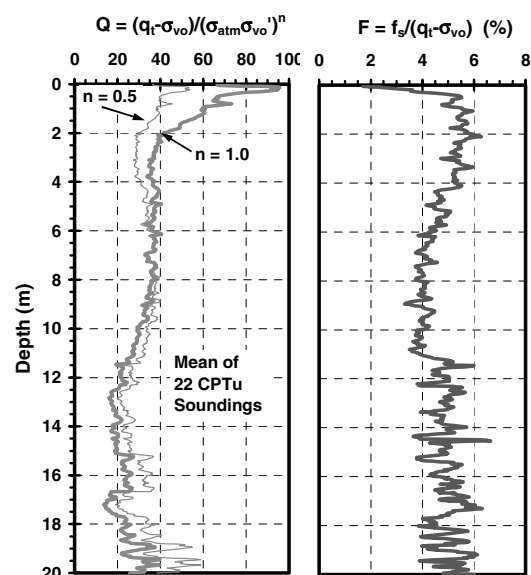


Figure 4.13. Dimensionless Q and F profiles at Opelika NGES, Alabama. (data from Mayne & Brown 2003).

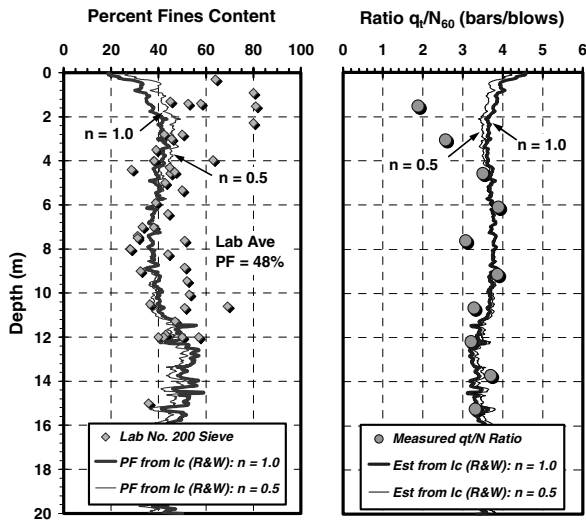


Figure 4.14. CPTu estimated values: (a) percent fines content with lab data; (b) ratio of q_t/N_{60} for CPT-SPT interrelationship.

Of final mention in the SBT systems, the use of SCPT can be useful in identifying cemented geomaterials by implementation of plots of the ratio G_{max}/q_t versus stress-normalized cone tip resistance: $q_{t1} = (q_t/\sigma_{atm})/(\sigma_{vo}'/\sigma_{atm})^{0.5}$. In this arrangement, Schnaid (2009) has provided expected guidelines in terms of the expression shown in Figure 4.17 with uncemented soils having a lower bound $B_x = 110$ and upper bound $B_x = 280$ and cemented geomaterials falling between a lower bound $B_x = 280$ and upper bound $B_x = 800$.

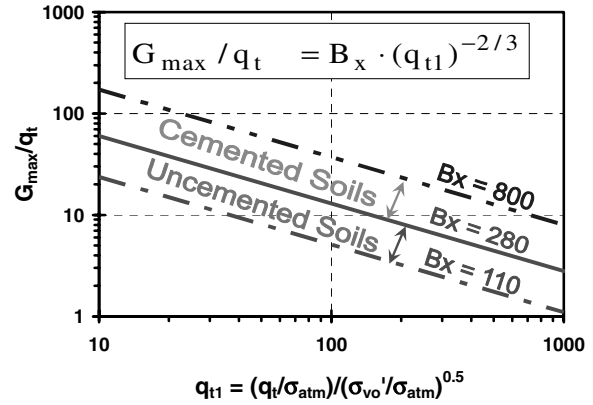


Figure 4.17. SCPT plot to identify cemented geomaterials from uncemented soil types (after Schnaid 2009).

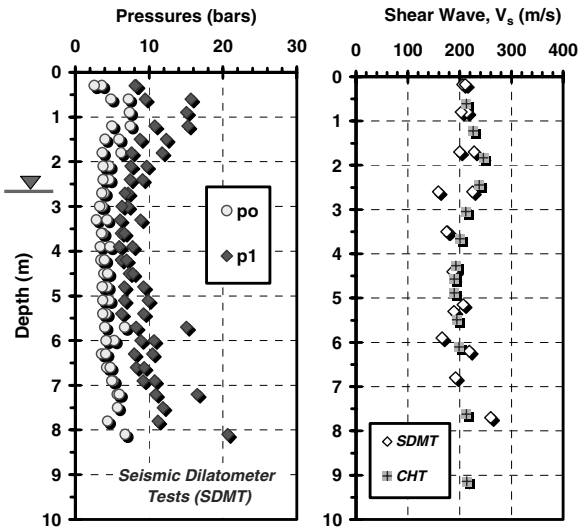


Figure 4.15. SDMTs in ML-SM residual soils at Opelika NGES.

4.2.3 Effective Yield Stress or Preconsolidation

Initially, normally-consolidated conditions prevail during the sedimentation process and formation and the subsequent consolidation of marine, lacustrine, alluvial, deltaic, aeolian, and fluvial deposits of sands, silts, and clays. Yet, the majority of soils on Planet Earth have become lightly- to moderately- to heavily-overconsolidated as a result of being exposed to a variety of physical, environmental, climatological, and thermal processes over many thousands to millions of years. These mechanisms of overconsolidation and/or apparent prestressing include: overburden erosion, ageing, rise in sea level, increased groundwater elevations, glaciation, freeze-thaw cycles, repeated wetting-drying, desiccation, mass wasting, earthquake loading, tidal cycles, and geochemical bonding. As such, the first step towards revealing the behavior of a soil formation would be a quantification of the yield stress profile of the material.

The effective yield stress (σ_y') is the key parameter separating NC soils (with primarily plastic response) from the OC region (associated pseudo-elastic response). In many cases, the yield stress is taken as the effective preconsolidation stress ($\sigma_p' = P_c' = \sigma_{vmax}'$), although technically the latter is associated with the mechanical unloading of stresses, whereas the former includes additional effects such as diagenesis, bonding, fabric, and structure. The classic reference test for determining the yield stress ratio ($YSR = \sigma_y'/\sigma_{vo}'$) is the one-dimensional consolidation test. In terms of the most common occurrence, the mechanical removal of overburden stresses results in the overconsolidation ratio ($OCR = \sigma_p'/\sigma_{vo}'$).

To develop a full profile of OCR with depth, series of undisturbed samples must be procured from various depths and subjected to lab consolidation testing. Yield stresses can also be defined for a variety of different stress paths conducted in the more versatile triaxial apparatus (Leroueil & Hight, 2003). Both the oedometric and triaxial specimens will be burdened by some degree of sample disturbance effects, thereby adding uncertainty or variance to the derived σ_p' profile. Undoubtedly,

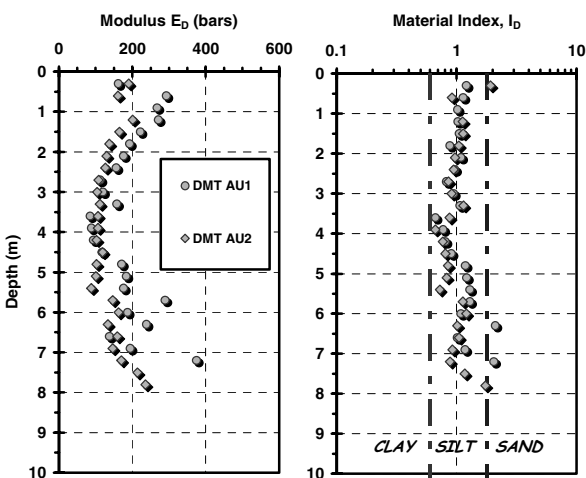


Figure 4.16. Interpreted dilatometer modulus and soil material index from SDMT soundings AU1 and AU2 at Opelika test site.

a detailed background and understanding of the geologic origins and subsequent geomorphological changes can be helpful in developing a mechanistic picture behind the causes for specific stress history events endured by a particular formation. In addition to direct σ_p' determination by laboratory testing, supplemental profiling can be provided by in-situ test measurements.

For the case of CPTs in clay, a link has been established between σ_p' and net cone tip resistance ($q_t - \sigma_{vo}$) via several different and independent methods, including empirical, statistical, and analytical approaches, as well as numerical simulations. For instance, Tavenas & Leroueil (1979) suggested a direct empirical link between yield stress and measured cone resistance (q_c), although now it is recognized that q_c must be corrected to a total tip resistance (q_t) because of porewater pressure effects (e.g., Lunne, et al. 1997). Also, the net tip resistance ($q_t - \sigma_{vo}$) is preferable for considerations of ambient overburden stresses per the remarks of Wroth (1988), as well as the utilization of dimensionless forms for yield stress and preconsolidation (YSR and OCR) with normalized cone tip resistance $Q = (q_t - \sigma_{vo})/\sigma_{vo}'$. A hybrid analytical model in terms of cavity expansion and CSSM showed (Mayne, 1991):

$$OCR = 2 \cdot \left[\frac{\frac{2}{M} \cdot Q}{\frac{4}{3} [\ln(I_R) + 1] + \frac{\pi}{2} + 1} \right]^{\frac{1}{\lambda}} \quad (4.13)$$

where I_R = rigidity index, defined as the shear modulus divided by the shear strength. A simplification can be made by adopting $\lambda = 1$, resulting in the expression (Mayne, 2005):

$$\sigma_p' = \frac{(q_t - \sigma_{vo})}{(M/3) \cdot [\ln(I_R) + 2.928]} \quad (4.14)$$

During the initial site investigation of a new clay, the effective friction angle [$\phi' = 3M/(6+M)$] and rigidity index (I_R) will not be known until extensive laboratory tests have been completed, thus assuming a set of characteristic values ($\phi' = 30^\circ$ and $I_R = 100$) produces a first-order estimation of yield stress as:

$$\sigma_p' = 0.33 (q_t - \sigma_{vo}) \quad (4.15)$$

Many experimental studies have now been completed that compare the lab consolidation value of σ_p' with the net cone tip

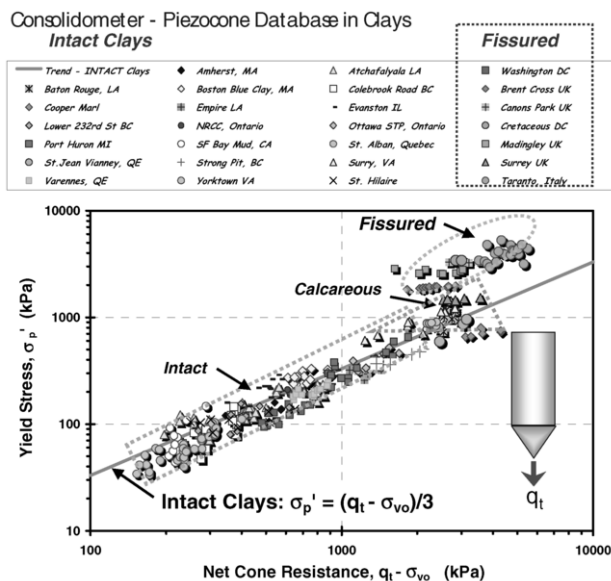


Figure. 4.18. Yield stress relation with net cone resistance in clays.

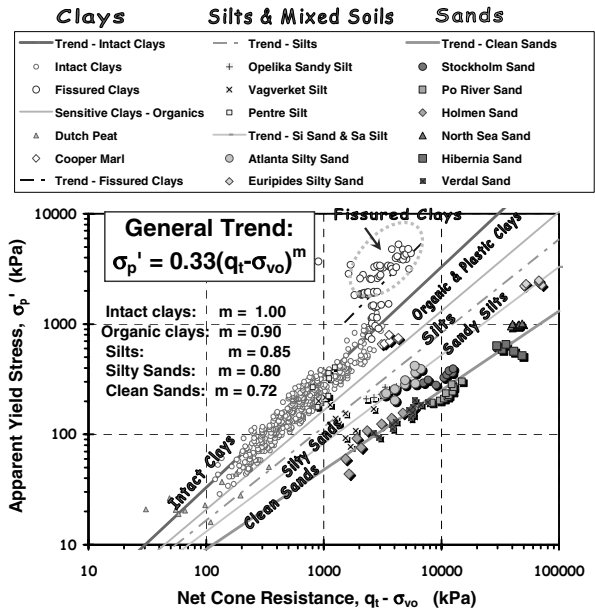


Figure 4.19. Generalized yield stress vs. net cone resistance for clays, silts, and sandy soils.

resistance, essentially validating (4.15) for general purpose use when evaluating intact clays (Chen & Mayne, 1996; Demers & Leroueil, 2002). In the case of fissured clays, the above tends to underestimate the yield stresses, as seen in Fig. 4.18.

In the evaluation of yield stresses for clean quartz and siliceous sands, a methodology has been developed on the basis of CPT data from large flexible-walled calibration chamber tests from 26 different laboratory series of tests. The measured cone tip resistances were corrected for the boundary effects (D/d ratio) because the chambers are of limited diameter size (D) relative to the cone diameter (d), as discussed by Kulhawy & Mayne (1990). The evaluation of overconsolidation ratio (OCR) from this approach determined (Mayne 2007):

$$OCR = \left[\frac{0.192(q_t / \sigma_{atm})^{0.22}}{(1 - \sin \phi')(\sigma_{vo}' / \sigma_{atm})^{0.31}} \right]^{\frac{1}{\sin \phi' - 0.27}} \quad (4.16)$$

A simplified form can be produced by adopting a representative friction angle (i.e., $\phi' = 35^\circ$):

$$OCR \approx \frac{(q_{tnet} / \sigma_{atm})^{0.72}}{13.8 \cdot (\sigma_{vo}' / \sigma_{atm})^{1.02}} \quad (4.17)$$

where the net cone tip resistance has been utilized in lieu of q_t since it is more proper and little error is introduced because the overburden stress (σ_{vo}) is so small relative to magnitude of q_t (Jamiołkowski & Robertson, 1988). Reducing equation (4.16) in terms of the preconsolidation stress and adopting specific SI units of kPa for stresses (1 atm = 100 kPa):

$$\sigma_p' (\text{kPa}) \approx 0.3 \cdot (q_t - \sigma_{vo})^{0.7} \quad (4.18)$$

which bears an uncanny resemblance to (4.14) derived for intact clays. Further investigation suggests a generalized methodology as presented in Figure 4.19. The generalized form may be a power law expression founded on a focal centerpoint:

$$\sigma_p' = 0.33 \cdot (q_t - \sigma_{vo})^m (\sigma_{atm} / 100)^{1-m} \quad (4.19)$$

where the exponent m apparently increases with fines content and/or decreases with mean grain size. Based on available observations, the parameter $m \approx 0.72$ in clean quartz sands, 0.8 in silty sands, 0.85 in silts, 0.90 in organic fine-grained geomaterials, up to $m = 1.0$ in intact clays of low sensitivity, and may even take on values of 1.1+ in fissured clays. In future studies, the CPT material index I_c may prove to be a means of identifying the magnitude of the parameter m for general profiling of σ_p' in homogeneous or heterogeneous deposits, as well as mixed soils and/or stratified formations. The above generalized approach for CPTs with a focal point is quite similar to a reported empirical form for SPT resistances in variety of soils (Mayne, 2007).

For DMTs in clays, an analogous cavity expansion-CSSM approach can be used to show an interrelationship between the OCR and the horizontal stress index, $K_D = (p_0 - u_0) / \sigma_{vo}'$ (Mayne, 2001). The simplified form for the DMT becomes:

$$\sigma_p' = 0.50 (p_0 - u_0) \tag{4.20}$$

which works well for obtaining a first-order estimation of yield stresses in intact clays, yet underestimates values in fissured clays, as indicated by Figure 4.20.

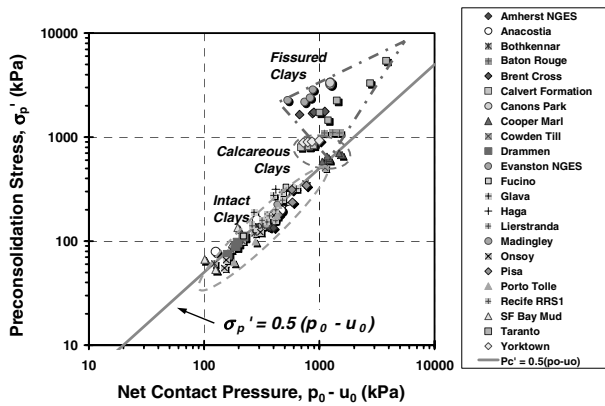


Figure 4.20. Yield stress estimation from DMTs in clays.

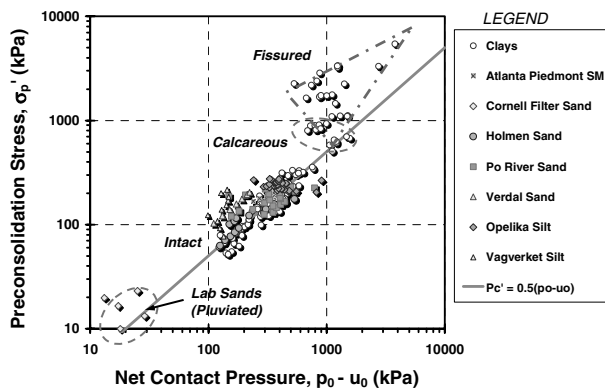


Figure 4.21. Yield stress estimation from DMTs in sands and silts.

Surprisingly, the trends for yield stresses with net dilatometer contact pressure ($p_0 - u_0$) do not appear to be focus point based. In fact, the relationship given by equation (4.20) seems to apply regardless of fines content and/or mean grain size, as seen with the DMT data from the few available documented sites presented in Fig. 4.21. Thus, for unknown reasons, the DMT relationship appears to capture the yield stress profile more directly without need to identify soil type or material index.

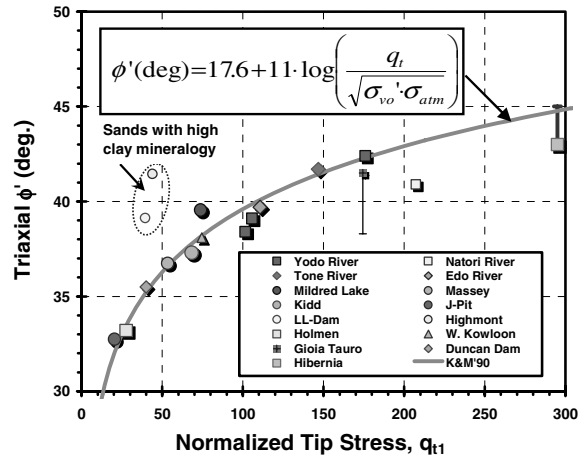


Figure 4.22. Triaxial friction angle vs. normalized CPT resistance for undisturbed clean sands (Mayne 2007).

4.2.4 Effective Stress Friction Angle

Using special "undisturbed" sampling methods, primarily based on one-dimensional freezing techniques and subsequent thawing within the triaxial apparatus, the effective stress friction angles of clean sands at 15 sites have been determined and cross-linked with in-situ SPT, CPT, and downhole V_s data (Mayne, 2006). For the CPT, Figure 4.22 shows the direct relationship between the laboratory-measured triaxial friction angle and stress-normalized cone tip resistance, defined by $q_{t1} = (q_t / \sigma_{atm}) / (\sigma_{vo}' / \sigma_{atm})^{0.5}$:

$$\phi' = 17.6^\circ + 11.0 \log(q_{t1}) \tag{4.21}$$

Since piezocone tests provide direct measurements of induced porewater pressures during penetration, the opportunity exists to ascertain the effective stress conditions surrounding a probe during insertion into all types of soils. This notion led Senneset et al. (1989) to develop an undrained effective stress analysis based in limit plasticity theory for the determination of the effective stress friction angle using the cone resistance number, $N_m = (q_t - \sigma_{vo}') / (\sigma_{vo}' + a')$, and normalized porewater pressure parameter, $B_q = (u_2 - u_0) / (q_t - \sigma_{vo}')$, where $a' = c' \cot \phi' =$ attraction term and $c' =$ effective cohesion intercept. Figure 4.23 shows the theoretical interrelationship between ϕ' , N_m , and B_q (for the case where the angle of plastification $B_p = 0$).

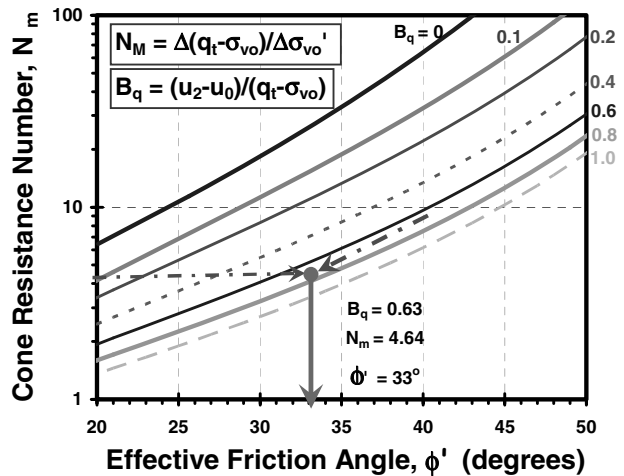


Figure 4.23. NTNH method for obtaining ϕ' from CPTu parameters.

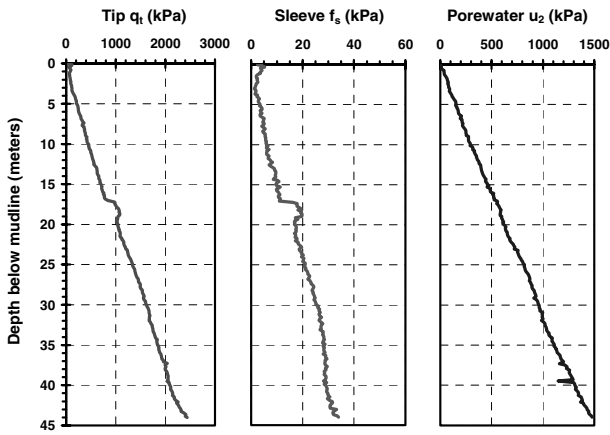


Figure 4.24. Representative CPTu sounding in soft seabed clays at Troll East site (data from Lunne & By 1989).

The value of N_m is obtained from the slope of a plot of net cone resistance vs. effective overburden stress, with a negative intercept on the latter equal to the value of the attraction. Likewise the parameter B_q can be defined as the slope of excess porewater pressure vs. net cone resistance. To illustrate the approach, CPTu data in soft seabed clays at the Troll East offshore platform site in the North Sea will be utilized (Lunne & By, 1989), with the measured readings presented in Fig. 4.24. The CPTu depths are relative to the mudline which is situated in seawater depths of about 330 m.

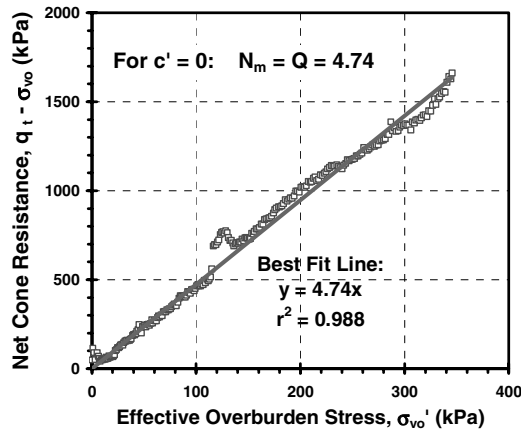


Figure 4.25. CPT post-processing for cone resistance number at Troll.

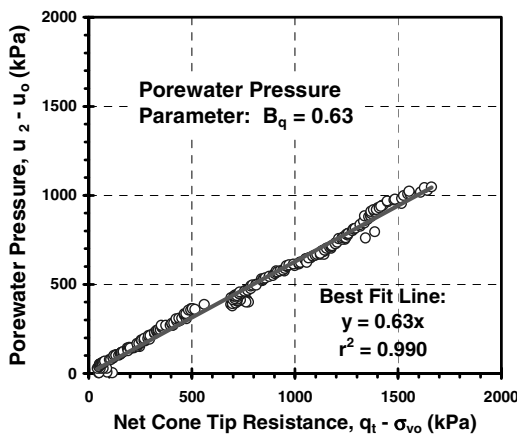


Figure 4.26. CPT post-processing for porewater pressure parameter from the Troll site.

The post-processing results of the piezocone data are shown in Figure 4.25 for obtaining the cone resistance number $N_m = 4.64$ and in Fig. 4.26 for determining the value of porewater pressure parameter $B_q = 0.63$. These are read into the chart solution developed by the Norwegian University of Science & Technology (NTNH) to obtain the effective stress friction angle $\phi' = 33^\circ$ for these marine clays (See Fig. 4.23). The derived friction angles are in excellent agreement with laboratory CAUC triaxial tests on undisturbed samples taken at the site and presented in Figure 4.27.

For most soils, the parameter c' is often quite low and close to zero (and thus $a' = 0$), the resistance number N_m reduces simply to the more well-known normalized tip resistance, Q . In that case, the expression for effective friction angle can be approximated (Mayne 2001):

$$\phi' \approx 29.5^\circ \cdot B_q^{0.121} \cdot (0.256 + 0.336B_q + \log(N_m)) \quad (4.22)$$

where valid ranges include: $0.1 \leq B_q \leq 1.0$ and $20^\circ \leq \phi' \leq 45^\circ$. This approach has been applied to the Troll clay data in Figure 4.28 with apparent good success with the triaxial results.

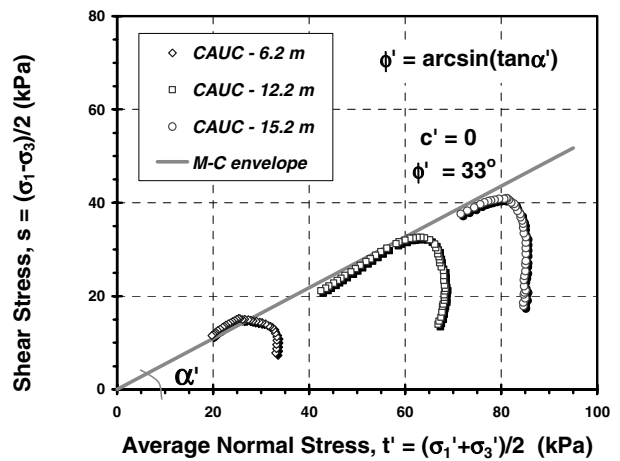


Figure 4.27. Laboratory effective stress paths from CAUC tests on upper Troll clay (data from Lunne & By 1989).

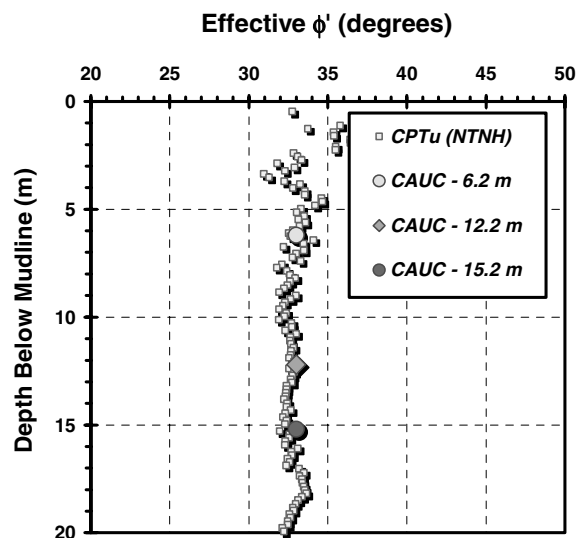


Figure 4.28. Approximate NTNU method for ϕ' applied to CPTu data from upper clay Troll site.

4.2.5 Stiffness

Quantification of the geomaterial stiffness can be represented by the appropriate elastic moduli (E' , D' , G' , K'), Poisson's ratio (ν), and their interrelationships, such as: $D' = E(1-\nu)/[(1+\nu)(1-2\nu)]$ and $E = 2G(1+\nu)$. As noted earlier, the fundamental stiffness begins in the nondestructive region corresponding to very small strains ($\gamma_s < 0.0001$) and best obtained from field measurements of the shear wave velocity (i.e., CHT, DHT, SCPT, SASW). The initial tangent shear modulus ($G_{max} = G_0 = \rho_t \cdot V_s^2$) is thus the beginning of all shear stress vs. shear strain curves and involves significant nonlinearity in the representation of modulus reduction as various phases of yielding, elastic straining, plastic behavior, strain rate, creep, and deformation occur.

For the case of simple static loading (monotonic case), a modulus reduction factor (G/G_{max}) can be applied for use in analytical models. Apparently, the mode of loading only slightly affects the amount of modulus reduction, as shown for four tests on Pisa clay in Figure 4.29 (data from LoPresti, et al. 1995, 1999, 2003). A compilation of undrained and drained tests on a variety of "hourglass" sands and "vanilla" clays show similar responses in modulus reduction. Figure 4.30 presents results in terms of G/G_{max} vs. mobilized strength (τ/τ_{max}), where the latter can be considered as the reciprocal of the factor of safety (FS).

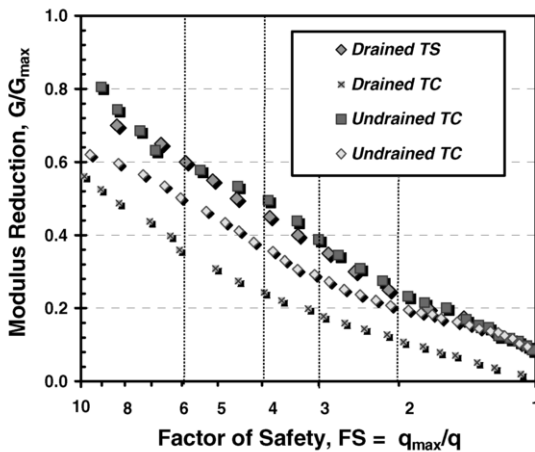


Figure 4.29. Modulus reduction curves for Pisa clay under drained torsional shear, drained triaxial, and undrained compression loading.

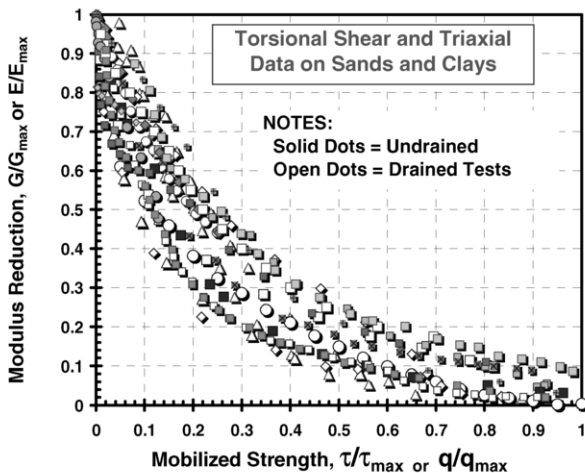


Figure 4.30. Measured modulus reduction curves for clean sands and low sensitivity clays during drained & undrained loading (Mayne 2007).

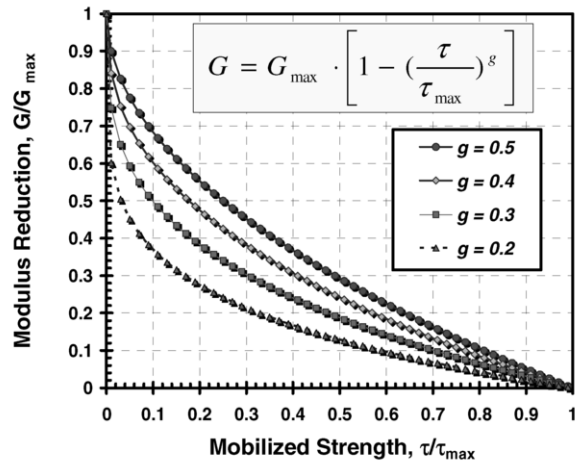


Figure 4.31. Algorithm for modulus reduction curves in terms of mobilized shear stress for "hourglass" sands and "vanilla" clays.

A number of mathematical expressions and algorithms for expressing modulus reduction curves in terms of strain level or mobilized strength have been proposed (Tatsuoka & Shibuya, 1991; Mayne 2005). One fairly simple method uses a type of modified hyperbolic form that is given by (Fahey & Carter, 1993; Fahey 1998):

$$G/G_{max} = 1 - (\tau/\tau_{max})^g \tag{4.23}$$

where g = fitted exponent parameter, as illustrated in Figure 4.31. From the laboratory stress-strain data shown in the prior graph, typical ranges for the parameter g are between 0.2 and 0.5, with a characteristic value $g = 0.3$ adopted for many soils and uncemented geomaterials (Mayne 2005).

4.3. New In-Situ Devices and Advanced Testing Methods

In addition to the SCPTu and SDMT, other valuable probes for site characterization include the pressuremeter (PMT) and its derivatives, especially the self-boring pressuremeter (SBPMT) that attempts to minimize soil disturbance during insertion, and the cone pressuremeter (CPMT) where a hybrid of penetrometer and inflation probing obtain multiple readings to quantify different aspects of soil behavior. Details on the conduct and interpretation of the PMT, SBPMT, and CPMT are given elsewhere (e.g., Gambin, et al. 2005).

A new approach to very soft soils includes full-flow penetrometers (FFP), including the T-bar, ball-, and plate-type probes, especially for offshore investigations (Randolph 2004; Boylan et al. 2007; Yafraie et al. 2007). These full-flow probes are in essence cone penetrometers with larger heads (usually 100-cm² in place of the standard conical tips of 60° apex and 10-cm² cross-sectional areas (see Figure 4.32). The cone tip is replaced with a new larger front end (either sphere, plate, and horizontal rod) that offer threefold advantages over CPTs in very soft soils: (a) increased resolution of the electronic load cell, (b) much less significance on the correction of penetration porewater effects on the unequal end areas, and (c) direct use of the measured resistance (in contrast to the net resistance: $q_t - \sigma_{vo}$ used in standard CPT) because the soil flows around the head, thus avoiding the uncertainty in calculation of total overburden stress (σ_{vo}). In addition to FFP measurements during the push downward, additional readings are taken during periodic depths with up-down cycles to look at strength degradation, as well as resistances during extraction of the probes to investigate and quantify the degree of soil remoulding and sensitivity.

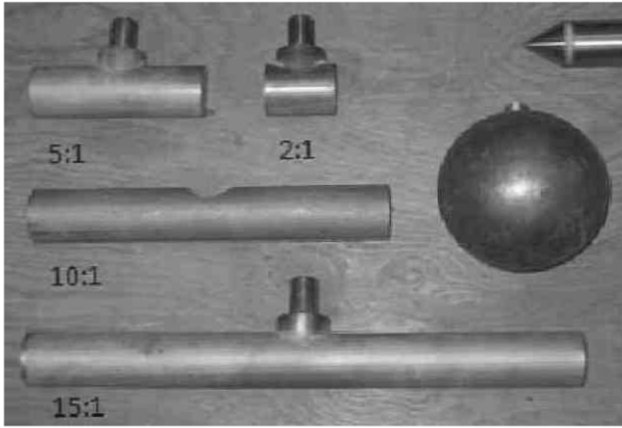


Figure 4.32. Full-flow penetrometers including the ball-penetrometer and various T-bars for strength testing of very soft offshore soils (Yafate et al. 2007).

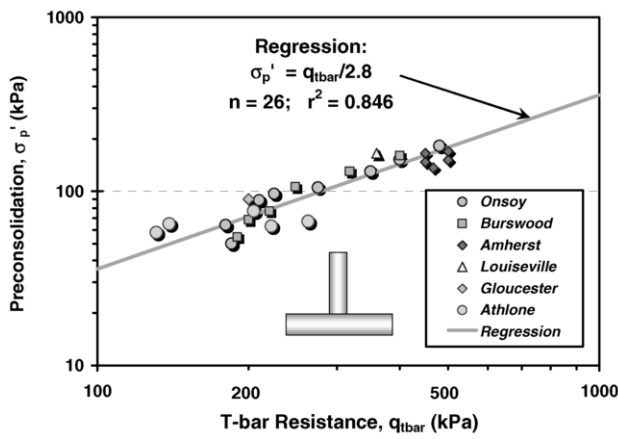


Figure 4.33. T-bar relationship for evaluating effective yield stresses in very soft clays and silts.

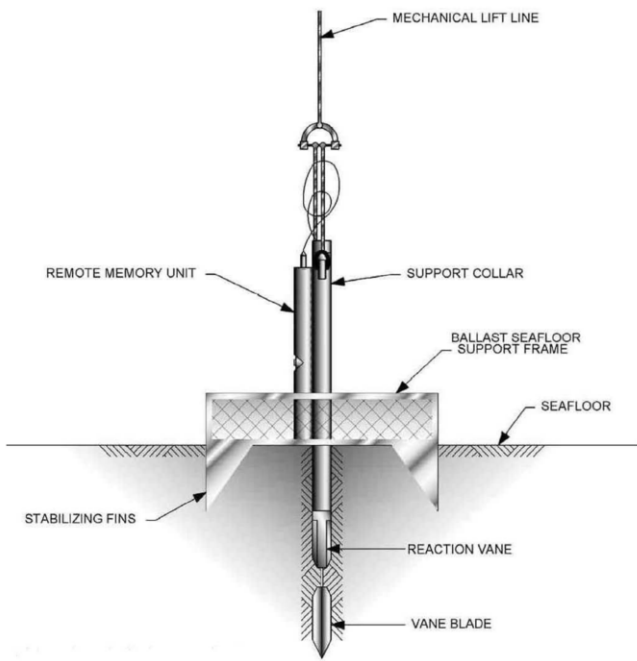


Figure 4.34. Seabed deployment of VST in offshore using the Halibut system (courtesy Fugro Engineers, The Netherlands).

For soft clays and silts, the vane shear test (VST) has traditionally been utilized to obtain in-situ shear strengths and sensitivity values. Older vane systems relied on a mechanical rod coupling in order to convey the torque uphole to a moment measuring system at the surface. Measured angles of rotation, as well as torque, were often in error due to poor rod connections, rust, wear, bending, and twisting of the steel rods. New electro-vane systems are now available that obtain the torque and rotation data downhole, just above the blade, and the data are transmitted by cable up to the surface computer, else stored digitally until downloaded upon retrieval. Figure 4.34 shows the Halibut electromechanical VST system that remotely deploys the vane from the reaction frame situated on the seabed floor. With the electrovane, the equivalent of a continuous stress-strain-strength curve is obtained from the data acquisition monitoring. Illustrative results from an electrovane shear test in offshore clay (Peuchen & Mayne, 2007) are presented in Figure 4.35 with three stages employed during the test: (a) initial shearing at standard rate of 0.1°/s to obtain the peak undrained shear strength (s_{uv}); (b) faster rate for remoulding phase; and (c) slowed rate at residual torque readings for sensitivity determination ($S_t = s_{uv}/s_{ur}$).

A new concept in VST is the helical vane which involves continuous torque measurements as the vane is pushed vertically at a constant rate of penetration (House et al. 2001). A comparison of the interpreted shear strength profiles in soft clays using helical vane shear tests (HVST) with those measured by T-bar tests are shown in Figure 4.35, with good results evident.

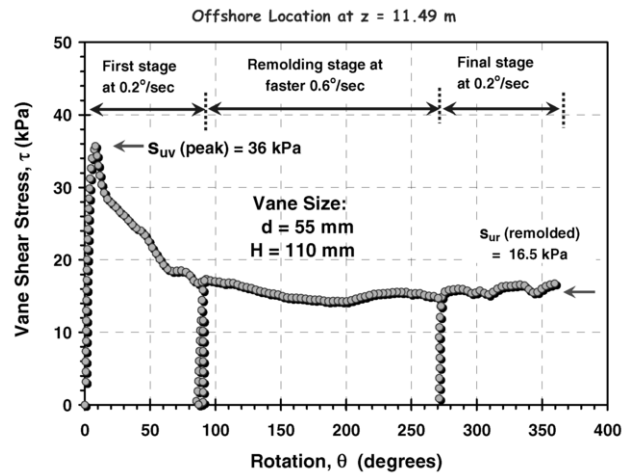


Figure 4.35. Electrovan tests in clay from offshore site in Eurasia (Peuchen & Mayne 2007).

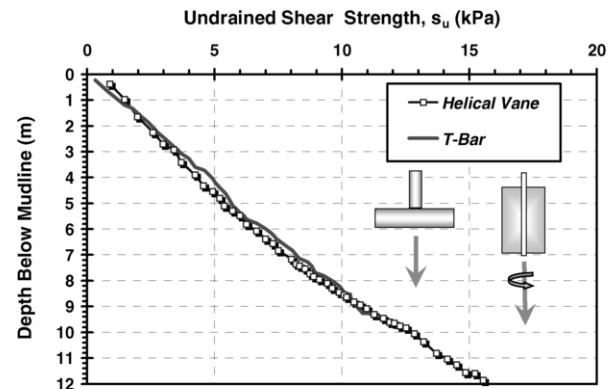


Figure 4.33. Profiles of undrained shear strength in clay from helical vane shear tests and T-bar penetrometer (House et al. 2001).

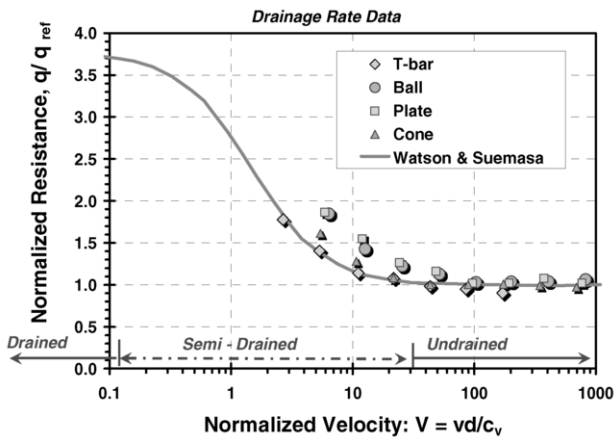


Figure 4.34. Results of twitch tests using cone, ball, plate, and T-bar in clay (Chung et al. 2006) in terms of normalized velocity to delineate undrained, drained, and semi-drained regions.

To evaluate the conditions of drainage and/or strain rate effects, variable rate penetration tests, termed *twitch* tests, have been proposed (Randolph 2004; Fun et al. 2006). Twitch testing can be conducted using the conventional cone, piezocone, or vane, as well as by the full-flow penetrometers such as the ball- and T-bar. Of particular vantage, the piezocone offers the opportunity to look at both cone tip resistance and porewater pressure effects as the rate of penetration is slowed by orders of magnitude; i.e., stepped rates of 20 mm/s to 2 mm/s to 0.2 mm/s, and so forth. This can be accomplished using a variable electric motor, although some new hydraulic systems are now available to control the rates quite accurately. Illustrative results of twitch testing in a clay reported by Fun et al. (2006) are presented in Figure 4.34 from data collected using a combination of various penetrometers, including: piezocone, ball, plate, and T-bar. For evaluation, a dimensionless and normalized velocity term is defined by:

$$V = v \cdot d / c_v \tag{4.24}$$

where v = velocity of the test, d = diameter, and c_v = coefficient of consolidation of the soil.

The results of twitch testing are significant in that they can be used for two major purposes: (a) investigate site-specific viscosity effects during undrained penetration, and thus a quantification on the strain-rate behavior of soils; and (b) discern the criteria that separate out “drained” from “undrained” response, as well as the intermediate phase which can be construed as “partially-drained”. This offers value in projects requiring staged construction of embankments as well as guidance in selection of total stress analyses (i.e, undrained shear strength = $s_u = c_u$) vs. effective stress analysis (i.e., ϕ'). In the case presented above, undrained response occurs when $V > 30$ while drained behavior evident when $V < 0.1$.

For offshore investigations, other new devices include special free-fall penetrometers which have been devised to facilitate quick deployment and collection of data without the need for long drill rod connections or seabed frames and setups (Mosher, et al., 2007). Instead, the probes are allowed to free-fall through the water column whereby they impact soils at the mudline and dynamically collect readings at a high rate of data sampling during the deceleration process. A tether is used to extract the probe for use on the next sounding.

With regards to improved geophysical testing, special methods for frequent-interval downhole testing and continuous V_s profiling with depth have been developed (McGillivray &

Mayne 2008). Both of these approaches provide better delineation of the small-strain stiffness variation with depth that benefit site-specific studies concerned with the evaluation of soil liquefaction potential, layered pavement subgrades, and comprehensive geotechnical investigations for critical and sensitive structures with stringent settlement criteria. An autoseis unit is employed to improve the repeatability and consistency of the wavelets. The autoseis also benefits field work as testing times are better controlled and automated.

Measured wavelets taken from a series of frequent-interval downhole testing are presented in Figure 4.35 and clearly show the detailed signature patterns in the profiling capabilities. The derived shear wave velocities from frequent-interval DHTs have been reported by McGillivray & Mayne (2004). A series of these types of measurements from the campus of Northwestern University are shown in Figure 4.36. Here, a sandy fill and crustal layer extend to 7 m, underlain by soft clay tills to depths of around 20 m. Another example of frequent-interval V_s profiling is shown in the prior Figure 4.5 taken at the Treport test embankment.

In the related continuous V_s profiling, a more expedient conduct of the SCPTu is also attained, since there is no halting of the penetration for DHT and V_s data are collected at 2-s intervals, comparable to the q_t , f_s , and u_2 readings (Mayne and McGillivray 2008). In these tests, two field computers are utilized with one taking the penetrometer readings and the second dedicated to collection of the faster wavelets data.

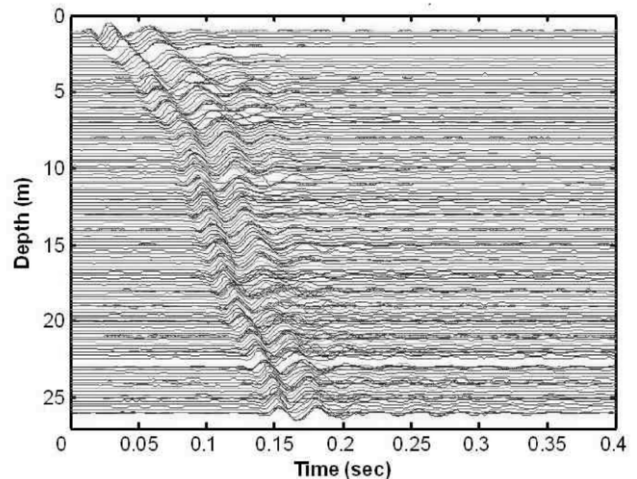


Figure 4.35. Paste-ups of wavelets from frequent-interval V_s testing.

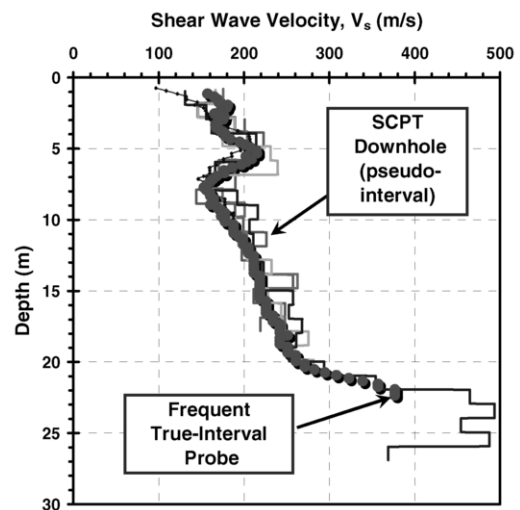


Figure 4.36. Frequent-interval V_s profile at Northwestern University.

5. CYCLIC BEHAVIOR AND LIQUEFACTION

According to Seed (1979), liquefaction denotes a condition where a soil will undergo continued deformation at constant low residual stress or with low residual resistance, due to the buildup and maintenance of high porewater pressures, which reduce the effective confining pressure to a very low value. Porewater pressure buildup leading to liquefaction may be due either to static or cyclic stress applications and the possibility of its occurrence will depend on the void ratio or relative density of a sand and the confining pressure. It may also be caused by a critical hydraulic gradient during an upward flow of water in a sand deposit. Historically, the most common form of soil liquefaction observed in the field has been liquefaction due to cyclic (e.g., earthquake) stress applications. Thus, much of the existing research on soil liquefaction has been related to earthquake-induced type cyclic liquefaction. Cyclic liquefaction is generally applied to level or gently sloping ground in which shear stress reversal occurs during repetitive seismic loading.

A major concern to geotechnical engineers from a soil behavioral point of view is the potential of cyclic liquefaction for a given seismic event (e.g., a design earthquake). There are generally two available approaches to assess the potential of cyclic liquefaction of a given soil deposit: (1) use of laboratory testing on undisturbed samples, and (2) use of semi-empirical relationships that involve correlations of observed field soil behavior with in situ index tests. Taking undisturbed samples in sand and conducting laboratory testing can be complicated and prohibitively expensive. Thus, the laboratory testing approach is usually reserved for research applications and rarely used in geotechnical engineering practice.

The semi-empirical field-based methods (Idriss & Boulanger, 2006), which evolved from the simplified procedure by Seed and Idriss (1971) are by far the most widely used methods in assessing the cyclic liquefaction potential of sand. The simplified procedure has two essential components: (1) an analytical framework to organize past case history experiences, and (2) a suitable in-situ index to represent soil liquefaction characteristics (Idriss & Boulanger, 2006). In-situ penetration tests have shown use in representing soil liquefaction characteristics because they not only provide an indication of denseness, but also reflect other important characteristics such as fabric, gradation, cementation, age, and stress history (Seed, 1979).

The simplified procedure provides a boundary curve that separates cases of observed liquefaction and those with no notable liquefaction in a two-dimensional plot of seismic loading, in terms of Cyclic Stress Ratio (CSR) versus a normalized in situ index test value. The boundary curve also serves as a correlation between the in situ index test value and the Cyclic Resistance Ratio (CRR). The term CRR may be considered as the maximum CSR that a soil can resist before liquefying. Traditionally, the result of the liquefaction potential analysis using the simplified procedure is presented in terms of a factor of safety (F_s) defined as the ratio of CRR over CSR. No soil liquefaction is predicted if $F_s > 1$. The assessment of liquefaction potential in terms of factor of safety is generally known as the deterministic approach. In recent years, there has been an increased effort to quantify the generally unknown degree of conservativeness that existed in the published boundary curves and to assess the liquefaction potential in terms of probability of liquefaction (Cetin et al., 2004; Juang et al., 2002; 2006). The probabilistic approaches have been prepared for the SPT, CPT, and in term of V_s data.

5.1 Liquefaction Potential Assessment for Clean Sands Using Simplified Procedures

Four in situ index test methods have been identified by Youd et al. (2001) as having reached a level of sufficient maturity for the purpose of soil liquefaction potential assessment under the

framework of simplified procedure. These tests include: (1) standard penetration test (SPT); (2) cone penetration test (CPT); (3) shear wave velocity (V_s); and (4) Becker penetration test (BPT). BPT is used primarily for tests in gravely deposits and readers interested in BPT are referred to Harder & Seed (1986).

The oldest and probably the most widely used in situ index test method is the SPT. A relationship between CRR and the SPT N value (number of hammer blows required to penetrate a split barrel sampler for 1 ft or 300 mm), corrected to a hammer energy ratio of 60% and normalized to an effective overburden stress (σ_{vo}') of 100kPa (or 1atm), [designated $(N_1)_{60}$] is used to represent the boundary curve. Figure 5.1 presents the CRR- $(N_1)_{60}$ correlations published in the past 3 decades for clean sands (fines content, $FC < 5\%$) and earthquake events of magnitude $M = 7.5$. Fines are defined as particles passing #200 sieve (material < 0.075 mm). The modifications in CRR- $(N_1)_{60}$ correlations over the years generally recognized a more significant increase of CRR as $(N_1)_{60}$ reached values about 30.

The SPT is a versatile testing method applicable to soils with a wide variety of gradation and density conditions. The equipment and skilled technicians required to perform the SPT are readily available in most parts of the world and thus there exists a large database. A soil sample, albeit disturbed, can be retrieved with the split barrel sampler along with the SPT. The gradation and other important basic physical soil properties can be measured directly in the laboratory. These are important advantages in favor of the use of SPT for soil liquefaction potential assessment. The equipment such as the rope, dimensions of the cathode, type of hammer and details in the split barrel sampler (Seed et al., 1984) can all affect the measured SPT N values. It is imperative to follow the relevant standards when using the SPT (ASTM D1586-08a and associated energy measurements in D4633-05).

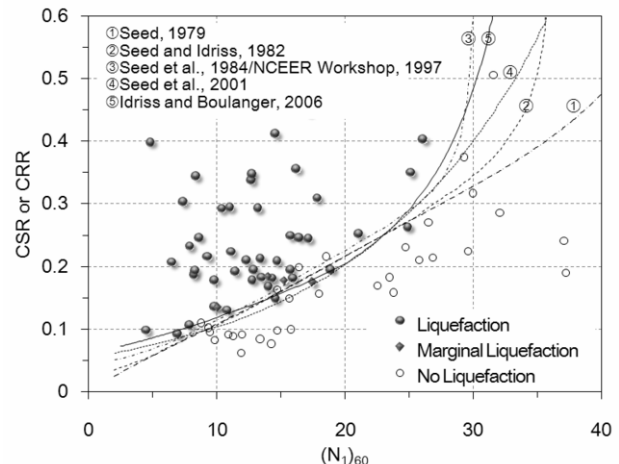


Figure 5.1 CRR- $(N_1)_{60}$ correlations published in the past 3 decades for clean sands (after Idriss and Boulanger, 2006).

Figure 5.2 shows a selection of correlations between CRR and normalized cone tip resistance (q_{cIN}) published within the last decade for clean sands and earthquake events of magnitude $M = 7.5$. The q_{cIN} represents a CPT tip resistance normalized to σ_{vo}' of 100 kPa and divided by atmospheric pressure and thus a dimensionless value. There are different levels in conservatism among these published CRR- q_{cIN} correlations as q_{cIN} exceeds 100. The CPT can be highly automated and yields an almost continuous stratigraphy of the soil deposit; thus the results are less equipment dependent. The quality of test data can be substantially enhanced with the addition of piezo unit(s) and seismometer(s); i.e., the seismic piezocone penetration test, SCPTu. The additional information can be helpful for soil liquefaction potential assessment. A disadvantage of CPT is that it does not routinely provide a soil sample. The soil gradation needed for liquefaction potential assessment is estimated from empirical rules, such as that presented in Section 4.

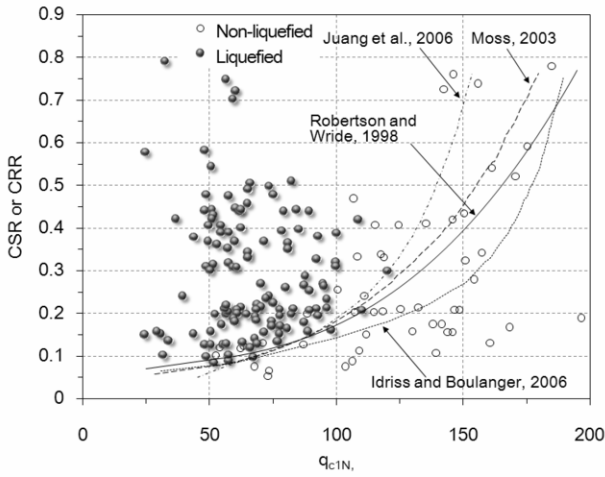


Figure 5.2. A selection of CRR- q_{c1N} correlations published recently (after Juang et al. 2006).

In addition to borehole methods (CHT and DHT), field shear wave velocity (V_s) measurement can be non-intrusive (e.g., surface wave method). This procedure can be especially useful for sites underlain with gravelly materials where penetration tests such as SPT or CPT are not feasible. The V_s can also be easily measured in a triaxial cell using bender elements. By comparing the V_s from bender element test to the CRR obtained using the same soil specimen through cyclic triaxial tests, it is possible to verify or establish the CRR- V_{s1} correlations using reconstituted (Huang et al., 2005) or undisturbed samples (Baxter et al., 2008). Figure 5.3 shows the CRR- V_{s1} (V_s normalized to a stress level σ'_{v0} of 100 kPa) correlations published by Andrus and Stokoe (2000). An important disadvantage in the use of V_s is a lack of sensitivity to the relative density, D_r . For a change of D_r of clean sand from 30 to 80%, the corresponding SPT N value would increase by a factor of 7.1 and q_c by a factor of 3.3. The same D_r would be expected to change the V_s by a factor of 1.4 based on available correlations (Idriss & Boulanger, 2006).

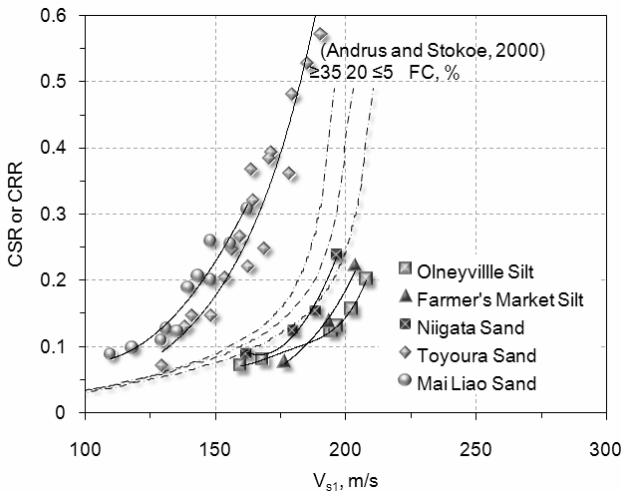


Figure 5.3 The CRR- V_{s1} correlation proposed by Andrus and Stokoe (2000) and other sands/silts (after Baxter, 2008).

For the flat dilatometer test (DMT) developed by Marchetti (1980), the horizontal stress index (K_D) has been demonstrated to have clear correlations with D_r (Reyna & Chameau, 1991), at rest lateral earth pressure coefficient (K_0) (Monaco et al., 2005) and most importantly, the age of sands (Marchetti et al., 2008). These characteristics make DMT favourable as a viable in situ

index test method for the assessment of soil liquefaction potential. Figure 5.4 summarizes the various CRR- K_D (for earthquake magnitude $M = 7.5$) for clean sands reported by Marchetti et al. (2008). The flat dilatometer is rugged and quite capable in penetrating through loose to dense granular materials. The DMT pressure control console and its test procedures are simple and results are not operator-dependent. A drawback with the use of DMT is the lack of a large database. As in the case of routine CPT, no soil sample is obtained in DMT. The soil gradation needed for liquefaction potential assessment is estimated from empirical rules.

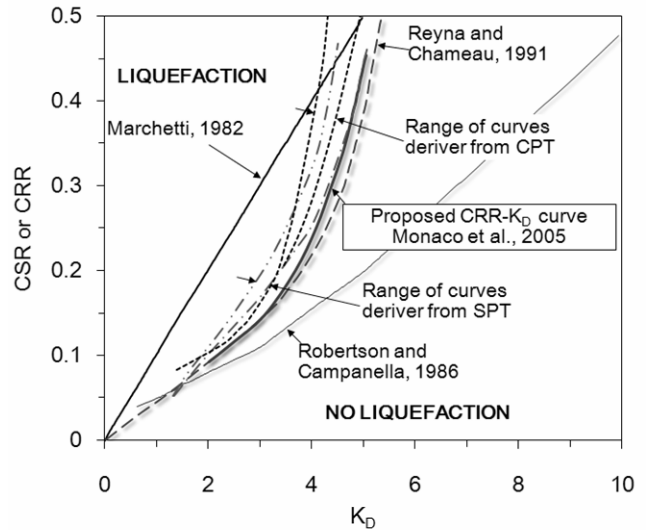


Figure 5.4. Available CRR- K_D correlations (after Marchetti et al., 2008).

Roy (2008) compiled a database from 24 sand test sites in different parts of the world to analyze the correlations among CRR, q_c , and V_s . The data included laboratory tests on high-quality (undisturbed) soil samples, field CPT soundings, and V_s measurements from near sampling locations. The sands had a wide range of fines contents, age, and soil grain compressibility. The analysis did not indicate a coherent correlation between q_{c1N} or V_{s1} and CRR. Instead, Roy (2008) reported that the ratio of q_c to maximum shear modulus (G_0) relates reasonably with CRR using separate correlations that depend on geologic age. Two boundary curves that separate the liquefaction region from no-liquefaction cases in the CRR- q_c/G_0 space can be identified as shown in Figure 5.5; one for Holocene and one for Pleistocene soils. The maximum shear modulus (G_0) is determined from V_s measurements. The CRR- q_c/G_0 correlations are independent of the fines content and soil grain compressibility. The use of CRR- q_c/G_0 correlations avoids the complexity of adjustment and/or normalizations of the individual index parameters to account for fines contents and stress conditions (Boulanger, 2003; Moss et al., 2006). When using the seismic cone penetration tests, V_s measurements can be easily coupled with CPT directly to obtain q_c/G_0 values.

Ishihara and Harada (2008) analyzed the correlations between SPT and CPT results and their relationship with the ratio of effective horizontal stress to vertical stress (K). The CRR values were estimated from D_r . The penetration resistance values from SPT and CPT were based on calibration chamber tests. Figure 5.6 shows the comparison of the CRR- q_{c1} correlations derived for three clean sands: Toyoura sand (average grain size, $D_{50} = 0.20$ mm), Da Nang sand ($D_{50} = 1.13$ mm) & Monterey sand ($D_{50} = 0.37$ mm), for $K = 0.5$. The correlations by Robertson & Wride (1998) and AIJ (2001) are also included for reference. For these three types of clean sands, the CRR- q_{c1} correlations can deviate significantly from the published curves and among themselves. Similarly, discrepancies can also be found among the CRR-N correlations

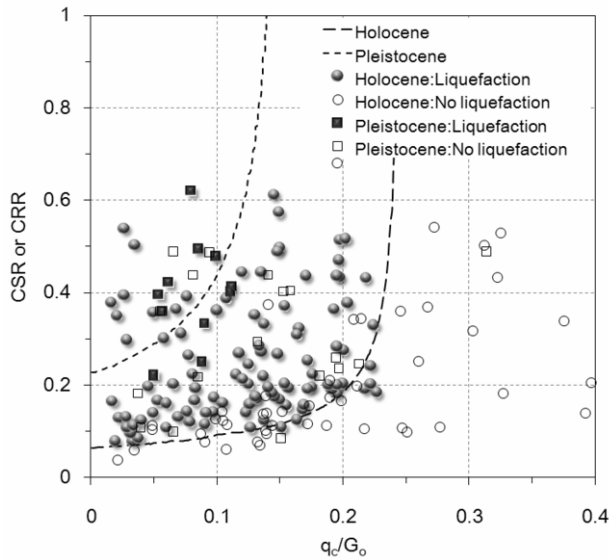


Figure 5.5 The CRR- q_c/G_0 correlations reported by Roy (2008).

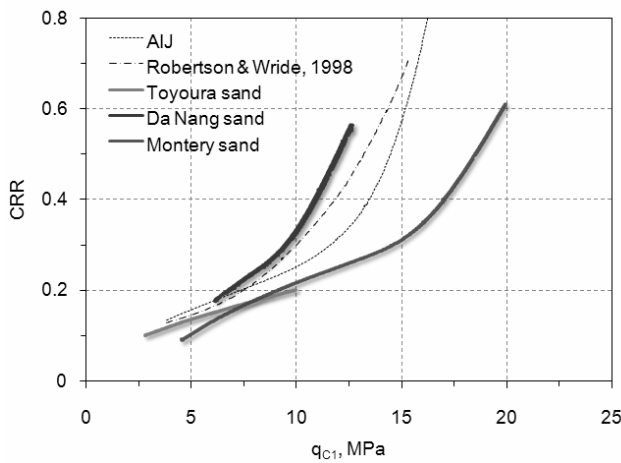


Figure 5.6 Comparison of the CRR- q_{c1N} correlations derived for three clean sands (after Ishihara and Harada, 2008).

derived for Toyoura sand and those reported by Youd et al. (2001) and JRA (1996).

5.2 Liquefaction Potential Assessment for Silty Sands Using Simplified Procedures

Natural sand deposits often contain various amounts of fines (silt and clay size particles). A comprehensive description on the behavior of silty sands is provided in the section 02 on soil behaviour of this paper. It has been reported that most cases of earthquake-induced liquefaction have actually occurred in silty sands (Yamamuro & Covert, 2001). Researchers have generally agreed that as fines contents exceed 5%, relative density ceased to be a reliable index to predict liquefaction potential (Seed et al., 1985; Ishihara, 1993). For fine grained soils, the cyclic resistance correlates well with the void ratio, where a lower void ratio corresponds to greater cyclic resistance (Ishihara, 1996). There is still a lack of consensus as to what role the fines content plays in relation to liquefaction.

Figure 5.7 shows the critical state lines (or steady state lines) of Kogyuk sand with FC ranging from 0 to 10%. The critical state lines rotate clockwise as the fines content increases. This rotation occurs around a pivot that corresponds to a mean effective confining stress ($p' = (\sigma'_v + 2\sigma'_h)/3$) between 20 and

80 kPa. According to this set of critical state lines, for a given void ratio, the soil with 10% FC is more dilatant than those with FC=0 to 5% at low effective confining stress. This trend is reversed as p' increases. Alternatively, it may be considered that the fines content effects can be stress dependent. Similar phenomenon has also been reported by Yamamuro & Covert (2001). Following this observation, Bouckovalas et al. (2003) idealized that for a sand with different fines contents, all corresponding critical state lines pass through a pivot point (defined by e_{piv} and p'_{piv}). The effect of fines contents is reflected in the slope of these critical state lines (steeper slope for higher fines content). Based on this framework, a stress dependent correction factor that considers the effect of fines on liquefaction resistance is proposed. For initial confining stress $p'_o < p'_{piv}$, liquefaction resistance increases with fines. The trend is reversed for $p'_o > p'_{piv}$.

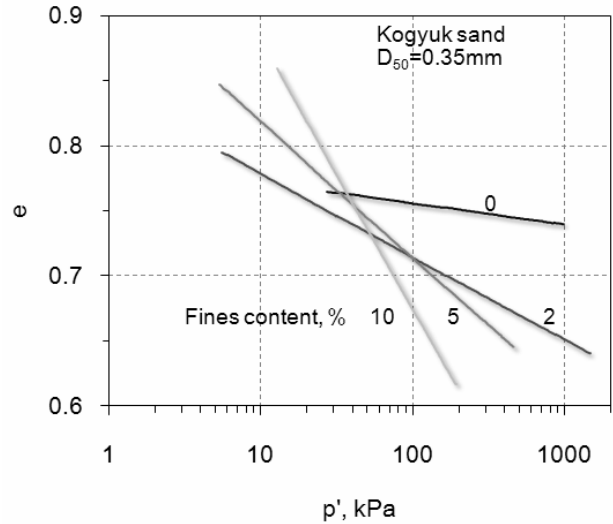


Figure 5.7 Critical state lines for Kogyuk 350 sand with different silt contents (from Been & Jefferies, 1985).

Depending on the mineralogy and grain characteristics of the soil, the sand and fines portions can both be compressible as it is the case of Mai Liao Sand (MLS) (Huang et al., 1999). The coarse grains of MLS are flaky in shape, with its average grain size (D_{50}) at approximately 0.15 mm. The fines of MLS have liquid limit (LL) of 32 and plasticity index (PI) < 8. The MLS represents a typical alluvial sand found in Central Western Taiwan. Because of the continued increase in compressibility with FC, the steady state lines of MLS are curved, and correspond to distinctly lower void ratios at more or less parallel positions with increasing FC, as shown in Figure 5.8. As a result, MLS becomes more contractive in undrained monotonic shearing and the CRR decreases consistently with FC (Huang et al., 2004). The relatively high compressibility renders the grain contact density index (Thevanayagam et al., 2002) not applicable for MLS.

Under a given confining stress, it is often not possible to maintain a constant grain contact density index as FC increases. Silty sands are likely to be more compressible than clean sands. When analyzing test results, it is essential to use the post consolidation void ratios. Ignoring changes in void ratio during consolidation can lead to unpredictable errors and more confusion in the fines content effects. The high compressibility can also result in differences in contractiveness in undrained shearing for soil with the same fines content but different initial void ratio and stress history. Also, the steady state line may not be unique as reported by Yamamuro & Covert (2001). Plasticity of the fines can cause further differences in the mechanical behavior of sand, silt/clay mixtures (Guo & Prakash, 1999; Boulanger & Idriss, 2006; Bray & Sancio, 2006).

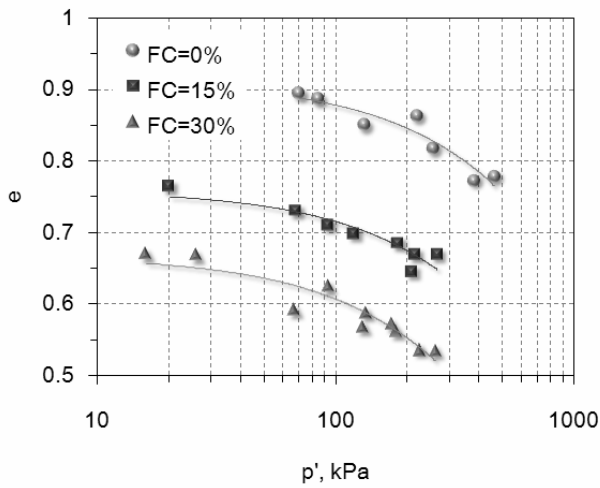


Figure 5.8 Steady state lines of MLS with FC = 0, 15 and 30% (from Huang et al., 2004).

Significant differences in the effects of fines between natural, undisturbed soil samples and those reconstituted in the laboratory have also been reported. Høeg et al. (2000) showed that undrained shearing tests on natural silt or silty sand had dilatant behavior while reconstituted specimens with the same fines contents and void ratios were contractive. Figure 5.9 compares the stress-strain curves and excess pore pressure relationships from undrained triaxial tests on soil samples from Yuan Lin, Taiwan (YLS) with fines contents ranged from 18 to 89%, reported by Huang & Huang (2007). The triaxial specimens were isotropically consolidated to 100 kPa effective confining stress. The YLS soils came from the same region as MLS. The coarse grain ($D_{50} = 0.18$ to 0.2 mm) characteristics and its mineralogy are similar to MLS. The plasticity of YLS increased as FC changed from 18% (LL=25, PI=11), to 43% (LL=21, PI=7) and 89% (LL=31, PI=12). Undisturbed samples were taken using a Laval sampler (LS) and all LS samples had natural water contents (w_c) larger than their respective LL. Details of the Laval sampling procedure are described later. The LS specimens were dismantled upon triaxial test and remixed to make reconstituted specimens with similar void ratios, using the water sedimentation (WS) and moist tamping (MT) methods. As in the case of Høeg et al. (2000) the LS (considered as undisturbed) specimens showed considerably less contractive behavior regardless of their fines contents.

Figure 5.10 compiles the relative values of CRR, V_{s1} taken from tests on LS, WS and MT specimens of YLS with similar void ratios, as a function of fines content for specimens prepared by different methods. The relative values are presented as ratios of the parameter normalized with respect to the same parameter from tests using 18% fines content specimens. The results show that for the three types of parameters compared, LS specimens were the least sensitive to fines contents. The MT Specimens were the most sensitive to fines content. These results imply that the effects of age or structure on sand, silt/clay, and mixed soils can be fines content dependent. Relative comparisons in various mechanical behaviors using freshly reconstituted specimens with different fines contents may be misleading.

When the CRR of a sand with fines is determined through in situ index test using simplified procedure, the situation is more complicated as the available correlations are empirically derived mainly from field observations of soil behavior following earthquakes. Although different in magnitude and/or format, most available CRRs based on in situ index test value correlations for cohesionless silty sands suggest that a given index test value should correspond to a higher CRR as fines content increases. Alternatively, the in-situ index test value

should be increased to obtain an equivalent clean sand value. For the V_s method by Andrus & Stokoe (2000), the adjustment in the CRR- V_{s1} correlations is included in Figure 5.3. The SPT penetration resistance (Idriss & Boulanger, 2006) is increased to an equivalent clean sand value, $(N_1)_{60cs}$ according to FC (in percent) as:

$$(N_1)_{60cs} = (N_1)_{60} + \Delta(N_1)_{60} \tag{5.1}$$

$$\Delta(N_1)_{60} = \exp\left(1.63 + \frac{9.7}{FC + 0.1} - \left(\frac{15.7}{FC + 0.1}\right)^2\right) \tag{5.2}$$

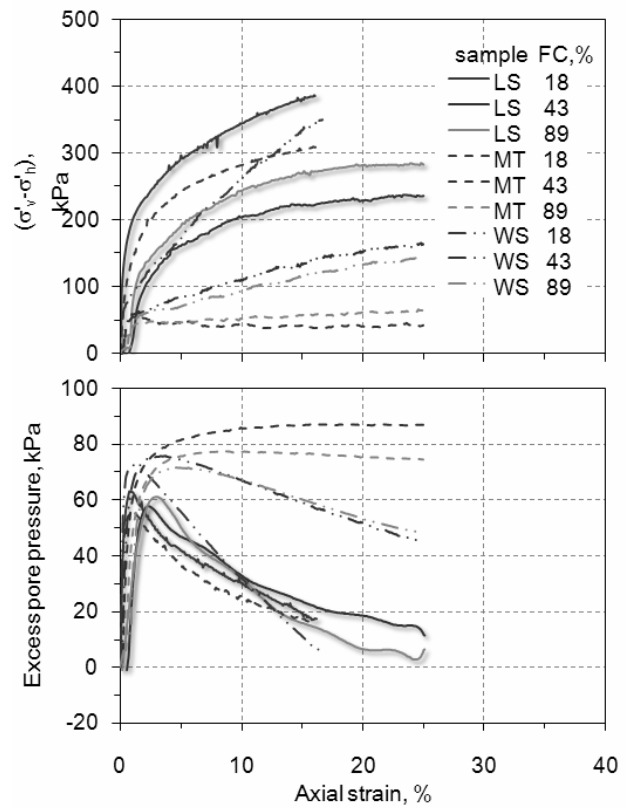


Figure 5.9. Stress-strain and excess porewater pressure relationships from triaxial tests on YLS (after Huang & Huang, 2007).

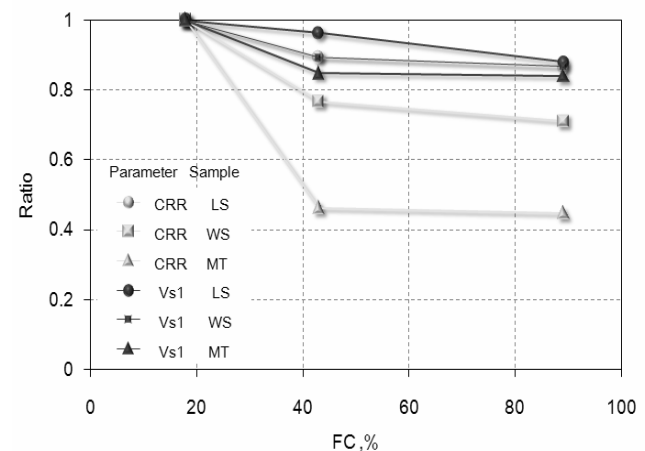


Figure 5.10. Relative values of cyclic resistance ratio (CRR) and stress-normalized shear wave velocity (V_{s1}) as a function of FC (after Huang & Huang, 2007).

Robertson & Wride (1998) suggested that for CPT the equivalent clean sand value should be determined based on the soil behavior index (I_c), using the following relationship:

$$(q_{tIN})_{cs} = K_c q_{tIN} \tag{5.3}$$

For $I_c \leq 1.64$: $K_c = 1.0$ (5.4)

For $I_c > 1.64$:

$$K_c = -0.403I_c^4 + 5.58I_c^3 - 21.63I_c^2 + 33.75I_c - 17.88 \tag{5.5}$$

where the CPT material index I_c is a function of normalized tip resistance Q_t and normalized sleeve friction F_s , as discussed in Section 4. The parameter I_c is related to soil type and fines content. The adjustment to account for the fines content can impact significantly the outcome of the calculated liquefaction potential assessment. Despite this significance, little explanation has been offered to justify the consideration of fines content effects (Ishihara, 1993; Youd et al., 2001).

Figure 5.11 shows a series of q_t profiles in dry and saturated specimens ($q_c = q_t$ in dry specimens) from laboratory calibration tests in MLS reported by Huang et al. (2004). For FC of 15%, the q_t profiles in dry and saturated specimens are essentially identical upon reaching a stabilized value, indicating that the cone penetration is drained. When FC exceeds 30%, the q_t in saturated specimens is significantly lowered than that in dry specimens. Similar partial drainage phenomena have also been reported by Campanella et al. (1981) for CPT in clayey silt.

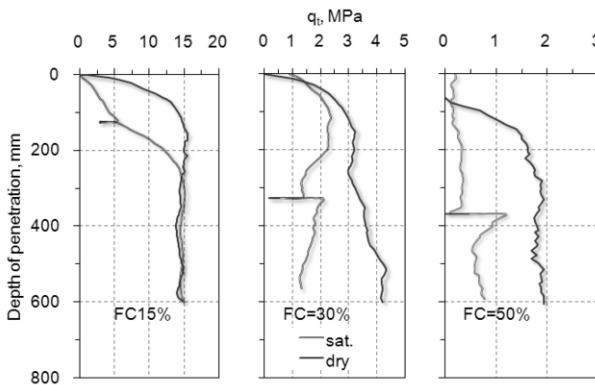


Figure 5.11 Measured q_t profiles from CPT calibration tests in MLS at different fines contents (after Huang and Hsu, 2004)

By comparing the CRR and q_t from CPT calibration tests in reconstituted specimens with comparable fines contents, density and stress states, it was possible to verify the CRR- q_{tIN} correlation by direct comparisons for MLS as shown in Figure 5.12 (Huang et al., 2005). The CRR values were determined based on cyclic strength obtained from a series of cyclic triaxial tests (CRR_{CTX}). The inference of CRR under anisotropic stress conditions from CRR_{CTX} follows the procedure by Ishihara (1996), given as:

$$CRR = CRR_{CTX} \frac{1+2K}{3} \tag{5.6}$$

The soil specimen in the cyclic triaxial test was consolidated under an isotropic effective confining stress ($K = 1$), σ'_o of 100kPa, and then subjected to a cyclic deviator stress, σ'_d in axial direction. The CRR_{CTX} was defined as the $\sigma'_d/2\sigma'_o$ that produced an axial strain of 5% in double amplitude and 20 cycles (N_c) of uniform load application. The results as shown in Figure 5.12 indicate that the fines content adjustment becomes significant only when the fines start affecting the drainage conditions in CPT and thus result in a group of data points with distinctly lower q_{tIN} . A similar explanation has

been postulated by Thevanayagam & Martin (2002). The laboratory study in MLS seems to suggest that a more effective q_{tIN} adjustment scheme should be based on CPT drainage conditions rather than fines content.

Additional CRR- q_{tIN} data points based on field CPTU and cyclic triaxial tests on undisturbed samples are also included in Figure 5.12. The data compiled by Tokimatsu et al. (1995) were collected from 6 test sites, where soil samples were retrieved by freeze sampling. The fines contents varied from <1% to as much as 30%. According to Tokimatsu et al. (1995), there was a unique CRR- q_{tIN} correlation irrespective of fines content. For a given q_{tIN} , the dispersiveness in CRR was attributed to changes in K and soil type, represented as a function of minimum void ratio, i.e. $f(e_{min})$. The CRR- q_{tIN} data points of YLS will be described later.

In light of the above findings, Huang et al. (2005) suggested that a porewater pressure dissipation test during CPTU may be used as a reference to scale the amounts of fines content adjustment. For the CPTU in saturated specimens included in Figure 5.11, a dissipation test was conducted in the chamber (at respective depths of 125, 325 and 375mm for FC of 15, 30 and 50%). In a dissipation test, the cone penetration was suspended and the dissipation of the excess pore pressure induced by cone penetration was monitored until its full dissipation. When the FC exceeded 30%, there was a distinct increase of q_t at the start of the subsequent push. The q_t setup increased further as the FC reached 50%. This phenomenon referred to as the q_t setup was also reported by McNeilan & Bugno (1984) in their experience of CPT in offshore California silts. The reason for setups is that partial drainage caused a lowered q_t due to pore pressure accumulation. The dissipation of pore pressure increases soil strength against cone penetration and generates the setup. There is no obvious q_t setup for the case of FC=15% in Figure 5.11, a result that is consistent with the fact that CPT is drained as mentioned above.

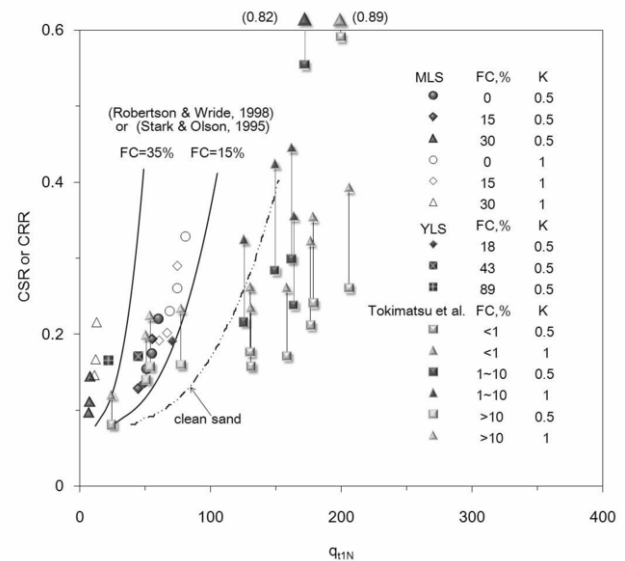


Figure 5.12 Laboratory and field calibrations of CRR- q_{tIN} correlations.

A series of CPTU using a standard cone (cone cross sectional area=10cm²) penetrating at 20mm/sec (the standard CPTU rate), a large cone (cone cross sectional area=15cm²) penetrating at 20mm/sec (the large CPTU), and a standard cone penetrating at 1mm/sec (the slow CPTU) were conducted at the Yuan Lin test site. The rate of consolidation for soil surrounding a cone tip is inversely proportional to the square of the cone diameter (Robertson et al., 1992). Therefore, changing the cone diameter can also duplicate the effects of penetration rate. The pore pressure element was located immediately behind

the cone tip, at the u_2 position. Profiles of CPTU results that include friction ratio, $R_f (= f_s/q_t \times 100\%)$ from tests at Yuan Lin site are shown in Figure 5.13. The results indicated no significant differences in q_t among three types of CPTU, considering drastic differences in cone size and/or penetration rate. The slow CPTU was conducted at depth levels where Laval samples were taken. The u_2 values from large CPTU were mostly identical to those from the standard CPTU. The u_2 readings in slow CPTU matched well with the hydrostatic pressure u_0 , indicating that 1mm/sec was slow enough to allow the penetration induced pore pressure to fully dissipate and reach equilibrium in most parts with the surrounding hydrostatic pressure.

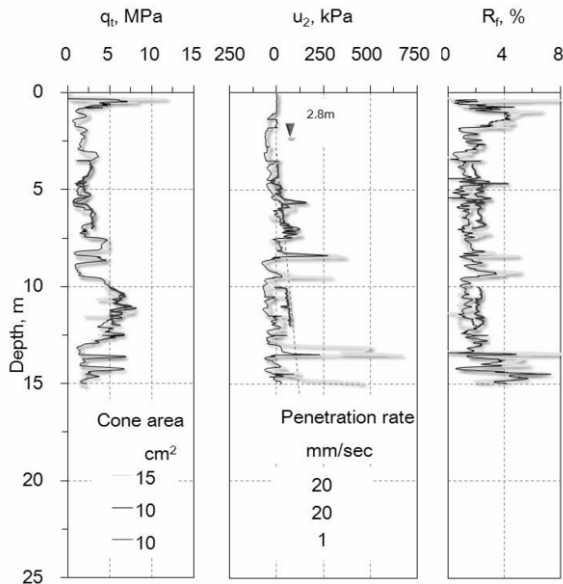


Figure 5.13 CPTU profiles from Yuan Lin site (after Huang, 2009).

The standard CPTU was coupled with dissipation tests at Yuan Lin test sites. The results in terms of q_t profile are plotted in Figure 5.14 along with fines contents (from tests on SPT samples). The comparison between Figures 5.11 and 5.14 allows the change in q_t and its relationship with pore pressure dissipation tests to be visualized. The effects of partial drainage for CPTU in MLS were demonstrated by the presence of significant setups following a pore pressure dissipation test as shown in Figure 5.11. The field CPTU was close to drained conditions with essentially no signs of q_t setup, even when the fines contents reached as high as almost 100%. The suspension of cone penetration in field pore pressure dissipation test caused a sharp decrease in q_t and followed by a resumption of the original q_t at the start of the subsequent push.

The drastic differences between CPTU in laboratory prepared, well mixed silty sand and natural silt/sand in the field are likely due to the heterogeneity existed in natural soil. It is believed that the presence of closely-spaced free draining sand layers made the field CPTU behave as a drained test in a silty soil mass. At much wider range of fines contents, the lateral spread of $CRR-q_{tIN}$ data points based on tests in YLS shown in Figure 5.12 was less than those from tests using the reconstituted MLS specimens or suggested by the available $CRR-q_{tIN}$ correlations. If differences in fines content are viewed as those of soil types, it can also be concluded that the fines content effects are less significant than soil types for the case of YLS.

Using bender elements, the V_s can be measured on the same soil specimen of cyclic shearing test. The $CRR-V_{sI}$ correlation can thus be conveniently calibrated completely based on laboratory tests (Huang et al., 2004; Baxter et al., 2008). Figure

5.3 shows $CRR-V_{sI}$ data points compiled by Baxter et al. (2008) that include clean sands (Toyoura and Niigata sand), silty sand (Mai Liao sand with $0\% \leq FC \leq 50\%$) and non-plastic silt. The silt specimens include those from undisturbed block samples, split-barrel samples and reconstituted samples by a modified moist tamping method. The result shows that the effects of soil type on $CRR-V_{sI}$ correlation overshadow those of fines content, sample preparation methods and applications of pre-shearing or pre-stressing.

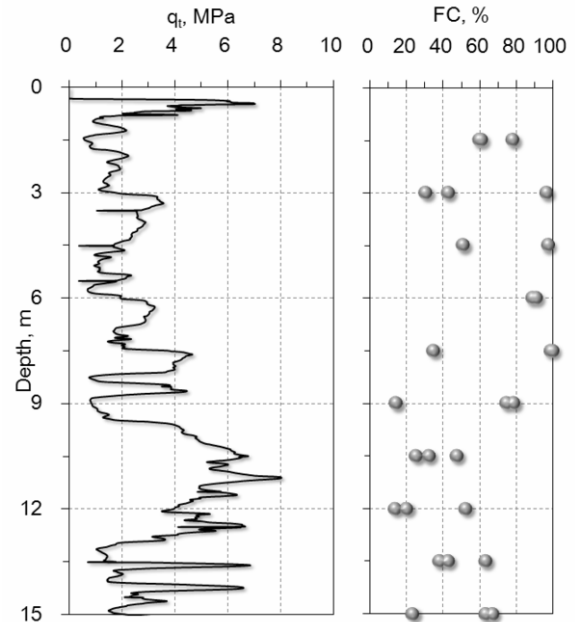


Figure 5.14 Enlarged q_t and fines content profiles from YLS site (after Huang, 2009).

5.3 Evaluation of Liquefaction Resistance Based on Undisturbed Samples

Attempts of taking high quality samples of cohesionless soils from below ground water table can be traced back by at least half a century (Singh et al., 1982). Challenges involved in taking good quality sand samples include prevention of the loss of sample during withdrawal and damaging soil structure during transportation. These challenges are formidable unless the samples are taken near the ground surface or by block sampling. Yoshimi et al. (1977) is believed to be the first among the more recent attempts in developing practical procedures of ground freezing and dry coring for sand sampling. A column of sand is frozen in situ and then cored out of the ground surface. Researchers from Japan and North America have generally considered in situ ground freezing (Hofmann et al., 2000) and coring to be a superior method for obtaining undisturbed samples of sand.

Driven by the demand in high-tech industry, the cost of liquid nitrogen continues to decrease. With a much lower temperature (-196°C), the efficiency and practicality of using liquid nitrogen for ground freezing can be much improved in contrast to the use of brine (-30°C). Provided that drainage is not impeded and that changes in void ratio are minimized during freezing, the in situ structure can be reserved. Studies have indicated that this structure preservation is possible if free drainage is allowed in at least one direction during freezing (Singh et al., 1982). The reservation of soil structure is further enhanced if freezing is conducted under a confining stress (Yoshimi et al., 1977).

For silty sands, especially when fines contents are high, drainage can be significantly constrained in the field. Ground freezing can cause void ratio changes due to frost heaving. It is

possible to retrieve samples in granular soils by pushing a piston tube sampler under ambient temperature. However, the friction between the sampling tube and the surrounding soil can be excessive when fines contents are low. The sampling by pushing tends to loosen dense sand and densify loose sand (Hofmann et al., 2000). Good quality sampling is possible if fines contents are high (Bray & Sancio, 2006) or samples are taken near the ground surface (Høeg et al., 2000) with either a piston tube sampler or by block sampling (Baxter et al., 2008).

Huang & Huang (2007) reported the use of Laval sampler to obtain high quality silty sand samples with fines contents ranging from 18 to 89% at Yuan Lin test site. The Laval sampler as schematically described in Figure 5.15 was developed at Laval University (La Rochelle et al., 1981), originally for taking high quality samples in sensitive clay. The sampler was made of two main parts; a sampling tube and an overcoring tube. To take a sample, the drill rig pushed the sampling tube into the bottom of the borehole while rotating the overcoring tube. No freezing was applied in the ground. The bottom of sampling tube was protruded at 20mm ahead of the steel teeth and cutters. During penetration, the head valve was kept open to allow drill mud circulation and thus removal of soil cuttings. The Laval sample can be 450 to 550 mm long. After a waiting period of 5 to 30 minutes, the head valve was closed and the bottom of the sample sheared by rotating the inner rod. The sample was then retrieved to the ground surface.

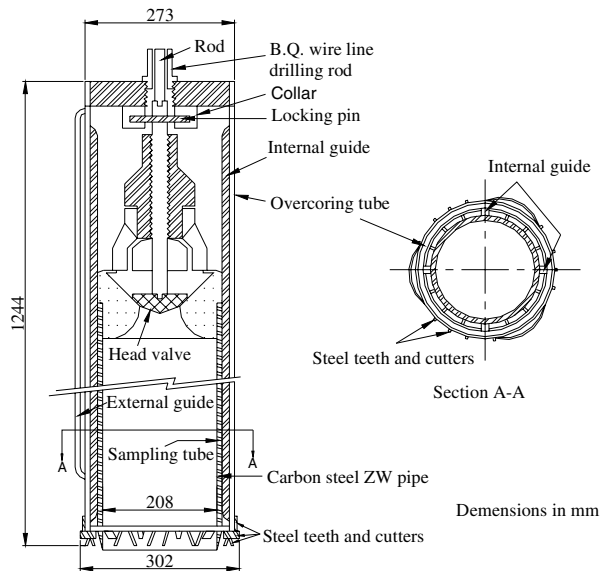


Figure 5.15 Schematic view of the modified Laval sampler (modified from La Rochelle et al., 1981).

The Laval samples with $FC > 30\%$ were cut into 120 to 180mm long segments and sealed in the field, without freezing. The samples taken from soil layers with low fines contents ($FC < 30\%$) remained in the sampling tube and kept vertical until it was completely frozen. The soil along with the sampling tube was placed in a Styrofoam lined wooden box and gradually frozen from top of the sample by dry ice at -80°C . A backpressure equal to the water head within the sample was applied by means of nylon tubing connected to the bottom of the sample to ensure that no water can drain under gravity. The bottom drainage and backpressure assured pore water drainage only due to water volume expansion during freezing (Konrad et al., 1995). The frozen samples were stored in a freezer during shipping and laboratory storage until the time of shearing test.

A specially designed coring device was used to cut 70mm diameter triaxial specimens from the frozen Laval sample, kept at -80°C by dry ice (Huang & Huang, 2007). The specimen was

then placed in the triaxial cell under a confining stress and thawed following the procedure suggested by Hofmann (1997). An important advantage of Laval sampler is its large size. Four 70mm diameter triaxial specimens can easily be cored from a single Laval sample at the same depth level. The number of specimens is ideally suited for the determination of a $CRR-N_c$ curve through cyclic triaxial tests. As shown in Figure 5.16, the values of V_{s1} taken from the triaxial test specimens fell within the general range of field measurements near the Laval sampling locations, indicating a reasonable quality of the soil samples.

Huang et al. (2008) reported the use of a gel-push sampler to recover high quality samples in silty sands at a test site in Kao Hsiung of Southern Taiwan, where the fines contents varied from 5 to over 60%. The gel-push sampler developed in Japan (Tani & Kaneko, 2006) was modified from a 75mm Osterberg piston sampler (also known as a Japanese sampler) as schematically shown in Figure 5.17. The sand sample was obtained by pushing the gel-push sampler under ambient temperature as typically done for piston sampling in clays. A water soluble polymeric lubricant (gel) was injected from the sampler shoe to lubricate and alleviate friction exerted on the sampling tube as it was pushed into the sand. A shutter located at the tip of the sampler remained open during pushing but forced into a closed position at the end of pushing. The closed shutter prevents the sample from falling during withdrawal. Upon withdrawal of the sampling tube above ground, the ends of the tube were sealed and waxed. No freezing was applied for the sample preservation. An accelerometer was attached to the sampling tube where the acceleration readings were continuously recorded during shipping.

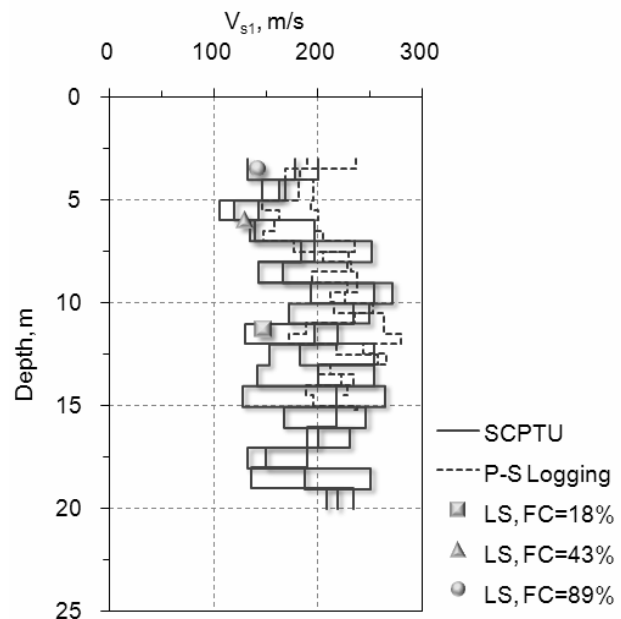


Figure 5.16 Comparison of laboratory and field V_{s1} measurements in YLS with varying fines content (after Huang & Huang, 2007).

The soil sample extruded out of the gel-push sampler was trimmed to a diameter of 70mm to fit the triaxial testing device and remove a shell of soil that was impregnated by the gel during field sampling. The trimmed soil specimen was inserted directly into a rubber membrane lined sample holder. The design of the sample holder shown in Figure 5.18 follows that of Dharma & Sanin (2006), where a layer of sponge was placed between the rubber membrane and the metal split mold. The sponge was compressed initially by the application of vacuum to give room for insertion of the soil specimen. Upon release of vacuum, the sponge expansion provides a confining stress on

the granular soil specimen until the specimen is seated in the triaxial cell and vacuum resumed through the drainage lines. By maintaining the confining stress the sample holder minimizes the chance of disturbance during triaxial test set up.

Figure 5.19 compares the V_s measurements on cyclic triaxial test (CTX) specimens using bender elements and those from the field seismic cone penetration tests (SCPTU). For the most part, the laboratory V_s falls within or close to the range of those from SCPTU at comparable depths.

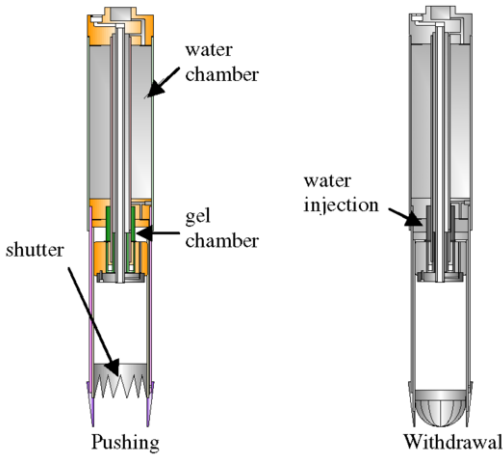


Figure 5.17 Schematic views of the gel-push sampler (after Huang & Huang, 2007).



Figure 5.18. The sample holder (photograph by A.B. Huang).

5.3 Liquefaction Potential Assessment for Silts and Clays

Except for organic soils, as fines content exceeds 50%, the soil is classified as either silts or clays. Experience learned in Northridge, Kocaeli and Chi-Chi earthquakes showed that the seismic motion could cause ground failures in low-plastic silts and clays (Chu et al., 2004; Bray & Sancio, 2006). Based on data collected in China that relate to earthquake induced liquefaction, Wang (1979) suggested that clayey soils containing less than 15 to 20% particles by weight smaller than 0.005 mm and having a water content (w_c) to LL ratio greater than 0.9, are susceptible to liquefaction. Seed & Idriss (1982)

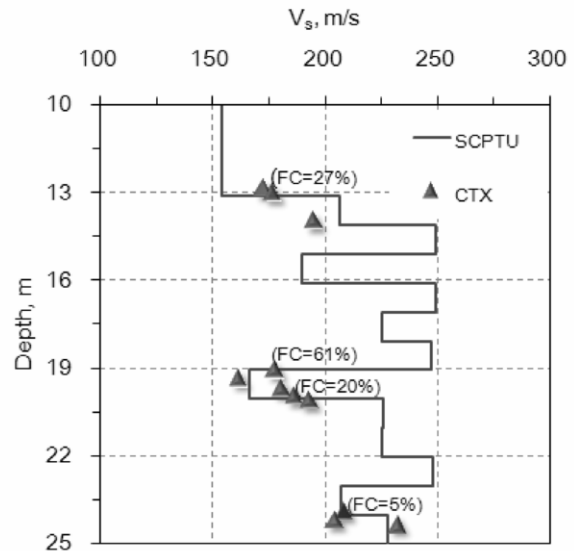


Figure 5.19 Comparison between the V_s measurements from bender elements and those from SCPTU (after Huang et al., 2008).

further refined that statement and indicated that all of the following three conditions must be met: (1) percent of particles smaller than 0.005 mm is less than 15%, (2) $LL < 35$, and (3) ratio of $w_c/LL > 0.9$. These conditions are referred to as the “Chinese criteria” because of their origins. Bray & Sancio (2006) compiled data that included observations in recent earthquake events and proposed new liquefaction susceptibility criteria for silts and clays using PI and w_c/LL ratio, as shown in Figure 5.20. The criteria proposed by Bray & Sancio (2006) consider liquefaction in a general term that includes the phenomenon of dramatic loss of shear strength due to increased porewater pressure and reduced effective stress. It also considers cases where liquefaction leads to transient softening and increased cyclic shear strains, due to dilation as undrained shearing continues (i.e., cyclic softening).

Boulanger & Idriss (2006) indicated that there can be fundamental differences in cyclic and monotonic undrained shearing behavior between clay-like and sand-like fine grain materials. Figure 5.21 shows screening criteria suggested by Boulanger & Idriss (2006) to first determine whether the liquefaction susceptibility should be evaluated as a clay-like (cyclic softening) or sand-like (liquefaction) material. For fine-grained soils considered as sand-like, the SPT or CPT based simplified procedure can be used to estimate their cyclic strength.

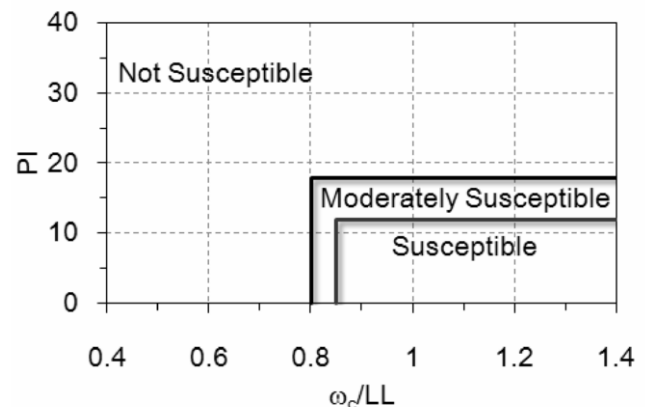


Figure 5.20 Liquefaction susceptibility criteria proposed by Bray & Sancio (2006).

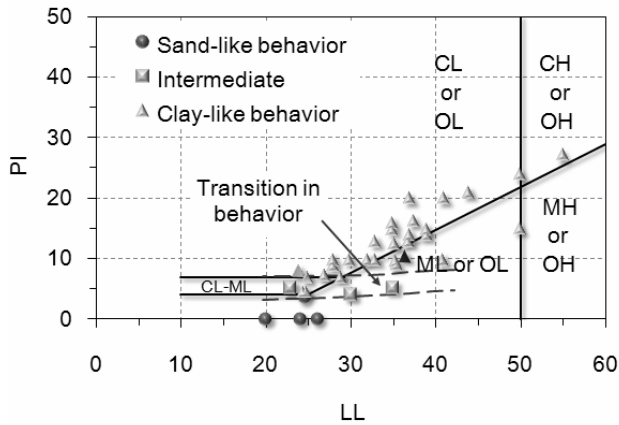


Figure 5.21 Atterberg limits chart showing representative values for clay-like, sand-like, or intermediate type soil behavior (from Boulanger & Idriss, 2006).

For practical purposes, fine-grained soils can confidently be expected to exhibit clay-like behavior if they have $PI \geq 7$ as shown in Figure 5.22. The clay-like soils are more likely to have stress-history normalized behavior. The cyclic strength can be evaluated based on information from in situ testing, laboratory testing and available empirical correlations. For clay-like fine-grained soils, undisturbed sampling is relatively simple and low cost. Evaluation of liquefaction resistance based on undisturbed samples can be a practical alternative.

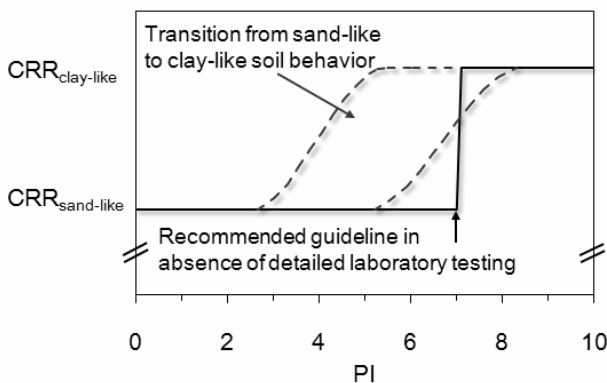


Figure 5.22 Transition from sand-like to clay-like behavior for fine-grained soils with increasing PI, and the recommended guideline (from Boulanger & Idriss, 2006).

5.4 The Critical State Approach

The background and details of the Critical State Soil Mechanics have been given in Section 2 on Soil Behaviour. In contrast to the semi-empirical and field-based methods in the simplified procedures, the critical state approach to cyclic response of granular materials has a sound theoretical framework. Following a critical state constitutive model developed by Papadimitriou et al. (2001), Bouckovalas et al. (2003) was able to systematically evaluate the effects of fines on the cyclic strength of silty sand. Qadimi & Coop (2007) investigated the undrained cyclic behavior of a carbonate sand based on a series of monotonic shearing tests using the critical state framework.

The critical state approach is anchored to the state parameter (ψ). The state parameter is the void ratio difference between the current state of the soil and the critical state at the same effective mean normal stress (p'). The more negative state parameter corresponds to higher soil dilatancy in shearing. Figure 5.23 shows results from cyclic triaxial tests on 13 sands compiled by Jefferies and Been (2006). The cyclic strength is referred to the cyclic resistance ratio at 15 cycles (CRR_{15}) of loading in triaxial tests. Consistent with the correlation between

state parameter and soil dilatancy, the data show that CRR_{15} increases as ψ becomes more negative. There are some scattering in the CRR_{15} - ψ correlation. This scattering correctly reflects the effects of soil fabric as specimens prepared by different methods but tested under the same initial state are likely to result in different CRR_{15} . On the other hand, fabric effects are not captured by ψ .

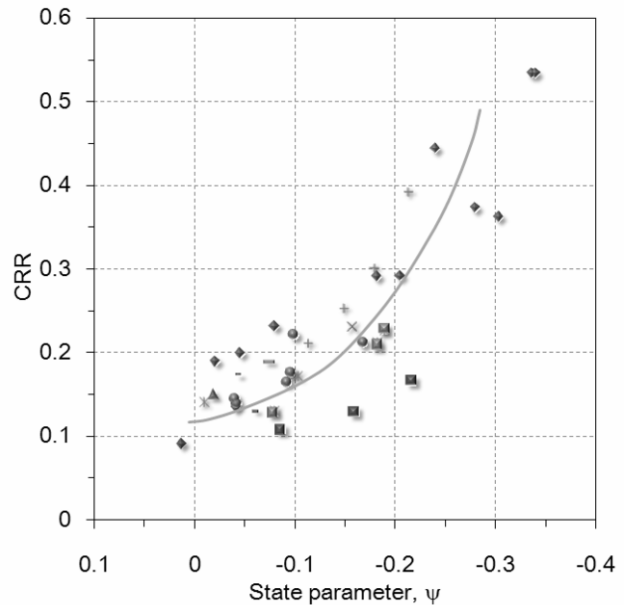


Figure 5.23 Cyclic strength as a function of state parameters for 13 sands (after Jefferies & Been, 2006).

The state parameter needed in assessing the cyclic strength according to Figure 5.23 can be determined from in situ tests. By analyzing a series of calibration chamber CPT data, Been et al. (1986; 1987) and Jefferies & Been (2006) demonstrated that the normalized cone tip resistance $Q_p (= (q_c - p)/p')$ in log scale has a linear relationship with ψ as shown in Figure 5.24. The trend line has a simple exponential form:

$$Q_p = k \exp(-m\psi) \tag{5.7}$$

This empirically derived equation based on dimensional grounds was consistent with the cavity expansion solution proposed by Carter et al. (1986). The values of k and m in Equation (7) correspond, respectively to the intercept and slope of the trend lines in Figure 5.24. These values are sand-specific and as such are functions of intrinsic properties of the sands. In addition, k and m should relate to the slope of the critical state line (λ).

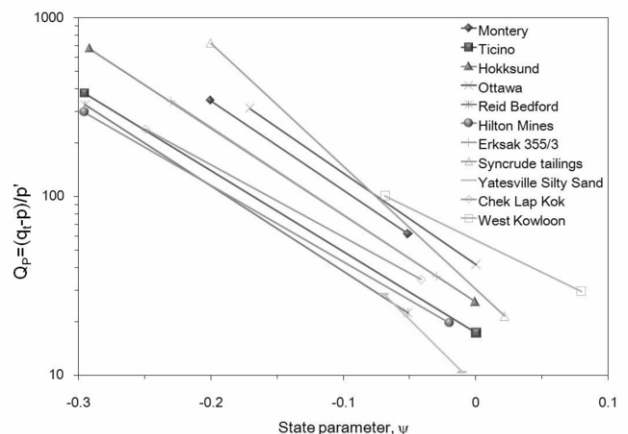


Figure 5.24 The Q_p - ψ trends for different sands (after Jefferies & Been, 2006).

The validity of Equation (7) was challenged by Sladen (1989) who indicated that k and possibly m were functions of p' . Shuttle & Jefferies (1998) developed a numerical framework for evaluating ψ from CPT. This framework was based on cavity expansion analysis and NorSand numerical model. Based on their analysis and those of Carter et al. (1986), the stress level bias pointed out by Sladen (1989) can be properly addressed by treating k and m as functions of rigidity index (I_r) defined as $I_r = G/p'_o$. Taking advantage of this revised Q_p - ψ correlation, Jefferies & Been (2006) demonstrated the potential of expressing the liquefaction boundary curve in terms of ψ for clean sands. Assuming a set of critical state parameters expected for typical clean sands, $\sigma'_{vo} = 100\text{kPa}$ and $K_o = 0.7$, a series of Q_p and ψ were computed using the critical state based numerical framework and Equation (7). The ψ -based boundary curve that separates liquefaction from no liquefaction is a simple exponential function as shown in Figure 5.25.

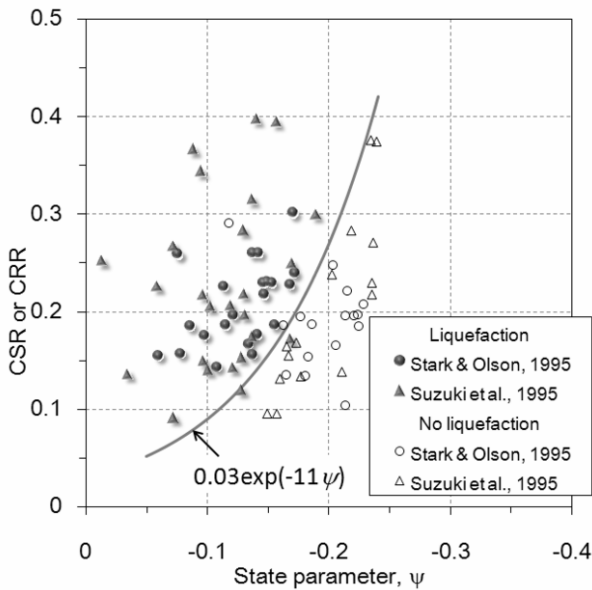


Figure 5.25 A liquefaction boundary curve expressed in terms of ψ (after Jefferies & Been, 2006).

As the boundary curve was derived based on a given set of critical state parameters, the coefficients of the exponential equation (i.e., the “0.03” and “-11”) included in Figure 5.25 are expected to be functions of soil properties. This implies that there can be multiple ψ -based boundary curves. The coefficients k and m of Equation (7) are sand-specific. For a given ψ , there can be multiple Q_p , depending on the soil properties. Following this logic, there should be no single CRR - q_{t1N} correlation for clean sands. Instead, it is expected that there are multiple CRR - q_{t1N} correlations that reflect the differences in the intrinsic properties among various sands. This is consistent with the results depicted in Figure 5.6, where a separate CRR - q_{t1N} correlation was obtained for different clean sands.

The critical state approach as above described can have many important advantages over the semi-empirical field-based simplified procedures. The effects of confining stress on CRR (i.e., the K_σ effect) are included in the CRR - ψ correlation. The cone tip resistance, Q_p is linearly normalized with p' , and thus avoids the potential error associated with the exponential stress normalization typically used to obtain q_{t1N} . As long as CPT remains drained, the fines content is part of the soil intrinsic properties (i.e., grain size, gradation, mineralogy, interparticle friction etc.). Their effects are reflected in the critical state parameters and coefficients of k and m . Potential confusion in the fines content adjustment, which is an integral part of the simplified procedure, can thus be minimized if not avoided.

In addition to Q_p , the use of other types of cone penetration as well as in-situ test methods to infer state parameters have also been reported. These methods include cone pressuremeter (Yu et al., 1996), seismic cone (Schnaid, 2005), pressuremeter (Yu, 1996) and the flat plate dilatometer (Konrad, 1988; Marchetti et al 2008).

5.5 Probabilistic Approaches to Liquefaction Evaluation

In addition to deterministic liquefaction methods, some new approaches using probability of occurrence have been developed by statistical analyses of the large databases. For clean sands, Figures 5.26 and 5.27 show illustrative sets of CRR at different degrees of certainty in liquefaction likelihood in terms of cyclic stress ratio (CSR) versus stress-normalized cone tip resistance (q_{t1}) and stress-normalized shear wave velocity (V_{s1}), respectively. Additional efforts are underway to help quantify the effects of fines content, age, and porewater pressures in terms of probability distributions for the CRRs.

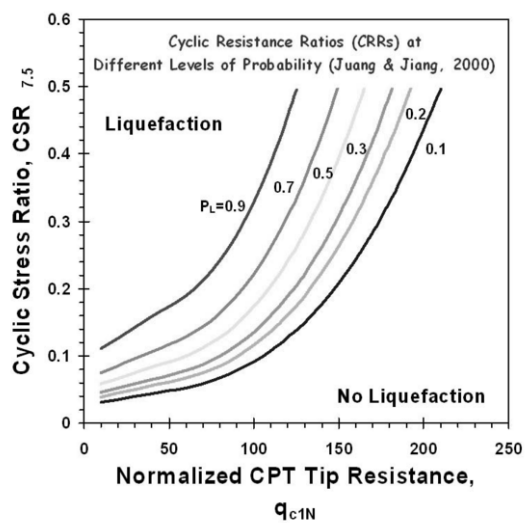


Figure 5.26 Probabilistic liquefaction boundary curves for normalized cone tip resistance (after Juang & Jiang 2000)

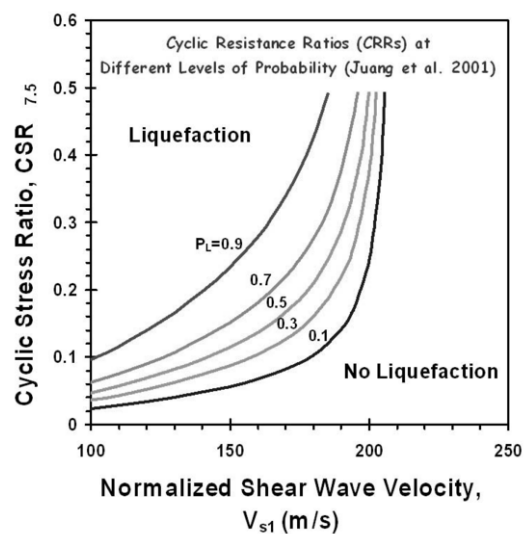


Figure 5.27 Probabilistic liquefaction boundary curves for normalized shear wave velocity (after Juang et al 2001)

6. BEHAVIOR AND TESTING OF SOIL-GEOSYNTHETIC INTERFACES

6.1 Overview of geosynthetics

Geosynthetics constitute well-established geomaterials in engineering practice, as they enhance or replace several of the functions of soils and rocks. According to Giroud (2008), it is justified to refer to geosynthetics as a full discipline, because, unlike other innovations in geotechnical engineering, geosynthetics have pervaded most branches of the geotechnical practice. The relevance of geosynthetics has increased rapidly due not only to their use in well-established applications but mainly to the increasing number of new applications involving their use.

Among the various properties used to characterize geosynthetics, proper characterization of the soil-geosynthetic interfaces requires particular attention. The shear behavior of these interfaces can be evaluated within frameworks already developed to characterize the shear behavior of soils. For example, as in the case of soils, aspects of the soil-geosynthetic interface behavior such as their drained and undrained response, characterization of the peak and residual interface shear strength, and plastic deformations along these interfaces can be evaluated using the framework of critical state soil mechanics. Yet, it is important to identify the differences between the shear behavior of soil and that of soil-geosynthetic interfaces. Indeed, shear failure along soil-geosynthetic interfaces often governs the behavior of earthen structures involving the use of geosynthetics. This section discusses the behavior and testing of various soil-geosynthetic interfaces, including comparisons among the behavior of various soil-geosynthetic interfaces.

Geosynthetics are defined as planar products manufactured from polymeric materials, which are used with soil, rock or other geotechnical engineering related material as an integral part of a man-made project, structure, or system (ASTM 1995). Numerous tests have been developed to characterize the hydraulic, mechanical, and rheological properties of geosynthetics. The material properties that are primarily related to the manufacture and quality control of geosynthetics are generally referred to as index properties and those related to the design are referred to as performance properties. As in the case of soils, some index properties are also used for design after developing correlations with performance properties.

Geosynthetics are widely used in many geotechnical, environmental, and hydraulic applications. In order to fulfill design needs of geotechnical-, environmental-, and hydraulic-related systems, the geosynthetic industry has developed a number of products to achieve multiple functions. The geosynthetic functions include (Bouazza et al. 2005; Zornberg and Christopher 2007):

- **Separation**, when a geosynthetic placed between two dissimilar geomaterials is used to maintain or improve the integrity and performance of both materials.
- **Reinforcement**, for the case in which the geosynthetic provides tensile strength to other geomaterials or systems that lack sufficient tensile capacity.
- **Filtration**, if the geosynthetic allows flow across its plane while retaining fine soil particles on its upstream side.
- **Drainage**, when the geosynthetic transmits flow within the plane of its own structure.
- **Hydraulic/Gas Barrier**, if the geosynthetic is relatively impervious and is used to contain liquids or gasses.
- **Protection**, when the geosynthetic provides a cushion to minimize damage of other products such as geomembranes.

In some cases, a geosynthetic may serve multiple functions (e.g., a geocomposite layer may provide in-plane drainage but also provide protection to an underlying geomembrane). Structures such as modern landfills often involve the use of all types of geosynthetics to perform all the aforementioned functions (Bouazza et al. 2005). The types of geosynthetics include:

- **Geogrids**, which are extensively used to reinforce steep slopes (Elias et al. 2001; Zornberg and Kavazanjian 2001; Zornberg and Arriaga 2003), and retaining walls (Abu-Hejleh et al. 2002, Allen et al. 2003, Benjamim et al. 2007, Hatami and Bathurst 2005). Geogrids are also used to reinforce and improve the performance of pavements (Perkins and Cortez 2005; Zornberg et al. 2008) and foundations (Gabr et al. 1994). In addition, geogrids have been recently used to reinforce slopes beneath the waste, as well as for veneer reinforcement of the cover soils above geomembranes (Zornberg et al. 2001; Zornberg 2005). Innovative uses of geogrids have involved their use in reinforced structures to increase the storage capacity in mining projects (Costa Filho and Sieira 2008).
- **Geotextiles** are common components in many geotechnical projects. For example, they are used in hydraulic systems, pavements and landfills for filtration purposes (Giroud 2009). Important advances are also currently underway regarding understanding of their rheological properties (Thornton et al. 1998, Zornberg et al. 2004). They are also used as cushion to protect the geomembrane from puncture (Koerner et al. 1996, Narejo et al. 1996, Wilson-Fahmy et al. 1996). Geotextiles are also used occasionally to reinforce the waste mass in order to increase its global stability (Gisbert et al. 1996). The hydraulic properties of geotextiles under unsaturated conditions are currently being investigated for multiple applications (Bouazza et al. 2006).
- **Geonets** are unitized sets of parallel ribs positioned in layers such that liquid can be transmitted within their open spaces. Their primary function is in-plane drainage (Giroud et al. 2000). There are basically two types of products in the market: biplanar and tri-planar geonets. The tri-planar geonets are a more recent development, which resist vertical compression under load and allow larger in-plane flows (Banks and Zhao 1997). Because of their open structure, geonets must be protected from clogging by soil. Geonets are used with geotextiles or geomembranes on one or both of their planar surfaces.
- **Geomembranes** involve relatively impermeable sheets of polymeric formulations used as a barrier to liquids and/or vapors. The most common types of geomembranes are high density polyethylene (HDPE), very flexible polyethylene (VFPE), polyvinyl chloride (PVC), and reinforced chlorosulfonated polyethylene (CSPE-R), although there are also other types available (Koerner 1991). Polypropylene (PP) has been used to manufacture geomembranes (Matichard et al. 1996, Bouazza 1998, Comer et al. 1998). The use of geomembranes as the primary water-proofing element at the Contrada Sabetta Dam, Italy (Cazzuffi 1987) and to control clay desiccation in the Mission Dam (today Terzaghi Dam), Canada (Terzaghi and Lacroix, 1964) in the late 1950's represent the precursors of the current use of geosynthetics in containment systems. Data are now available regarding their expected lifetime, indicating that long-term durability of geomembranes is less of a concern than initially anticipated (Hsuan and Koerner 1998; Rowe and Sangam 2002, Koerner et al. 2008, Tisinger et al. 1991). Indeed, exposed geomembranes are also being used nowadays in the design of waste containment cover systems (Giroud et al. 1995, Zornberg and Giroud 1997, Giroud et al. 1999).

Construction quality control issues are considered the main limitation in the performance of geomembranes.

- **Geocomposites** represent a subset of geosynthetics whereby two or more individual materials are utilized together. They are often laminated and/or bonded to one another in the manufacturing facility and are shipped to the project as a completed unit. A type of geocomposite most commonly used in landfills is a geotextile/geonet composite (Banks and Zhao 1997). The geotextile serves as both a separator and a filter, and the geonet or built-up core serves as a drain. There can be geotextiles on both the top and bottom of the drainage core and they may be different from one another.
- **Geosynthetic clay liners (GCLs)** represent a composite material consisting of bentonite and geosynthetics (Bouazza 2002). The geosynthetics are either geotextiles or a geomembrane. With geotextile-encased bentonite, the bentonite is contained by geotextiles on both sides. The geotextiles are bonded with an adhesive, needle-punching, or stitch-bonding. For the geomembrane-supported GCL, the bentonite is bonded to the geomembrane using a water-soluble adhesive. Due to the flexibility of production and rapid innovation, different types of GCLs are also available with variation in their performances. Of the various types of geosynthetics used for containment of waste, GCLs are one of the newest and their use is rapidly expanding.
- **Geopipes** are commonly used in hydraulic, pavement, and landfill applications. A geopipe system is used in the sand or aggregate leachate collection layer to facilitate collection and rapid drainage of the leachate to a sump and removal system. Landfill facilities that operate wet cells (i.e. with leachate recirculation) employ geopipes to transport and redistribute leachate back into the waste fill (Reinhart and Townsend 1998). The pipes may be made of PVC or HDPE. The latter can be solid wall or corrugated.
- **Geocells** are three-dimensional, expandable panels made from HDPE or polyester strips (Yuu et al. 2008). When expanded during installation, the interconnected strips form the walls of a flexible, three-dimensional cellular structure into which infill materials are placed and compacted. This creates a system that holds the infill material in place and prevents mass movements. Cellular confinement systems improve the structural and functional behavior of soil infill materials. Geocells have been used to protect and stabilize steep slope surfaces and to reinforce foundations and landfill liners.
- **Fiber reinforcement** typically involves polypropylene fibers with lengths ranging from 25 to 50 mm mixed with soil. Two internal failure mechanisms, pullout and breakage, can be identified for fiber-reinforced soil (Maher and Gray 1988, Zornberg 2002). Under relatively low confining pressures, the fibers will develop a maximum tension under which they will be pulled out from the soil matrix being sheared. Under relatively high confining pressure, the fibers will develop a maximum tension under which they will break. For practical applications, and unlike a soil mass reinforced using uniaxial inclusions, the failure mechanism governing the behavior of a soil mass reinforced using polymeric fibers is pullout.

Recent advances on the behavior of the interfaces involving the various types of geosynthetics are described next in this section, with particular emphasis on the characteristics and differences in their shear stress-strain-strength response. Focus is on soil-geogrid interfaces, soil-geotextile interfaces, interfaces involving GCLs, and shear behavior of fiber reinforced soil.

6.2 Soil-Geogrid Interfaces

Geogrids are geosynthetic products designed preliminarily to fulfill a reinforcement function. They involve a uniformly-distributed array of apertures between their longitudinal and transverse elements. The apertures allow direct contact between soil particles on either side of the installed sheet, thereby increasing the interaction between the geogrid and the backfill soil. Geogrids are manufactured using polypropylene, polyethylene, polyester, or coated polyester. The coated polyester geogrids are typically woven or knitted. Coating is generally performed using PVC or acrylics to protect the filaments from construction damage and to maintain the grid structure. The polypropylene geogrids are either extruded or punched sheet drawn, and polyethylene geogrids are exclusively punched sheet drawn.

Since geogrids are primarily used as reinforcement elements, the shear behavior of interfaces involving geogrids has been typically characterized using pullout tests (Koerner et al. 1989; Jewell 1990; Bergado et al. 1993; Sugimoto et al. 2001; Palmeria 2004; Teixeira et al. 2007). The pullout interaction mechanisms between soil and geogrid reinforcements are more complex than those between soil and strip or sheet reinforcements. This is because the pullout resistance of geogrids includes two components: the interface shear resistance that takes place along the longitudinal ribs (and to a lesser extent along the transverse ribs), and the passive resistance that develops against the front of transverse ribs (Koerner et al. 1989). While the first mechanism could be quantified using parameters obtained from direct shear tests, the latter can only be evaluated using pullout tests. Evaluations of pullout test results have showed that geogrids may develop an equivalent interface shear strength that even exceeds the interface shear strength of the backfill soil (Ingold 1983).

Figure 6.1 shows the results obtained from a typical large-scale pullout test (Teixeira et al. 2007). The figure shows the applied pullout force as function of internal displacements, measured using telltales attached at different locations within the geogrid specimen. Figure 6.2 shows the displacement profiles along the geogrid length. The profiles are presented for increasing values of the pullout force, which is shown in the figure as a percentage of the maximum pullout resistance. The maximum displacement occurs at the point of application of the pullout load and decreases towards the back of the geogrid following a non-linear trend that reflects the effect of reinforcement extensibility.

The effect of the geogrid length on the pullout resistance is an important aspect that has been evaluated using large-scale pullout tests. Figure 6.3(a) shows the results of a pullout testing program conducted using geogrids with specimen lengths of 350, 600, and 1200 mm. The tests were conducted using a normal stress of 25 kPa. As shown in the figure, an increasing specimen length leads to increasing pullout resistance, increased initial stiffness, and increased displacement at peak pullout resistance. It should be noted that the pullout resistance increases approximately linearly with the geogrid specimen length. Indeed, the three pullout force-displacement curves appear to collapse into a single normalized curve when the pullout force and the frontal displacement are normalized in relation to the specimen length [Figure 6.3(b)]. The pullout resistance was found to be directly proportional to reinforcement length in spite of the complex stress transfer mechanisms that take place during pullout testing of geogrids (Teixeira et al. 2007).

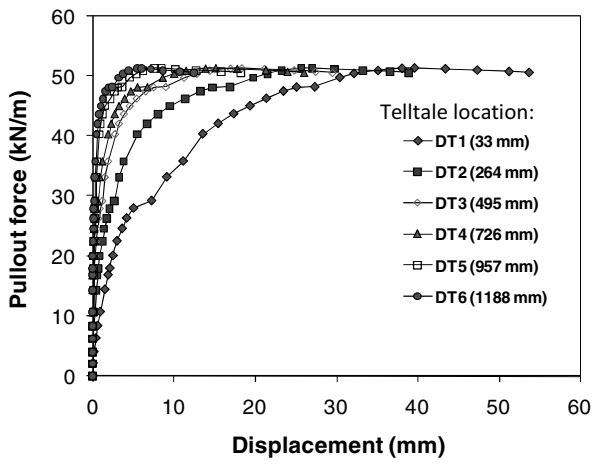


Figure 6.1. Load-displacement curves obtained from tell-tails located along a geogrid specimen during a large-scale pullout test (Teixeira et al. 2007).

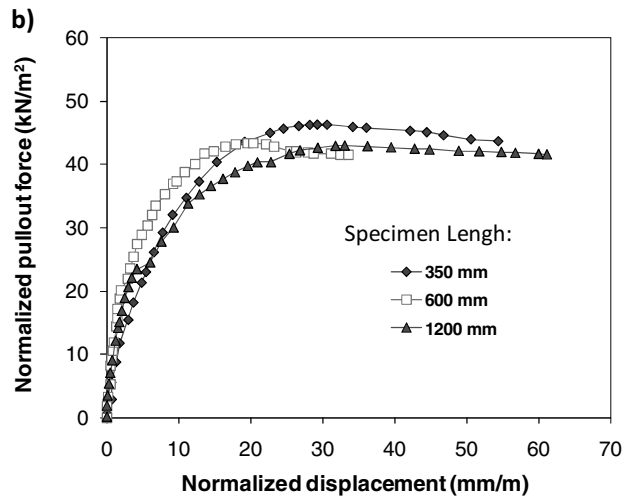
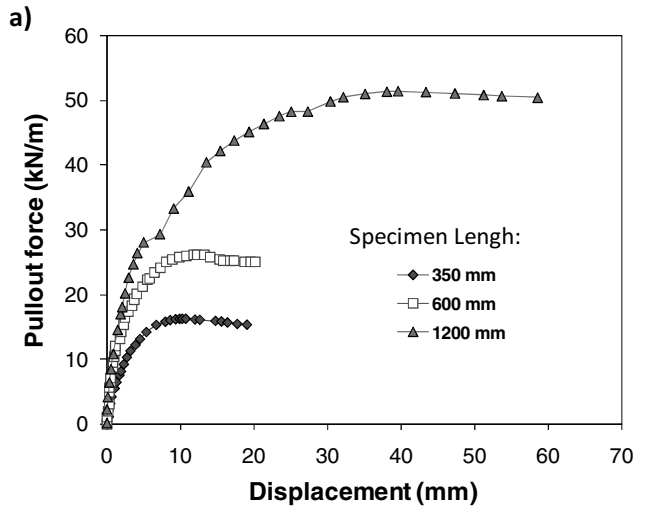


Figure 6.3: Effect of specimen length on pullout resistance: a) force vs. displacement curve; b) normalized force vs. displacement curve (Teixeira et al. 2007).

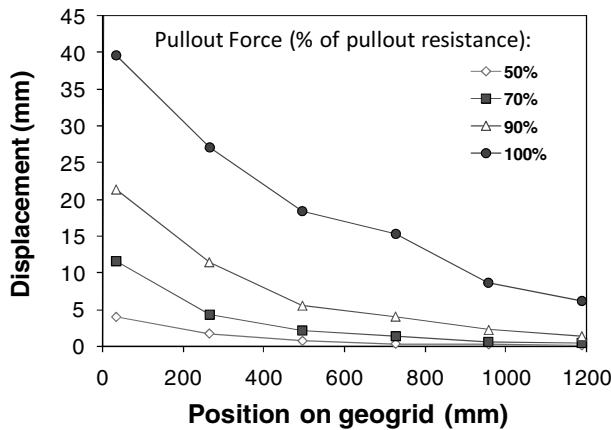


Figure 6.2. Distribution of displacements along a geogrid as obtained from a pullout test (Teixeira et al. 2007).

The ultimate pullout resistance has been typically interpreted as the sum of the passive and interface shear components (Jewell 1996). However, any synergism between these two load transfer mechanisms has often been neglected. Several failure mechanisms have been proposed to estimate the passive pullout resistance that develops against transverse ribs. These include the general shear failure mechanism (Peterson and Anderson 1980), the punching failure mechanism (Jewell *et al.* 1984), and a modified punching failure mechanism (Chai 1992). The general shear and punching shear failure mechanisms have been reported to provide upper and lower bounds of experimental pullout test results (Palmeira and Milligan 1989a; Jewell 1990b). The interface shear component between geogrid surface and soil has been generally estimated considering the surface area of the geogrid and the interface shear strength properties between the soil and geogrid.

Figure 6.4 compares the results of pullout tests, conducted using geogrid specimens with and without transverse ribs (Teixeira et al. 2007). The tests were conducted using a normal stress of 25 kPa. As expected, the pullout resistance of the geogrid with transverse ribs is higher than that of the geogrid without transverse ribs. Since the pullout resistance of the geogrid with transverse ribs is only 26 % higher than that of the geogrid without transverse ribs, a cursory interpretation of these

results could erroneously suggest that the passive resistance mechanisms provides only a comparatively small contribution to the overall pullout resistance. However, the pullout resistance of geogrids without transverse ribs should not be considered representative of the contribution of interface shear to the pullout resistance of geogrids. This is because the contribution of interface shear to the geogrid pullout resistance may be significantly reduced due to the interaction between longitudinal and transverse ribs.

A comprehensive discussion on the prediction of interface shear and passive resistance mechanisms has been summarized by Jewell (1990a) and Bergado et al. (1994). However, many of the available equations for interpretation of pullout tests correspond to inextensible inclusions and may not rigorously apply to polymeric extensible geogrids. Nonetheless, Milligan and Palmeira (1987) reported good comparison between experimental results and predictions obtained using bearing capacity equations that are valid for rigid reinforcement. Slightly modified analytical procedures were also successfully used to compute the pullout resistance of HDPE geogrids, as reported by Bergado and Chiai (1994) and Alfaro et al. (1995). Teixeira et al. (2007) showed that experimental results from large-scale pullout tests on Polyester (PET) geogrids could be predicted very accurately after defining separately the contribution of longitudinal ribs and transverse ribs.

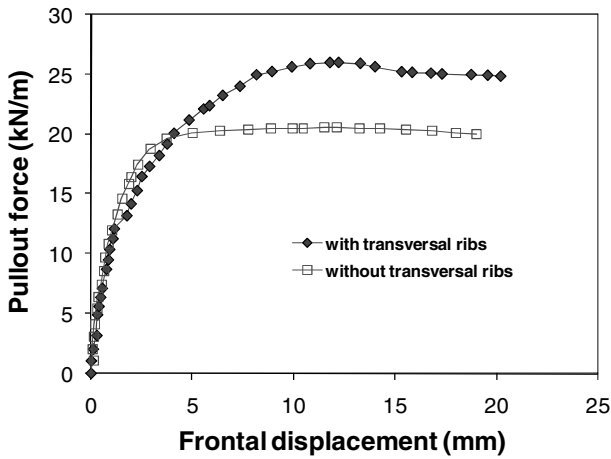


Figure 6.4. Results of pullout tests conducted using geogrids with and without transversal ribs (Teixeira et al. 2007).

Previous studies have reported that the interface and passive resistance contributions to the total pullout resistance depend on the geogrid geometry, soil grain size distribution and soil density. Specifically, Jewell (1990a) and Bergado *et al.* (1993) reported that geogrid pullout failure mechanism is a function of the ratio between transverse rib spacing (S) and the transverse rib diameter, the average particle size (D_{50}), the compaction moisture content, and the soil stiffness. Jewell (1990a) identified limiting values of the S/D_{50} ratio that characterize either interface shear or full interaction mechanisms (i.e. interface shear plus passive resistance). Additional studies on the variables governing the pullout resistance of geogrids were reported by Sarsby (1985), Lopes and Ladeira (1996), Ochiai *et al.* (1996), Teixeira and Bueno (1999) and Sugimoto *et al.* (2001).

Figure 6.5 shows the results from tests performed using different geogrid mesh densities (Teixeira et al. 2007). Specifically, pullout tests were conducted using the same geogrid but with transverse rib spacing ranging from 22 to 66 mm. While a decreasing pullout resistance is expected for increasing transverse rib spacing, the pullout test results indicate that there is an optimum spacing that maximizes the pullout resistance. When the transverse rib spacing is below the optimum value, the pullout response appears to be detrimentally affected by the effect that transverse ribs cause on the interface shear component of the pullout resistance. On the other hand, when the transverse rib spacing is above the optimum value, the pullout resistance is comparatively decreased because of the small number of transverse ribs that provide passive resistance contribution to the overall pullout resistance. Additional studies conducted using a variety of geogrid types and mesh densities in order to quantify the various pullout mechanisms include Palmeira and Milligan (1989b), Bergado and Chiai (1994), Alfaro *et al.* (1995), Lopes and Ladeira (1996), Ochiai *et al.* (1996), Teixeira and Bueno (1999), and Sugimoto *et al.* (2001).

An important aspect that can affect the pullout of geogrids is the interference that transverse ribs may have on the interface shear resistance component (Dyer 1985, Palmeira and Milligan 1989b). For example, the interference between transverse and longitudinal ribs in rigid metal grids buried in dense sand was reported to be function of the geogrid length, spacing between transverse ribs, and thickness of transverse ribs (Palmeira 1987, Palmeira and Milligan 1989b). Such interference has been attributed to increased localized vertical stresses that develop during pullout towards the front of the transverse ribs, as well as to a decrease in vertical stresses developing behind the transverse ribs (Palmeira 2004).

Figure 6.6 presents the localized normal stresses, as measured by two total stress cells (TSC1 and TSC2) located approximately 10 mm over the soil-geogrid interface (Teixeira et al. 2007). The total stress cells were aligned at the central portion of the geogrid apertures (in between two longitudinal ribs). Cell TSC1 was initially located between two transverse ribs while cell TSC2 was initially located directly over a transverse rib. The localized normal stresses in the beginning of the test (i.e. for zero frontal displacement) correspond to the applied normal stress of 25 kPa. However, as the test progresses, the localized stresses measured by the total stress cells oscillate and show normal stress values ranging from approximately 10 to 50 kPa. It should be noted that the distance between peaks in the measured localized stresses is consistent with the spacing between transverse ribs of the geogrid used in the test.

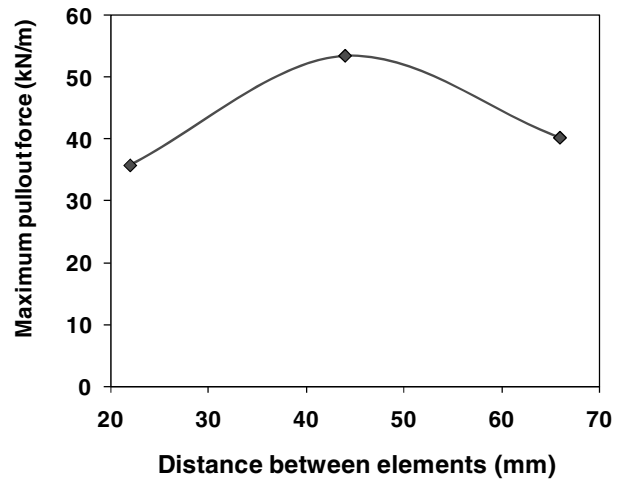


Figure 6.5. Effect of transverse-rib spacing on pullout resistance (Teixeira et al. 2007).

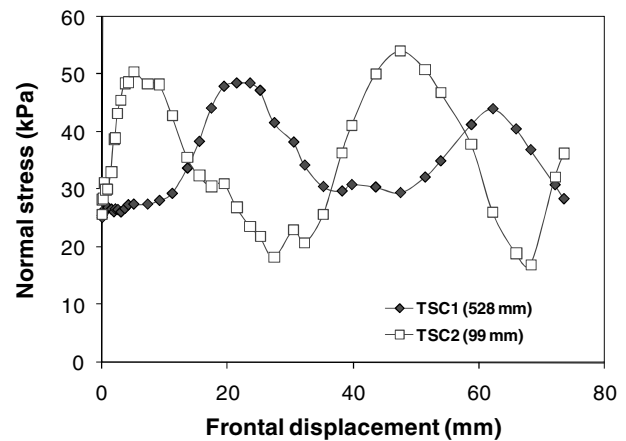


Figure 6.6. Localized normal stress in the vicinity of the soil-geogrid interface, as measured using stress cells located between longitudinal ribs (Teixeira et al. 2007).

During pullout, the soil in front of the transverse ribs is displaced above and below the transverse ribs, causing a tendency to dilation over the transverse ribs (Dyer 1985). As dilation is partially inhibited, the normal stresses tend to increase in the vicinity of the transverse ribs and to decrease between consecutive transverse ribs. This is consistent with the oscillation of normal stress measurements shown in Figure 6.6,

where the soil directly over transverse ribs is overstressed while the soil in the zone between transverse ribs (i.e. over the apertures) shows a comparative decrease in normal stress. Additional experimental data suggested that the redistribution of normal stresses induced by the transverse ribs appears to have a detrimental effect on the interface shear resistance component that develops along longitudinal ribs.

6.2 Soil-Geotextile Interfaces

Among the different geosynthetics, geotextiles are the products that present the widest range of properties. They can be used to fulfill all the different functions for many different geotechnical, environmental, and hydraulic applications. Geotextiles are manufactured from polymer fibers or filaments which are later combined to develop the final product. Approximately 85% of the geotextiles used today are based on polypropylene resin. An additional 10% are polyester and the remaining 5% consist of a range of polymers including polyethylene, nylon and other resins used for specialty purposes. As with all geosynthetics, however, the base resin has various additives, such as for ultraviolet light protection and long-term oxidative stability (Zornberg and Christopher 2007).

The filaments, fibers or yarns are formed into geotextiles using either woven or nonwoven methods. Woven geotextiles are manufactured using traditional weaving methods and a variety of weave types. Nonwoven geotextiles are manufactured by placing and orienting the filaments or fibers onto a conveyor belt, which are subsequently bonded by needle punching or by melt bonding. The needle-punching process consists of pushing numerous barbed needles through the fiber web. The fibers are thus mechanically interlocked into a stable configuration. As the name implies, the heat (or melt) bonding process consists of melting and pressurizing the fibers together.

The failure mode of interfaces involving geotextiles in projects such as landfill liners has been generally evaluated using direct shear tests. In contrast, the failure mode in projects such as reinforced soil structures has been generally evaluated using pullout tests. However, modeling of soil-geosynthetic interfaces under direct shear mode for the case of reinforced soil structures has also proven to be relevant, particularly for numerical simulation of their response (e.g. Springman et al. 1997, Hatami and Bathurst 2006). Studies involving direct shear tests have been reported by Jarret and Bathurst (1985), Cancelli et al. (1992), Bauer and Zhao (1993), Cazzuffi et al. (1993), Bakeer et al. (1998), and Abu-Farsakh and Coronel (2006).

Figure 6.7 shows the results of direct shear test results conducted using sand (conventional direct shear test), geotextile only, and sand-geotextile interfaces (Tupa 1994, Palmeira 2008). The materials used in the testing program included a fine sand and a nonwoven geotextile. The geotextile-only test was conducted by fixing the nonwoven geotextile to two rigid blocks and conducting a simple shear. As shown in the figure, the results indicate that the initial shear displacements of the soil-geotextile interface are consistent with those of the geotextile-only test and are then associated to the distortion of the geotextile. Yet, shear failure of the soil-geotextile interface was consistent with the shear failure of the fine sand. Specifically, the shear strength of the soil-geotextile interface and its post-peak behavior are essentially the same as those obtained by the direct shear test on sand.

A comparative evaluation of the response in direct shear mode of interfaces involving sand, sand-geotextile, and sand-geogrid is reported by Liu et al. (2009). The soil testing program involved large-scale direct shear tests performed using Ottawa sand, a polyester woven geotextile, and polyester geogrids manufactured using polyester yarns. It should be noted that the geogrids and woven geotextiles used in this testing program are the same material (PVC-coated PET yarns). The

direct shear test results conducted on sand, sand-geotextile interfaces, and sand-geogrid interfaces are shown in Figure 6.8. The sand and sand-geotextile interfaces show a reasonably well-defined peak shear strength, which is reached at comparatively small shear displacements. The shear stress at any shear displacement value (and in particular the peak shear strength) obtained from direct shear tests on sand is consistently higher than that obtained from direct shear tests on the sand-geotextile interface. On the other hand, the shear stress-displacement behavior of the sand-geogrid interface shows a different pattern. Specifically, a "yield" shear stress with a value slightly higher than the peak shear strength of the sand-geotextile interface develops at a shear displacement similar to the shear displacement at peak of the sand-geotextile interface (below 20 mm). The shear stress in the sand-geogrid interface continues to increase beyond this "yield" shear stress, approaching the value of the sand peak shear strength for comparatively large shear displacement values.

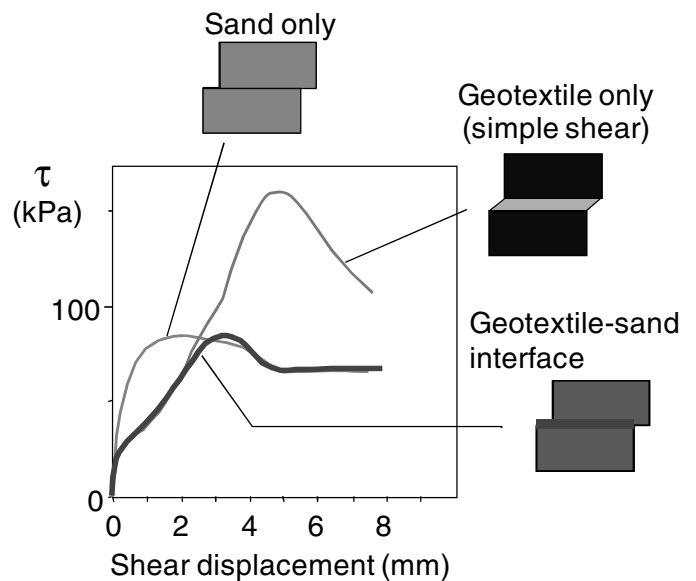


Figure 6.7. Influence of nonwoven geotextile distortion on the results of direct shear tests (Palmeira 2008).

The higher interface shear strength of the sand-geogrid interface in relation to that of the sand-geotextile interface can be attributed to the effect of the transverse ribs, which provide passive resistance even under direct shear mode. Specifically, the additional strength is developed from passive resistance induced by the transverse ribs. As shown in Figure 6.8, passive resistance mechanisms in the sand-geogrid interface develop at comparatively larger shear displacements than mechanisms in the sand or the sand-geotextile interfaces. In summary, for the same polymeric products, the sand-geogrid response was found to be bound between the sand-geotextile and sand shear stress-displacement curves.

6.3 Geosynthetic Clay Liner (GCL) Interfaces

Geosynthetic clay liners (GCLs) are infiltration barriers consisting of a layer of unhydrated, loose granular or powdered bentonite placed between two or on top of one geosynthetic layer (geotextile or geomembrane). GCLs are produced in panels which are joined in the field by overlapping. They are generally used as an alternative to compacted clay liners (Bouazza, 2002). Due to the inherent low shear strength of hydrated bentonite, GCL usage had initially been limited to applications where stability of the overlying materials was not a

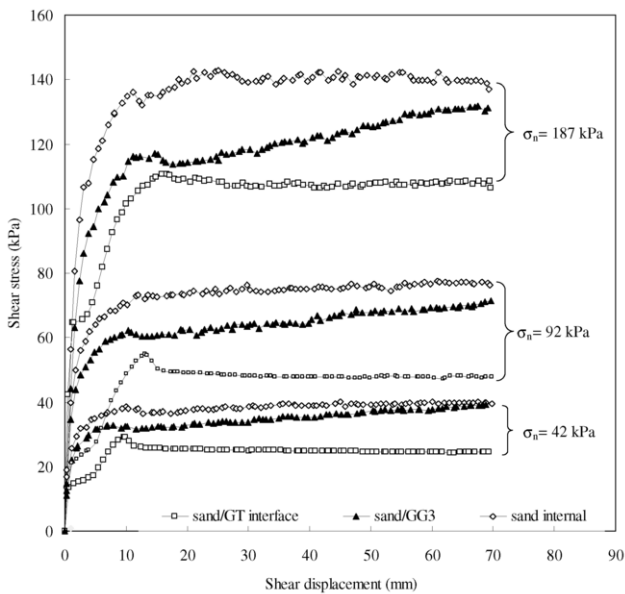


Figure 6.8. Shear stress-displacement behavior obtained from large-scale direct shear tests on sand, sand-geotextile interface, and sand-geogrid interface (Liu et al. 2009).

concern. In the late 1980s, however, methods were developed to reinforce the GCLs, producing a composite material with higher shear strength properties.

Some advantages of GCLs over compacted clay liners are that they occupy significantly less space to achieve equivalent performance, plus they are flexible, self-healing, and easy to install. In locations where low hydraulic conductivity clays are not readily available, they may offer significant construction cost savings. In addition, since they are factory manufactured with good quality control, field construction quality assurance costs are typically less than with compacted clay liners.

Geosynthetic clay liners are manufactured by placing a layer of dry bentonite, approximately 5-mm thick, on a geosynthetic material and attaching the bentonite to the geosynthetic. Two general configurations are currently employed in commercial processes: bentonite sandwiched between two geotextiles or bentonite glued to a geomembrane. The outer geosynthetic layer of GCLs can be mechanically bonded using stitching or needle punching (resulting in reinforced GCLs). A different process involves using an adhesive bond to glue the bentonite to the geosynthetic (resulting in unreinforced GCLs). The mechanical bonding of reinforced GCLs increases their internal shear strength.

A relevant failure mechanism in GCL liners correspond to failure surfaces that develop through the central portion of the GCL itself (internal shear failure). Several investigators have evaluated the GCL internal shear strength using direct shear and ring shear tests (Gilbert et al. 1996, 1997; Stark et al. 1996; Eid and Stark 1997; Fox et al. 1998; Eid et al. 1999). The evaluation of recent landfill failures and the availability of databases with shear strength results are making feasible the use of risk assessment to quantify uncertainty in selection of appropriate interface shear strengths (Koerner and Koerner 2001; Sabatini et al. 2002; McCartney et al. 2004; Dixon et al. 2005). Recently, a database of 414 large-scale direct shear tests conducted by a single laboratory was assembled and evaluated by Zornberg et al. (2005). This database allowed evaluation of the performance of GCLs manufactured using different types of reinforcement, indirect evaluation of the porewater pressures during shearing, and assessment of the GCL internal shear strength variability.

Figure 6.9 shows shear stress-displacement curves for three different types of GCLs: GCL A (needle-punched), GCL B (stitch-bonded), and GCL C (thermal-locked). The three GCL types were tested using the same normal stress σ_n (310.3 kPa), same hydration time t_h (168 hrs), same consolidation period t_c (48 hrs), and same shear displacement rate, SDR (0.1 mm/min.). GCL A shows a well-defined peak shear strength (τ_p) and a marked post-peak shear strength loss. Unlike GCL A, GCL B shows a rapid initial mobilization of shear strength until reaching a “yield” stress level, beyond which a less pronounced hardening takes place until reaching τ_p . The displacement at peak for GCL B is significantly larger than that observed for GCL A. The post-peak behavior of GCL B could not be evaluated since this GCL did not reach a steady large-displacement strength value at the maximum displacement of the device. Thermal-locked GCL C shows a behavior similar to that of needle-punched GCL A, although the τ_p value is below that obtained for GCL A. GCLs A and C were reinforced using similar needle-punching techniques and have the same specified peel strength. Consequently, differences in their behavior are attributed to the effect of thermal-locking.

Figure 6.10 shows shear stress-displacement curves for an unreinforced GCL tested under hydrated and unhydrated conditions. Although a direct comparison of τ_p is not possible as the specimens were tested using different normal stresses, σ_n , the results indicate that the hydrated GCL has lower peak and large displacement shear strength values than the unhydrated GCL. Both specimens, however, show a significantly lower τ_p

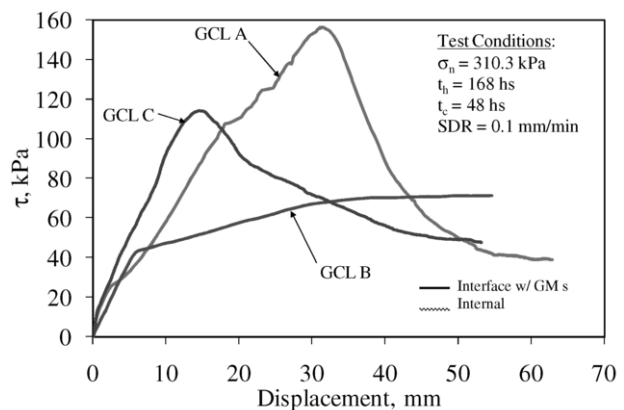


Figure 6.9. Shear stress-displacement curves for different GCLs: GCLs A (needle-punched), B (stitch-bonded), and C (thermally-locked) (Zornberg et al. 2005).

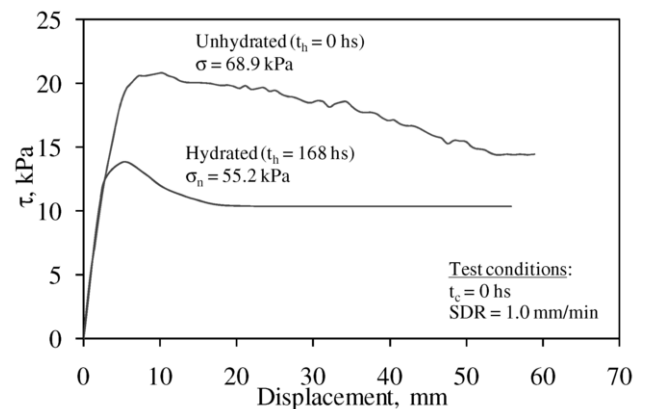


Figure 6.10. Shear stress-displacement curves for unreinforced GCLs (Zornberg et al. 2005).

than that obtained for reinforced GCLs. While both hydrated and unhydrated unreinforced GCLs show post-peak shear strength loss, the hydrated GCL appears to reach residual conditions at lower shear displacement than the unhydrated GCL.

The effect of shear displacement rate, SDR , on the peak and large displacement shear strength has been reported by Stark and Eid (1996), Gilbert et al. (1997), Eid and Stark (1997), Fox et al. (1998) and Eid et al. (1999). These studies, which primarily focused on the response of tests conducted under relatively low σ_n , reported an increasing τ_p with increasing SDR . Zornberg et al. (2005) reports the effect of SDR on internal shear strength using tests conducted under σ_n values beyond those reported in previous studies. Figure 6.11 shows the results of tests on a needle-punched GCL conducted under comparatively low σ_n (50 kPa) using the same test conditions, but varying $SDRs$. Consistent with the trend reported in past studies for tests conducted under low σ_n , the results show an increasing τ_p with increasing SDR . Figure 6.12 shows the results of tests on the same GCL conducted under high σ_n (520 kPa) using the same test conditions, but varying $SDRs$. Unlike the trend shown in Figure 6.11 for tests conducted under low σ_n , the results in Figure 6.12 show a decreasing τ_p with increasing SDR .

Figure 6.13 summarizes the peak shear strength results from Figures 6.11 and 6.12, and includes additional tests conducted to verify the repeatability of results (Zornberg et al. 2005). Explanations proposed to justify the trend of increasing τ_p with increasing SDR observed in previous studies, conducted under relatively low σ_n , have included shear-induced porewater pressures, secondary creep, undrained frictional resistance of bentonite at low water content, and SDR -dependent pullout behavior of fibers during shearing. However, the results obtained from tests conducted under both low and high σ_n suggest that the observed trends are consistent with the generation of shear-induced porewater pressures. Shear-induced porewater pressures are expected to be negative in tests conducted under low σ_n (i.e., below the swell pressure of GCLs). Consequently, increasing SDR will lead to increasingly negative porewater pressures and thus higher τ_p . This trend was also observed for tests conducted on unreinforced GCLs (Gilbert et al. 1997). On the other hand, shear-induced porewater pressures are expected to be positive in tests conducted under high σ_n (i.e., above the swell pressure of GCLs). In this case, increasing SDR will lead to increasingly positive porewater pressures and thus lower τ_p .

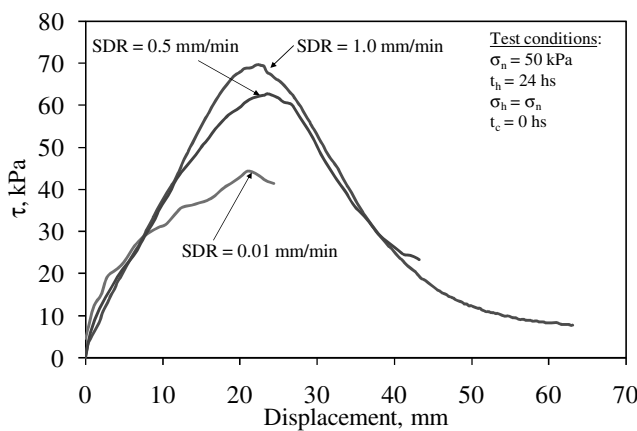


Figure 6.11. Effect of shear displacement rate on peak shear strength of needle-punched GCL: (a) Shear stress-displacement curves for tests under low σ_n (50 kPa) (Zornberg et al. 2005).

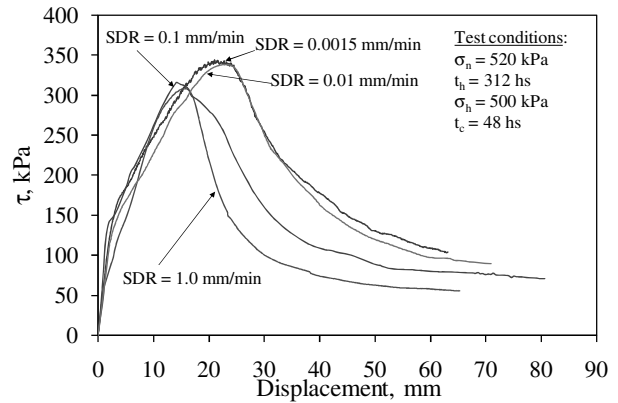


Figure 6.12. Effect of shear displacement rate on peak shear strength of needle-punched GCL: Shear stress-displacement curves for tests under high σ_n (520 kPa) (Zornberg et al. 2005)

In addition to internal GCL failure, a relevant interface that should be evaluated is that between GCL and geomembranes (GMs). This is because GMs are typically used directly above GCLs in hydraulic barrier systems such as landfill covers or bottom liners. In this case, stability is a major concern for side slopes in liners that include GCLs and GMs because of the very low shear strength of hydrated sodium bentonite, which has been reported to extrude from the GCL leading to weakening of the interface (Triplett and Fox 2001). Several investigators have evaluated the GCL-GM interface shear strength using direct shear and ring shear tests (Gilbert et al. 1996, 1997; Hewitt et al. 1997; Triplett and Fox 2001; Chiu and Fox 2004). Also, a database of results from 534 direct shear tests on the interface between different GCLs and GMs, conducted by a single laboratory, was assembled by McCartney et al. (2009) to identify and quantify the variables governing GCL-GM interface shear strength.

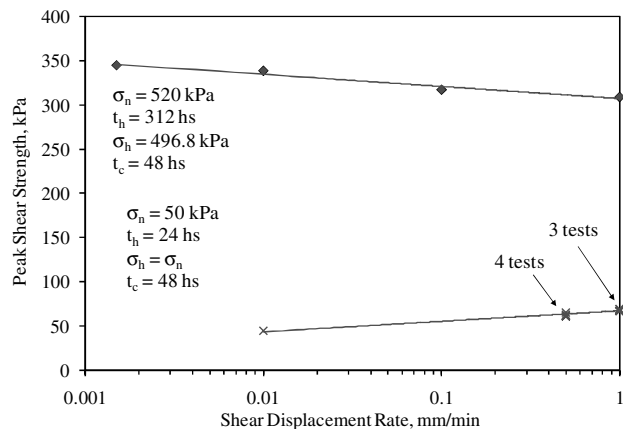
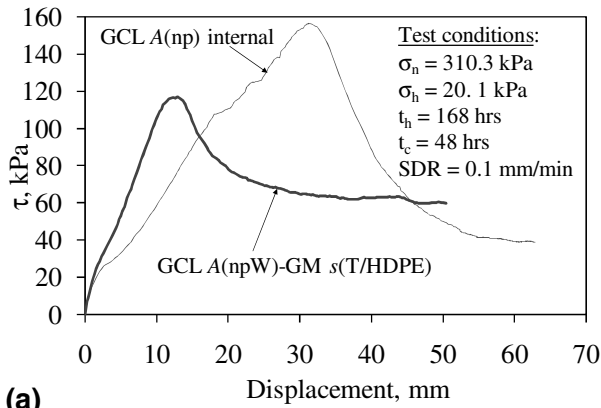
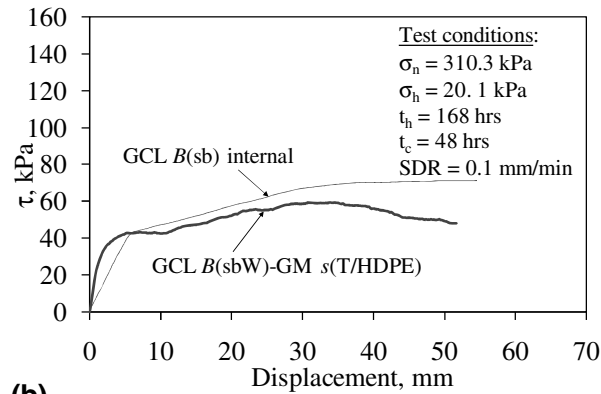


Figure 6.13. Summary trends of peak shear strength as a function of shear displacement rate (Zornberg et al. 2005).

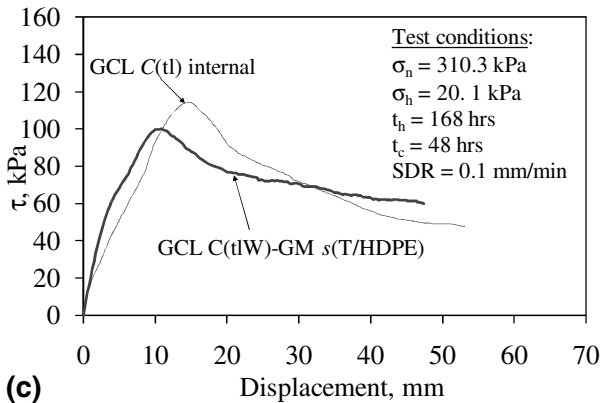
Figures 6.14(a), 6.14(b), and 6.14(c) show typical shear stress-displacement curves for the interfaces between an 80-mil textured HDPE GM and the woven carrier geotextiles of GCLs A (needle-punched), B (stitch-bonded) and C (thermal-locked), respectively (McCartney et al. 2009). The three interfaces shown in these figures were tested using the same σ_n (310.3 kPa), same t_h (168 hrs), same t_c (48 hrs), and same SDR (1.0 mm/min). For comparison, the three figures also show internal shear stress-displacement curves for GCLs A, B, and C tested under the same conditions (see Figure 6.9).



(a)



(b)



(c)

Figure 6.14. Comparison between shear stress-displacement curves from GCL internal tests and GCL-GM interface tests involving: (a) Woven side of GCL A (needle-punched) with textured GCL s; (b) Woven side of GCL B (stitch-bonded) with textured GCL s; and (c) Woven side of GCL C (thermally-locked) with textured GCL s (McCartney et al. 2009).

Although the three interface direct shear tests involve the same combination of geosynthetics in contact (woven carrier geotextile of a GCL and a GM), the interface shear-displacement responses are significantly different. Indeed, the curves follow patterns similar to the corresponding internal shear-displacement curves. Specifically, the GCL A-GM interface shows a well defined peak (the highest τ_p) and a significant post-peak shear strength loss. This pattern is similar to that for GCL A when sheared internally, although it should be noted that the GCL A internal large-displacement shear strength, τ_{ld} , is lower than the GCL A-GM interface τ_{ld} . The

GCL B-GM interface shows a rapid initial mobilization of shear strength until reaching a “yield” stress level, beyond which less pronounced hardening takes place until reaching τ_p . The displacement at peak for the GCL B-GM interface is larger than that observed for the GCL A-GM interface and only little post-peak shear strength loss is observed for larger displacements. Also in this case, the GCL B-GM interface shows a similar shear displacement pattern as the GCL B internal curve. The GCL C-GM interface shows lower τ_p than the GCL A-GM interface, but both interfaces show a similar τ_{ld} . The GCL C internal shear-displacement curve also shows a similar response as the GCL C-GM interface curve.

It should be noted that GCLs A and C are reinforced using similar needle-punching techniques and have the same specified peel-strength. Consequently, the differences in behavior can be attributed to the effects of the thermal-locking process of GCL C. Although a similar pattern could have been expected among all interface shear-displacement curves (all interfaces involved a woven carrier geotextile and the same textured GM), the GCL-GM interface results show different patterns. However, the pattern of each GCL-GM interface shear displacement curve corresponds with that of the GCL sheared internally. As in the case of internal shear strength, the GCL fiber reinforcement is shown to also influence significantly the behavior of GCL-GM interfaces.

6.4 Shear Behavior of Fiber-Reinforced Soil

Fiber reinforcement constitutes a promising solution to the stabilization of thin soil veneers and localized repair of failed slopes. Randomly distributed fibers can maintain strength isotropy and avoid the existence of the potential planes of weakness that can develop parallel to continuous planar reinforcement elements. The design of fiber-reinforced soil slopes has typically been performed using composite approaches, where the fiber-reinforced soil is considered a single homogenized material. Accordingly, fiber-reinforced soil design has required non-conventional laboratory testing of composite fiber-reinforced soil specimens which has discouraged implementation of fiber-reinforcement in engineering practice.

Relevant contributions have been made on the behavior of fibers. The advantages of randomly distributed fibers over continuous inclusions include the maintenance of strength isotropy and the absence of the potential planes of weakness that can develop parallel to continuous planar reinforcement elements (Gray and Al-Refeai, 1986; Maher and Gray, 1990; Consoli et al., 1998). Micro-reinforcement techniques for soils also include Texol, which consists of monofilament fibers injected randomly into sand (Leflaive, 1985), and randomly distributed polymeric mesh elements (McGown et al., 1985; Morel and Gourc, 1997). The use of fiber-reinforced clay backfill to mitigate the development of tension cracks has also been evaluated (Maher and Ho, 1994).

A discrete approach for the design of fiber-reinforced soil slopes was recently proposed to characterize the contribution of randomly distributed fibers to stability (Zornberg, 2002). In this approach, fiber-reinforced soil is characterized as a two-component (soil and fibers) material. Fibers are treated as discrete elements that contribute to stability by mobilizing tensile stresses along the shear plane. Consequently, independent testing of soil specimens and of fiber specimens, but not of fiber-reinforced soil specimens, can be used to characterize fiber-reinforced soil performance.

When failure is governed by the pullout of the fibers, the fiber-induced distributed tension, t_p , is defined as the average of the tensile forces inside the fibers over the control area. Consequently, t_p can be estimated as:

$$t_p = \chi \cdot \eta \cdot (c_{i,c} \cdot c + c_{i,\phi} \cdot \tan \phi \cdot \sigma_{n,ave}) \tag{6.1}$$

where χ is the volumetric fiber content, $c_{i,c}$ and $c_{i,\phi}$ are the interaction coefficients corresponding to the cohesive and frictional components of the interface shear strength, and η is the aspect ratio defined as:

$$\eta = \frac{l_f}{d_f} \tag{6.2}$$

where l_f is the fiber length and d_f is the equivalent diameter of the fiber. When failure is governed by the yielding of the fibers, the distributed tension, t , is determined from the tensile strength of the fiber:

$$t_t = \chi \cdot \sigma_{f,ult} \tag{6.3}$$

where $\sigma_{f,ult}$ is the ultimate tensile strength of the individual fibers. Ultimately, the fiber-induced distributed tension t to be used in the discrete approach to account for the tensile contribution of the fibers in limit equilibrium analysis is:

$$t = \min(t_p, t_t) \tag{6.4}$$

Figure 6.15 shows the stress-strain behavior of sand specimens reinforced with fibers placed at gravimetric fiber contents of 0, 0.2, and 0.4 %. Specimens were tested under an applied confining pressure of 70 kPa. These results are part of a testing program on fiber-reinforced soil conducted to validate the proposed discrete framework (Zornberg 2002, Zornberg and Li 2005). The tests were conducted using commercially-available polypropylene fibers. The peak deviator stress increases approximately linearly with increasing fiber content, which is consistent with the discrete framework. The post-peak shear strength loss is smaller in the reinforced specimens than in the unreinforced specimens. However, the initial portions of the stress-strain curves of the reinforced and unreinforced specimens are approximately similar. Accordingly, the soil appears to take most of the applied load at small strain levels, while the load resisted by the fibers is more substantial at higher strain level. The larger strain corresponding to the peak deviator stress displayed by the fiber-reinforced specimens suggests that fibers increase the ductility of the reinforced soil specimen. These findings are confirmed in Figure 6.16, which shows the test results obtained under higher confining stress (140 kPa).

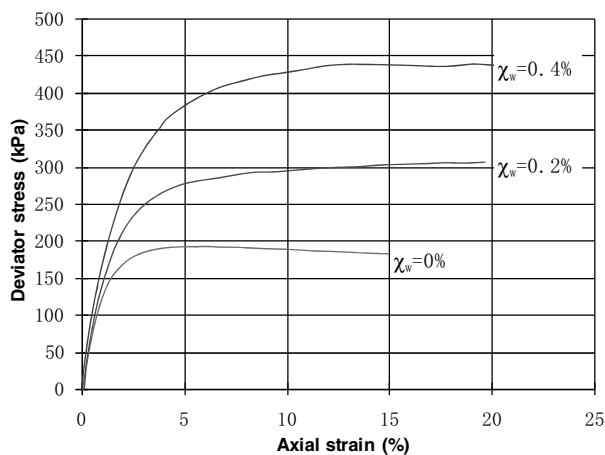


Figure 6.15. Stress-strain behavior of specimens prepared using fiber contents of 0.0, 0.2 and 0.4% with 25 mm-long fibers, $\sigma_3=70$ kPa (Zornberg and Li 2003).

The effect of fiber length on the stress-strain behavior is shown in Figure 6.17. The specimens were prepared using fibers with a different fiber type. The specimens were prepared using the same gravimetric fiber content, but with varying fiber length. The specimens reinforced with longer (50 mm) fibers displayed higher shear strength. The peak deviator stress increases linearly with increasing aspect ratio, which is also consistent with the discrete framework (Zornberg 2002). The strain corresponding to the peak strength increases with increasing fiber length. When the governing failure mode is pullout, the fiber-induced distributed tension reaches its peak when the pullout resistance is fully mobilized. For longer fibers, it usually requires a larger interface shear deformation to fully mobilize the interface strength. Consequently, the macroscopic axial strain at peak stress should be larger for specimen reinforced with longer fibers.

Additional insight into the validity of the discrete approach was obtained by comparing the results obtained for specimens reinforced with 50 mm-long fibers placed at a fiber content of 0.2% with those obtained for specimens reinforced with 25 mm-long fibers placed at a fiber content of 0.4%. That is specimens with a constant value of the product of fiber content and fiber aspect ratio ($\chi \cdot \eta$). In theory, the fiber-induced distributed

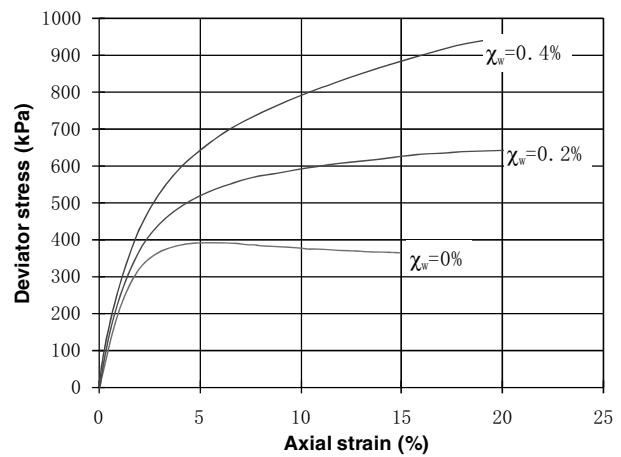


Figure 6.16. Stress-strain behavior of specimens prepared using fiber contents of 0.0, 0.2 and 0.4% with 25 mm-long fibers, $\sigma_3=140$ kPa (Zornberg and Li 2003).

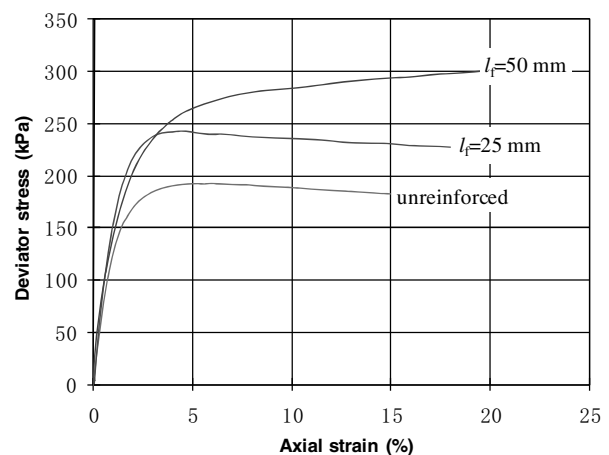


Figure 6.17. Stress-strain behavior of specimen prepared using fiber content of 0.2 %, with fiber lengths of 25 mm and 50 mm, $\sigma_3=70$ kPa (Zornberg and Li 2003).

tension is directly proportional to both the fiber content and the fiber aspect ratio. As shown in Figure 6.18, the predicted equivalent shear strength parameters for the above combinations of fiber length and fiber content are essentially the same, confirming the theoretical predictions. From the practical standpoint, it should be noted that using 50 mm-long fibers placed at a fiber content of 0.2% corresponds to half the reinforcement material than using 25 mm-long fibers placed at a fiber content of 0.4%. That is, for the same target equivalent shear strength the first combination leads to half the material costs than the second one.

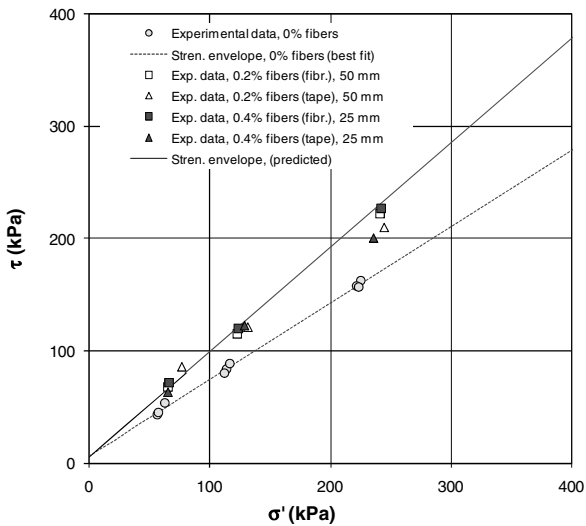


Figure 6.18. Shear strength results for specimen reinforced with 50 mm-long fibers placed at a fiber content of 0.2% and 25 mm fibers placed at a fiber content of 0.4% (Zornberg 2002).

Figure 6.19 shows the stress-strain behavior of specimen reinforced with 50 mm fibers placed at a fiber content of 0.2% and 25 mm fibers placed at a fiber content of 0.4%. While the discrete approach was developed only to predict the shear strength response, the results in the figure show that fiber-reinforced specimens prepared using a constant value of $(\chi \cdot \eta)$ display similar stress-strain behavior. The experimental results suggest that the proportionality of shear strength with the fiber content and fiber aspect ratio predicted by the discrete framework can be extrapolated to the entire stress-strain response of fiber-reinforced specimens.

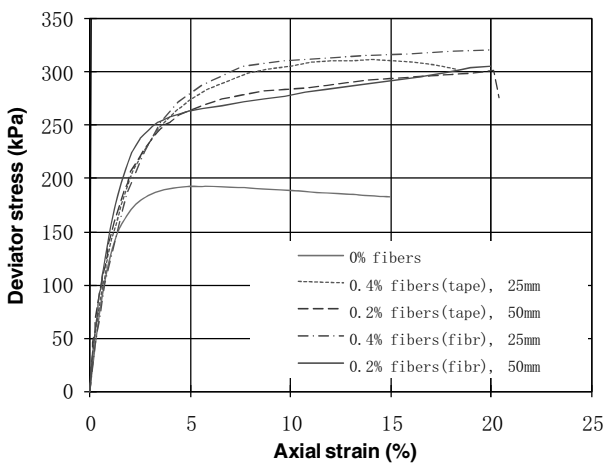


Figure 6.19. Stress-strain behavior for specimen reinforced with 50mm-long fibers placed at a fiber content of 0.2% and 25 mm fibers placed at a fiber content of 0.4%, $\sigma_3=70$ kPa (Zornberg and Li 2003).

7. CONCLUSIONS

This SOA-1 on geomaterial behavior and testing has been prepared to reflect on recent developments and understandings on natural soils, reconstituted and compacted fills, and geosynthetic-reinforced soils. Some of the highlights may be summarized as follows:

- (a) Geomaterials are inherently complex and difficult to characterize fully because of their varied origins, constitutive and compositional assemblages of particle sizes, shapes, and mineralogies, old ages and exposure to different geological, environmental, and environmental factors over long time periods. As a consequence, there have been a great number of soil parameters defined to describe the initial conditions (indices and state), as well as quantifiable values on their mechanical, hydraulic, and rheological aspects. Coupled with a proper background in engineering geology, any given geomaterial will require a combination of laboratory testing, in-situ probings, and geophysical measurements in order to realize a thorough geotechnical site characterization.
- (b) While the interpretation of in-situ and physical tests now uses Critical State Soil Mechanics extensively as the baseline theory, experimental and to some extent numerical research has moved on to examine the limitations of the current paradigm. Limitations have been identified that are associated with the particulate nature of soils, as well as how the particles evolve under load, for example through breakage. The role of the arrangement of particles, defining the fabric has also been found to be of key importance, giving rise to difficulties in the application of Critical State Soil Mechanics to many “transitional” soils of intermediate grading.
- (c) Physical modeling can reveal valuable insights into understanding soil behaviour within a boundary value problem. The advantages and disadvantages of each method have been discussed in this contribution and linked to predictions of soil behavior and validation of numerical models. Physical modelling techniques have become increasingly sophisticated with improvements in capacity and capability in many areas from miniaturisation to mechatronics, imaging techniques, data acquisition, handling and storage. If, however, the geotechnical aspects for creating a suitable model are forgotten due to greater complexity, the results will be less valid.
- (d) Advances in geotechnical in-situ testing have sought to expedite and optimize the subsurface investigation studies by the efficient collection of multi-data measurements. For routine explorations, use of the hybrid geotechnical – geophysical devices such as seismic piezocone (SCPT_u) and seismic flat dilatometer (SDMT_a) are advantageous since up to five independent readings are captured in a single sounding; i.e., SCPT_u: q_t , f_s , u_2 , t_{50} , and V_s ; and SDMT_a: p_0 , p_1 , p_2 , t_{nex} , and V_s . Of specific significance, these soundings provide direct information with depth on the geostratigraphy, fundamental stiffness (G_{max}), stress state, strength, and flow characteristics of geomaterials within a single sounding.
- (e) The evaluation of soil liquefaction potential of young loose sands below the groundwater table must include considerations on the fines contents, types of fines, fabric, and structure of these geomaterials. Frameworks in terms of penetration resistance and shear wave velocity measurements have been identified and developed using databases on ground conditions that have undergone earthquake loadings.

(f) Geosynthetics have become well-established geomaterials in engineering practice, as they enhance or replace several of the functions of soils and rocks. Among the various properties used to characterize geosynthetics, the interface shear strength between soil and several geosynthetics. The shear behavior of these interfaces can be evaluated within frameworks already developed to characterize the shear behavior of soils. Of particular relevance are the characterization of soil-geogrid interfaces used in soil reinforcement applications, of soil-geotextile interfaces used for multiple applications, of interfaces involving GCLs in waste containment applications, and the shear behavior of fiber-reinforced soil. It should be recognized that shear failure along soil-geosynthetic interfaces often governs the stability of earthen structures that incorporate geosynthetics.

ACKNOWLEDGMENTS

The authors appreciate the honor of selection to prepare the SOA-1 by ISSMGE President Pedro Sêco e Pinto. Financial and technical support of the five co-authors has been provided individually to each, including: National Science Foundation (USA), US Dept. of Energy, National Highway Institute, ConeTec Investigations, Fugro Engineers, Swiss National Science Foundation, ETH Research Fund, and the Marie Curie Research Training Network from the European Community "Human Resources and Mobility".

The authors extend their gratitude to the following individuals who provided technical assistance and support during the preparation of this document: Mengia Amberg, Béatrice Baudet, David Woeller, Alessandra Carrera, Michael Jefferies, Alessandra Nocilla, James A. Schneider, Peter K. Robertson, Barbara Shipton, Joek Peuchen, Lukas Arenson (BGC Engineering), Malcolm Bolton (University of Cambridge), Jan Laue, André Arnold, Bernd Imre, Emma Pooley, Ravi Chikatamarla, Philippe Nater, Thomas Weber (ETH Zürich), David Muir Wood (University of Bristol), Mark Randolph and David White (University of Western Australia), Andrew Take (University of Western Ontario), Sidney Teixeira (Federal U. of Parana, Brazil), Chianan Liu (National Chi-Nan University, Taiwan), John McCartney (Univ. Colorado-Boulder), and Chunling Li (Geosyntec Consultants, USA).

REFERENCES

- Abu-Farsakh, M.Y. & Coronel, J. 2006. Characterization of cohesive soil-geosynthetic interaction from large direct shear test. *85th Transportation Research Board Annual Meeting*, Washington, D.C.
- Abu-Hejleh, N., Zomberg, J.G., Wang, T. & Watcharamonthein, J. 2002. Monitored displacements of unique geosynthetic-reinforced soil bridge abutment. *Geosynthetics International* 9 (1): 71-95.
- Adachi, Y., Urano, K., Sakuma, T., Suehiro, S. & Kawamura, M. 2004. *Full-Scale Model Test for Earthquake Resistant Reinforcement Method for Pile Foundations Based on Ground Solidification Techniques*. Tech. Res. Rept., Hazama Corporation. Vol. 36: 9-14.
- Addenbrooke, T. I., Potts, D. M. & Puzrin, A. M. 1997. The influence of pre-failure soil stiffness on the numerical analysis of tunnel construction. *Geotechnique* 47, (3): 693-712.
- Adrian, R.J. 1991. Particle imaging techniques for experimental fluid mechanics. *Ann. Rev. Fluid Mech.* 23: 261-302.
- Ackerley, S.K., Hellings, J.E. & Jardine, R. J. 1987. Discussion: A new device for measuring local axial strains on triaxial specimens. *Geotechnique* 37 (4): 414-415.
- Adianopolous, K.I., Bouckovalas, G.D. & Papadimitiou, A.G. 2001. A critical state evaluation of fines effect on liquefaction potential. *Proc. Fourth Intl. Conf. on Recent Advances in Geotechnical Earthquake Engineering and Soil Dynamics*, San Diego, California.
- Airey, D.W. 1993. Triaxial testing of a naturally cemented carbonate soil. *J. of Geotechnical Engineering*, ASCE. 119 (9): 1379-1398.
- Alfaro, M.C., Miura, N. & Bergado, D. 1995. Soil-geogrid reinforcement interaction by pullout and direct shear tests. *ASTM Geotechnical Testing Journal* 18 (2): 157-167.
- Al-Khafaji, Z. A. & Craig, W. H. 2000. Drainage and reinforcement of soft clay tank foundation by sand columns. *Geotechnique* 50 (6): 709-713.
- Allard, M.A. 1984. Tests on piles installed in flight on the centrifuge. *Proc. of the Symposium on Recent Advances in Geotechnical Centrifuge Modeling*, University of California, Davis: 140-148.
- Allen, T.M. & Bathurst, R.J. 2002. Soil reinforcement loads in geosynthetic walls at working stress conditions. *Geosynthetics International* 9 (5-6): 525-566.
- Allen, T.M., Bathurst, R.J., Holtz, R.D., Walters, D. & Lee, W.F. 2003. A new working stress method for prediction of reinforcement loads in geosynthetic walls. *Canadian Geotechnical J.* 40 (5): 976-994.
- Almeida, M.S.S. & Gurung, S.B. 2000. Migration of some pollutants through clayey and sandy soils: *Proc. of the International Symposium on Physical Modelling and Testing in Environmental Geotechnics*, La Baule, France, May 15-17, 2000: 379-385. LCPC.
- Alonso, E.E., Gens, A. & Josa A. 1990. A constitutive model for partially saturated soils. *Geotechnique* 40 (3): 405-430.
- Altuhaifi, F. 2007. On the mechanical behaviour of glacial sediments. *PhD Thesis*, University College London, U.K.
- Altuhaifi, F., Baudet, B.A. & Sammonds, P. 2006. Particle breakage in glacial sediments. *Geomechanics and Geotechnics of Particulate Media*, Taylor and Francis Group, London: 21-24.
- Andrus, R.D. & Stokoe, K.H., II. 2000. Liquefaction resistance of soils from shear wave velocity. *Journal of Geotechnical and Geoenvironmental Engineering* 126 (11): 1015-1025.
- Architectural Institute of Japan (AIJ). 2001. *Recommendations for design of building foundations*, Tokyo, p.65.
- Arenson, L.U., Take, W.A. & Sego, D.C. 2007. Measurement of ice lens growth and soil consolidation during frost penetration using particle image velocimetry (PIV). *Proc. of the 60th Canadian Geotechnical Conference*, Ottawa: 2046-2053.
- Arenson, L.U., Azmatch, T.F. & Sego, D.C. 2008. A new hypothesis on ice lens formation in frost-susceptible soils. D.L. Kane, K.M. Hinkel (eds). *Proc. of the Ninth International Conference on Permafrost*. Fairbanks, Alaska, USA, June 29-July 3, 2008, Vol. 1: 59-64.
- Arnold, A., Thielen, A. & Springman, S.M. 2005. On the stability of active layers in alpine permafrost. *Proc. of the 11th International Conference and Field Trip on Landslides (ICFL)*, Trondheim, Norway, September 1-10, 2005: 19-25. London: Taylor & Francis.
- Arnold, A. & Laue, J. 2009. Influence of unloaded walls on the stress distribution under a raft foundation. *17th International Conference on Soil Mechanics and Geotechnical*, Alexandria, Egypt, October 5-9, 2009, Rotterdam: Millpress.
- Arthur, J.R.F., Koenders, M.A. & Wong, R.K.S. 1986) Anisotropy in particle contacts associated with shearing in granular media, *Acta Mechanica* 64: 20-29.
- Askarinejad, A., Shahnazari, H., Salehzadeh, H. & Zare, M. 2008. Failure surface determination using image processing in geotechnical centrifuge tests. *Proc. Second British Geotechnical Association Intl. Conf. on Foundations, ICOF*, Dundee Scotland, UK, Vol. 1: 653-662. Bracknell: IHS BRE Press.
- ASTM 1995. *ASTM Standards on Geosynthetics*. Sponsored by ASTM Committee D-35 on Geosynthetics, Fourth Edition, 178 p.
- ASTM 1289.5.4.2-2007 Methods of testing soils for engineering purposes - Soil compaction and density tests - Compaction control test - Assignment of maximum dry density and optimum moisture content values. American Society for Testing & Materials, PA.
- ASTM D1586-08a. 2008. Standard test method for standard penetration test (SPT) and split-barrel sampling of soils. *Annual Book of ASTM Standards*, Volume 04.08, American Soc. Testing Materials, PA.
- ASTM D4633-05. 2005. Standard test method for energy measurement for dynamic penetrometers. *Annual Book of ASTM Standards* 04.08.
- Atkinson, J.A. 2000. Non-linear soil stiffness in routine design. *Geotechnique* 50 (5): 487-508.
- Atkinson, J.H. & Richardson, D. 1987. The effect of local drainage in shear zones on the undrained strength of overconsolidated clay. *Geotechnique* 37 (3): 393-403.
- Baharom, B. & Stallebrass, S.E. 1998. A constitutive model combining the microscopic and macroscopic behaviour of sands in shear and volumetric deformation. *Proc. 4th European Conf. on Numerical Methods in Geotech. Engng.*, Udine.
- Bakeer, R.M., Sayed, M., Cates, P. & Subramanian, R. 1998. Pullout and shear test on geogrid reinforced lightweight aggregate. *Geotextiles and Geomembranes*, 16 (2): 119-133.

- Banks, J.A. & Zhao, A. 1997. Installation of tri-planar drainage geonet at Sarasota landfill project. *Proceedings 11th Geosynthetic Research Institute Conference*, Philadelphia: 251-263.
- Barker, H.R. 1998. *Physical Modelling of Construction Processes in The Mini-Drum Centrifuge*. PhD Thesis, Cambridge, Geotechnical Group, UK: 136 p.
- Barry D.A., Lisle, I.G., Li, L. Prommer, H., Parlange, J.-Y., Sander, G. & Griffioen, J.W. 2001. Similitude applied to centrifugal scaling of unsaturated flow. *Water Resources Res.* 37 (10): 2471-2479.
- Bathurst, R.J., Walters, D.L., Esfehiani, M. El-Emam, M. & Blatz, J.A. 2002. Physical modelling of geosynthetic walls and embankments. R. Phillips, P.J. Guo, R. Popescu (eds), *Proc. of the International Conference on Physical Modelling in Geotechnics/ICPMG*, St. John's, Newfoundland, Swets & Zeitlinger/Balkema: 21-30.
- Bathurst, R.J. & Hatami, K. 2006. Physical to computational modelling of reinforced soil walls under static loading. C.W.W. Ng, L-M. Zhang, Y.H. Wang (eds), *Proc. of the Physical Modelling in Geotechnics - 6th ICPMG '06*, Hong Kong, August 4-6, 2006, Vol. 1: 3-18. Leiden: Taylor & Francis/Balkema.
- Baudet, B.A. & Stallebrass, S.E. 2004. A constitutive model for structured clays. *Géotechnique* 54 (4): 269-278.
- Bauer, G.E. & Zhao, Y. 1993. Evaluation of shear strength and dilatancy behavior of reinforced soil from direct shear tests. *Geosynthetic Soil Reinforcement Testing Procedures*, STP 1190, ASTM, West Conshohocken/PA: 138-157.
- Baxter, C.D., Bradshaw, A.S., Green, R.A. & Wang, J-H. 2008. Correlation between cyclic resistance and shear-wave velocity for Providence silts. *Journal of Geotechnical and Geoenvironmental Engineering* 134 (1): 37-46.
- Been, K. & Jefferies, M.G., 1985. A state parameter for sands. *Géotechnique* 35 (2): 99-112.
- Been, K., Crooks, J.F.A. & Jefferies, M.G. 1988. Interpretation of material state from the CPT in sands and clays. *Penetration Testing in the UK*, Thomas Telford, London: 89-92.
- Been, K., Crooks, J.H.A., Becker, D.E. & Jefferies, M.G., 1986. The cone penetration test in sands: Part I, state parameter interpretation. *Géotechnique* 36 (2): 239-249.
- Been, K., Jefferies, M.G., Crooks, J.H.A. & Rothenberg, L., 1987. The cone penetration test in sands: Part II, general inference of state. *Géotechnique* 37 (2): 285-299.
- Been, K. & Jefferies, M.G. 1985. A state parameter for sands. *Geotechnique* 35 (2): 99-112.
- Benjamin, C.V.S., Bueno, B., Zornberg, J.G. 2007. Field monitoring evaluation of geotextile-reinforced soil retaining walls. *Geosynthetic International Journal* 14 (2): 100-118.
- Benoît, J. & Lutenecker, A.J., editors 2000. *National Geotechnical Experimentation Sites*. GSP 93, ASCE, Reston/Virginia: 398 p.
- Bergado, D.T. & Chai, J.C. 1994. Pullout force-displacement relationship of extensible grid reinforcement. *Geotextiles and Geomembranes* 13 (5): 295-316.
- Bergado, D.T., Chai, J.C., Abiera, H.O., Alfaro, M.C. & Balasubramaniam, A.S. 1993. Interaction between cohesive-frictional soil and various grid reinforcements. *Geotextiles and Geomembranes*, 12 (4): 327-349.
- Bergado, D.T., Chai, J.C., Alfaro, M.C. & Balasubramaniam, A.S. 1994. *Improvement Techniques of Soft Ground in Subsiding and Lowland Environment*. Balkema, Rotterdam, Netherlands.
- Bergado, D.T., Shivashankar, R., Alfaro, M.C., Chai, J.C. & Balasubramaniam, A.S. 1993. Interaction behavior of steel grid reinforcements in clayey sand. *Géotechnique* 43 (4): 589-603.
- Birmingham, P. & Janes, M. 1991. An innovative approach to load testing of high capacity piles. *Piling and Deep Foundations*. Deep Foundations Institute, Vol. 1: 409-415.
- Bezuijen, J. & den Adel, H. 2006. Dike failure due to surface erosion, N-g and 1-g tests. C.W.W. Ng, L-M. Zhang, Y.H. Wang (eds), *Proc. of the Physical Modelling in Geotechnics - 6th ICPMG '06*, Hong Kong, Vol. 2, Leiden: Taylor & Francis/Balkema: 1307-1312.
- Bienen, B., W. Byrne, B., Houlisby, G. T. & Cassidy, M. J. 2006. Investigating six degree-of-freedom loading of shallow foundations on sand, *Géotechnique* 56 (6): 367-379.
- Bienen, B., Gaudin, C. & Cassidy, M. J. 2007. Centrifuge tests of shallow footing behaviour on sand under combined vertical-torsional loading. *International Journal of Physical Modelling in Geotechnics* 7(2): 1-21.
- Bilotta, E. 2008. Use of diaphragm walls to mitigate ground movements induced by tunneling, *Géotechnique* 58 (2): 143-155.
- Bolton, M.D. 1986. The strength and dilatancy of sands, *Géotechnique* 35 (1): 65-78.
- Bolton, M.D. & Powrie, W. 1987. The collapse of diaphragm walls retaining clay. *Géotechnique* 37 (3): 335-353.
- Bolton, M. D. & Powrie, W. 1988. Behaviour of diaphragm walls in clay prior to collapse, *Géotechnique* 38 (2): 167-189.
- Bolton, M.D., Gui, M.W., Garnier, J., Corte, J.F., Bagge, G., Laue, J. & Renzi, R. 1999. Centrifuge cone penetration tests in sand. *Géotechnique* 49 (4): 543-552.
- Bolton, M.D., Nakata, Y. & Cheng, Y.P. 2008. Micro- and macro-mechanical behaviour of DEM crushable materials. *Géotechnique* 58 (6): 471-480.
- Bolton, M.D., Lam, S.Y. & Osman, A.S. 2008. Supporting excavations in clay: from analysis to decision-making. *Proc., 6th International Symposium on Geotechnical Aspects of Underground Construction in Soft Ground*, IS-Shanghai, Vol. 1: 15-28.
- Bolton, M.D. 2009. Private communication.
- Borsic, A., Comina, C., Foti, S., Lancelotta, R. & Musso, G. 2005. Imaging heterogeneities with electrical impedance tomography: laboratory results. *Géotechnique* 55 (8): 539-548.
- Bouazza, A. 1998. Clay-polypropylene geomembrane interface friction. *Proc. 3rd Intl. Congress on Environmental Geotechnics*, Lisbon.
- Bouazza, A. 2002. Geosynthetic clay liners. *Geotextiles and Geomembranes* 20 (1): 1-17.
- Bouazza, A., Zornberg, J.G. & Adam, D. 2002. Geosynthetics in waste containment facilities: recent advances. State-of-the-art keynote paper, *Proceedings Seventh International Conference on Geosynthetics*, Nice, France. Balkema, Rotterdam, Vol. 2: 445-510.
- Bouazza, A., Zornberg, J.G., McCartney, J.S. & Nahlawi, H. 2006. Significance of unsaturated behaviour of geotextiles in earthen structures. *Australian Geomechanics Journal* 41 (3): 133-142.
- Bouckovalas, G.D., Andrianopoulos, K.I. & Papadimitriou, A.G. 2003. A critical state interpretation for the cyclic liquefaction resistance of silty sands. *Soil Dynamics and Earthquake Engineering* 23: 115-125.
- Boudali, M., Leroueil, S. & Murthy, B.R.S. 1994. Viscous behaviour of natural soft clays. *Proc. 13th Int. Conf. on Soil Mech and Foundation Engng.*, New Delhi, Vol. 1: 411-416.
- Bouferra, R. & Shahrour, I. 2004. Influence of fines on the resistance to liquefaction of a clayey sand. *Ground Improvement* 8 (1): 1-5.
- Boulanger, R.W. 2003. High overburden stress effects in liquefaction analyses. *Journal of Geotechnical and Geoenvironmental Engineering* 129 (12): 1071-1082.
- Boulanger, R.W. & Idriss, I.M. 2006. Liquefaction susceptibility criteria for silts and clays. *Journal of Geotechnical and Geoenvironmental Engineering* 132 (11): 1413-1426.
- Bowman, E.T., Laue, J., Imre, B., Zweidler, A. Springman, S.M. 2006. Debris flows in a geotechnical centrifuge. C.W.W. Ng, L-M. Zhang, Y.H. Wang (eds), *Proc. Physical Modelling in Geotechnics - 6th ICPMG '06*, Hong Kong, Vol. 1: 311-316. Taylor & Francis, UK.
- Bowman, E.T., Imre, B., Laue, J. & Springman, S.M. 2007. Geotechnical centrifuge modelling of debris flows. *4th International Conference on Debris-Flow Hazards Mitigation: Mechanics, Prediction, and Assessment (DFHM Conference)*, Chengdu, China.
- Boylan, N., Long, M., Ward, D., Barwise, A. & Georgiouis, B. 2007. Full-flow penetrometer testing in Bothkennar clay. *Proc. 6th Intl. Offshore Site Investigation and Geotechnics Conf.*, Society of Underwater Technology, London: 177-186.
- Bransby, M.F., Davies, M.C.R., Michovski, S.B., Sonnenberg, R., Bengoug, A.G. & Hallett, P.D. 2006. Stabilisation of slopes by vegetation reinforcement. C.W.W. Ng, L-M. Zhang, Y.H. Wang (eds), *Proc. of the Physical Modelling in Geotechnics - 6th ICPMG '06*, Hong Kong, Vol. 1: 317-324. Taylor & Francis/Balkema.
- Bray, J.D. & Sancio, R.B. 2006. Assessment of the liquefaction susceptibility of fine-grained soils. *Journal of Geotechnical and Geoenvironmental Engineering* 132 (9): 1165-1177.
- Brinkgreve, R.B.J. (ed). 2002. *PLAXIS, Finite Element Code for Soil and Rock Analyses, 2D - Version 8*. Lisse: Balkema.
- Britto, A.M. & Gunn, M.J. (eds). 1987. *Critical state soil mechanics via finite elements*. Chichester: Ellis Horwood Limited.
- Broms, B.B. & Flodin, N. 1988. History of soil penetration testing, *Proc. of 1st International Symposium on Penetration Testing, ISOPT-1*, Orlando: 157-220.
- Bucher, F. 1996. Zentrifugen Modellversuche und Ihre Anwendung zur Beurteilung von geotechnischen Stabilitätsproblemen. Instabile Hänge und andere risikorelevante natürliche Prozesse, NDK Erdwissenschaften Monte Verità, Ascona, Switzerland.
- Bucher, F. 2000. Demonstration Models for Undergraduate Teaching in Geotechnics, *Proc. 1st International Conference on Geotechnical Engineering Education and Training*, Sinaia, Romania: 325-328. Rotterdam: Balkema.

- Bucky P. B. 1931. *The use of models for the study of mining problems*. Technical Publication 425. New York: American Inst. of Min. & Metal. Engineering.
- Burland, J.B. 1989. Small is beautiful: the stiffness of soils at small strains. *Canadian Geotechnical Journal* 26 (4): 499-516.
- Burland, J.B. 1990. Thirtieth Rankine Lecture: On the compressibility and shear strength of natural clays. *Géotechnique* 40 (3): 327-378.
- Burland, J.B. & Symes, M. 1982. A simple axial displacement gauge for use in the triaxial apparatus. *Géotechnique* 32 (1): 62-65.
- Burns, S.E., Santamarina, J.C. & Mayne, P.W. ed. 2008. *Deformational Characteristics of Geomaterials*, Vols. 1 and 2, Millpress - IOS Press, Rotterdam: 944 p.
- Byrne, B.W. & Houlsby, G.T. 2002. Experimental investigations of the response of suction caissons to transient vertical loading. *Journal of Geotechnical Engineering* 128 (11): 926-939.
- Byrne, B.W. & Houlsby, G.T. 2004. Experimental investigations of the response of suction caissons to transient combined loading. *Journal of Geotechnical and Geoenvironmental Engrg.* 130 (3): 240-253.
- Campanella, R.G., Robertson, P.K. & Gillespie, D. 1981. In-situ testing in saturated silt (drained or undrained?)", *Proc. 34th Canadian Geotechnical Conference*, Fredericton, New Brunswick.
- Cancelli, A., Rimoldi, P. & Togni, S. 1992. Frictional characteristics of geogrids by means of direct shear and pullout tests. *Proc. Intl. Symposium on Earth Reinforcement Practice*, Vol. 1, 29-34.
- Caprez, M., Springman, S.M., Anagnostou, G. & Puzrin, A.M. 2008. Geotechnical engineering education and training in Switzerland. *1st Intl. Conf. on Education and Training in Geo-Engineering Sciences: Soil Mechanics, Geotechnical Engineering, Engineering Geology and Rock Mechanics*, Constantza, Romania, June 2-4, 2008.
- Carter, J.P. Booker, J.R. & Yeung, S.K. 1986. Cavity expansion in cohesive frictional soils. *Géotechnique* 36 (3): 349-358.
- Cazzuffi, D., 1987. The use of geomembranes in Italian dams. *Intl. Journal of Water Power and Dam Construction* 26 (2): 44-52.
- Cazzuffi, D., Picarelli, L., Ricciuti, A. & Rimoldi, P. 1993. Laboratory investigations on the shear strength of geogrid reinforced soils. *Geosynthetic Soil Reinforcement Testing Procedures*, STP 1190, ASTM, West Conshohocken/PA: 119-137.
- Cetin, K.O., Seed, R.B., Kjureghian, A.D., Tokimatsu, K., Harder, L.F., Kayen, R.E. & Moss, R.E.S. 2004. Standard penetration test-based probabilistic & deterministic assessment of seismic soil liquefaction potential. *Jour. Geotechnical & Geoenvironmental Engineering* 130 (12): 1314-1340.
- Chai, J.C. 1992. Interaction between grid reinforcement and cohesive-frictional soil and performance of reinforced wall/embankment on soft ground. *Ph.D. Dissertation*, Asian Institute of Technology, Bangkok, Thailand.
- Chandler, H.W. 1985. A plasticity theory without Drucker's postulate, suitable for granular materials. *J. Mech. Phys. of Solids* 33: 215-226.
- Chen, B.S.-Y. & Mayne, P.W. 1996. Statistical relationships between piezocone measurements and stress history of clays. *Canadian Geotechnical Journal* 33 (3): 488-498.
- Chen, Y.C. & Chuang, J.C. 2001. Effects of fabric on steady state and liquefaction resistance. *Proc. 11th Intl. Offshore and Polar Engrg. Conf.*, Stavanger: 524-529.
- Chen, Y.-C., Ishibashi, I. & Jenkins, J.T. 1988. Dynamic shear modulus and fabric: Part 1: Depositional and induced anisotropy. *Géotechnique*, 38 (1): 25-32.
- Chen, Z.Y., Zhang, J.H., Wang, W.X. & Xing, Y.C. 2006. Centrifuge modeling for rock slopes. *Proc. Physical Modelling in Geotechnics - 6th ICPMG '06*, Hong Kong, Vol. 1: 19-28. Taylor & Francis, UK.
- Chen, W. & Randolph, M.F. 2007. External radial stress changes and axial capacity for suction caissons in soft clay. *Géotechnique* 57 (6): 499-511.
- Cheng, Y.P., Nakata, Y. & Bolton, M.D. 2003. Discrete element simulation of crushable soil. *Géotechnique* 53 (7): 633-641.
- Cheng, Y.P., Nakata, Y. & Bolton, M.D. 2004. Crushing and plastic deformation of soils simulated using DEM. *Géotechnique* 54 (2): 131-141.
- Cheng, Y.P., Nakata, Y. & Bolton, M.D. 2005. Grain crushing and critical states observed in DEM simulations. *Powders and Grains*, Taylor and Francis, London, Vol. 2: 1393-1397.
- Chikatamarla, R., Laue, J. & Springman, S.M. 2004. *Verbesserung der Schutzwirkung von Galerien gegen Steinschlag*. Geotechnical Innovations - Festkolloquium zum 60. Geburtstag von P. Vermeer, Stuttgart, 25.6.2004.
- Chikatamarla, R., Laue, J. & Springman, S.M. 2006. Centrifuge scaling laws for guided free fall events including rockfalls. *Intl. Journal of Physical Modelling in Geotechnics* 2: 14-25.
- Chin E.L., Craig, W.H. & Cruickshank, M. 2006. Uplift resistance of pipelines buried in cohesionless soil. *Proc. of the Physical Modelling in Geotechnics - 6th ICPMG '06*, Hong Kong, Vol. 1: 723-728. Leiden: Taylor & Francis/Balkema.
- Chiu, P. & Fox, P.J. (2004). "Internal and interface shear strengths of unreinforced and needle-punched geosynthetic clay liners." *Geosynthetics International*, 11(3), 176-199.
- Choy, C.K., Standing, J.R. & Mair, R.J. 2007. Stability of a loaded pile adjacent to a slurry-supported trench. *Géotechnique* 57 (10): 807-819.
- Chu, J., Leroueil, S. & Leong, W.K. 2003. Unstable behaviour of sand and its implication for slope instability. *Canadian Geotechnical Journal* 40 (5): 873-885.
- Chu et al. 2004. Documentation of soil conditions at liquefaction and non-liquefaction sites from 1999 Chi-Chi (Taiwan) earthquake. *Soil Dynamics and Earthquake Engineering* 24: 647-657.
- Chu, J. & Leong, W.K. 2002. Effect of fines on instability behaviour of loose sands. *Géotechnique* 52 (10): 751-755.
- Chu, J., Leong, W.K. & Loke, W.L. 2003. Discussion: Defining an appropriate steady state line for Marriespruit gold tailings. *Canadian Geotech. J.* 40 (2): 484-486.
- Chung, K.H., Mair, R.J. & Choy, C.K. 2006a. Centrifuge modelling of pile-tunnel interaction. *Proc. Physical Modelling in Geotechnics - 6th ICPMG '06*, Hong Kong, August 4-6, 2006, Vol. 2: 1151-1156. Leiden: Taylor & Francis/Balkema.
- Chung, S.F. 2005. *Characterisation of soft soils for deep water developments*. PhD dissertation, Univ. of Western Australia, Perth.
- Chung, S. F., Randolph, M. F. & Schneider, J. A. 2006. Effect of penetration rate on penetrometer resistance in clay, *Journal of Geotechnical and Geoenvironmental Engrg.* 132 (9): 1188-1196.
- Clayton, C.R.I. & Khatrush, S.A. 1986. A new device for measuring local axial strains on triaxial specimens. *Géotechnique* 36 (4): 593-597.
- Clementino, R.V. 2005. Discussion: An oedometer test study on the preconsolidation stress of glaciomarine clays. *Canadian Geotechnical J.* 42 (3): 972-976.
- Clough, G.W., Sitar, N., Bachus, R.C. & Rad, N.S., 1981. Cemented sands under static loading. *J. Geotech. Engrg.*, 107 (GT6): 799-817.
- Comer, A.I., Hsuan, Y.G. & Konrath, L. 1998. Performance of flexible polypropylene geomembranes in covered and exposed environments. *Proc. 6th International Conference on Geosynthetics*, Atlanta, Vol. 1: 359-362.
- Conca, J., and Wright, J. 1992. Diffusion and Flow in Gravel, Soil, and Whole Rock. *Applied Hydrogeology*. Vol. 1: 5-24.
- Consoli, N.C., Prietto, P.D.M. & Ulbrich, L.A. 1998. Influence of fibre and cement addition on behavior of sandy soil. *ASCE J. Geotech Geoenviron. Engrg.* 124 (12): 1211-1214.
- Coop, M.R. 1990. The mechanics of uncemented carbonate sands. *Géotechnique* 40 (4): 607-626.
- Coop, M.R. 2003. On the mechanics of reconstituted and natural sands. Keynote Lecture: *Deformation Characteristics of Geomaterials*, Swets and Zeitlinger, Lisse, Vol. 2: 29-58.
- Coop, M.R. & Atkinson, J.H. 1993. The mechanics of cemented carbonate sands. *Géotechnique*.43 (1): 53-67.
- Coop, M.R. & Cotecchia, F. 1995. The compression of sediments at the archaeological site of Sibari. *Proc. 11th ECSMFE*, Copenhagen, Vol. 1: 55-62.
- Coop, M.R. & Lee, I.K. 1993. The behaviour of granular soils at elevated stresses. *Predictive Soil Mechanics*, Thomas Telford, London: 186-198.
- Coop, M.R. & Willson, S.M. 2003. On the behavior of hydrocarbon reservoir sands and sandstones. *J. Geotechnical Engrg* 129 (11): 1010-1019.
- Coop, M.R., Atkinson, J.H. & Taylor, R.N. 1995. Strength, yielding, and stiffness of structured and unstructured soils. *Proc. 11th ECSMFE*, Copenhagen, Vol. 1: 55-62.
- Coop, M.R., Klotz, E.U. & Clinton, L. 2005. The influence of the in-situ state of sands on the load-deflection behaviour of driven piles. *Géotechnique* 55 (10): 721-730.
- Coop, M.R., Sorensen, K.K., Bodas Freitas, T. & Georgoutsos, G. 2004. Particle breakage during shearing of a carbonate sand, *Géotechnique* 54 (3): 157-163.
- Corté, J-F. (ed). 1988. *Proc. of the International Conference Centrifuge 88*, Paris, France, April 25-27, 1988. Rotterdam: Balkema
- Costa, Y.D., Cintra, J.C. & Zornberg, J.G. 2003. Influence of Matrix Suction on the Results of Plate Load Tests Performed on a Lateritic Soil Deposit. *Geotechnical Testing Journal (ASTM)* 26 (2): 219-227.

- Costa Filho, L.M. & Sieira, A.C.C.F. 2008. Recent applications of geosynthetics in mining and industrial waste disposal. *Proceedings of GeoAmericas 2008*, First PanAmerican Geosynthetics Conference and Exhibition, Cancún, Mexico: 29-44.
- Cotecchia, F. & Chandler, R.J. 1998. One-dimensional compression of natural clay: Structural changes & mechanical effects. *The Geotechnics of Hard Soils-Soft Rocks*, Balkema, NL: 103-113.
- Cotecchia, F. & Chandler, R.J. 2000. A general framework for the mechanical behaviour of clays. *Géotechnique* 50 (4): 431-447.
- Craig, W.H. (ed). 1984. *The application of centrifuge modeling to geotechnical design*. Manchester, April 16-18, 1984.
- Craig, W.H., James, R.G. & Schofield, A.N. (eds) 1988. *Centrifuges in Soil Mechanics*. Rotterdam: Balkema.
- Craig, W. H. 1989. Edouard Phillips (1821-89) and the idea of centrifuge modelling. *Géotechnique* 39 (4): 697-700.
- Craig, W.H. 1994. Size effects in anchor performance, *Canadian Geotechnical Journal* 31 (3): 450-454.
- Craig, W.H. 2002. The Seven Ages of centrifuge modelling. S.M. Springman (ed), *Proc. of the workshop on constitutive and centrifuge modelling: two extremes*, Monte Verità, Ascona, Switzerland: 165-174. Lisse: Swets & Zeitlinger /Balkema.
- Cresswell, A. & Powrie, W. 2004. Triaxial tests on an unbonded locked sand, *Géotechnique* 54 (2): 107-115.
- Cuccovillo, T. & Coop, M.R. 1997. The measurement of local axial strains in triaxial tests using LVDTs. *Géotechnique* 47 (1): 167-171.
- Cuccovillo, T. & Coop, M.R. 1999. On the mechanics of structured sands, *Géotechnique* 49 (6): 741-760.
- Cui, L. & O'Sullivan, C. 2006. Exploring the macro- and micro-scale response of an idealized granular material in the direct shear apparatus. *Géotechnique* 56 (7): 455-466.
- Cui, L., O'Sullivan, C. & O'Neil, S. 2007. Analysis of the triaxial apparatus using a mixed boundary three-dimensional discrete element model. *Géotechnique* 57 (10): 831-844.
- Culligan, P. & Soga, K. 2006. Non-aqueous phase liquid behavior in the subsurface: Transportation, seepage zone characterization and remediation. *Proc. Physical Modelling in Geotechnics - 6th ICPMG '06*, Hong Kong, Vol. 1: 29-46. Leiden: Taylor & Francis/Balkema.
- Culligan, P.J. & Barry, D.A. 1998. Similitude requirements for modeling NAPL movement with a geotechnical centrifuge. *Proc. Instn Civ. Engrs Geotech. Engng.*, 131: 151-162.
- Daouadji, A., Hicher, P-Y. & Rahma, A. 2001. An elasto-plastic model for granular materials taking into account grain breakage. *Eur. J. Mech A/Solids*, 20: 113-127.
- Davies, M.C.R., Hamza, O. & Harris, C. 2003. Physical modelkling of permafrost warming in rock slopes. M. Philips, S.M. Springman, L.U. Arenson (eds), *Proc. of the eighth International Conference on Permafrost ICOP 2003*, Zurich, Switzerland, July 21-25 July 2003, Vol. 1: 169-194. Lisse; Balkema.
- Davison, L.R., Springman, S.M. & Sharma, J.S. 2002. Integrating web based courseware in different environments. *Proc. 4th International Conference on New Educational Environments*, Lugano, Switzerland: 1.117-10.
- Dean, T.T.R., James, R.G. & Schofield, A.N. 1990. *Drum centrifuge studies for EEPUK*. Contract No. EP-022R Task Order 1-022. Phase 1. Draft report, Cambridge.
- DeGroot, D.J. & Lutenecker, A.J. 2003. Geology and engineering properties of Connecticut Valley Varved Clay. *Characterisation and Engineering Properties of Natural Soils*, Vol. 1, Swets and Zeitlinger, Lisse: 695-724.
- Dell'Avanzi, E., Zornberg, J.G., and Cabral, A.R. 2004. Suction profiles and scale factors for unsaturated flow under increased gravitational field. *Soils and Foundations* 44 (3): 79-89.
- Deluzarche, R. & Cambou, B. 2006. Discrete numerical modeling of rockfill dams. *Intl. J. Numerical. and Analytical Methods in Geomechanics* 30 (11): 1075-1096.
- Demers, D. & Leroueil, S. 2002. Evaluation of preconsolidation pressure and OCR from piezocone tests of clay deposits in Quebec. *Canadian Geotechnical J.* 39 (1): 174-192.
- DeNicola, A. & Randolph, M.F. 1997. The plugging behaviour of driven and jacked piles in sand. *Géotechnique* 47 (4): 841-856.
- Derkx, F., Merliot, E., Garnier, J. & Cottineau, M. 1998. On-board remote-controlled centrifuge robot. *Proc. of the International Conference Centrifuge 98*, Tokyo, Vol. 1: 97-102. Balkema.
- Derkx, F., Thorel, L., Chazelas, J.L., Escoffier, S., Rault, G., Buttigieg, S., Cottineau, L.M. & Garnier, J. 2006. Dynamic tests and simulation of earthquakes in the LCPC's centrifuge. *Proc. Physical Modelling in Geotechnics - 6th ICPMG '06*, Hong Kong, Vol. 1: 181-186. Leiden: Taylor & Francis/Balkema.
- Desrues, J., Chambon, R., Mokni, M. & Mazerolle, F. 1996. Void ratio evolution inside shear bands in triaxial sand specimens studied by computed tomography. *Géotechnique* 46 (3): 529-546.
- Dewoolkar, M.M., Goddery, T. & Znidarcic, D. 2003. Centrifuge modeling for undergraduate geotechnical engineering education. *Geotechnical Testing Journal* 26 (2): 201-209.
- Dharma, D. & Sanin, M.V. 2006. New sample holder for the preparation of undisturbed fined-grained soil specimens for laboratory element testing. *ASTM Geotechnical Testing Journal* 29 (3): 1-8.
- Diaz-Rodriguez, J.A., Leroueil, S. & Aleman, J. 1992. Yielding of Mexico City clay and other natural clays. *Journal of Geotechnical Engineering* 118 (7): 981-995.
- DiBenedetto, H., Doanh, T., Geoffroy, H. & Sauzéat, C., ed. 2003. *Deformation Characteristics of Geomaterials*, Vol. 1: Swets and Zeitlinger, Lisse: 1426 p. Vol. 2: Taylor and Francis, UK: 247 p.
- Dixon, N., Jones, D. R. V. & Fowmes, G. J. 2006. Interface shear strength variability and its use in reliability-based landfill stability analysis. *Geosynthetics International* 13 (1): 1-14.
- Dusseault, M.B. & Morgenstern, N.R. 1979. Locked sands. *Journal Engineering Geology* 12: 117-131.
- Dyer, M.R. 1985. Observations of the stress distribution in crushed glass with applications to soil reinforcement. *PhD dissertation*, University of Oxford, Oxford, UK.
- Dyson, J. & Randolph, M. F. 2001. Monotonic Lateral Loading of Piles in Calcareous Sand. *Journal of Geotechnical and Geoenvironmental Engineering* 127 (4): 346-352.
- Edelmann, L. 1998. *Beitrag zum Grenzverformungsverhalten und zur Gebrauchstauglichkeit horizontaler mineralischer Deponiebarrieren*. Dissertation, TU Darmstadt.
- Edelmann, L., Hertweck, M. & Amann, P. 1999. Mechanical behaviour of landfill barrier systems. *Geotechnical Engineering*, 137 (4), ICE, London: 215-224.
- Eid, H.T. & Stark, T.D. 1997. Shear behavior of an unreinforced geosynthetic clay liner. *Geosynthetics International* 4 (6): 645-659.
- Eid, H.T., Stark, T.D. & Doerfler, C.K. 1999. Effect of shear displacement rate on internal shear strength of a reinforced geosynthetic clay liner. *Geosynthetics International* 6 (3): 219-239.
- Einav, I. 2006. Breakage mechanics—Part I: theory. *J. Mech. Phys. Solids*, 55 (6): 1274-1297.
- Einav, I. 2006. Breakage mechanics—Part II: modelling granular materials. *J. Mech. Phys. Solids* 55 (6): 1298-1320.
- El-Emam, M.M., Bathurst, R.J. & Hatami, K. 2002. Effect of reinforcement design on seismic response of reinforced soil retaining walls. *Proc. Intl. Conference on Physical Modelling in Geotechnics/ICPMG*, St. John's, Newfoundland: 1011-1016. Lisse: Swets & Zeitlinger/Balkema.
- Elias, V., Christopher, B.R. & Berg, R.R. 2001. *Mechanically Stabilized Earth Walls and Reinforced Soil Slopes*. Publication No. FHWA NHI-00-043, Federal Highway Administration, Washington, DC.
- Ellis, E.A. & Springman, S.M. 2001a. Full-height piled bridge abutments constructed on soft clay. *Géotechnique* 51 (1): 3-14.
- Ellis, E.A. & Springman, S.M. 2001b. Modelling of soil-structure-interaction for a piled bridge abutment in plane strain FEM analyses. *Computers & Geotechnics* 28 (2): 79-98.
- Ellis, E.A., Cox, C., Yu, H.S., Ainsworth, A. & Baker, N. 2006. A new geotechnical centrifuge at the University of Nottingham, UK. *Proc. Physical Modelling in Geotechnics (6th ICPMG '06*, Hong Kong), Vol. 1: 129-133. Leiden: Taylor & Francis/Balkema.
- El Nimr, A. 2009. Private Communication.
- Fahey, M. 1998. Deformation and in-situ stress measurement. *Geotechnical Site Characterization*, Vol. 1 (ISC-1, Atlanta), Balkema, Rotterdam: 49-68.
- Fahey, M. & Carter, J.P. 1993. A finite element study of the pressuremeter in sand using a nonlinear elastic plastic model. *Canadian Geotechnical Journal* 30 (2): 348-362.
- Fang, Z & Yin, J-H. 2006. Physical modelling of consolidation of Hong Kong marine clay with prefabricated vertical drains. *Canadian Geotechnical Journal* 43 (6): 638-652.
- Fannin, R.J., Eliadorani, A. & Wilkinson J.M.T. 2005. Shear strength of cohesionless soils at low stress. *Géotechnique* 55 (6): 467-478.
- Fearon, R.E. & Coop, M.R. 2000. Reconstitution - what makes an appropriate reference material? *Géotechnique* 50 (4): 471-477.
- Fearon, R.E. & Coop, M.R. 2002. The effect of landsliding on the properties of a structurally complex clay. *Quarterly Journal. Engng Geol. and Hydrogeology* 35 (1): 25-32.
- Ferguson, E.S. 1992. *Engineering and the Mind's Eye*. MIT Press, Cambridge Massachusetts: 221 p.

- Fernandez, A.L. & Santamarina, J.C. 2001. Effect of cementation on the small-strain parameters of sand. *Canadian Geot. J.* 38 (1): 191-199.
- Ferreira, P.M.V. & Bica, A.V.D. 2006. Problems on the identification of structure in a soil with a transitional behaviour. *Géotechnique* 56 (7): 445-454.
- Fletcher, G.F.A. 1965. Standard penetration test: its uses and abuses. *J. Soil Mech. and Foundations Div.* (ASCE), Vol. 91 (SM4): 67-76.
- Fourie, A.B. & Papageorgiou, G. 2001. Defining an appropriate steady state line for Merriespruit gold tailings. *Canadian Geotechnical J.* 28 (5): 695-706.
- Fox, P.J., Rowland, M.G. & Scheithe, J.R. 1998. Internal shear strength of three geosynthetic clay liners. *Journal of Geotechnical and Geoenvironmental Engineering* 124 (10): 933-944.
- Franzius, J. N., Potts, D. M. & Burland J. B. 2005. The influence of soil anisotropy and K_0 on ground surface movements resulting from tunnel excavation, *Géotechnique* 55 (3): 189-199.
- Frost, J.D., Jang, D.J., Park, J.Y., & Chen, C.C. 1999. Quantitative Characterization of Microstructure Evolution. *Proc. of International Workshop on Physics and Mechanics of Soil Liquefaction*: 169-177.
- Fukumoto, F. 1992. Particle breakage characteristics in granular soils. *Soils and Foundations* 32 (1): 26-40.
- Gabr, M.A., Bowders, J.J. & Mooney, D.T. 1994. Settlement analysis of a reinforced landfill liner over a deep mined area. *Vertical and Horizontal Deformations of Foundations and Embankments*, Vol. 1, (GSP 40), ASCE, Reston/VA: 436-450.
- Gajo, A. & Muir Wood, D. 1999. Severn-Trent sand: a kinematic hardening constitutive model for sands: the q-p formulation. *Géotechnique* 49 (5): 595-614.
- Gambin, M., Magnan, J-P. & Mestat, P., editors (2005). *ISPS - Pressio 2005*, Vols. 1 and 2, (IS-Pressuremeters), LCPC, Paris: 1484 p.
- Gardner, R.A. 1937. The method of measuring the capillary pressures in small core samples. *Soil Science*. 43:277-283.
- Garnier, J., Rault, G., Favraud, C. & Laue, J. 1992. *Homogénéité de massifs de sable reconstitués par différentes méthodes de pluviation*. Procope 90/92, RUB-LCPC, Bericht an Ministère de la Recherche et de l'Espace, Nantes.
- Garnier, J., Ternet, O., Cottineau, L.-M. & Brown, C.J. 1999. Placement of embedded pressure cells. *Géotechnique* 49 (3): 405-414.
- Garnier, J., Thorel, L. & Haza, E. (eds). 2000. *Physical modelling and testing in environmental geotechnics*. La Baule, France, LCPC.
- Garnier, J., Thorel, L., König, D., Lynch, R. & Weststrate, F. 2002. European cooperation on the application of centrifuge modelling to environmental geotechnics: the NECER network. *Proc. Intl. Conf. Physical Modelling in Geotechnics (ICPMG)*, St. John's, Newfoundland: 333-335. Swets & Zeitlinger/Balkema.
- Garnier, J., Gaudin, C., Springman, S.M., Culligan, P.J., Goodings, D., König, D., Kutter, B., Phillips, R., Randolph, M.F. & Thorel L. 2007. Catalogue of Scaling Laws and Similitude Questions in Geotechnical Centrifuge Modelling, *IJPMG-International Journal of Physical Modelling in Geotechnics* Vol. 7 (3): 1-23.
- Gasparre, A., Nishimura, S., Anh-Minh, N., Coop, M.R. & Jardine, R.J. 2007. The stiffness of natural London clay. *Symposium in Print on Stiff Clays*. *Géotechnique* 57 (2): 33-47.
- Garnier, J., Gaudin, C., Springman, S.M., Culligan, P.J., Goodings, D., König, D., Kutter, B., Phillips, R., Randolph, M.F. & Thorel L. 2007. Catalogue of Scaling Laws and Similitude Questions in Geotechnical Centrifuge Modelling, *IJPMG-International Journal of Physical Modelling in Geotechnics* 7 (3): 1-23.
- Gaudin, C., Garnier, J., Gaudicheau, P. & Rault, G. 2002. Use of a robot for in-flight excavation in front of an embedded wall. R. Phillips, P.J. Guo, R. Popescu (eds), *Proc. of the International Conference on Physical Modelling in Geotechnics/ICPMG*, St. John's, Newfoundland, Canada, July 10-12, 2002: 77-82. Lisse: Swets & Zeitlinger/Balkema.
- Gaudin, C. & Lehane, B. M. 2006. Centrifuge modelling of pile groups in sand. *Proc. Physical Modelling in Geotechnics - 6th ICPMG '06*, Hong Kong, Vol. 2: 835-840. Leiden: Taylor & Francis/Balkema.
- Gaudin, C., O'Loughlin, C. D. & Randolph, M. F. 2006a. Centrifuge tests on suction embedded plate anchors. *Proc. Physical Modelling in Geotechnics - 6th ICPMG '06*, Hong Kong, Vol. 1: 639-644. Leiden: Taylor & Francis/Balkema.
- Gaudin, C., O'Loughlin, C.D., Randolph, M.F. & Lowmass, A.C. 2006b. Influence of the installation process on the performance of suction embedded plate anchors. *Géotechnique* 56 (6): 381-391.
- Gaudin, C., Randolph, M. F. & O'Loughlin, C. D. 2006c. New insights from model tests of foundations and anchoring systems in offshore Geotechnics. *6th International Offshore and Polar Engineering Conference*, Hong Kong, Vol. 1: 47-61. Taylor & Francis/Balkema.
- Gaudin, C., Vlahos, G. & Randolph, M. F. 2006d. Centrifuge tests to design pipeline rock protection. *6th International Offshore and Polar Engineering Conference*, International Society of Offshore and Polar Engineers, California, USA, 2: 336-341.
- Gaudin, C., Vlahos, G. & Randolph, M. F. 2007. Investigation in centrifuge of anchor-pipeline interaction, *International Journal Offshore and Polar Engineering* 17 (1): 67-73.
- Gay, G. & Azoumi, A. 2000. Forced migration of heavy metals ahead of solid-liquid interface. *Physical Modelling and testing in environmental geotechnics*. La Baule, France: 69-75.
- Georgiannou, V.N. & Burland, J.B. 2001. A laboratory study of post-rupture strength. *Géotechnique* 51 (8): 665-675.
- Georgiannou, V.N., Hight, D.W. & Burland, J.B. 1990. The undrained behaviour of clayey sands in triaxial compression and extension. *Géotechnique* 40 (3): 431-449.
- Georgiannou, V.N., Rampello, S. & Silvestri, F. 1991. Static and dynamic measurements of undrained stiffness on natural overconsolidated clays. *Proc. 10th European Conf. Soil Mech. and Foundation Engrg*, Vol. 1, Florence: 91-95.
- Geotip. Institute for Geotechnical Engineering, ETH Zurich, <http://geotip.igt.ethz.ch>.
- Ghahremannejad, B., Surjadinata, J., Poon, B. & Carter, J.P. 2006. Effects of tunnelling on model pile foundations. *Proc. of the Physical Modelling in Geotechnics - 6th ICPMG '06*, Hong Kong, Vol. 2: 1157-1162. Leiden: Taylor & Francis/Balkema.
- Ghionna, V.N., Jamiolkowski, M., Pedroni, S. & Salgado, R. 1994. The tip displacement of drilled shaft in sands. *Vertical and Horizontal Deformations of Foundations and Embankments*, Vol. 2, (GSP 40), ASCE, Reston/VA: 1039-1057.
- Gilbert, R.B., Fernandez, F.F. & Horsfield, D. 1996. Shear strength of a reinforced clay liner. *Journal of Geotechnical and Geoenvironmental Engineering* 122 (4): 259-266.
- Gilbert, R.B., Scranton, H.B. & Daniel, D.E. 1997. Shear strength testing for geosynthetic clay liners. *Testing and Acceptance Criteria for Geosynthetic Clay Liners* (STP 1308), ASTM: 121-138.
- Giroud, J.P. 2008. The geosynthetics discipline: achievements and challenges. *Proceedings of GeoAmericas 2008*, First PanAmerican Geosynthetics Conference and Exhibition, Cancún, Mexico: 1-3.
- Giroud, J.P., Gleason, M.H. & Zornberg, J.G. 1999. Design of geomembrane anchorage against wind action. *Geosynthetics International* 6 (6): 481-507.
- Giroud, J.P., Pelte, T. & Bathurst, R.J. 1995. Uplift of geomembranes by wind. *Geosynthetics International* 2 (6): 897-952.
- Giroud, J.P., Zornberg, J.G. & Zhao, A. 2000. Hydraulic design of geosynthetic and granular liquid collection layers. *Geosynthetics International*, Vol. 7 (Nos. 4-6): 285-380.
- Gisbert, T., Oberti, O., Bloquet, C., Gourc, J.P. & Ouvry, J.F. 1996. Geosynthetics in french landfills: particular geotechnical aspects. *Proc. 1st European Conf. on Geosynthetics*, Maastricht: 563-568.
- Gourvenec, S. & O'Loughlin, C.D. 2006. Drum centrifuge tests of shallow skirted foundations on soft clay. *Proc. of the Physical Modelling in Geotechnics - 6th ICPMG '06*, Hong Kong, Vol. 1: 645-650. Leiden: Taylor & Francis/Balkema.
- Grämiger, E. 2001. *Einbauverfahren und Bodenerkundung im Sand in der geotechnischen Zentrifuge Zürich*. Diplomarbeit, Institut für Geotechnik, ETH Zürich.
- Gray, D.H. & Al-Refeai, T. 1986. Behavior of fabric versus fiber-reinforced sand. *J. Geotech. Engrg.* 112 (8): 804-820.
- Gray, D.H. & Ohashi, H. 1983. Mechanics of fiber-reinforcement in sand. *J. Geotechnical Engrg.* 109 (3): 335-353.
- Grozić, J.L.H., Lunne, T. & Pande, S. 2003. An oedometer test study on the preconsolidation stress of glaciomarine clays. *Canadian Geotechnical Journal* 40 (3): 857-872.
- Gudehus, G. 1996. A comprehensive constitutive equation for granular materials. *Soils and Foundations* 36 (1): 1-12.
- Günzel, F.K. & Davies, M.C.R. 2006. Influence of warming permafrost on the stability of ice filled rock joints. *Proc. Physical Modelling in Geotechnics - 6th ICPMG '06*, Hong Kong, Vol. 1: 343-348. Leiden: Taylor & Francis/Balkema.
- Guo, T. & Prakash, S. 1999. Liquefaction of silts and silt-clay mixtures. *J. Geotech. and Geoenvironmental Engrg* 125 (8): 706-710.
- Gurung, S.B., Almeida, M.S.S. & Bicalho, K.V. 1998. Migration of zinc through sedimentary soil models. *Proc. International Conf. Centrifuge 98*, Tokyo, Vol. 1: 589-594. Rotterdam: Balkema.
- Ha, I.S., Seo, M.W., Jung, W.S., Kim H.S., D.S., Sobolevsky, A. & Van Laak, P. 2006. Park Development of a large scale geotechnical centrifuge in KOWACO. *Proc. Physical Modelling in Geotechnics - 6th ICPMG '06*, Hong Kong, Vol. 1: 135-139. Taylor & Francis.

- Hao, J., Neilson, R. D., Ivanovic, A., Rodger, A.A., Starkey, A.J., Li, J. & Davies, M.C.R. 2006. Model testing to assess a novel technique for condition monitoring of soil anchorages. *Proc. Physical Modelling in Geotechnics - 6th ICPMG '06*, Hong Kong, Vol. 2: 1429-1435. Leiden: Taylor & Francis/Balkema.
- Harder, L.F., Jr. & Seed, H.B. 1986. Determination of penetration resistance for coarse grained soils using the Becker hammer drill. *Rept. USB/ERC-86/06*, Earthquake Engineering Research Center, University of California at Berkeley.
- Hardin, B.O. 1985. Crushing of soil particles. *Journal of Geotechnical Engineering* 111 (10): 1177-1192.
- Harris, C., Smith, J.S., Davies, M.C.R. & Rea, B. 2008. An investigation of periglacial slope stability in relation to soil properties based on physical modelling in the geotechnical centrifuge. *Geomorphology* 93: 437-459.
- Hassler, G. L. and Brunner, E. 1945. Measurements of capillary pressure in small core samples. *Trans. AIME*. Vol. 160, 114-123.
- Hatami, K. & Bathurst, R.J. 2005. Development and verification of a numerical model for the analysis of geosynthetic-reinforced soil segmental walls under working stress conditions. *Canadian Geotechnical Journal* 42 (10): 1066-1085.
- Hatami, K. & Bathurst, R.J. 2006. Numerical model for reinforced soil segmental walls under surcharge loading. *Journal of Geotechnical and Geoenvironmental Engineering* 132 (6): 673-684.
- Hauswirth, D. 2008. *Ausziehversuche von Mikroankern*. Technischer Bericht. Masterarbeit, ETH Zürich.
- Hertweck M. 2000. *Untersuchung des Tragverhaltens von Steilwandbarrieren im Deponiebau mit grossmassstäblichen Modellversuchen*. ETH Dissertation 12616, Zürich, vdf Verlag.
- Hewitt, R.D., Soydemir, C., Stulgis, R.P. & Coombs, M.T. 1997. Effect of normal stress during hydration and shear on the shear strength of gcl/textured geomembrane interfaces. *Testing and Acceptance Criteria for Geosynthetic Clay Liners*, American Society for Testing and Materials, West Conshohocken/PA: 55-71.
- Hight, D.W., Bond, A.J. & Legge, J.D. 1992. Characterization of the Bothkennar clay. *Geotechnique* 42 (2): 303-347.
- Hight, D.W., et al. 2003. The characterization of Bothkennar clay. *Characterization and Engineering Properties of Natural Soils*, Vol. 1, Swets and Zeitlinger, Lisse: 543-598.
- Hight, D.W., McMillan, F., Powell, J.J.M., Jardine, R.J. & Allenou, C.P. 2002a. Some characteristics of London clay. *Characterisation and Engineering Properties of Natural Soils*, Vol. 2, Swets and Zeitlinger, Lisse, Netherlands: 851-908
- Hird, C.C. & Springman, S.M. 2006. Comparative performance of a 5 cm² and 10 cm² piezocones in a lacustrine clay. *Géotechnique* 56 (6): 427-438.
- Høeg, K., Dyvik, R. & Sandbækken, G. 2000. Strength of undisturbed versus reconstituted silt and silty sand specimens. *Journal of Geotechnical and Geoenvironmental Engineering* 126 (7): 606-617.
- Hofmann, B.A. 1997. In-situ ground freezing to obtain undisturbed samples of loose sand for liquefaction assessment. *PhD thesis*, Dept. of Civil & Environmental Engrg, University of Alberta, Edmonton.
- Hofmann, B.A., Sego, D.C. & Robertson, P.K. 2000. In-situ ground freezing to obtain undisturbed samples of loose sand. *Canadian Geotechnical Journal* 126 (11): 979-989.
- Honda, T., Hibino, T. & Kuwano, J. 2001. Centrifuge model tests on deformation mechanism of nail reinforced sand ground around shallow tunnel. *Proc. Regional Conference on Geotechnical Aspects of Underground Construction in Soft Ground*, Shanghai: 554-559.
- Honeywell 2003. *Technical manual for Optoschmitt Detector*: 179-183.
- Hossain, M. S., Randolph, M. F., Hu, Y. & White, D. J. 2006. Cavity stability and bearing capacity of spudcan foundations on clay. *Offshore Technology Conference*, Houston, Texas, OTC 17770.
- Houlsby, G. T., Kelly, R. B., Huxtable, J. & Byrne, B. W. 2005. Field trials of suction caissons in clay for offshore wind turbine foundations. *Géotechnique* 55 (4): 287-296.
- House, A.R., Randolph M.F. & Watson P.G. 2001. In-situ assessment of shear strength and consolidation characteristics of soft sediments. *Proc. Offshore Technology Conf.*, Houston: 52-63.
- Hsuan, Y.G. & Koerner, R.M. 1998. Antioxidant depletion lifetime in high density polyethylene geomembranes. *Journal of Geotechnical and Geoenvironmental Engineering* 124 (6): 532-541.
- Huang, A.B. (ed). 1991. Calibration Chamber Testing. *Proc. First Intl. Symposium on Calibration Chamber Testing (ISOCCT1)*, Potsdam, Elsevier, New York: 405 p.
- Huang J.T & Airey D.W. 1998. Properties of an artificially cemented carbonate sand. *J. Geotechnical and Geoenvironmental Engrg* 124 (6): 492-499
- Huang, A.B., Hsu, H.H. & Chang, J.W. 1999. The behavior of a compressible silty fine sand. *Canadian Geotech. J.* 36 (1): 88-101.
- Huang, A.B. & Hsu, H.H. 2004. Advanced calibration chambers for cone penetration testing in cohesionless soils. *Geotechnical and Geophysical Site Characterization (ISC-2, Porto)*, Vol. 1: 147-167.
- Huang, A.B. & Hsu, H.H. 2005. Cone penetration tests under simulated field conditions. *Géotechnique* 55 (5): 345-354.
- Huang, A.B., Huang, Y.T. & Ho, F.J. 2005. Assessment of liquefaction potential for a silty sand in Central Western Taiwan. *Proc. XVI ICSMGE*, Vol. 4, Osaka: 2653-2657.
- Huang, A.B., & Huang, Y.T. 2006. Correlating q_c and Cyclic Resistance of a Silty Sand through Laboratory Calibration Tests. *Site and Geomaterial Characterization (GSP No. 149, GeoShanghai 2006)*, ASCE, Reston/VA: 16-31.
- Huang, A.B. & Huang, Y.T. 2007. Undisturbed sampling and laboratory shearing tests on a sand with various fines contents. *Soils and Foundations* 47 (4): 771-781.
- Huang, A.B., Tai, Y.Y., Lee, W.F. & Ishihara, K. 2008. Sampling and field characterization of the silty sand in Central and Southern Taiwan. *Proc. 3rd Intl. Conference on Site Characterization, (ISC-3, Taipei)*, Taylor and Francis, London: 1457-1463.
- Huang, Y.T, Huang, A.B., Kuo, Y.C. & Tsai, M.D. 2004. A laboratory study on the undrained strength of a silty sand from Central Western Taiwan. *Soil Dynamics & Earthquake Engrg* 24 (9-10): 733-743.
- Huang, A.B. 2009. Lessons learned from sampling and CPT in silt/sand soils. *International Conference on Performance-Based Design in Earthquake Geotechnical Engineering*, Tokyo.
- Hufenus, R., Rüegger, R., Weingart, K., Banjac, R., Mayor, P., Springman, S.M., Brönnimann, R. & Feltrin, G. 2006. Full-scale field tests on geosynthetic reinforced unpaved roads on soft subgrade. *Geotextiles and Geomembranes* 24 (1): 21-37.
- Idriss, I.M. & Boulanger, R.W. 2006. Semi-empirical procedures for evaluating liquefaction potential during earthquakes. *Soil Dynamics & Earthquake Engineering* 26: 115-130.
- Ilamparuthi, K. & Dickin, E.A. 2001. Predictions of the uplift response of model belled piles in geogrid-cell-reinforced sand. *Geotextiles and Geomembranes*, 19 (2): 89-109.
- Ilankatharan, M., Kutter, B.L., Shin, H., Arduino, P., Kramer, S.L., Johnson, N. & Sasaki, T. 2006. Comparison of centrifuge and 1 g shake table models of a pile supported bridge structure. *Proc. Physical Modelling in Geotechnics - 6th ICPMG '06*, Hong Kong, Vol. 2: 1313-1318. Taylor & Francis, London.
- Imamura, S., Hirano, T., Hagiwara, T., Sato, Miyazaki, Y., Tsukamoto K.Y. & Ishihara K. 2006a. Use of small-diameter plastic vertical drains in sand deposits against seismically induced lateral spreading in centrifuge model tests. *Proc. Physical Modelling in Geotechnics - 6th ICPMG '06*, Hong Kong, Vol. 1: 457-462. Taylor & Francis.
- Imamura, S., Hagiwara T. & Miyazaki, Y. 2006b. Centrifuge modeling tests on an application of vacuum drainage method to soft marine clay. *Proc. Physical Modelling in Geotechnics - 6th ICPMG '06*, Hong Kong, Vol. 1: 513-519. Leiden: Taylor & Francis/Balkema.
- Imre, B. & Springman, S.M. 2006. Micromechanical Analysis of the Particulate Nature of Sturzstroms. *Intl. Symposium on Geotechnics and Geotechnics of Particulate Media*, Ube, Yamaguchi, Japan, 2006: 267-272. Taylor & Francis/Balkema.
- Imre, B., Räsänen, S. & Springman, S.M. 2008. A coefficient of restitution of rock materials. *Computers & Geosciences* 34: 339-350.
- Imre, B. 2008. Private Communication.
- Ingold, T.S. 1983. Laboratory pull-out testing of grid reinforcements in sand. *ASTM Geotechnical Testing Journal* 6 (3): 101-111.
- Interagency Performance Evaluation Taskforce (IPET). 2007. *Performance evaluation of the New Orleans and Southeast Louisiana Hurricane Protection System*. Final Volume V: The performance - levees and floodwalls. US Army Corps of Engineers, Washington, DC.
- Ishihara, K. 1993. Liquefaction and flow failure during earthquakes. *Géotechnique* 43 (3):351-415.
- Ishihara, K. 1996. *Soil Behavior in Earthquake Geotechnics*. Clarendon Press, Oxford, UK: 350p.
- Ishihara, K. & Harada, K. 2008. Effects of lateral stress on relations between penetration resistances and cyclic strength to liquefaction. *Proc. 3rd International Conf. on Site Characterization, (ISC-3, Taipei)*: Taylor & Francis, London: 1043-1050.
- Iverson, R.M. 1997. The physics of debris flows. *Review of Geophysics* 35 (3): 245-296.

- Iwasaki, K., Tanizawa, F., Zhou, S., & Tatsuoka, F. 1988. Cone resistance and liquefaction of sand. *Penetration Testing 1988*, Vol. 2, (ISOPT-1, Orlando): Balkema, Rotterdam: 785-791.
- Jacobsz, S.W., Standing, J.R., Mair, R.J., Soga, K., Hagiwara, T. & Sugiyama, T. 2001. The effects of tunneling near single driven piles in dry sand. *Proc. Regional Conference on Geotechnical Aspects of Underground Construction in Soft Ground*, Shanghai, China.
- Jamiolkowski, M. 1998. Closing remarks. *Pre-failure Deformation Behaviour of Geomaterials*, Thomas Telford, London: 413-416.
- Jamiolkowski, M. & Robertson, P.K. 1988. Future trends for penetration testing. *Penetration Testing in the UK*, Thomas Telford, London: 321-342.
- Jamiolkowski, M., Lancellotta, R. & LoPresti, D.C.F., editors. 1999. *Pre-Failure Deformation Characteristics of Geomaterials*, Vol. 1, Balkema, Rotterdam; Vol. 2, Swets and Zeitlinger, Lisse: 1419 p.
- Jamiolkowski, M., Lancellotta, R. & LoPresti, D.C.F. 1995. Remarks on the stiffness at small strains of six Italian clays. *Pre-failure Deformation of Geomaterials (2)*, Balkema, Rotterdam: 817-836.
- Jamiolkowski, M., Lancellotta, R., LoPresti, D.C.F. & Pallara, O. 1994. Stiffness of Toyoura sand at small and intermediate strain. *Proc. 13th ICSMFE.*, Vol. 1, New Delhi: 169-172.
- Jang, D.J. & Frost, J.D. 1998. Sand structure differences resulting from specimen preparation procedures. *Geotechnical Earthquake Engng. and Soil Dynamics*, (Proc. Seattle), ASCE, Vol.1: 235-245.
- Jang, D.J., Frost, J.D. & Park, J.Y. 1999. Preparation of epoxy impregnated sand couplers for image analysis. *ASTM Geotechnical Testing Journal* 22 (2): 147-159.
- Japan Road Association (JRA) 1996. *Specifications for Highway Bridges*, Part III, Seismic design.
- Jardine, R. J., Symes, M. J. & Burland, J. B. 1984. The measurement of soil stiffness in the triaxial apparatus. *Géotechnique* 34 (3): 323-340.
- Jardine, R.J., Davies, M.C.R., Hight, D.W., Smith, A.K.C. & Stallebrass, S.E., editors. 1998. *Pre-Failure Deformation Behaviour of Geomaterials*, Thomas Telford, London: 416 p.
- Jardine, R.J., Lehane, B.M., Smith, P.R. & Gildea, P.A. 1995. Vertical loading experiments on rigid pad foundations at Bothkennar. *Géotechnique* 45 (4): 573-597.
- Jarret, P.M. & Bathurst, R.J. 1985. Frictional development at a gravel geosynthetic peat interface. *Proc. Second Canadian Symposium on Geotextiles and Geomembranes*, Edmonton: 1-6.
- Jefferies, M. & Been, K. 2006. *Soil Liquefaction: A Critical State Approach*, Taylor and Francis Group, London: 480 p.
- Jefferies, M.G. 1993. NorSand: a simple critical state model for sand. *Géotechnique* 43 (1): 91-103.
- Jefferies, M.G. & Shuttle, D.A. 2005. NorSand: features calibration, and use. *Soil Constitutive Models: Evaluation, Selection, and Calibration* (GSP 128), ASCE, Reston/VA: 204-235.
- Jewell, R.A. 1990a. Reinforcement bond capacity. *Géotechnique* 40 (3): 513-518.
- Jewell, R.A. 1990b. Strength and deformation in reinforced soil design." *Proc. 4th International Conference on Geotextiles, Geomembranes and Related Products*, The Hague, Netherlands, Vol. 3: 913-946.
- Jewell, R.A. 1996. *Soil Reinforcement with Geotextiles*. Ciria Special Publication 123, Thomas Telford, London: 332 p.
- Jewell, R.A., Milligan, G.W.E., Sarsby, R.W. & Dubois, D. 1984. Interaction between soil and geogrids. *Proc. Symp. Polymer Grid Reinforcement in Civil Engineering*, Science and Engineering Research Council and Netlon Limited: 18-30.
- Juang, C.H. and Jiang, T. 2000. Assessing probabilistic methods for liquefaction potential evaluation. *Soil Dynamics and Liquefaction* (GSP 107), ASCE, Reston, Virginia: 148-162.
- Juang, C.H., Chen, C.J., and Jiang, T. 2001. Probabilistic framework for liquefaction potential by shear wave velocity. *Journal of Geotechnical & Geoenvironmental Engng.* 127 (8): 670-678.
- Juang, C.H., Jiang, T. & Andrus, R.D. 2002. Assessing probability-based methods for liquefaction potential evaluation. *Journal of Geotechnical and Geoenvironmental Engineering* 128 (7): 580-589.
- Juang, C.H., Fang, S.Y. & Khor, E.H. 2006. First-order reliability method for probabilistic liquefaction triggering analysis using CPT. *J. Geotechnical and Geoenvironmental Engng* 132 (3): 337-350.
- Jung, M.S., Shibuya, S. & Chae, J.G. 2008. Strain rate effects on undrained behavior of natural sedimentary clay at Kobe Airport. *Deformational Characteristics of Geomaterials*, Vol. 1, Millpress - IOS Press, Amsterdam: 437-443.
- Katagiri, M., & Takemura, J. 1998. Test programme. *Proc. Intl. Conference Centrifuge 98*, Tokyo, Vol. 2: 1091-1094. Balkema.
- Katagiri, M., Ueno, K. & Takemura, J. 1998. Test results and discussions: C1 and C3. *Proc. International Conference Centrifuge 98*, Tokyo, Vol. 2: 1095-1108. Rotterdam: Balkema.
- Katzenbach, R., Gutberlet, C., Bachmann, G. & Pudasaini, S.P. 2006. Development of a numerical model for the determination of pile-soil-wall-interaction during excavation works. *Proc. Physical Modelling in Geotechnics - 6th ICPMG '06*, Hong Kong, Vol. 2: 1449-1454. Leiden: Taylor & Francis/Balkema.
- Kavvasdas, M. & Amorosi, A. 2000. A constitutive model for structured soils. *Géotechnique* 50 (3): 263-273.
- Kerisel J., Bassett R.H., Andersen K.H., Ovesen N.K. & Mair R.J. 1979. The use of physical models in design. *Proc. VII European Conf. Soil Mech. and Foundation Engng*, Brighton, Vol. 4: 315-360.
- Kim, S.R., Hwang, J.I., Kim, M.M., Bao, Y. & Ko, H.Y. 2006. Comparison of 1-g and centrifuge model tests for liquefied sands. *Proc. Physical Modelling in Geotechnics - 6th ICPMG '06*, Hong Kong, Vol. 2: 1319-1324. Leiden: Taylor & Francis/Balkema.
- Kimura, T., Takemura, J., Hiro-oka, A., Okamura, M. & Park, J. 1994. Excavation in soft clay using an in-flight excavator. *Proc. of the International Conference Centrifuge 94*, Singapore: 649-654. Rotterdam: Balkema
- Kimura, T., Kusakabe, O. & Takemura, J. (eds). 1998. *Proc. of the International Conference Centrifuge 98*, Tokyo. Balkema.
- King, R. & Lodge, M. 1988. North-West shelf development - the foundation engineering challenge. *Engineering for Calcareous Sediments*, Balkema, Rotterdam, Vol. 2: 333-342.
- Kitazume, M., Okano, K. & Miyajima, S. 2000. Centrifuge model tests on failure envelope of column type DMM improved ground. *Soils and Foundations* 40 (4): 43-55.
- Kitazume, M. 2006. Application of physical modeling for investigating ground failure pattern. *Proc. of the Physical Modelling in Geotechnics - 6th ICPMG '06*, Hong Kong, Vol. 1: 63-74. Leiden: Taylor & Francis/Balkema.
- Kitazume, M. & Maruyama K. 2007. Internal stability of group column type deep mixing improved ground under embankment loading. *Soils & Foundations* 47 (3): 437-456.
- Klotz, E.U. & Coop, M.R. 2001. An investigation of the effect of soil state on the capacity of driven piles in sands. *Géotechnique* 51 (9): 733-751.
- Ko, H.Y. & McLean, F.G. (eds). 1991. *Proc. of the International Conference Centrifuge 91*, Boulder, Colorado, USA, June 13-14, 1991. Rotterdam: Balkema
- Koerner, R.M. 1991. Geomembrane overview – significance and background. *Geomembrane Identification and Performance Testing*, Chapman Hall: 3-21.
- Koerner, R.M. & Koerner, G.R. 2001. Geosynthetics design beyond factor of safety: risk assessment using probability of failure analysis. *Proc. Geosynthetic Research Institute (GRI-15)*, Houston: 235-253.
- Koerner, R.M., Hsuan, Y.G. & Koerner, G.R. 2008. Freshwater and geosynthetics: a perfect marriage. *Proc. GeoAmericas 2008*, First PanAmerican Geosynthetics Conf. & Exhibition, Cancún: 4-28.
- Koerner, R.M., Wilson-Fahmy, R.F. & Narejo, D. 1996. Puncture protection for geomembranes Part III: examples. *Geosynthetics International* 3 (5): 655-653.
- Komoto, N., Tatsuoka, F. & Nishi, T. 2003. Viscous stress-strain properties of undisturbed Pleistocene clay and its constitutive modelling. *Proc. 3rd Intl. Symp. Deformation Characteristics of Geomaterials* (IS Lyon), Vol. 2: 579-587.
- Kong, L.G. & Zhang L.M. 2006. Use of a robotic manipulator to conduct pile tests in centrifuge. *Proc. Physical Modelling in Geotechnics - 6th ICPMG '06*, Hong Kong, Vol. 1: 199-204. Taylor & Francis/Balkema.
- Konrad, J. M., St-Laurent, S. Gilbert, F. & Leroueil, S. 1995. Sand sampling below the water table using the 200 mm diameter Laval sampler. *Canadian Geotechnical Journal* 32 (6): 1079-1086.
- Konrad, J.M. 1988. Interpretation of flat plate dilatometer tests in sand in terms of state parameter. *Géotechnique* 38 (2): 263-278.
- Konrad, J.M. 1998. Sand state from cone penetrometer tests: framework considering grain crushing stress. *Géotechnique* 48 (2): 201-215.
- Kuerbis, R., Nigussey, D. & Vaid, Y.P. 1988. Effect of gradation and fines content on the undrained response of sand. *Hydraulic Fill Structures*, Fort Collins, Colorado: 330-345.
- Kulhawy, F.H. & Mayne, P.W. 1990. *Manual on Estimating Soil Properties for Foundation Design*, Report EL-6800, Electric Power Research Institute, Palo Alto: 306 p.
- Küng, H. 2003. *Undrainierte Scherfestigkeit an aufbereitetem Seebodenlehm*. Diplomarbeit, Institut für Geotechnik, ETH Zürich.

- Kuo, C.Y. & Frost, J.D. 1996. Uniformity evaluation of cohesionless specimens using digital image analysis. *Journal Geotechnical and Geoenvironmental Engng.* 122 (5): 390-396.
- Kutter, B.L., Idriss, I.M., Khonke, T., Lakeland, J., Li, X.S., Sluis, W., Zeng, X., Tauscher, R.C., Goto, Y. & Kubodera, I. 1994. Design of a large earthquake simulator at UC Davis. *Proc. of the International Conference Centrifuge 94*, Singapore, 1994: 169-175. Balkema.
- Kutter, B.L. 2006. Phenomena associated with undrained and partly drained dilatant soil. *Proc. of the Physical Modelling in Geotechnics - 6th ICPMG '06*, Hong Kong, Vol. 1: 75-86. Taylor & Francis.
- Kwag, J.M., Ochiai, H. & Yasafuku, N. 1999. Yielding stress characteristics of carbonate sand in relation to individual particle fragmentation strength. *Engineering for Calcareous Sediments*, Balkema, Rotterdam, Vol. 1: 79-86.
- La Rochelle, P., Sarraih, J., Tavenas, F., Roy, M. & Leroueil, S. 1981. Causes of sampling disturbance and design of a new sampler for sensitive soils. *Canadian Geotechnical Journal* 18 (1): 52-66.
- Lacasse, S. 1988. Design parameters of clays from in-situ and lab tests. *Proc. Symposium on New Concepts in Geotechnical Engineering*, Rio de Janeiro; also NGI Report No. 52155-50, Oslo.
- Lacasse, S., Berre, T. & Lefebvre, G. 1985. Block sampling of sensitive clays. *Proceedings, 11th Intl. Conf. on Soil Mechanics and Foundations Engineering*, Vol. 2, San Francisco: 887-892.
- Ladd, C.C. 1991. Stability evaluation during staged construction: 22nd Terzaghi Lecture. *J. Geotechnical Engineering* 117 (4): 540-615.
- Ladd, C.C. & DeGroot, D.J. 2003. Recommended practice for soft ground site characterization. *Soil and Rock America*, Vol. 1 (Proc. 12th PanAmerican Conf., MIT), Verlag Glückauf, Essen: 3-57.
- Ladd, C.C. & Lambe, T.W. 1963. The strength of undisturbed clay determined from undrained tests. *Laboratory Shear Testing of Soils*, STP 361, ASTM, West Conshohocken/PA: 342-371.
- Ladd, C.C., Germaine, J.T., Baligh, M.M. & Lacasse, S.M. 1980. Evaluation of self-boring pressuremeter tests in Boston Blue clay. *Report FHWA-RD-80/052*, MIT, Cambridge/Massachusetts: 239 p.
- Ladd, R.S. 1974. Specimen preparation and liquefaction of sands. *Journal Geotechnical Engng. Div.(ASCE)* 100 (GT1): 1180-1184.
- Ladd, R.S. 1977. Specimen preparation and cyclic stability of sands. *J. Geotechnical Engineering Div. (ASCE)* 103 (GT6): 535-547.
- Lade, P.V. & Overton, D.D. 1989. Cementation effects in frictional materials. *Journal Geotechnical Engineering* 115 (10): 1373-1387.
- Lade, P.V. & Yamamuro, J.A. 1996. Undrained sand behavior in axisymmetric tests at high pressures. *Journal Geotechnical Engineering* 122 (2): 120-129.
- Lade, P.V. & Yamamuro, J.A. 1997. Effects of nonplastic fines on static liquefaction of sands. *Canadian Geotechnical J.* 34 (6): 918-928.
- Lagioia, R. & Nova, R. 1995. An experimental and theoretical study of the behaviour of a calcarenite in triaxial compression. *Géotechnique* 45 (4): 633- 648.
- Lambe, T.W. & Lambe, R.V. 1979. *Soil Mechanics, SI Version*, Wiley and Sons, New York: 554 p.
- Last, N.C. 1979a. The use of calibration chambers to study cone penetration behavior in dry samples of Hokksund sand. *NGI Internal Report* 52108-6.
- Last, N.C. 1979b. The introduction of CPT on saturated samples of Hokksund sand in the NGI calibration chamber. *NGI Internal Report* 52108-7.
- Last, N.C. 1979c. Cone penetration tests on samples of dry Hokksund sand in a rigid walled chamber. *NGI Internal Report* 52108-8.
- Laue, J., Nater, P. & Springman S.M. 2002a. Preparation of soil samples in drum centrifuges. *Proc. of the International Conference on Physical Modelling in Geotechnics, ICPMG*, St. John's, Newfoundland: 143-148. Lisse: Swets & Zeitlinger/Balkema.
- Laue, J., Nater, P., Chikatamarla, R. & Springman, S.M. 2002b. *Der Einsatz von "pressure pads" in geotechnischen Labor und Modellversuchen*, Institut für Grundbau & Bodenmechanik, TU Braunschweig, Fach-Symposium, Messen in der Geotechnik.
- Laue, J. 2002a. Centrifuge Technology. (invited keynote lecture). S.M. Springman (ed), *Proc. of the workshop on constitutive and centrifuge modelling: two extremes*, Monte Verità, Ascona, Switzerland: 75-105, Discussion: 105-112. Lisse: Swets & Zeitlinger/Balkema.
- Laue, J. 2002b. *The use of physical modelling and teleobservation in Undergraduate and graduate education*. Invited Lecture Workshop on the Role of Geotechnical Physical Modelling in Education. C-CORE, Memorial University, St. John's, Newfoundland.
- Laue, J., Springman, S.M., Nater, P., Graemiger, P. & Ducksch, A. 2005. Creating seafloor conditions in geotechnical centrifuges. *Proc. 16th International Conference on Soil Mechanics and Geotechnical Engineering*, Osaka, Japan, Vol. 3: 1741-1744. Millpress.
- Laue, J. & Arnold A. 2008. Physical Modelling of Soil - Structure Interaction of Flexible Raft Foundations. *Foundations, 2nd BGA Intl. Conference on Foundations: 1569-1580*. Norfolk: Brepres.
- Laue, J., Herzog, R. & Springman, S.M. 2009. A soil exploration exercise in Bachelor's level education in soil mechanics. *Proc. 17th International Conference on Soil Mechanics and Geotechnical*, (ICSMGE, Alexandria), Millpress, Rotterdam.
- Lee, F.H., Ng, Y.W. & Yong, K.Y. 1996. Centrifuge modelling of sand compaction piles in soft ground. *Proc. 2nd Int. Conf. Soft Soil Engineering*, Nanjing, China, Vol. 2: 407-412.
- Lee, J. & Salgado, R. 2000. Analysis of calibration chamber plate load tests. *Canadian Geotechnical Journal* 37 (1): 14-25.
- Lee, F.H., Ng, Y.W. & Yong, K.Y. 2001. Effects of installation method on sand compaction piles in clay in the centrifuge. *Geotechnical Testing Journal (ASTM)*, 24 (3): 314-323.
- Lee, F.H. 2002. *The philosophy of modelling versus testing. Constitutive and centrifuge modelling: two extremes*. S.M. Springman (ed): 113-134 Lisse: Swets & Zeitlinger.
- Lee, F.H., Juneja, A., Wen, C., Dasari, G.R. & Tan, T.S. 2002. Performance of total stress cells in model experiments in soft clays. *Proc. of the International Conference on Physical Modelling in Geotechnics, ICPMG*, St. John's, Newfoundland: 101-106. Lisse: Swets & Zeitlinger/Balkema.
- Leflaive, E. 1985. Soils reinforced with continuous yarns: the Texol. *Proc. Eleventh Intl. Conf. on Soil Mech. and Found. Engrg.* Vol. 3, San Francisco: 1787-1790.
- Lehane, B.M. 2003. Vertically loaded shallow foundation on soft clayey silt. *Geotechnical Engineering* 156 (1): 17-26.
- Lehane, B.M. & Jardine, R.J. 2003. Effects of long-term pre-loading on the performance of a footing on clay. *Géotechnique* 53 (8): 689-695.
- Leoni, M., Karstunen, M. & Vermeer, P.A. 2008. Anisotropic creep model for soft soils. *Géotechnique* 58 (3): 215-26.
- Leroueil, S. & Hight, D.W. 2003. Behaviour and properties of natural soils and soft rocks. *Characterization and Engineering Properties of Natural Soils*, Vol. 1, Swets and Zeitlinger, Lisse: 29-254.
- Leroueil, S. & Marques, M.E.S. 1996. State of the art: importance of strain rate and temperature effects in geotechnical engineering. *Measuring and Modelling Time Dependent Behaviour of Soils*. GSP 61, ASCE, Reston, Virginia: 1-60.
- Leroueil, S. & Vaughan, P.R. 1990. The general and congruent effects of structure in natural soils and weak rocks. *Géotechnique* 40 (3): 467-488.
- Leroueil, S., Kabbaj, M., Tavenas, F. & Bouchard, R. 1985. Stress-strain-strain rate relationship for the compressibility of sensitive natural clays. *Géotechnique* 35 (2): 159-180.
- Leung, C.F., Lee, F.H. & Tan, E.S. (eds). 1994. *Proc. of the International Conference Centrifuge 94*, Singapore, August 31-September 2, 1994. Rotterdam: Balkema
- Levy, L.C., Adams, K.A., Culligan, P.J. & Germaine, J.T. 2000. DNAPL transport in fractures using the centrifuge: Modelling and physical data. *Proc. of the International Symposium on Physical Modelling and Testing in Environmental Geotechnics*, La Baule, France: 309-316. LCPC.
- Levy, N., Gaudin, C. & Einav, I. 2007. The behaviour of piles undergoing a change in lateral loading direction, *International Journal of Physical Modelling in Geotechnics* 7 (1): 13-23.
- Li, X.S. & Dafalias, Y.F. 2000. Dilatancy for cohesionless soils. *Géotechnique* 50 (4): 449-460.
- Li, X.S. & Dafalias, Y.F. 2002. Constitutive modeling of inherently anisotropic sand behavior. *J. Geotechnical and Geoenviron. Engng.*, 128 (10): 868-880.
- Ling, H.I., Mohri, Y., Leshchinsky, D., Burke, C., Matsushima, K. & Liu, H. 2003. Behavior of A Large-Scale Modular-Block Reinforced Soil Retaining Wall Subject to Earthquake Shaking. *ASCE 16th Engineering Mechanics Conference*, Seattle, July 16-18, 2003.
- Lings, M.L. 2001. Drained and undrained elastic stiffness parameters. *Géotechnique* 51 (6): 555-565.
- Lings, M.L., Pennington, D.S. & Nash, D.F.T. 2000. Anisotropic stiffness parameters and their measurement in a stiff natural clay. *Géotechnique* 50 (2): 109-125.
- Liu, C., Zornberg, J.G., Chen, T.-C., Ho, Y. & Lin, B. (2009). Behavior of geogrid-sand interfaces in direct shear mode. Submitted to the *Journal of Geotechnical and Geotechnical Engineering*, ASCE.
- Liu, S.H. 2006. Simulating a direct shear box test by DEM. *Canadian Geotechnical J.* 43 (2): 155-168.

- Lobo-Guerrero, S. & Vallejo, L.E. 2005. Analysis of crushing of granular material under isotropic and biaxial stress conditions. *Soils and Foundations* 45 (4): 79-88.
- Loh, C.K., Tan, T.S. & Lee, F.H. 1998. Three-dimensional excavation tests. *Proc. of the International Conference Centrifuge 98*, Tokyo, Japan, Vol. 1: 649-654. Rotterdam: Balkema.
- Lopes, M.L. & Ladeira, M. 1996. Influence of the confinement, soil density and displacement ratio on soil-geogrid interaction. *Geotextiles and Geomembranes* 14 (10): 543-554.
- LoPresti, D.C.F., Pallara, O. & Puci, I. 1995. A modified commercial triaxial testing system for small-strain measurements. *Geotechnical Testing Journal* 18 (1), ASTM: 15-31.
- Lunne, et al. 2006. Effects of sample disturbance and consolidation procedures. *Canadian Geotechnical Journal* 43 (7): 726-750.
- Lunne, T. & By, T. 1989. Troll phase 1 soil investigation. *Report No. 892512* to Statoil Corp., Norwegian Geot. Institute, Oslo.
- Lunne, T., Long, M. & Forsberg, C. 2003. Characterisation and engineering properties of Holmen sand. *Characterization and Engineering Prop. of Natural Soils* (1) Swets and Zeitlinger, Lisse: 1121-1148.
- Lunne, T., Powell, J.J.M., Hague, E.A., Mokkalbost, K.H. & Uglow, I.M. 1990. Correlation of dilatometer readings with lateral stress in clays. *Transportation Research Record No. 1278*, Transportation Research Board, Washington, DC: 183-193.
- Lunne, T., Robertson, P.K. & Powell, J.J.M. 1997. *Cone Penetration Testing in Geotechnical Practice*, Routledge-Blackie Academic and Professional, London: 312 p.
- Luong, M.P. 1994. Efficiency of stress-wave mitigation barrier. 1994. Leung, C.F., Lee, F.H. & Tan, E.S. (eds). *Proc. of the International Conference Centrifuge 94*, Singapore, August 31-September 2, 1994: 283-288. Rotterdam: Balkema.
- Lupini, J.F., Skinner, A.E. & Vaughan, P.R. 1981. The drained residual strength of cohesive soils. *Géotechnique* 31 (1): 181-213.
- Lynch, R.J., Treadaway, A.C.J., Bailey, G., Bolton, M.D., Chandler, S.G., Collison, C.H., Sentenac, P., Garrett, J.A., Santos, C.A. & Silva, M.A.G. 2000. Fibre-optic photometric probes for tracking groundwater pollutant tracers in geotechnical centrifuge studies. *Proc. of the International Symposium on Physical Modelling and Testing in Environmental Geotechnics*, La Baule, France, May 15-17, 2000: 35-42. LCPC.
- Lynch, R.J., Allersma, H., Barker, H., Bezuijen, A., Bolton, M.D. & Cartwright, M., Davies, M.C.R., Depountis, N., Esposito, G., Garnier, J., de Almeida Garrett, J.L.L., Harris, C., Kechavarzi, C., Oung, O., da Silva, M.A.G., Santos, C., Sentenac, P., Soga, K., Spiessl, S., Taylor, R.N., Treadaway, A.C.J. & Weststrate, F. 2001. Development of sensors, probes and imaging techniques for pollutant monitoring in geo-environmental model tests. *Intl. Journal of Physical Modelling in Geotechnics* 1 (4): 17-27.
- Ma, X.F., He Z.M., Zhu, H.H. & Lin, M. 2006. Development of a new geotechnical centrifuge at Tongji University in Shanghai. *Proc. of the Physical Modelling in Geotechnics - 6th ICPMG '06*, Hong Kong, Vol. 1: 151-156. Leiden: Taylor & Francis/Balkema.
- Madabhushi, S.P.G., Schofield, A.N. & Lesley, S. 1998. A New Stored Angular Momentum (SAM) based earthquake actuator. *Proc. of the International Conference Centrifuge 98*, Tokyo, Japan, Vol. 1: 111-116. Rotterdam: Balkema.
- Madabhushi, S.P.G. & Take, W.A. 2002. Use of a mini-drum centrifuge for teaching of geotechnical engineering. *Proc. of the International Conference on Physical Modelling in Geotechnics/ICPMG*, St. John's, Newfoundland, Canada: 221-228. Swets & Zeitlinger.
- Madabhushi, S.P.G., Houghton, N.E. & Haigh, S.K. 2006. A new automatic sand pourer for model preparation at University of Cambridge. *Proc. Physical Modelling in Geotechnics - 6th ICPMG '06*, Hong Kong, Vol. 1: 217-222. Taylor & Francis/Balkema.
- Maher, M.H. & Gray, D.H. 1990. Static response of sand reinforced with randomly distributed fibers. *J. Geotechnical Engrg.* 116 (11): 1661-1677.
- Maher, M.H. & Ho, Y.C. 1994. Mechanical Properties of Kaolinite - Fiber Soil Composite. *J. Geotech. Engineering* 120 (8): 1381-1393.
- Mair, R.J. 2008. Tunnelling and geotechnics: new horizons. *Géotechnique* 58 (9): 695-736.
- Manzari, M.T. & Dafalias, Y.F. 1997. A critical state two-surface plasticity model for sands. *Géotechnique* 47 (2): 255-272.
- Marchetti, D., Marchetti, S., Monaco, P. & Totani, G. 2008. Experience with seismic dilatometer (SDMT) in various soil types. *Geotechnical and Geophysical Site Characterization*, (ISC-3, Taipei), Taylor and Francis, London: 1339-1345.
- Marchetti, S. 1980. In-situ tests by flat dilatometer. *Journal of Geotechnical Engineering* 106 (GT3): 299-321.
- Marchetti, S., Monaco, P., Calabrese, M. & Totani, G. 2004. DMT-predicted vs. measured settlements under a full-scale instrumented embankment at Treporti, Italy. *Geotechnical and Geophysical Site Characterization*, Vol. 2, Millpress, Rotterdam: 1511-1518.
- Marchetti, S., Monaco, P., Totani, G. & Calabrese, M. 2006. The flat dilatometer test (DMT) in soil investigations. *Proc. 2nd Intl. Conf. on the Flat Dilatometer*, Washington, DC: 7-48.
- Martins, F., Bressani, L.A., Coop, M.R. & Bica, V.D. 2002. Some aspects of the compressibility behaviour of a clayey sand. *Canadian Geotechnical J.* 38 (6): 1177-1186.
- Marulanda, C., Culligan, P.J. & Germaine, J.T. 2000. Study of air flow through saturated porous media and applications in situ air sparging. *Proc. of the Intl. Symposium on Physical Modelling and Testing in Environmental Geotechnics*, La Baule, France: 165-172. LCPC.
- Masin, D., Stallebrass, S.E. & Atkinson, J.H. 2003. Laboratory modelling of natural structured clays. *Proc Intl. Workshop on Geotechnics of Soft Soils: Theory and Practice*, VGE, The Netherlands: 491-496.
- Matichard, Y., Potie, G., Bloquet, C. & Gisbert, T. 1996. Lining system using polypropylene geomembrane in waste landfill. *Proceedings 1st European Geosynthetics Conf.*, Maastricht: 709-714.
- Maynar, M.J.M. & Rodriguez, L.E. 2005. Discrete numerical model for analysis of earth pressure balance tunnel excavation. *J. Geotechnical and Geoenvironmental Engrg* 131 (10): 1234-1242.
- Mayne, P.W. 1991. Determination of OCR in clays by piezocone tests using cavity expansion and critical state concepts. *Soils and Foundations* 31 (1): 65-76.
- Mayne, P.W., & Kulhawy, F.H. 1991. Calibration chamber database and boundary effects correction for CPT data. *Proc. 1st Intl. Symp. on Calibration Chamber Testing: 257-264*. New York: Elsevier.
- Mayne, P.W. 2001. Stress-strain-strength-flow parameters from enhanced in-situ tests. *Proc. Intl. Conf. on In-Situ Measurements of Soil Properties and Case Histories*, Bali, Indonesia: 27-48.
- Mayne, P.W. 2004. Lateral drilled shaft response from dilatometer tests. *GeoSupport 2004* (GSP 124), ASCE, Reston/VA: 415-428.
- Mayne, P.W. 2005. Keynote: Integrated ground behavior: in-situ and laboratory tests. *Deformation Characteristics of Geomaterials*, Vol. 2. (Proc. IS-Lyon), Taylor and Francis Group, London: 155-177.
- Mayne, P.W. 2006. The 2006 James K. Mitchell lecture: Undisturbed sand strength from seismic cone tests. *Geomechanics and Geoengineering*, Vol. 1 (4), Taylor and Francis, London: 239-247.
- Mayne, P.W. 2007. Invited overview paper: In-situ test calibrations for evaluating soil parameters. *Characterization and Engineering Prop. of Natural Soils*, Vol. 3, Taylor and Francis, London: 1602-1652.
- Mayne, P.W. 2007. *NCHRP Synthesis 368: Cone Penetration Testing*, Transportation Research Board, Washington, DC: 118 p.
- Mayne, P.W. & Brown, D.A. 2003. Site characterization of Piedmont residuum of North America. *Characterization and Engineering Properties of Natural Soils*, Vol. 2, Swets and Zeitlinger, Lisse: 1323-1339.
- Mayne, P.W. & Kulhawy, F.H. 1991. Calibration chamber database and boundary effects correction for CPT data. *Calibration Chamber Testing*, (Proc. ISOCCT, Potsdam), Elsevier, New York: 257-264.
- Mayne, P.W., Christopher, B.R. & DeJong, J. 2002. *Subsurface Investigations: Geotechnical Site Characterization*. Publication No. FHWA-NHI-01-031, National Highway Institute, Federal Highway Administration, Washington, DC: 301 p.
- Mayne, P.W. and McGillivray, A. 2008. Improved shear wave measurements using autoseis sources. *Deformational Characteristics of Geomaterials*, Vol. 2, Millpress/IOS Press, Amsterdam: 853-860.
- McAlister, C.M. & Pierce, C.E. 2001. Calibration of small diameter TDR cables for measuring displacement in physical soil models. *In TDR 2001 Symposium*. Evanston IL: Northwestern University, USA.
- McCartney, J.S., and Zornberg, J.G. 2005. The Centrifuge Permeameter for Unsaturated Soils (CPUS). *Proceedings of the International Symposium on Advanced Experimental Unsaturated Soil Mechanics, Experus 2005*, Trento, Italy, June 27-29, A.A. Balkema, pp. 299-304.
- McCartney, J.S., Zornberg, J.G. & Swan, R.H. 2009. Analysis of a large database of gcl-geomembrane interface shear strength results *Journal of Geotechnical and Geotechnical Engineering* 134 (2), 209-223.
- McCartney, J.S., Zornberg, J.G., Swan, R.H. Jr & Gilbert, R.B. 2004. Reliability-based stability analysis considering GCL shear strength variability. *Geosynthetics International* 11 (3): 212-232.
- McDowell, G.R. & Bolton, M.D. 1998. On the micromechanics of crushable aggregates. *Géotechnique* 48 (5): 667-679.
- McDowell, G.R. & Harireche, O. 2002. Discrete element modelling of soil particle fracture. *Géotechnique* 52 (2): 131-135.

- McDowell, G.R., Bolton, M.D. 1998. One the micromechanics of crush-able aggregates. *Geotechnique* 48 (5): 667-679.
- McGillivray, A. & Mayne, P.W. 2004. Seismic piezocone and seismic flat dilatometer tests at Treporti. *Geotechnical and Geophysical Site Characterization*, Vol. 2 (ISC-2, Porto), Millpress: 1695-1700.
- McGillivray, A.V. and Mayne, P.W. 2008. Automated seismic source for continuous shear wave profiling. *Geotechnical & Geophysical Site Characterization 2008*, Taylor & Francis, London: 1347-1352.
- McGown, A., Andrawes, K.Z., Hytiris, N. & Mercel, F.B. 1985. Soil strengthening using randomly distributed mesh elements. *Proc. 11th Intl. Conf. on Soil Mech. and Foundation Engrg.* Vol. 3, San Francisco: 1735-1738.
- McNamara, A.M. & Taylor, R.N. 2002. Use of heave reducing piles to control ground movements around excavations. *Proc. of the International Conference on Physical Modelling in Geotechnics/ICPMG*, St. John's, Newfoundland: 847-857. Swets & Zeitlinger/Balkema.
- McNeilan, T.W. & Bugno, W.T. 1985. Cone penetration test results in offshore California silts. *Strength Testing of Marine Sediments. Laboratory and In-Situ Measurements*, STP 883, ASTM, West Conshohocken/PA: 55-71.
- McRostie, G.C. & Crawford, C.B. 2001. Canadian geotechnical research site no. 1 at Gloucester. *Canadian Geotechnical Journal* 38 (5): 1134-1141.
- Mesri, G. 1975. Discussion: New design procedures for stability of soft clays. *Journal of Soil Mechanics and Foundation Engrg Division (ASCE)* 101 (SM4): 409-412.
- Mesri, G. & Olson, R.E. 1970. Shear strength of montmorillonite. *Geotechnique* 20 (3): 261-270.
- Michalowski, R.L. & Zhao, A. 1996. Failure of fiber-reinforced granular soils. *J. Geotechnical Engineering* 122 (3): 226-234.
- Milligan, G.W.E. & Palmeira, E.M. 1987. Prediction of bond between soil and reinforcement. *Prediction and Performance in Geotechnical Engineering*, Calgary: 147-153.
- Mimura, M. 2003. Characteristics of some Japanese natural sands – data from undisturbed frozen samples. Disaster Prevention Research Institute Report, Kyoto University, Japan.
- Mimura, M. 2003. Characteristics of some Japanese natural sands from undisturbed frozen samples. *Characterization and Engrg. Properties of Natural Soils*, Vol. 2, Swets and Zeitlinger, Lisse: 1149-1168.
- Mirghasemi, A.A., Rothenburg, L. & Matyas, E.L. 2002. Influence of particle shape on engineering properties of assemblies of two-dimensional polygon-shape. *Geotechnique* 52 (3): 209-217.
- Mitchell, J.K. 1976. *Fundamentals of Soil Behaviour*. John Wiley and Sons, New York.
- Miura, N & O-Hara, S. 1979. Particle-crushing of a decomposed granite soil under shear stresses. *Soils and Foundations*.19 (3): 1-14.
- Miura, N. & Yamanouchi, T. 1977. Effect of particle-crushing on the shear characteristics of a sand. *Proc. of Japanese Society of Civil Engrgs (JSCE)* No. 260: 109-118 (in Japanese), Trans. JSCE, Vol. 9, 1978.
- Miura, S. & Toki, S. 1982. A sample preparation method and its effect on static and cyclic deformation-strength properties of sand. *Soils and Foundations* 22 (1): 61-77.
- Miyake, M., Yanagihata, T., Tsurugasaki, K. & Baba, S. 2001. Dynamic loading to sea bed by district dumping. *Proc. Intl. Symposium on Offshore & Polar Engineering (ISOPE 2001)*, Stavanger, Norway, Vol. II: 631-638.
- Miyake, M., Yanagihata, T., Baba, S. & Tsurugasaki, K. 2002. A large-scale drum type centrifuge facilities and its application. *Proc. of the Intl. Conf. on Physical Modelling in Geotechnics/ICPMG*, St. John's, Newfoundland: 43-48. Lisse: Swets & Zeitlinger.
- Monaco, P., Marchetti, S., Totani, G. & Calabrese, M. 2005. Sand liquefiability assessment by flat dilatometer test (DMT). *Proc. XVI ICSMGE*, Osaka, Vol. 4: 2693-2697.
- Morel, J.C. & Gourc, J.P. 1997. Mechanical behavior of sand reinforced with mesh elements. *Geosynthetics Intl.* 4 (5): 481-508.
- Moriwaki, H., Inokuchi, T., Hattani, T., Sassa, K., Ochiai, H. & Wang, G. 2004. Failure processes in a full-scale landslide experiment using a rainfall simulator. *Landsides* 1 (4): 277-288.
- Mosher, D.C., Christian, H., Cunningham, D., MacKillip, K., Furlong, A. and Jarret, K. 2007. The harpoon free-fall cone penetrometer for rapid offshore geotechnical assessment. *Proc. 6th Intl. Offshore Site Investigation and Geotechnics Conf.*, Society of Underwater Technology, London: 195-202.
- Moss, R.E.S. 2003. CPT-based probabilistic assessment of seismic soil liquefaction initiation. *Ph.D. dissertation*, Dept. Civil Engineering, University of California, Berkeley, CA.
- Moss, R.E.S., Seed, R.B. & Olen, R.S. 2006. Normalizing the CPT for overburden stress. *Journal of Geotechnical and Geoenvironmental Engineering* 132 (3): 378-387.
- Muir Wood, D. 1990. *Soil Behaviour and Critical State Soil Mechanics*, Cambridge Univ. Press, UK, 462 p.
- Muir Wood, D. 2002. Constitutive cladistics: the progeny of Critical state soil mechanics. S.M. Springman (ed), *Proc. of the workshop on constitutive and centrifuge modelling: two extremes*, Monte Verità, Ascona, Switzerland: 35-57. Lisse: Swets & Zeitlinger/Balkema.
- Muir Wood, D. & Maeda, K. 2007. Changing grading of soil: effect on critical states. *Acta Geotechnica*, online.
- Muir Wood, D. 2008. Critical states and soil modeling. *Deformational Characteristics of Geomaterials*, Vol. 1, IOS Amsterdam: 51-72.
- Murillo, C., Caicedo, B., Thorel, L. & Garnier, J. 2006. Characterization of centrifuge model using SASW techniques. *Proc. of the Physical Modelling in Geotechnics - 6th ICPMG '06*, Hong Kong, Vol. 1: 223-228. Taylor & Francis/Balkema.
- Murthy, T.G., Loukidis, D., Carraro, J.A.H., Prezzi, M. & Salgado, R. 2007. Undrained monotonic response of clean and silty sands. *Geotechnique* 57 (3): 273-288.
- Najser, J., Pooley, E., Springman, S.M., Laue, J. & Boháč, J. 2008. Construction of motorway on double porosity clay fill. *6th International Conference on Case Histories in Geotechnical Engineering*, Arlington, Virginia, USA, August 11-16, 2008.
- Najser, J., Pooley, E. & Springman, S.M. 2009a. Technical note: Modelling of double porosity clays in a small centrifuge. *Int. Journal of Physical Modelling in Geotechnics*: In press.
- Najser, J., Pooley, E., Springman, S.M., Laue, J. & Boháč, J. 2009b. Mechanisms controlling the behaviour of double porosity clayfills – in situ and centrifuge study. *Quarterly Journal of Engineering Geology and Hydrogeology*: Submitted for review.
- Narejo, D., Wilson-Fahmy, R.F. & Koerner, R.M. 1996. "Puncture protection of geomembranes Part II: Experimental." *Geosynthetics International* 3(5), pp. 629-653.
- Nater, P., Laue, J. & Springman, S.M. 2001. Physical modelling of loading on shallow foundations on homogeneous and layered soils. *XVth International Conference on Soil Mechanics & Geotechnical Engineering*, Istanbul, Turkey: 755-760. Lisse: Balkema.
- Nater, P. 2002. Construction of models in the ETH Zurich drum centrifuge. S.M. Springman (ed), *Proc. of the workshop on constitutive and centrifuge modelling: two extremes*, Monte Verità, Ascona, Switzerland: 155-161. Lisse: Swets & Zeitlinger/Balkema.
- Nater, P., Laue, J., Springman, S.M. & Glanzmann, P. 2003. *Stress distribution under a shallow foundation on layered soil - Physical and Numerical Investigations*. International Symposium FONDSUP, November 2003, ECP, Paris.
- Nater, P. 2005. *Verhalten von Flachfundationen auf geschichteten Böden*. Vortrag an SGBF Tagung, Jahresbericht IGT.
- Nater, P. 2006. *Belastungs- und Verformungsverhalten von geschichteten Bodensystemen unter starren Kreisfundamenten*. ETH Dissertation 16319, Zürich: vdf Verlag.
- National Center for Earthquake Engineering Research (NCEER). 1997. *Proceedings of the NCEER Workshop on Evaluation of Liquefaction Resistance of Soils*, T.L. Youd & I.M. Idriss, Editors, Technical Report NCEER-97-022.
- NEA/CSRI/R 2004. *Experimental Facilities for Earthquake Engineering Simulation Worldwide*. Organisation for Economic Co-operation and Development, JT00167275.
- Newson, T.A. 1998. Validation of a non-associated critical state model. *Computers and Geotechnics*, Vol. 23, (4): 277-287.
- Newson, T.A., Bransby, M.F. & Kainourgiaki, G. 2002. The use of small centrifuges for geotechnical education. *Proc. International Conference on Physical Modelling in Geotechnics/ICPMG*, St. John's, Newfoundland: 215-228. Lisse: Swets & Zeitlinger.
- Ng, Y.W., Lee, F.H. & Yong, K.Y. 1998. Development of an inflight sand compaction piles (SCPs) installer. *Proc. Intl. Conf. Centrifuge 98*, Tokyo, Vol. 1: 837-843. Rotterdam: Balkema.
- Ng, C.W.W. Van Laak, P.A., Zhang, L.M., Tang, W.H., Zong, G.H., Wanf, Z.L., Xu, G.M. & Liu, S.H. 2002. Development of a four-axis robotic manipulator for centrifuge modeling at HKUST. *Proc. of the Intl. Conf. on Physical Modelling in Geotechnics/ICPMG*, St. John's, Newfoundland: 71-76. Lisse: Swets & Zeitlinger/Balkema.
- Ng, T-T. 2004. Behavior of ellipsoids of two sizes. *J. Geotechnical and Geoenvironmental Engrg*, 130 (10): 1077-1083.
- Ng, C.W.W., Zhang, L.M. & Wang, Y.H. (eds). 2006. *Proc. of the Physical Modelling in Geotechnics - 6th ICPMG '06*, Hong Kong. Leiden: Taylor & Francis/Balkema.

- Ni, Q., Tan, T.S., Dasari, G.R. & Hight, D.W. 2004. Contribution of fines to the compressive strength of mixed soils. *Géotechnique*, 54 (9): 561-569.
- Nimmo, J.R., Rubin, J., and Hammermeister, D.P. 1987. Unsaturated flow in a centrifugal field: measurement of hydraulic conductivity and testing of Darcy's law. *Water Resources Res.* 23 (1): 124-134.
- Nocilla, A., Coop, M.R. & Colleselli, F. 2006. The mechanics of an Italian silt: an example of transitional behaviour. *Géotechnique* 56 (4): 261-271.
- Nougier-Lehon, C., Vincens, E. & Cambou, B. 2005. Structural changes in granular materials: the case of irregular polygonal particles. *Intl. J. Solids and Structures* 42 (24-25): 6356-6375.
- Ochiai, H., Otani, J., Hayashic, S. & Hirai, T. 1996. The pullout resistance of geogrids reinforced soil. *Geotextiles and Geomembranes*, 14 (1): 19-42.
- Oda, M. 1972b. The mechanism of fabric changes during compressional deformation of sand. *Soils and Foundations* 12 (2): 1-18.
- Oda, M. 1972a. Initial fabrics and their relations to mechanical properties of granular materials. *Soils and Foundations* 12 (1): 17-36.
- Oda, M. & Iwashita, K., editors 1999. *Mechanics of Granular Materials: An Introduction*. Balkema, Rotterdam.
- Oda, M., Takemura T. & Takahashi M. 2004. Microstructure in shear band observed by microfocuss X-ray computed tomography. *Géotechnique* 54 (8): 539-542.
- Oka, F., Kodaka, T., Kimoto, S., Ishigaki, S. & Tsuji, C. 2003. Step-changed strain rate effect on the stress-strain relations of clay and a constitutive modelling. *Soils and Foundations* 43 (4): 189-202.
- Olivares, L. & Picarelli, L. 2006. Modelling of flowslides behaviour for risk mitigation. *Proc. Physical Modelling in Geotechnics - 6th ICPMG '06*, Hong Kong, Vol. 1: 99-112. Taylor & Francis.
- O'Loughlin, C.D., Lowmass, A., Gaudin, C. & Randolph, M.F. 2006. Physical modelling to assess keying characteristics of plate anchors. *Proc. of the Physical Modelling in Geotechnics - 6th ICPMG '06*, Hong Kong, Vol. 1: 659-666. Taylor & Francis/Balkema.
- Osman, A.S. & Bolton, M.D. 2004. A new design method for retaining walls in clay. *Canadian Geotechnical Journal* 41 (3): 451-466.
- Osman, A.S., Mair, R.J. & Bolton, M.D. 2006. On the kinematics of 2D tunnel collapse in undrained clay. *Géotechnique* 56 (9): 585-595
- Osterberg, J. 1991. New device for load testing driven piles and drilled shafts separates friction and end bearing. *Piling and Deep Foundations*, Vol. 1. Deep Foundations Institute: 421-427.
- Oung, O., Bezuijen, A., Weststrate, F., Haza, E., Favraud, C., Garnier, J., Spiessl, S., Taylor, N., Coumoulos, H., Soga, K., Esposito, G. & Allersma, H. 2005. Investigations of a European network of geotechnical centrifuges on multiphase flow. *International Journal of Physical Modelling in Geotechnics* 5 (1): 1-14.
- Ovesen, N.K. 1975. Centrifugal testing applied to bearing capacity problems of footing on sand. *Géotechnique* 25 (2): 394-401.
- Ovesen N.K. 1979. The use of physical models in design. *Proc. of the VII European Conference on Soil Mechanics and Foundation Engineering*, Brighton, UK, Vol. 4: 336-339.
- Paikowsky, S.G. & Xi, F. 2000. Particle motion tracking utilizing a high-resolution digital CCD camera. *Geotechnical Testing Journal (ASTM)*, 23 (1): 123-134.
- Palmeira, E.M. 2004. Bearing force mobilisation in pull-out tests on geogrids. *Geotextiles and Geomembranes* 22 (6): 481-509.
- Palmeira, E.M. 1987. The study of soil-reinforcement interaction by means of large scale laboratory tests. *Ph.D. Dissertation*, University of Oxford, Oxford, UK, 238 p.
- Palmeira, E.M. 2008. Soil-geosynthetic interaction: modelling and analysis. Mercel Lecture. *Proceedings of EuroGeo4, Fourth European Geosynthetics Conference*, Edinburgh, U.K. (CD-ROM).
- Palmeira, E.M. & Milligan, G.W.E. 1989a. Large scale direct shear tests on reinforced soil. *Soil and Foundations* 29 (1): 18-30.
- Palmeira, E.M. & Milligan, G.W.E. 1989b. Scale and other factors affecting the results of the pullout tests of grids buried in sand. *Géotechnique* 39 (3): 551-584.
- Palmer, A.C., White, D.J., Baumgard, A.J., Bolton, M.D., Barefoot, A.J., Finch, M., Powell, T., Faranski, A.S. & Baldry, J.A.S. 2003. Uplift resistance of buried submarine pipelines: comparison between centrifuge modelling and full-scale tests. *Géotechnique* 53 (10): 877-883.
- Palmer, A.C. 2008. *Dimensional Analysis and Intelligent Experimentation*. World Scientific, Singapore.
- Pan, S.S., Pu, J.L., Yin, K.T. & Liu, F.D. 1999. Development of pile driver and load set for pile group in centrifuge. *Geotechnical Testing Journal (ASTM)*, 22 (4): 917-923.
- Papadimitiou, A.G. & Bouckovalas, G.D. 2002. Plasticity model for sands under small and large cyclic strains: A multiaxial formulation. *Soil Dynamics and Earthquake Engng.* 22: 203-221.
- Papadimitriou, A.G., Bouckovalas, G.D. & Dafalias, Y.F. 2001. Plasticity model for sand under small and large cyclic strains. *Journal of Geotechnical and Geoenvironmental Engineering* 127 (11): 73-983.
- Parkin, A.K., & Lunne, T. 1982. Boundary effects in the laboratory calibration of a cone penetrometer for sand. *Proc. Second European Symposium on Penetration Testing*, Amsterdam, Vol. 2: 761-768.
- Pennington, D.S., Nash, D.F.T. & Lings, M.L. 1997. Anisotropy of G_0 shear stiffness of Gault clay. *Géotechnique* 47 (3): 391-398.
- Perkins, S. W. & Cortez, E. R. 2005. Evaluation of base-reinforced pavements using a heavy vehicle simulator. *Geosynthetics Intl.* 12 (2): 86-98.
- Pestana, J.M. & Whittle, A.J. 1995. A compression model for cohesionless soils. *Géotechnique* 45 (4): 611-631.
- Peterson, L. M. & Anderson, L.R. 1980. *Pullout Resistance of Welded Wire Mats Embedded in Soil*. Res. Report Submitted to Hilfiker Co., Civil and Envir. Eng. Dept., Utah State Univ., Logan, Utah.
- Peuchen, J. & Mayne, P.W. 2007. Rate effects in vane shear testing. *Proc. 6th Intl. Offshore Site Investigation and Geotechnics Conf.*, Society of Underwater Technology, London: 187-194.
- Phillips, E. 1869a. *De l'équilibre des solides élastiques semblables*. C. R. Acad. Sci., Paris, 68: 75-79.
- Phillips, E. 1898b. *Du mouvement des corps solides élastiques semblables*. C. R. Acad. Sci., Paris, 69: 911-912.
- Phillips, R., Guo, P.J. & Popescu, R. (eds). 2002. *Proc. of the Intl. Conf. on Physical Modelling in Geotechnics (ICPMG)*, St. John's, Newfoundland. Swets & Zeitlinger.
- Picarelli, L., Olivares, L., Di Maio, C., Silvestri, F., Di Nocera, S. & Urciuoli, G. 2002. Structure, properties and mechanical behaviour of the highly plastic intensely fissured Bisaccia clay shale. *Characterisation and Engineering Properties of Natural Soils*, Vol. 2, Balkema, Rotterdam: 947-982.
- Pitman, T.D., Robertson, P.K. & Sego, D.C. 1994. Influence of fines on the collapse of loose sands. *Canadian Geot. J.* 31 (4): 728-739.
- Pokrovsky, G. Y. 1933. On the application of centrifugal force for modelling earth works in clay. *Journal Tech. Physics* 3: 537-539, Moscow (In Russian).
- Polito, C.P. & Martin, J.R. II 2001. Effects of nonplastic fines on the liquefaction resistance of sands. *J. Geotechnical and Geoenvironmental Engineering* 127 (5): 408-415.
- Pooley, E., Najser, J., Laue, J. & Springman, S.M. 2007. Centrifuge Modelling of an embankment on double porosity clay landfill. *60th Canadian Geotechnical Conference & 8th Joint CGS/IAH-CNC Groundwater Conference*, Ottawa, Ontario.
- Pooley, E., Laue, J. & Springman, S.M. 2008a. Centrifuge modelling of foundations on double porosity clay landfills. *Proc. Second British Geotechnical Association International Conference on Foundations, ICOF 2008*, Dundee, Scotland, Vol. 2. 1391-1401. IHS BRE Press.
- Pooley, E., Springman, S.M., Laue, J. & Najser, J. 2008b. Centrifuge modelling to compare ground improvement techniques on double porosity clay landfills. *Geotechnics of Soft Soils - Focus on Ground Improvement, 2nd International Workshop on Geotechnics of Soft Soils (IWGSS)*, University of Strathclyde, Scotland: 281-285.
- Pooley, E., Laue, J. & Springman, S.M. 2009. Assessment of the use of dynamic compaction on double porosity clay landfill. *17th International Conference on Soil Mechanics & Geotechnical Engineering (ICSMGE)*, Alexandria), Millpress, Rotterdam.
- Potts, D.M., Dounia, G.T. & Vaughan, P.R. 1987. Finite element analysis of the direct shear box test. *Géotechnique* 37 (1): 11-23.
- Powrie, W. & Kantartzi, C. 1996. Ground response during diaphragm wall installation in clay: centrifuge model tests. *Géotechnique* 46 (4): 725-739.
- Powrie, W., Ni, Q., Harkness, R.M. & Zhang, X. 2005. Numerical modeling of plane strain tests on sands using a particulate approach. *Géotechnique* 55 (4): 297-306.
- Prandtl, L. 1920. Über die Eindringungsfestigkeit (Härte) plastischer Baustoffe und die Festigkeit von Schneiden. *Zeitschrift für angewandte Mathematik und Mechanik*, Vol. 1 (1): 15-20.
- Qadimi, A. & Coop, M.R. 2007. The undrained cyclic behavior of a carbonate sand. *Géotechnique* 57 (9): 739-750.
- Rammah, K.I., Ismail, M.A. & Fahey, M. 2006. Development of a centrifuge seismic tomography system at UWA. *Proc. Physical Modelling in Geotechnics - 6th ICPMG '06*, Hong Kong, Vol. 1: 229-234. Taylor & Francis/Balkema.

- Rampello, S. & Silvestri, F. 1993. The stress-strain behaviour of natural and reconstituted samples of two overconsolidated clays. *Geotechnical Engineering of Hard Soils and Soft Rocks*, Balkema, Rotterdam: 769-778.
- Randolph, M.F. 2003. Science and empiricism in pile foundation design. *Géotechnique* 53 (10): 847-875.
- Randolph, M.F. 2004. Characterization of soft sediments for offshore applications. *Geotechnical and Geophysical Site Characterization*, Vol. 1 (Proc. ISC-2, Porto), Millpress, Rotterdam: 209-232.
- Ranjan, G., Vassan, R.M. & Charan, H.D. 1996. Probabilistic analysis of randomly distributed fiber-reinforced soil. *J. Geotechnical Engrg.* 120 (6): 419-426.
- Rechenmacher, A.L. 2005. Grain-scale processes governing shear band initiation and evolution in sands. *J. Mechs and Physics of Solids* 54: 22-45.
- Reddy, K.R. & Saxena, S.K. 1993. Effects of cementation on stress-strain and strength characteristics of sands. *Soils and Foundations* 33 (4): 121-134.
- Reinhart, D.R. & Townsend, T.G. 1998. *Landfill Bioreactor Design and Operation*. CRC Press, Lewis Pub., New York: 189 p.
- Reyna, F. & Chameau, J.L. 1991. Dilatometer based liquefaction potential of sites in the Imperial Valley. *Proc. 2nd Intl. Conf. on Recent Advances in Geot. Earthquake Engrg. and Soil Dynamics*, Vol. 1, St. Louis: 385-392.
- Richards, D.J. & Powrie, W. 1998. Centrifuge model tests on doubly propped embedded retaining walls in overconsolidated kaolin clay. *Géotechnique* 48 (6): 833-846.
- Richardson, M. D., O'Loughlin, C. D., Randolph M. F. & Cunningham T. J. 2006. Drum centrifuge modelling of dynamically penetrating anchors. *Proc. of the Physical Modelling in Geotechnics - 6th ICPMG '06*, Hong Kong, Vol. 1: 673-678. Taylor & Francis.
- Riemer, M.F. & Seed, R.B. 1997. Factors affecting apparent position of steady-state line. *J. Geotechnical and Geoenviron. Engrg* 123 (3): 281-288.
- Rittirong, A., Shang, J. Q., Ismail, M. A. & Randolph M. F. 2006. Effect of electric field intensity on electro-cementation of caissons in calcareous sand. *16th International Offshore and Polar Engineering Conference (ISOPE)*, California, Vol. 2: 408-415.
- Rittirong, A., Shang, J.Q., Ismail, M.A. & Randolph, M.F. 2007. Effect of electric field intensity on electro-cementation of caissons in calcareous sand, *Intl. Journal of Offshore and Polar Engineering*, 17 (1): 74-79.
- Robertson, P.K. 2004. Evaluating soil liquefaction and post-earthquake deformations using the CPT. *Geotechnical and Geophysical Site Characterization*, Vol. 1 (ISC-2, Porto), Millpress: 233-249.
- Robertson, P.K. & Campanella, R.G. 1986. Estimating liquefaction potential of sands using the flat plate dilatometer. *ASTM Geotechnical Testing Journal* 9 (1): 38-40.
- Robertson, P.K. & Wride, C.E. 1998. Evaluating cyclic liquefaction potential using the CPT. *Canadian Geotech. J.* 35 (3): 442-459.
- Robertson, P.K., Sully, J.O., Woeller, D.J., Lunne, T., Powell, J.J.M. & Gillespie. 1992. Estimating coefficient of consolidation from piezocone tests. *Canadian Geotechnical Journal* 29 (4): 539-550.
- Robertson, P.K. 2009. Review of CPT-DMT correlations. *Journal of Geotechnical & Geoenvironmental Engineering* 135, in press.
- Rombi, J., Pooley, E.J. & Bowman, E.T. 2006. Factors influencing granular debris flow behaviour: An experimental investigation. *Proc. of the Physical Modelling in Geotechnics - 6th ICPMG '06*, Hong Kong, Vol. 1: 379-384. Taylor & Francis/Balkema.
- Roscoe, K.H. 1970. The influence of strains in soil mechanics. The 10th Rankine Lecture, *Géotechnique* 20 (1): 129-170.
- Roscoe, K.H. & Burland J.B. 1968. On the generalised stress-strain behaviour of "wet" clay. *Engineering Plasticity*, Cambridge University Press, UK: 535-609.
- Roscoe, K. H. 1970. The influence of strains in soil mechanics. *Géotechnique* 20 (2): 129-170.
- Roth, S. & Cheney, D. 2001. *Directory of International Earthquake Engineering Research Facilities*. The National Science Foundation, George E. Brown, Jr., Network for Earthquake Engineering Simulation, Arlington, Virginia.
- Rotta, G.V., Consoli, N.C., Prietto, P.D.M., Coop, M.R. & Graham, J. 2003. Isotropic yielding in an artificially cemented soil cured under stress, *Géotechnique* 53 (5): 493-502.
- Rouainia, N. & Muir Wood, D. (2000). A kinematic hardening constitutive model for natural clays with loss of structure. *Géotechnique* 50 (2): 153-164.
- Rowe, P.W. 1962. The stress-dilatancy relation for static equilibrium of an assembly of particles in contact. *Proc. Royal Society*, Vol. 269: 500-27.
- Rowe, R.K. & Sangam, H.P. 2002. Durability of HDPE geomembranes. *Geotextiles and Geomembranes* 20 (2): 77-95.
- Roy, D. 2008. Coupled use of cone tip resistance and small strain shear modulus to assess liquefaction potential. *Journal of Geotechnical and Geoenvironmental Engineering* 134 (4): 519-530.
- Russell, B. 1912, reprinted 1998. *The problems of philosophy*. Oxford: Oxford University Press.
- Sabatini, P.J., Griffin, L.M., Bonaparte, R., Espinoza, R.D. & Giroud, J. P. (2002). Reliability of state of practice for selection of shear strength parameters for waste containment system stability analysis. *Geotextiles and Geomembranes* 20 (4): 241-262.
- Salgado, R., Mitchell, J.K., & Jamiolkowski, M. 1997. Cavity Expansion and Penetration Resistance in Sand. *Journal of Geotechnical and Geoenvironmental Engineering* 123 (4): 344-354.
- Salgado, R., Mitchell, J.K. & Jamiolkowski, M. 1998. Chamber size effects on penetration resistance measured in calibration chambers. *J. Geotechnical and Geoenvironmental Engrg* 124 (9): 878-888.
- Sarsby, R. W. 1985. The influence of aperture size/particulate size on efficiency of grid reinforcement. *Proc. 2nd Canadian Symposium on Geotextiles and Geomembranes*, Edmonton, Alberta: 7-12
- Schaminée, P.E.L., den Adel, H. & Bezuijen, A. 2006. Geotechnical exchange format language a base for a physical modelling data standard? *Proc. of the Physical Modelling in Geotechnics - 6th ICPMG '06*, Hong Kong, Vol. 1: 241-246. Taylor & Francis.
- Schnaid, F. 2006. Geo-characterization and properties of natural soils by in situ tests. *Proc. XVI International Conference on Soil Mechanics and Geotechnical Engineering*, Osaka, Vol. 1: 3-45.
- Schnaid, F. 2009. *In-Situ Testing in Geomechanics - the main tests*. Taylor & Francis Group, London: 327 p.
- Schneider, J.A., Randolph, M.F., Mayne, P.W. & Ramsey, N.R. 2008. Analysis of factors influencing soil classification using normalized piezocone tip resistance and pore pressure parameters. *Journal Geotechnical and Geoenvironmental Engrg.* 134 (11): 1569-1586.
- Schofield, A.N. 1980. Cambridge geotechnical centrifuge operations, *Géotechnique* 30 (2): 227-268.
- Schofield, A.N. 1998. Geotechnical centrifuge development can correct a soil mechanics error. *Proc. International Conference Centrifuge 98*, Tokyo, Japan, Vol. 2: 923-929. Rotterdam: Balkema.
- Schofield, A.N. 2005. *Disturbed Soil Properties and Geotechnical Design*, Thomas Telford, London: 142 p.
- Schofield, A.N. & Wroth, C.P. 1968. *Critical State Soil Mechanics*, McGraw-Hill, London: 310 p. Download: www.geotechnique.info
- Seed, H.B. 1979. Soil liquefaction and cyclic mobility evaluation for level ground during earthquakes. *Journal of the Geotechnical Engineering Division*, ASCE 105 (GT2): 201-255.
- Seed, H.B. & Idriss, I.M. 1971. Simplified procedure for evaluating soil liquefaction potential. *Journal of Soil Mechanics and Foundations Division*, ASCE 97 (SM9): 1249-1273.
- Seed, H.B. & Idriss, I.M. 1982. Ground motions and soil liquefaction during earthquakes, *Monograph No.5*, Earthquake Engrg. Research Institute, Berkeley, CA.
- Seed, H.B., Tokimatsu, K., Harder, L.F. & Chung, R. 1984. The influence of SPT procedures on soil liquefaction resistance evaluations, *Rept. UCB/EERC-84/15*, University of California, Berkeley.
- Seed, H.B., Tokimatsu, K., Harder, L.F. & Chung, R.M. 1985. Influence of SPT procedures in soil liquefaction resistance evaluation. *Journal of Geotechnical Engineering* 111(2):1425-1445.
- Seed, R.B., Cetin, K.O., Moss, R.E., Kammerer, A., Wu, J., Pestana, J. 2001. Recent advances in soil liquefaction engineering and seismic site response evaluation. *Proc. 4th International Conference and Symposium on Recent Advances in Geotechnical Earthquake Engineering and Soil Dynamics*, Univ. of Missouri, Rolla.
- Senders, M., Randolph, M. F. & Gaudin, C. 2006. Centrifuge test set up for installations and cyclic loading of suction caissons in sand. *Proc. Physical Modelling in Geotechnics - 6th ICPMG '06*, Hong Kong, Vol. 1: 679-684. Leiden: Taylor & Francis/Balkema.
- Senneset, K., Sandven, R. & Janbu, N. 1989. Evaluation of soil parameters from piezocone tests. *Transportation Research Record* 1235, National Research Council, Washington, DC: 24-37.
- Sharma, J.S. & Bolton, M.D. 2001. Centrifugal and numerical modelling of reinforced embankments on soft clay installed with wick drains. *Geotextiles and Geomembranes* 19 (1): 23-24.
- Sharma, J.S., Springman, S.M. & Davison, L.R. 2001. An internet-based multi-threaded approach to computer-aided learning in civil

- engineering, *Proc. 7th International NETTIES Conference. 3rd International Conf. on New Learning Technologies: 7.2.1-7.2.8.*
- Sharma, J.S. 2002. Measurement of displacement – Trends or numbers?. S.M. Springman (ed), *Proc. of the workshop on constitutive and centrifuge modelling: two extremes*, Monte Verità, Ascona, Switzerland: 249-257. Lisse: Swets & Zeitlinger/Balkema.
- Shen, C.K., Li, X.S., Ng, C.W.W., Van Laak, P.A., Kutter, B.L., Cappel, K. & Tauscher, R.C. 1998. Development of a geotechnical centrifuge in Hong Kong. *Proc. Physical Modelling in Geotechnics - 6th ICPMG '06*, Hong Kong, Vol. 1: 13-18. Taylor & Francis.
- Shewbridge, S.E. & Sitar, N. 1990. Deformation based model for reinforced sand. *J. Geotechnical Engineering* 116 (7): 1153-1170.
- Shiau, J., Pather, S. & Ayers, R. 2006. Developing physical models for geotechnical teaching and research. *Proc. Physical Modelling in Geotechnics - 6th ICPMG '06*, Hong Kong, Vol. 1: 157-162.
- Shibuya, S., Mitachi, T. & Miura, S, editors 1994. *Pre-Failure Deformation of Geomaterials*, Balkema, Rotterdam: 1269 p.
- Shipton, B.J.I., Coop, M.R. & Nocilla, A. 2006. Particle breakage in transitional soils. *Geomechanics and Geotechnics of Particulate Media*, Taylor and Francis, London: 143-147.
- Shuttle, D.A. & Jefferies, M.G. 1998. Dimensionless and unbiased CPT interpretation in sand. *International Journal of Numerical and Analytical Methods in Geomechanics* 22: 351-391.
- SIA 267, *Geotechnik*, Schweizer Norm, 2003.
- Siemer, T. 2000. Centrifuge model investigations towards the dynamic shear modulus in the subsoil. *Proc. of the International Symposium on Physical Modelling and Testing in Environmental Geotechnics*, La Baule, France, May 15-17, 2000: 361-368. LCPC.
- Simonini, P., Ricceri, G. & Cola, S. 2007. Geotechnical characterization and properties of Venice lagoon heterogeneous silts. *Characterization and Engrg Properties of Natural Soils*, Vol. 4, Taylor and Francis Group, London: 2289-2327.
- Simons, N., Menzies, B. & Matthews, M. 2002. *A Short Course in Geotechnical Site Investigation*. Thomas Telford, London: 353 p.
- Singh, H., Henkel, D.J. & Sangrey, D.A. 1973. Shear and K_0 swelling of overconsolidated clay. *Proc. 8th Intl. Conf. Soil Mechanics and Foundation Engrg.*, Vol. 1.2 Moscow: 367-376.
- Singh, S., Seed, H.B. & Chan, C.K. 1982. Undisturbed sampling of saturated sands by freezing. *Journal of the Geotechnical Engrg. Division*, ASCE 108 (2): 247-264.
- Sitharam, T.G., Vinod, J.S. & Ravishankar, B.V. 2008. Evaluation of undrained response from drained triaxial shear tests: DEM simulations and experiments. *Géotechnique* 58 (7): 605-608.
- Skinner, A.E. 1969. A note on the influence of interparticle friction on the shearing strength of a random assembly of spherical particles. *Géotechnique* 19 (1): 150-157.
- Sladen, J.A. 1989. Problems with interpretation of sand state from cone penetration test. *Geotechnique* 39 (2): 323-332.
- Soga, K. & Mitchell, J.K. 1996. Rate-dependent deformation of structured natural clays. *Measuring & Modeling Time Dependent Soil Behavior*, GSP 61, ASCE, Reston, Virginia: 243-257.
- Springman, S.M. 1993. Buttonhole pile foundations: Design methods. *Symposium on Novel Foundation Techniques*, Cambridge, Cambridge Programme for Industry: 25p.
- Springman, S.M. 1997. Course notes. *Modelling in Geotechnics*, ETH Zurich.
- Springman, S.M., Balachandran, S. & Jommi, C. 1997. Modelling pre-failure deformation behaviour of reinforced soil walls, *Géotechnique* 48 (3): 653-663. also published in *Pre-failure Deformation Behaviour of Geomaterials*, Thomas Telford, London.
- Springman, S.M. 2000. Discussion on Displacement of structures adjacent to cantilever sheet pile walls. *Soils and Foundations* 39 (2): 99-104; Vol. 40 (5): 4, 2000.
- Springman, S.M. 2001. Soil structure interaction: idealisation, validation and calibration of models. *Proc. 1st Albert Caquot Conf.*, Paris.
- Springman, S. M., Laue, J., Boyle, R., White, J. & Zweidler, A. 2001. The ETH Zurich geotechnical drum centrifuge. *International Journal of Physical Modelling in Geotechnics* 1 (1): 59-70.
- Springman, S.M. (ed). 2002. *Constitutive and Centrifuge Modelling: Two Extremes*, Proc. of the workshop on constitutive and centrifuge modelling: two extremes, Monte Verità, Ascona, Switzerland, July 8-13. 2001. Lisse: Swets & Zeitlinger/Balkema: 379 p.
- Springman, S.M., Laue, J., Nater, P. & Chikatamarla, R. 2002. Use of flexible tactile pressure sensors in geotechnical centrifuges. *Proc. Intl. Conf. on Physical Modelling in Geotechnics/ICPMG*, St. John's, Newfoundland: 113-118. Swets & Zeitlinger/Balkema.
- Springman, S.M. & Weber, T. 2002. Discussion on problems governed by failure. S.M. Springman (ed), *Proc. of the workshop on constitutive and centrifuge modelling: two extremes*, Monte Verità, Ascona, Switzerland: 223-236. Lisse: Swets & Zeitlinger/Balkema.
- Springman, S.M., Jommi, C. & Teyssie, P. 2003a. Instabilities on moraine slopes induced by loss of suction: a case history, *Géotechnique* 53 (1): 3-10.
- Springman, S.M., Mayor, P.A. & Banjac, R. 2003b. CALICE: Entwicklung und Erfahrungen, EDV-Programme in der Geotechnik, *Mitteilungen der Schweizerische Gesellschaft für Boden- und Felsmechanik SGBF*, Frühjahrstagung, Zürich, März 28., 2003, 146: 28-36.
- Stallebrass, S.E. & Taylor, R.N. 1997. The development and evaluation of a constitutive model for the prediction of ground movements in overconsolidated clay. *Géotechnique* 47 (2): 235-253.
- Stark, T.D. & Eid, H.T. 1996. Shear behavior of a reinforced geosynthetic clay liner. *Geosynthetics Intl.*, IFAL, 3 (6): 771-785.
- Stark, T.D. & Olson, S.M. 1995. Liquefaction resistance using CPT and field case histories. *Journal of Geotechnical Engineering Division* 121 (12): 856-869.
- Steedman, R.S. 2006. Investigating New Orleans. *Ingenia, Magazine of the Royal Academy of Engineering* 28: 24-28.
- Steenfelt, J.S., Mikkelsen, H., Leth, C.T. & Madsen, J. 2003. Design and verification of shallow glass roof foundations by large scale plate loading tests. *Symposium International FONDSUP*.
- Stewart, D.P., Boyle, R.S. & Randolph, M.F. 1998. Experience with a new drum centrifuge. *Proc. International Conference Centrifuge 98*, Tokyo, Japan, Vol. 1: 35-40. Rotterdam: Balkema.
- Stewart, D.P. & Randolph, M.F. 1991. A new site investigation tool for the centrifuge. *Proc. International Conference Centrifuge 91*, Boulder, Colorado: 531-538. Rotterdam: Balkema.
- Sugimoto, M., Alagiyawanna, A.M.N. & Kadoguchi, K. 2001. Influence of rigid and flexible face on geogrid pullout tests. *Geotextiles and Geomembranes* 19 (5): 257-328.
- Susuki, Y., Tokimatsu, K., Koyamada, K., Taya, Y. & Kubota, Y. 1995. Field correlation of soil liquefaction based on CPT data. *Intl. Symposium on Cone Penetration Testing, CPT'95*, Vol. 2, Swedish Geot. Society, Linköping: 583-588.
- Swift, J., Eng, J., Bardet, J.P., Luil, F., Mokarram, N. & Pekcan, G. 2004. *Using the NEES reference data model and the NEES metadata browser for centrifuge experiments*. Version 1.1. National Earthquake Engineering Simulation, National Science Foundation: <http://it.nees.org/documentation/pdf/TR-2004-50.pdf>
- Take, W.A. & Bolton, M.D. 2002. The use of centrifuge modeling to investigate progressive failure of overconsolidated clay embankment. S.M. Springman (ed), *Proc. of the workshop on constitutive and centrifuge modelling: two extremes*, Monte Verità, Ascona, Switzerland: 191-197. Lisse: Swets & Zeitlinger/Balkema.
- Take, W.A. & Bolton, M.D. 2003. Tensiometer saturation and the reliable measurement of matric suction. *Géotechnique* 53 (2): 159-172.
- Take, W.A., Bolton, M.D., Yeung, F.J. & Wong P.C.P. 2004. Evaluation of landslide triggering mechanisms in model fill slopes. *Landslides* 1: 173-184.
- Takemura, J. & Kouda, M. 1998. Test results and discussions: Cone penetration tests (C2-cone). *Proc. of the International Conference Centrifuge 98*, Tokyo, Vol. 2: 1109-1116. Rotterdam: Balkema.
- Takemura, J. 1998a. General. T. Kimura, O. Kusakabe, J. Takemura (eds), *Proc. of the International Conference Centrifuge 98*, Tokyo, Japan, Vol. 2: 1045-1046. Rotterdam: Balkema.
- Takemura, J. 1998b. Methods for preparation of clay samples (not completed). *Proc. of the International Conference Centrifuge 98*, Tokyo, Vol. 2: 1057-1058. Rotterdam: Balkema.
- Takemura J., Kondoh, M., Esaki, T., Kouda, M. & Kusakabe, O. 1999. Centrifuge model tests on double propped wall excavation in soft clay. *Soils and Foundations* 39 (3): 75-87.
- Tanaka, H. 2000. Sample quality of cohesive soils: Lessons from three sites: Ariake, Bothkennar, and Drammen. *Soils and Foundations* 40 (4): 54-74.
- Tang, Y.X., Hanzawa, H. & Yasuhara, K. 1995. Direct shear and direct simple shear test results on Japanese marine clay. *Pre-failure Deformation of Geomaterials* (1), Balkema, Rotterdam: 107-112.
- Tani, K. & Kaneko, S., 2006. Method of recovering undisturbed samples using water-soluble thick polymer. (in Japanese) Tsuchi-to-Kiso, *Journal of Japanese Geotechnical Society* 54 (4): 145-148.
- Tanner, S. 2004. Fundamentsbelastung von geschichteten Bodensystemen, Diplomarbeit ETH Zürich.
- Tatsuoka, F. 2006. Inelastic deformation characteristics of geomaterials and their simulation. *Soil Stress-Strain Behavior: Measurement,*

- Modeling and Analysis*. Proceeding of the Geotechnical Symposium in Roma 2006. Springer, Netherlands: 1-108.
- Tatsuoka, F. & Shibuya, S. 1991. Deformation characteristics of soils and rocks from field and laboratory tests. *Report of the Institute of Industrial Science*, Univ. of Tokyo, Vol. 37 (1), Serial 235: 136 p.
- Tatsuoka, F., Hirakawa, D., Nojiri, M., Aizawa, H., Tateyama, M. & Watanabe, K. 2008. Integral bridge with geosynthetic-reinforced backfill. *Proc. GeoAmericas 2008*, First PanAmerican Geosynthetics Conference and Exhibition, Cancún, Mexico: 1199-1208.
- Tatsuoka, F., Ishihara, M., Di Benedetto, H. & Kuwano, R. 2002. Time-dependent shear deformation characteristics of geomaterials and their simulation. *Soils and Foundations* 42 (2): 103-129.
- Tatsuoka, F., Jardine, R.J., LoPresti, D., DiBenedetto, H. & Kodaka, T. 1997. Theme lecture: characterising the pre-failure deformation properties of geomaterials. *Proc. 14th Intl. Conf. on Soil Mech. and Foundation Engrg* (4), Hamburg, Balkema/Rotterdam: 2129-2164.
- Tatsuoka, F., Ochi, K., Fujii, S. & Okamoto, M. 1986. Cyclic undrained triaxial and torsional shear strength of sands for different sample preparation methods. *Soils and Foundations* 26 (3): 23-41.
- Tavenas, F. & Leroueil, S. 1979. Clay behavior and the selection of design parameters. *Proc. 7th ECSMFE* (1), Brighton, UK: 281-291.
- Taylor, D. 1948. *Fundamentals of Soil Mechanics*, John Wiley & Sons, New York.
- Taylor, R.N. (ed.) 1995. *Geotechnical centrifuge technology*. London: Blackie Academic & Professional.
- Taylor, R.N., Grant, R.J., Robson, S. & Kuwano, J. 1998: An image analysis system for determining plane and 3-D displacements in soil models. *Proc. of the International Conference Centrifuge 98*, Tokyo, Vol. 1: 73-78. Rotterdam: Balkema.
- Taylor, R.N. 2004. Tunnels and Excavations: Ground movements and their control. Colloquium at ETH Zürich.
- Teixeira, S.H.C & Bueno, B.S. 1999. An equipment for pullout test of geosynthetics. *Proc. Geossintéticos '99*, Rio de Janeiro: 215-222 (In Portuguese).
- Teixeira, S.H.C., Bueno, B.S. & Zornberg, J.G. 2007. Pullout resistance of individual longitudinal and transverse geogrid ribs. *Journal of Geotechnical and Geoenvironmental Engineering* 133 (1): 37-50.
- TEKSCAN 2002. www.tekscan.com/technology.html.
- Tefera, T.H., Sandven, R. & Kleppe, O. 2006a. Response of laterally loaded round wooden roadside piles in dense sand. *Proc. of the Physical Modelling in Geotechnics - 6th ICPMG '06*, Hong Kong, Vol. 2: 951-956. Leiden: Taylor & Francis/Balkema.
- Tefera, T.H., Grande, L. & Athanasias, C. 2006b. Large scale model test on single strutted sheet pile wall in sand and numerical analysis. *Proc. of the Physical Modelling in Geotechnics - 6th ICPMG '06*, Hong Kong, Vol. 2: 1567-1572. Taylor & Francis/Balkema.
- Terzaghi, K. 1934a. Large retaining wall tests - I. Pressure in dry sand. *Engineering News Record*, February: 136-140.
- Terzaghi, K. 1943b. *Theoretical Soil Mechanics*, John Wiley and Sons, New York: 510 p.
- Terzaghi, K. & Lacroix, Y. 1964. Mission Dam: earth and rockfill dam on a highly compressible foundation. *Geotechnique* 14 (1): 13-50.
- Thevanayagam, S. 1998. Effects of fines and confining stress on undrained shear strength of silty sands. *Journal of Geotechnical and Geoenvironmental Engineering* 124 (6): 479-491.
- Thevanayagam, S. & Martin, G.R. 2002. Liquefaction in silty soils – screening and remediation issues. *Soil Dynamics and Earthquake Engineering* 22: 1035-1042.
- Thevanayagam, S. & Mohan, S. 2000. Intergranular state variables and stress-strain behaviour of silty sands. *Geotechnique* 50 (1): 1-23.
- Thevanayagam, S., Shentham T., Mohan, S. & Liang, J. 2002. Undrained fragility of clean sands, silty sands and sandy silts. *J. Geotechnical and Geoenviron. Engrg.* 128 (10): 849-859.
- Thomas, P.A. & Bray, J.D. 1999. Capturing nonspherical shape of granular media with disk clusters. *J. Geotechnical and Geoenviron. Engrg.* 125 (3): 169-178.
- Thorel, L., Gaudin, C. & Garnier, J. 2007. A cone pressuremeter for soil characterisation in centrifuge, *International Journal of Physical Modelling in Geotechnics* 7 (1): 23-30.
- Thornton, C. 2000. Numerical simulations of deviatoric shear deformation of granular media. *Geotechnique* 50 (1): 43-53.
- Thornton, J.S., Allen, S.R., Thomas, R.W. & Sandri, D. 1998. The stepped isothermal method for time-temperature superposition and its application to creep data on polyester yarn. *Proc. 6th Intl. Conference on Geosynthetics*, Atlanta, GA, Vol. 2: 699-706.
- Tisinger, L.G., Peggs, I.D. & Haxo, H.E. 1991. Chemical compatibility testing of geomembranes. *Geomembrane Identification and Performance Testing*, Chapman Hall.
- Tokimatsu, K., Suzuki, Y., Taya, Y. & Kubota, Y. 1995. Correlation between liquefaction resistance of in-situ frozen samples and CPT resistance. *Proc. 10th Asian Regional Conference on Soil Mechanics and Foundation Engineering*, Beijing: 493-496.
- Triplet, E.J. & Fox, P.J. 2001. Shear strength of hdpe geomembrane/geosynthetic clay liner interfaces. *Journal of Geotechnical and Geoenvironmental Engineering* 127 (6): 543-552.
- Tristancho, J., Caicedo, B. & Duque, M. 2006. New device to control the atmospheric boundary condition in centrifuge. *Proc. of the Physical Modelling in Geotechnics - 6th ICPMG '06*, Hong Kong, Vol. 1: 253-258. Leiden: Taylor & Francis/Balkema.
- Tsai, J-S, Liou, Y-J, Liu, F-C & Chen, C-H. 2004. Effect of hammer shape on energy transfer measurement in the standard penetration test. *Soils and Foundations* 33 (3): 103-114.
- Tupa, N. 1994. A study on adherence and interaction between soils and geosynthetics. *MSc. Dissertation*, University of Brasilia, Brasilia, Brazil, 188 p. (in Portuguese).
- Ubilla, J., Abdoun, T. & Zimmie, T. 2006. Application of in-flight robot in centrifuge modeling of laterally loaded stiff pile foundations. *Proc. of the Physical Modelling in Geotechnics - 6th ICPMG '06*, Hong Kong, Vol. 1: 259-264. Leiden: Taylor & Francis/Balkema.
- Ueno, K., Yokoyama, Y. & Murata, M. 1998. Bending moments and subgrade acting on sheet pile walls. *Proc. of the International Conference Centrifuge 98*, Tokyo, Vol. 1: 661-666. Balkema.
- Vaid, Y.P. & Negussey, D. 1984. Relative density of pluviated sand samplers. *Soils and Foundations* 24 (2): 101-105.
- Vaid, Y.P. & Negussey, D. 1988. Preparation of reconstituted sand specimens. *Advanced Triaxial Testing of Soil and Rock (STP 977)*, ASTM, West Conshohocken/PA: 405-417.
- Vaid, Y.P. 1994. Liquefaction of silty soils. *Ground Failures Under Seismic Conditions (GSP 44)*, ASCE, Reston, Virginia: 1-16.
- Vaid, Y.P. & Sivathayalan, S. 2007. Fundamental factors affecting liquefaction susceptibility of sands. *Canadian Geot. J.* 37: 592-606.
- Van, M.A. 2003. Innovation cycle in a Dutch polder. Discussion session 5.1, *Proc. XIIIth European Conference*, Prague.
- Van Laak, P.A., Adalier, K., Dobry, R. & Elgamal, A.W. 1998. Design of RPI's large servo hydraulic centrifuge shaker. *Proc. International Conference Centrifuge 98*, Tokyo, Vol. 2: 923-929. Balkema.
- Ventouras, K. & Coop, M.R. 2009. On the behaviour of Thanet sand: an example of an uncemented natural sand. *Geotechnique*, in press.
- Verdugo, R. and Ishihara, K. 1996. The steady state of sandy soils. *Soils and Foundations* 36 (2): 81-91.
- Vesic, A.B. 1963. *Bearing Capacity of Deep Foundations in Sand*. Highway Research Record, Washington, DC.
- Viggiani, G. & Desrués, J. 2004. Experimental observations of shear banding in stiff clay. *Geotechnical Innovations*, Verlag Glückauf, Essen: 649-658.
- Viswanadham, B.V.S. & Mahajan, R.R. 2007. Centrifuge model tests on geotextile-reinforced slopes. *Geosynthetics Intl.* 14 (6): 365-379.
- Wang, W. 1970. *Some findings in soil liquefaction*. Water Conservancy and Hydroelectric Power Scientific Res. Institute, Beijing, China.
- Wang, G. & Sassa, K. 2001. Factors affecting rainfall-induced flowslides in laboratory flume tests. *Geotechnique* 51 (7): 587-599.
- Wang, G. & Sassa, K. 2006. Physical modeling of landslides in ring shear tests and flume tests. *Proc. of the Physical Modelling in Geotechnics - 6th ICPMG '06*, Hong Kong, Vol. 1: 113-125. Taylor & Francis.
- Wang, J., Dove, N.S. & Gutierrez, M.S. 2007. Discrete-continuum analysis of shear banding in the direct shear test. *Geotechnique* 57 (6): 513-526.
- Walz, B. 2005. *Möglichkeiten und Grenzen 1-g Modellversuche (Opportunities & limitations to 1g model tests)* Entwicklungen in der Bodenmechanik, Bodendynamik & Geotechnik. Frank Rackwitz (ed.), Festschrift zum 60. Geburtstag von Univ.-Professor Dr.-Ing. habil. Stavros A. Savidis: 63-78. Berlin: Springer.
- Watson, P. G. & Randolph, M. F. 2006. A centrifuge study into cyclic loading of caisson foundations. *Proc. of the Physical Modelling in Geotechnics*, Hong Kong, Vol. 1: 693-699. Taylor & Francis.
- Weber, T.M. 2007 *Modellierung der Baugrundverbesserung mit Schotterssäulen*, ETH Dissertation 17321, Zürich, vdf Verlag.
- Weber, T.M., Laue, J., Springman, S.M. 2005. Modelling the inflight construction of sand compaction piles in the centrifuge, *Proc. 16th Intl. Conference on Soil Mechanics and Geotechnical Engineering* Osaka, Japan: 1291-1294. Rotterdam: Millpress.
- Weber, T.M., Laue, J., Springman, S.M. 2006. Centrifuge modelling of sand compaction piles in soft clay under embankment load, *Proc. 6th International Conference on Physical Modelling in Geotechnics*, Hong Kong: 603-608.

- Weber, T.M., Plötze, M., Laue, J., Springman, S.M. & Peschke G. 2009. Smear zone identification and soil properties around stone columns constructed in-flight in centrifuge model tests. *Géotechnique*. in print.
- Weiler, W.A. Jr & Kulhawy, F.H. 1982. Factors affecting stress cell measurements in soil. *Journal of Geotechnical Engineering* 108, (GT12): 1529-1548.
- Wheeler, S. J. & Sivakumar, V. 1995. An elastoplastic critical state framework for unsaturated soil. *Géotechnique* 45 (1): 35-53.
- White, M. 1990. *Leonardo da Vinci: the first scientist*. Abacus.
- White, D.J. 2002. An investigation into the behaviour of pressed-in piles. *PhD thesis*, University of Cambridge.
- White, D.J. & Bolton, M.D. 2002. Observing friction fatigue on a jacked pile. S.M. Springman (ed), *Proc. of the workshop on constitutive and centrifuge modelling: two extremes*, Monte Verità, Ascona, Switzerland: 347-354. Lisse: Swets & Zeitlinger/Balkema.
- White, D.J., Take, W.A. & Bolton, M.D. 2003. Soil deformation measurement using particle image velocimetry (PIV) and photogrammetry. *Géotechnique* 53 (7): 619-631.
- White, D.J. & Lehane, B.M. 2004. Friction fatigue on displacement piles in sand. *Géotechnique* 54 (10): 645-658.
- White, D.J., Randolph, M.F. & Thompson, B. 2005. An image-based deformation measurement system for the geotechnical centrifuge. *Intl. Journal of Physical Modelling in Geotechnics* 5 (3): 1-12.
- Whittle, A.J. & Kavvas, M.J. 1994. Formulation of MIT-E3 constitutive model for overconsolidated clay. *Journal of Geotechnical Engrg.* 120 (1): 173-224.
- Whittle, A.J. et al. 2001. Prediction and interpretation of pore pressure dissipation for a tapered piezoprobe. *Géotechnique* 51 (7): 601-617.
- Wilson-Fahmy, R.F., Narejo, D. & Koerner, R.M. 1996. Puncture protection of geomembranes Part I: theory. *Geosynthetics Intl.* 3 (5): 605-628.
- Wolf, H., König, D. & Triantafyllidis, T. 2003. Experimental investigation of shear band patterns in granular material. *Journal of Structural Geology* 25: 1229-1240.
- Wood, F.M., Yamamoto, J.A. & Lade, P.V. 2008. Effect of depositional method on undrained response of silty sand. *Canadian Geotechnical J.* 45: 1525-1537.
- Woods, R.D. 1978. Measurement of dynamic soil properties. *Earthquake Engineering and Soil Dynamics*, Vol. I (Proc. Pasadena), ASCE, Reston, Virginia: 91-178.
- Wroth, C.P. 1984. The interpretation of in-situ soil tests. *Geotechnique* 34 (4): 449-489.
- Wroth, C.P. 1988. Penetration testing: a more rigorous approach to interpretation. *Penetration Testing 1988*, Vol. 1, Balkema: 303-311.
- Wroth, C.P. & Bassett, R.H. 1965. A stress-strain relationship for the shearing behaviour of a sand. *Géotechnique* 15 (1): 32-56.
- Yafrate, N.J., DeJong, J.T. & DeGroot, D.J. 2007. The influence of full-flow penetrometer area ratio on penetration resistance and undrained shear strength. *Proc. 6th Intl. Offshore Site Investigation and Geotechnics Conf.*, Soc. Underwater Tech., London: 461-468.
- Yamamoto, J.A. & Lade, P.V. 1997. Static liquefaction of very loose sands. *Canadian Geotechnical Journal* 34: 905-917
- Yamamoto J.A. & Lade P.L. 1998. Steady-state concepts and static liquefaction of silty sands. *Journal of Geotechnical and Geoenvironmental Engrg.* 124 (9): 868-877.
- Yamamoto, J.A. & Covert, K.M. 2001. Monotonic and cyclic liquefaction of very loose sands with high silt content. *Journal of Geotechnical and Geoenvironmental Engineering* 127 (4): 314-324.
- Yamamoto, J.A. & Wood F.M. 2004. Effect of depositional method on the undrained behavior and microstructure of sand with silt. *Soil Dynamics and Earthquake Engineering* 24 (9-10): 751-760.
- Yamamoto, J.A., Wood, F.M. & Lade, P.V. 2008. Effect of depositional method on the microstructure of silty sand. *Canadian Geotechnical Journal* 45: 1538-1555.
- Yan, L. & Byrne, P.M. 1989. Application of hydraulic gradient similitude method to small scale footing tests on sand. *Canadian Geotechnical Journal* 26 (2): 246-259.
- Yang, Z.X., Li, X.S. & Yang, J. 2008. Quantifying and modelling fabric anisotropy of granular soils. *Géotechnique* 58 (4): 237-248.
- Yin, J-H., Zhu, J-G. & Graham, J. 2002. A new viscoplastic model for time-dependent behaviour of normally and overconsolidated clays: theory and verification. *Canadian Geotechnical J.* 39: 157-173.
- Yoshimi, Y., Hatanaka, M. & Oh-oka, H. 1977. A simple method for undisturbed sand sampling by freezing. *Proc. 9th Intl. Conf. on Soil Mechanics and Foundation Engineering*, Special Session 2, Tokyo, Japan: 23-28.
- Yoshimi, Y., Tokimatsu, K. & Hosaka, Y. 1989. Evaluation of liquefaction resistance of clean sands based on high quality undisturbed samples. *Soils and Foundations* 29 (1): 3-104.
- Youd, T.L. et al. 2001. Liquefaction resistance of soils: summary report from the 1996 NCEER and 1998 NCEER/NSF workshops on evaluation of liquefaction resistance of soils. *Journal of Geotechnical and Geoenvironmental Engrg.* 127 (10): 817-833.
- Yu, H.S. 1996. Interpretation of pressuremeter unloading tests in sand. *Geotechnique* 46 (1): 17-32.
- Yu, H.S. 2008. Non-coaxial theories of plasticity for granular materials. *Proceedings 12th Intl. Conf. Intl. Assoc. for Computer Methods and Advances in Geomechanics (IACMAG)*: 361-378.
- Yu, H.S., Schnaid, F. & Collins, I.F. 1996. Analysis of cone pressuremeter tests in sands. *Journal of Geotechnical and Geoenvironmental Engineering* 122 (8): 623-632.
- Yuu, J., Han, J., Rosen, A., Parsons, R.L. & Leshchinsky, D. (2008). Technical review of geocell-reinforced base courses over weak subgrade. *Proc. GeoAmericas 2008*, First PanAmerican Geosynthetics Conference and Exhibition, Cancún, Mexico: 1022-1030.
- Zhang, J., Rai, C.S. & Sondergeld, C.H. 1998. Mechanical strength of reservoir materials: key information for sand prediction. *Eurock '98 Soc. Petroleum Engrs and ISRM*, Trondheim: 291-298.
- Zhao, Y., Gafar, K., Elshafie, M.Z.E.B., Deeks, A.D., Knappett, J.A. & Madabhushi, S.P.G. 2006. Calibration and use of a new automatic sand pourer. *Proc. of the Physical Modelling in Geotechnics - 6th ICPMG '06*, Hong Kong, Vol. 1: 265-272. Taylor & Francis.
- Zlatovic, S. & Ishihara, K. 1997. Normalized behavior of very loose non-plastic soils: effects of fabric. *Soils & Foundations* 37 (4): 47-56.
- Zornberg, J.G. 2002. Discrete framework for limit equilibrium analysis of fibre-reinforced soil. *Géotechnique* 52 (8): 593-604.
- Zornberg, J.G. 2002. Peak versus Residual Shear Strength in Geosynthetic-Reinforced Soil Design. *Geosynthetics International*, Vol. 9, No. 4, pp. 301-318.
- Zornberg, J.G. 2005. Geosynthetic reinforcement in landfill design: us perspectives. *International Perspectives on Soil Reinforcement Applications*. GSP 141, ASCE, Reston, Virginia (CD-ROM).
- Zornberg, J.G., Sitar, N., & Mitchell, J.K. 1998. Limit Equilibrium as Basis for Design of Geosynthetic Reinforced Slopes. *Journal of Geotechnical and Geoenvironmental Engineering* 124 (8): 684-698.
- Zornberg, J.G., Sitar, N., & Mitchell, J.K. 1998. Performance of Geosynthetic Reinforced Slopes at Failure. *Journal of Geotechnical and Geoenvironmental Engineering* 124 (8): 670-683.
- Zornberg, J.G. & Arriaga, F. 2003. Strain distribution within geosynthetic-reinforced slopes. *J. Geotechnical and Geoenvironmental Engrg.* 129 (1): 32-45.
- Zornberg, J.G. & McCartney, J.S. 2009. Chapter 6: Internal and interface shear strength of GCLs. *Geosynthetic Clay Liners for Waste Containment*, Balkema, Rotterdam, in press.
- Zornberg, J.G. & Christopher, B.R. 2007. Chapter 37: Geosynthetics. *The Handbook of Groundwater Engineering*, 2nd Edition, CRC Press, Taylor and Francis, Boca Raton, Florida.
- Zornberg, J.G. & Giroud, J.P. 1997. Uplift of geomembranes by wind - extension of equations. *Geosynthetics Intl.* 4 (2): 187-207.
- Zornberg, J.G. & Kavazanjian, E. 2001. Prediction of the performance of a geogrid-reinforced slope founded on solid waste. *Soils and Foundations* 41 (6): 1-16.
- Zornberg, J.G. LaFountain, L. & Caldwell, J.A. 2003. Analysis and Design of Evapotranspirative Cover for Hazardous Waste Landfill. *Jour. Geotechnical and Geoenvironmental Engrg* 129 (6): 427-438.
- Zornberg, J.G. & Li, C. 2003. Design of fiber-reinforced soil." *Proc. 12th Panamerican Conference of Soil Mechanics and Geotechnical Engineering*, Cambridge, Massachusetts, Vol. 2: 2193-2200.
- Zornberg, J.G., Byler, B.R. & Knudsen, J. (2004). "Creep of Geotextiles using Time-Temperature Superposition Methods." *Journal of Geotechnical and Geoenvironmental Engineering* 130 (11): 1158-1168.
- Zornberg, J.G., Gupta, R., Prozzi, J.A. & Goehl, D. 2008. Case histories on geogrid-reinforced pavements to mitigate problems associated with expansive subgrade soils. *Proceedings GeoAmericas 2008*, First PanAmerican Geosynthetics Conf., Cancún, Mexico: 983-991.
- Zornberg, J.G., McCartney, J.S. & Swan, R.H. 2005. Analysis of a large database of gcl internal shear strength results. *Journal of Geotechnical and Geotechnical Engineering* 131 (3): 367-380.
- Zornberg, J.G., Somasundaram, S. & LaFountain, L. 2001. Design of geosynthetic-reinforced veneer slopes. *Proc. Intl. Symp. on Earth Reinforcement: Landmarks in Earth Reinforcement*, Fukuoka: 305-310.